Contents of issue 1 – 2 vol. XLVI

Archives
of
Mechanics

Archiwum Mechaniki Stosowanej

Plane-stress deformation of a flat plate
by slip between elastic elements

R. L. BISH (MELBOURNE)

PRINCIPLES previously published and concerned with the plane-strain deformation of a textured polycrystalline solid are extended to the plane-stress deformation of a flat plate. An example is given illustrating the method.

Notation

ω	vorticity,
τ	principal shear stress,
γ	principal shear strain,
$\dot{\gamma}$	principal shear strain rate,
ϕ, ϕ_1, ϕ_2	rotations in principal stress planes,
σ_{ij}	stress tensor,
τ_{ij}	deviator of stress,
h	yield function,
J_2	second invariant of τ_{ij},
J_3	third invariant of τ_{ij},
G	elastic shear modulus,
λ	a multiplier,
σ_1, σ_2	principal stresses,
$d\varepsilon_{ij}$	total strain increment,
de_{ij}	plastic strain increment,
α, β	slip-line coordinates,
h_α, h_β	scale factors for α- and β-lines,
∇^2	Laplacian,
p	external pressure,
P	power,
(r, θ)	plane-polar coordinates.

1. Introduction

IN EARLIER PAPERS the author proposed, for solids flowing by slip along banales (Appendix 1), two principles which may be expressed as follows.

(i) The rotation rate remains continuous. If ω is the vorticity, this principle may be expressed mathematically in the form [1]

$$(1.1) \qquad \qquad \text{curl}\,\omega = 0.$$

or, if $\dot{e}_{ij}$ denotes the plastic strain-rate tensor [2],

$$(1.2) \qquad \qquad \partial_i\,\dot{e}_{ij} = 0.$$

(ii) Under plane-strain, a fully textured solid work-hardens [3] in such a way that the relation between the principal shear stress, τ, and the principal shear strain, γ remains valid when γ is replaced by the rotation ϕ.

Thus the yield curve described by

$$\tau = \tau(\gamma)$$

becomes

(1.3) $$\tau = \tau(\phi),$$

where it is understood that the reference direction for ϕ must be properly chosen (Appendix 2).

Work-hardening was also the subject of refined experimental investigation by FARMER and OXLEY [4], who extruded split prisms of 5052-H34 temper aluminium through a lubricated wedge-shaped die, of semi-angle 30°, at 0.006 mm/sec. Their samples were pre-machined to fit the die cavity and measured 2.54 mm × 10.16 mm in cross-section. Grids were photo-engraved on the central planes in these split prisms and from the deformed grid patterns, rotations may be measured. The samples were coated with alodine and the die cavity was lubricated using sodium stearate. Friction, it was shown, remained very small. On loading the extrusion force rose rapidly to its maximum value of 7.5 kN.

The plane-strain theory developed from Eqs. (1.1) and (1.2) in conjunction with the stress-strain data provided by Farmer and Oxley leads to a force of 7.4 kN [5], whereas by neglecting work-hardening and choosing for the yield stress the value on Farmer and Oxley's yield curve, at a shear strain of 0.1, one obtains an extrusion force of 6.3 kN. Clearly work-hardening made an important contribution to the extrusion load measured in these experiments and the measurements of Farmer and Oxley support (1.3).

In extending this theory to the plane-stress deformation of a flat plate, the form of the yield criterion assumes central importance. Let us therefore consider the mechanics of yielding in a fully textured metal.

2. The yield criterion

A principal shear stress surface in a solid that has been aligned or textured by cold-work (Appendix 1) is enveloped by a polyhedral surface that consists of faces that are in fact crystallographic slip-planes. Each of these slip-planes is confined within a grain that the principal shear stress surface intersects. It follows, at once, assuming these slip-planes to remain perfectly aligned (tangent planes to the principal shear stress surface concerned), that Tresca's criterion must govern yielding. This insight allows the previously developed plane-strain theory [2, 3] to be extended to plane-stress as follows.

If σ_{ij} denotes the stress tensor and τ_{ij} is the deviator of stress, while J_2 and J_3 denote the second and third invariants of τ_{ij}, then the yield condition may be expressed in the form

(2.1) $$h(J_2, J_3) = 0.$$

The associated flow rule, if $d\varepsilon_{ij}$ is the total strain increment, is [6]

(2.2) $$d\varepsilon_{ij} = \frac{d\tau_{ij}}{2G} + \frac{\partial h}{\partial \sigma_{ij}} d\lambda,$$

where G is the elastic shear modulus, and λ is a multiplier.

In the case of Tresca's criterion, (2.1) being replaced by

(2.3) $$\sigma_1 - \sigma_2 = \pm 2\tau,$$
(2.4) $$\sigma_2 - \sigma_3 = \pm 2\tau,$$
(2.5) $$\sigma_3 - \sigma_1 = \pm 2\tau,$$

we have, from Eq. (2.3),

$$\frac{\partial h}{\partial \sigma_3} = 0,$$

while by Eq. (2.2),

$$d\varepsilon_3 = 0.$$

Similarly from Eq. (2.4)

$$d\varepsilon_1 = 0.$$

while in view of Eq. (2.5)

$$d\varepsilon_2 = 0.$$

We see that the pairs of opposite sides of the hexagonal cylinder represented by Eqs. (2.3)–(2.5) describe deformation that, if the principal surfaces remained plane, would equal deformation under plane strain. How we may interpret this result for a flat plate is illustrated in Fig. 1, where the principal stress σ_3 is constant (or zero) and the three rotations in the principal planes are ϕ_1, φ_2 and ϕ. The angle ϕ is associated with the side of the yield locus CD in Fig. 1a, which corresponds to the Hencky–Prandtl net in the plane of the plate shown in Fig. 1d. There are no Hencky–Prandtl nets in the plane of the plate in Figs. 1b and 1c, and these cases are associated, respectively, with sides AB and BC in Fig. 1a. In these two cases the plate extends uni-directionally at the expense of a reduction in its thickness, the extension being along one of the two families of principal stress lines in the plane of the plate.

a)

b)

AB
$de_2 = 0$

c)

BC
$de_1 = 0$

d)

CD
$de_n = 0$
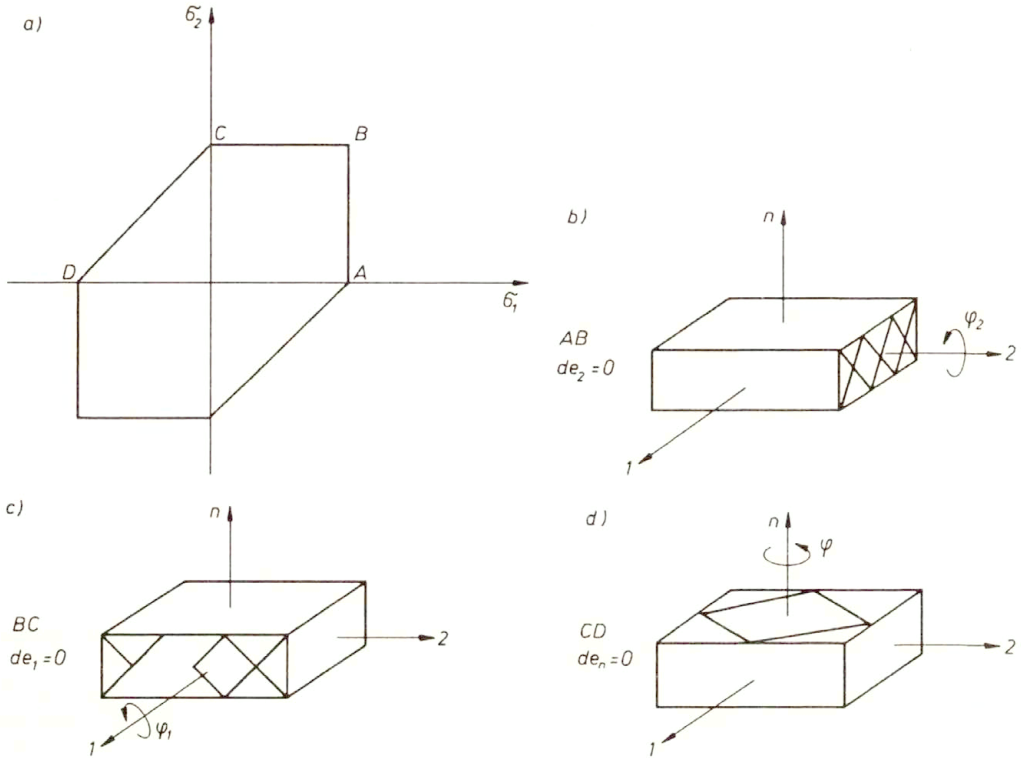
FIG. 1. Modes of deformation of a flat textured plate.

3. Continuity of rotation rate

That the rotation rate, in the case of a deforming single crystal, must remain spatially continuous is obvious. It is not so obvious where textured polycrystalline solids are concerned; but the banales remain parallel to the principal shear stress surfaces, which are smooth and continuous and, at the same time, the banales remain embedded in the solid. By the same principle a banale could not cross grain boundaries without deflection if the rotation rates in the two adjoining grains differed substantially.

If α and β are the coordinates measured along the two families of slip-lines in the plane of the plate and if h_α and h_β are the respective scale factors, with $\dot{\gamma}$ equal to the principal shear strain rate, then Eq. (1.2) reduces to the pair of equations

$$-2\dot{\gamma}\,\frac{\partial\phi}{h_\alpha\partial\alpha} + \frac{\partial\dot{\gamma}}{h_\beta\partial\beta} = 0.$$

$$2\dot{\gamma}\,\frac{\partial\phi}{h_\beta\partial\beta} + \frac{\partial\dot{\gamma}}{h_\alpha\partial\alpha} = 0.$$

and from these equations, using the formula [7],

$$(3.1) \qquad h_\alpha h_\beta \nabla^2 = \frac{\partial}{\partial\alpha}\left(\frac{h_\beta}{h_\alpha}\frac{\partial}{\partial\alpha}\right) + \frac{\partial}{\partial\beta}\left(\frac{h_\alpha}{h_\beta}\frac{\partial}{\partial\beta}\right)$$

we obtain

$$(3.2) \qquad \nabla^2\phi = 0,$$
$$(3.3) \qquad \nabla^2\ln\dot\gamma = 0.$$

4. Work-hardening

In order to extend Eq. (1.3) to a flat plate, in view of the fact that the three modes of deformation shown in Fig. 1 are, in fact, instances of plane strain (or would be if the first and second principal surfaces were plane), we need only note the additional fact [8], that work-hardening produced on one slip-plane, by slip on that plane, extends to all other slip-planes in a crystal. This must also be true of banales made up, as they are, from individual crystallographic slip-planes. Thus it follows for the plate in Fig. 1, irrespective of where the stress point lies on the yield locus, that

$$(4.1) \qquad \tau = \tau(\phi + \phi_1 + \phi_2).$$

5. Stress-equilibrium

If

$$\sigma = (\sigma_1 + \sigma_2)/2$$

and

$$\tau = (\sigma_2 - \sigma_1)/2$$

represent the respective normal and principal shear stresses in the plane of the plate, then the stress equilibrium equations for the plate are

$$(5.1) \qquad \frac{\partial\sigma}{h_\alpha\partial\alpha} - 2\tau\frac{\partial\phi}{h_\alpha\partial\alpha} + \frac{\partial\tau}{h_\beta\partial\beta} = 0,$$

$$(5.2) \qquad \frac{\partial\sigma}{h_\beta\partial\beta} + 2\tau\frac{\partial\phi}{h_\beta\partial\beta} + \frac{\partial\tau}{h_\alpha\partial\alpha} = 0.$$

If, moreover, the plate remains flat

$$(5.3) \qquad \frac{\partial\phi_1}{\partial\alpha} = \frac{\partial\phi_2}{\partial\alpha} = \frac{\partial\phi_1}{\partial\beta} = \frac{\partial\phi_2}{\partial\beta} = 0.$$

and by Eq. (4.1)

$$(5.4) \qquad \frac{\partial \tau}{\partial \alpha} \frac{\partial \phi}{\partial \beta} - \frac{\partial \tau}{\partial \beta} \frac{\partial \phi}{\partial \alpha} = 0.$$

The consistency condition for Eqs. (5.1) and (5.2) (which are in effect simultaneous equations in the first derivatives of ϕ) is

$$(5.5) \qquad d\sigma^2 = d\tau^2 + 4\tau^2 d\phi^2,$$

while we obtain, from Eqs. (5.1), (5.2) and (5.4), using Eq. (3.1), the second order equation

$$(5.6) \qquad 2\frac{\partial^2 \sigma}{\partial \alpha \partial \beta} + h_\alpha h_\beta \nabla^2 \tau = 0.$$

These equations are identical to the corresponding equations of the plane-strain theory [3].

6. Method

Before we can apply Eqs. (3.2), (3.3), (5.5) and (5.6) to a flat plate problem, it is essential to establish that the stress point lies on CD in Fig. 1a. We know that C cannot lie simultaneously on BC and CD [9] and if the plate exhibits a Hencky–Prandtl net, in its plane, then the stress point will lie on CD which includes its two end points.

If, moreover, an α – slip-line starts from an edge at which $\phi = \phi_0$ then, by Eq. (5.5),

$$(6.1) \qquad \sigma(\phi) = -\tau(\phi_0) + \int\limits_{\phi_0}^{\phi} \sqrt{\left(\frac{d\tau}{d\phi}\right)^2 + 4\tau^2}\, d\varphi.$$

since

$$\sigma(\phi_0) + \tau(\phi_0) = 0.$$

while, if p is the pressure on a principal surface in the plate,

$$(6.2) \qquad p(\phi) = \tau(\phi) - \tau(\phi_0) + \int\limits_{\phi_0}^{\phi} \sqrt{\left(\frac{d\tau}{d\phi}\right)^2 + 4\tau^2}\, d\varphi.$$

and by means of this formula the external load may be calculated.

Alternately we may calculate the power, P by means of the formula

$$(6.3) \qquad P = 2T \int_A \tau(\phi)\, \dot{\gamma}\; dS,$$

where T is the plate thickness and dS is an element of the area A of the deforming region in the plate.

In those problems where the free edges in the plate are radial lines or circular arcs, or where there are radial slip-lines, appropriate solutions to Eq. (3.2) are, if (x, y) and (r, θ) are rectangular and plane polar coordinates in the plane of the plate,

$$(6.4) \qquad \begin{aligned} \phi &= \tan^{-1}(y/C + x), \\ \phi &= \theta, \\ \phi &= C + \ln r, \end{aligned}$$

where C is a constant. The first of these formulae describe slip-lines in a rectangular net, while the second describes the radial lines in a centred fan; Eq. (6.4) being the equation for equi-angular spirals. The solution to Eq. (3.3) associated with Eq. (6.4) is

$$(6.5) \qquad \dot{\gamma} = av/r^2,$$

where v is the radial velocity across the circle $r = a$.

7. An example

The problem of an annulus cut from a textured plate and to which forces sufficient to cause plastic flow are applied at its inner edge, has relevance to cup drawing and may be studied by means of the above theory. While there is no buckling, Eq. (5.3) applies, and the stress point will lie on CD in Fig. 1a for the plate must then deform as in Fig. 1d. In the investigation of this problem the values of stress and strain obtained in the slow blanking of hard-drawn brass were used, [10]; the data are approximated by $\tau = 250 + 100 \exp(-11.5\gamma)\,\text{MNm}^{-2}$.

Material is not able to undergo slip at certain points of the annulus unless it first re-orientates. The delay due to this effect, in conjunction with the form of Eq. (3.3), leads to the "ears" familiar in deep-drawn cups. For an α-line that starts from such a point we obtain from Eqs. (5.6) or (6.1) and (6.4), in the case of hard-drawn brass,

$$\sigma = -k + 2k\ln(r/a),$$

where $\tau = k$ is the limiting value of shear stress given by the above equation for τ, while a is the radius of the outer edge of the blank. This relation may also have been obtained from Eqs. (6.3) and (6.5), using $p = \sigma + k$.

On the other hand, material in the annulus at the four intermediate points
on its outer edge is free to undergo slip immediately along the α-lines given by
Eq. (6.4), and the lower curve in Fig. 2 gives the variation in σ along a slip-line
starting from one of these "free" points. The integrations were carried out by
means of Simpson's rule. Note that the two curves in Fig. 2 become parallel on
moving in from the outer edge of the annulus. From these results the contribution
made by work-hardening to the external load may be readily calculated.
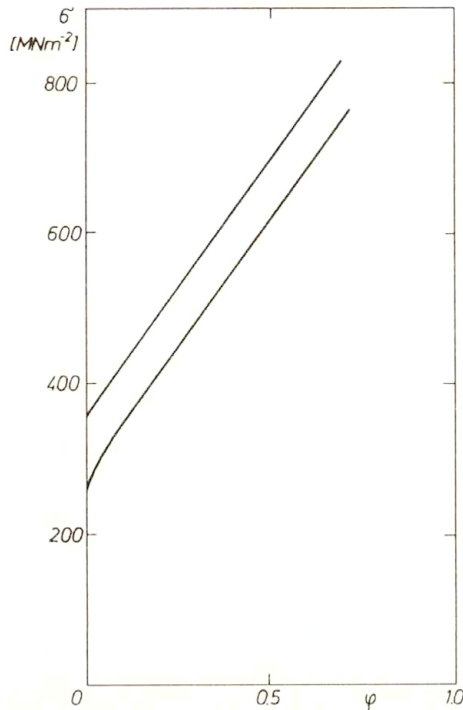
FIG. 2. Computed initial distributions of σ in a flat annulus cut from a textured plate, to which
forces are applied at its inner edge. The upper curve applies to a slip-line starting from a point
at which an "ear" develops, while the lower curve applies to slip-lines from points free
to undergo immediate deformation without re-orientation.

Appendix 1

OSMOND, in 1904 [11], described "lines" that he had observed in deformed
iron, and that he called "deformation banales". These trammels for extended slip
crossed grain boundaries without deflection and remained parallel to the principal
shear stress surfaces. The fact that banales may be revealed by illuminating etched
metal surfaces using polarised light testifies to the crystallographic character of
banales [12].

When a polycrystalline metal is plastically deformed, its grains rotate (see Appendix 2) so as to align their slip-planes parallel to the principal shear stress surfaces. Flow then takes place, in this aligned solid, by slip of the material along the lines of the banale network.

Appendix 2

When a solid is cold-worked, its grains rotate so as to align their slip-planes parallel to the principal shear stress axes. Clearly the grains cannot rotate as rigid bodies during this cold-working but must sub-divide into elastic blocks that slip past one another on at least two intersecting families of slip-planes, since single-slip can never accomodate a rotation. In the limit as the banale spacing tends to zero the rotation rate becomes equal to the vorticity; indeed vorticity, like strain, cannot otherwise be defined, in the case of plastic deformation.

Work-hardening also demands double or multiple slip [8], and the relation between rotation during deformation and work-hardening may be illustrated as follows.

We might imagine the yield curve replaced by a stepped curve such that the horizontal portions (constant τ) result from alternating single-slip on the banales, while the vertical portions (constant γ) are due to re-alignment of the banales; since the banales are embedded in the solid and so they must constantly re-align with the principal shear stress surfaces, and re-alignment, as just pointed out, demands double slip. In the limit as the increments in τ and γ on the stepped curve become infinitesimally small, the original yield curve is recovered, but the principal shear stress τ remains a function of the angle, ϕ, of re-alignment; since it is only during re-alignment that τ can increase.

References

1. R.L. BISH, *The flow of a polycrystalline solid by slip between elastic volume elements*, Phil. Mag., A56, 3, 385–390, 1987.

2. R.L. BISH, *The flow of a solid by viscous slip between elastic domains*, Acta Mech., **81**, 39–45, 1990.

3. R.L. BISH, *The flow of a work-hardening solid by inviscid slip between elastic domains*, Acta Mech., **83**, 1–7, 1990.

4. L.E. FARMER and P.L.B. OXLEY, *A slip-line field for plane-strain extrusion of a strain hardening material*, J. Mech. Phys. Solids, **19**, 6, 369–388, 1971.

5. R.L. BISH, *The plane-strain extrusion of a work-hardening solid*, Acta Mech., **85**, 125–130, 1990.

6. W. PRAGER, *Recent developments in the mathematical theory of plasticity*, J. Appl. Phys., **20**, 3, 235–241, 1949.

7. B. SPAIN, *Vector analysis*, D. Van Nostrand, 1965.

8. W. BOAS, *Physics of metals and alloys*, Melbourne University Press, 1947.

9. W.T. KOITER, *Stress-strain relations, uniqueness and variational theorems for elastic-plastic materials with a singular yield surface*, Quart. Appl. Math., **11**, 3, 350–354, 1953.

10. A.R. DOWLING, J. HARDING and J.D. CAMPBELL, *The dynamic punching of metals*, J.I.M., **96**, 215–224, 1970.

11. F. OSMOND, C.H. FREMONT and G. CARTAUD, *Les modes de déformation et de rupture des fers et des aciers doux*, Revue Métall., **1**, 11–45, 1904.

12. I.E. FRENCH and P.F. WEINRICH, *The tensile fracture mechanisms of fcc metals and alloys – a review of the influence of pressure*, J. Aust. Inst. Metals, **22**, 1, 40–50, 1977.

MATERIALS RESEARCH LABORATORY, ASCOT VALE, AUSTRALIA.

Analysis of dynamic shear bands in porous thermally softening viscoplastic materials

R. C. BATRA and X. S. JIN (BLACKSBURG)

WE STUDY THE INITIATION and growth of shear bands in a porous thermally softening viscoplastic block of square cross-section and deformed in plane strain tension. The impact load is modelled by prescribing a time-dependent axial velocity on the top and bottom surfaces which are taken to be free of the tangential tractions. The material defect is modelled by assuming that the material in a small region surrounding the centroid of the cross-section is weaker than the rest of the material. The finite element mesh consisting of constant strain triangular elements is refined adaptively so that the integral of the effective plastic strain-rate over an element is nearly the same for all elements in the mesh. The effects of the presumed variation in the initial porosity and the impact speed on the nominal strain at which a shear band initiates have been examined. For a typical steel alloy, we have also ascertained the effect, on the initiation of the shear band, of the softening caused by the increase in the porosity and/or the increase in the temperature.

1. Introduction

MICROSCOPIC OBSERVATIONS [1–10] of the failure process in several metallic alloys (e.g., AISI 1018 cold-rolled steel, AISI 4340 vacuum arc remelted steel, HY-100 steel, titanium and titanium alloys) have revealed that fracture occurs by a process of nucleation and coalescence of voids and microcracks. Under dynamic loads, the fracture of the specimen is usually preceded by the formation of a shear band [1-6], which is a narrow region, a few micrometers (μm) wide, of intense plastic deformation that forms during high strain-rate processes such as shock loading, ballistic penetration, metal forming, machining, grinding, high speed fabrication, and explosive fragmentation. ZENER and HOLLOMON [11] observed $32\,\mu$m wide shear bands during the punching of a hole in a low carbon steel plate, and postulated that the heat generated due to plastic working made the material softer, and the material became unstable when the thermal softening equalled or exceeded the hardening of the material due to strain and strain-rate effects. Since then, there have been numerous analytical, numerical, and experimental studies aimed at analyzing the initiation and growth of shear bands; the reader is referred to SHAWKI and CLIFTON [12] and BATRA and ZHU [13] for a list of references. Our objective here is to delineate the effect of additional softening caused by the nucleation of voids on the formation of shear bands in a prismatic body made of a thermally softening viscoplastic material and deformed in plane strain tension.

A general theory of elastic materials with voids has been developed by NUNZIATO and COWIN [14] and phenomenological constitutive relations for porous ductile solids have been proposed by KUHN and DOWNEY [15], GREEN [16],

GURSON [17], and SHIMA and OYANE [18]. Gurson's model has been modified
by TVERGAARD [19, 20], TVERGAARD and NEEDLEMAN [21], and PAN *et al.* [22] to
include work hardening, strain-rate hardening and a generalization of the flow
potential. The phenomenon of shear strain localization in porous materials has
been studied by PAN *et al.* [22], SAJE *et al.* [23], KOBAYASHI and DODD [24], and
ZAVALIANGOS and ANAND [25]. Here we study a dynamic two-dimensional prob-
lem and account for the effect of inertia forces and the dependence of the ther-
mophysical properties of the material upon the porosity. Also we use adaptively
refined finite element meshes to analyze the problem. The voids are assumed to
grow due to plastic dilatation, and a plastic strain controlled nucleation criterion
is used to account for the nucleation of voids throughout the deformation history.

2. Formulation of the problem

We assume that voids are randomly distributed throughout the body and de-
note their volume fraction by f. In terms of the referential description, the
thermomechanical deformations of the body are governed by the following equa-
tions:
balance of mass

$$(2.1) \qquad\qquad (\rho J(1 - f))^{\cdot} = 0,$$

balance of linear momentum

$$(2.2) \qquad\qquad \rho_r(1 - f_r) \dot{\mathbf{v}} = \text{Div}\,\mathbf{T},$$

balance of moment of momentum

$$(2.3) \qquad\qquad \mathbf{T}\mathbf{F}^T = \mathbf{F}\mathbf{T}^T,$$

balance of internal energy

$$(2.4) \qquad\qquad \rho_r(1 - f_r)\, \dot{e} = -\text{Div}\,\mathbf{Q} + \text{tr}\left(\mathbf{T}\,\dot{\mathbf{F}}^T\right),$$

where

$$(2.5) \qquad\qquad \mathbf{F} = \text{Grad}\,\mathbf{x}$$

is the deformation gradient, $\mathbf{x}$ is the present position of a material particle that
occupied place $\mathbf{X}$ in the reference configuration, $J = \det\mathbf{F}$, ρ is the present mass
density of the matrix or void-free material, ρ_r its mass density in the reference
configuration, f_r equals the volume fraction of voids in the reference configura-
tion, $\mathbf{v}$ is the velocity of a material particle, $\mathbf{T}$ is the first Piola – Kirchhoff stress
tensor, e is the specific internal energy for the matrix, $\mathbf{Q}$ is the heat flux per

unit undeformed area, a superimposed dot indicates a material time derivative, and Grad and Div signify, respectively, the gradient and the divergence operators applied to a field quantity defined as a function of $\mathbf{X}$ and time t. We have neglected the balance of equilibrated forces considered by NUNZIATO and COWIN [14], and have also assumed that the supplies of linear momentum and internal energy equal zero.

We presume that the strain-rate tensor $\mathbf{D}$, defined by

$$(2.6) \qquad 2\mathbf{D} = \operatorname{grad}\mathbf{v} + (\operatorname{grad}\mathbf{v})^T,$$

with grad denoting the gradient operator applied to a field quantity defined as a function of $\mathbf{x}$ and t, has the additive decomposition into elastic $\mathbf{D}^e$ and plastic $\mathbf{D}^p$ parts, and make the following constitutive assumptions:

$$(2.7) \qquad \dot{\sigma} + \sigma\Omega - \Omega\sigma = \frac{E(1-f)}{(1+\nu)}(\mathbf{D}-\mathbf{D}^p) + \frac{E\nu(1-f)}{(1+\nu)(1-2\nu)}(\operatorname{tr}(\mathbf{D}-\mathbf{D}^p) - \alpha\dot{\theta})\mathbf{1},$$

$$(2.8) \qquad \Phi = \frac{3}{2}\frac{\operatorname{tr}(\mathbf{s}\,\mathbf{s}^T)}{\sigma_m^2} + 2f^*\beta_1\cosh\left(\frac{\beta_2\operatorname{tr}\sigma}{2\sigma_m}\right) - 1 - \beta_1^2 f^{*2} = 0,$$

$$(2.9) \qquad \mathbf{s} = \sigma - \frac{1}{3}(\operatorname{tr}\sigma)\mathbf{1},$$

$$(2.10) \qquad \mathbf{D}^p = \frac{(1-f)\sigma_m\,\dot{\varepsilon}_m^p}{\operatorname{tr}(\sigma\mathbf{N}^T)}\mathbf{N},$$

$$(2.11) \qquad \mathbf{N} = \frac{3}{\sigma_m^2}\left(\sigma - \frac{1}{3}(\operatorname{tr}\sigma)\mathbf{1}\right) + \frac{f^*\beta_1\beta_2}{\sigma_m}\left[\sinh\left(\frac{\beta_2\operatorname{tr}\sigma}{2\sigma_m}\right)\right]\mathbf{1},$$

$$(2.12) \qquad f^* = \begin{cases} f & \text{if } f \le f_c, \\ f_c + \left(\dfrac{f_u^* - f_c}{f_f - f_c}\right)(f - f_c) & \text{otherwise}. \end{cases}$$

$$(2.13) \qquad \sigma_m = \sigma_0\left(1 + b\,\dot{\varepsilon}_m^p\right)^m\left(1 + \frac{\varepsilon_m^p}{\varepsilon_y}\right)^n(1 - \nu_s\theta).$$

$$(2.14) \qquad \dot{f} = (1-f)\operatorname{tr}\mathbf{D}^p + \frac{f_2\,\dot{\varepsilon}_m^p}{s_2\sqrt{2\pi}}\exp\left(-\frac{1}{2}\left(\frac{\varepsilon_m^p - \epsilon_N}{s_2}\right)^2\right),$$

$$(2.15) \qquad \mathbf{q} = -k\left(1 - \frac{3}{2}f\right)\operatorname{grad}\theta,$$

$$(2.16) \qquad \dot{e} = c\,\dot{\theta} + \operatorname{tr}(\sigma(\mathbf{D} - \mathbf{D}^p)).$$

where

(2.17) $\mathbf{T} = J\boldsymbol{\sigma}\left(\mathbf{F}^{-1}\right)^{T}$,

(2.18) $\mathbf{Q} = J\mathbf{F}^{-1}\mathbf{q}$,

(2.19) $2\boldsymbol{\Omega} = \text{grad}\,\mathbf{v} - (\text{grad}\,\mathbf{v})^{T}$.

Equation (2.7) is Hooke's law written in the rate form with the left-hand side equal to the Jaumann derivative of the Cauchy stress tensor $\boldsymbol{\sigma}$, $\boldsymbol{\Omega}$ defined by Eq. (2.19) is the skew-symmetric part of the velocity gradient, E, ν, and α, respectively, are Young's modulus, Poisson's ratio, and the coefficient of thermal expansion for the matrix material, and $\mathbf{1}$ is the unit tensor. We have included the factor $(1 - f)$ on the right-hand side of the constitutive relation (2.7) to account for the porosity of the material; this was also considered by PASSMAN and BATRA [26] and KOBAYASHI and DODD [24]. BUDIANSKY [27] has given the dependence of the material parameters upon f for a macroscopically isotropic composite consisting of a random dispersion of roughly spherical voids in a matrix material. These relations are more involved than the simple reduction of E by the factor $(1 - f)$ we have used in Eq. (2.7). Equations (2.10) and (2.11) follow from the plastic yield function (2.8) proposed by Gurson and subsequently modified by Tvergaard, and the assumptions that $\mathbf{D}^{p}$ is directed along the outward normal $\mathbf{N}$ to the yield function Φ, and the plastic working $\text{tr}\,(\boldsymbol{\sigma}\mathbf{D}^{p})$ equals $(1 - f)\sigma_{m}\,\dot{\varepsilon}_{m}^{p}$ with σ_{m} and $\dot{\varepsilon}_{m}^{p}$ denoting the effective stress and the equivalent plastic strain-rate in the matrix material. The expressions (2.12) for f^{*} were given by TVERGAARD and NEEDLEMAN [21] so that the computed results matched well the test findings for the cup-cone fracture in a round tensile bar. They suggest the values $f_{c} \approx 0.15$ and $f_{f} \approx 0.25$. As $f - f_{f}$, $f^{*} - f_{u}^{*}$, and the material loses all stress-carrying capacity. In Eq. (2.8), β_{1} and β_{2} are material parameters and $\mathbf{s}$ is the deviatoric Cauchy stress tensor.

Equation (2.13) relating the effective stress σ_{m} in the matrix to the equivalent plastic strain, equivalent plastic strain-rate, and the temperature is a generalization, due to BATRA [28], to the three-dimensional state of deformation of that proposed by LITOŃSKI [29] for the simple shearing problem. In that equation, σ_{0} equals the yield stress of the matrix material in a quasistatic simple compression test, the parameters b and m characterize strain-rate sensitivity of the material, ε_{y} and n the strain-hardening, and ν_{s} the thermal softening of the matrix material. The first term on the right-hand side of Eq. (2.14) describes the growth of voids due to plastic dilatation, and the second term describes the plastic strain-controlled nucleation of voids. CHU and NEEDLEMAN [30] suggested this form by assuming that void nucleation follows a normal distribution about some mean critical plastic strain. In Eq. (2.14), s_{2} is the standard deviation of the normal distribution, f_{2} equals the volume fraction of voids that would be nucleated if deformation continued infinitely, and e_{N} equals the strain at which the void

nucleation rate reaches a maximum. The experimental studies of LEROY [31] and
FISHER [32] on spheroidized carbon steel indicate that, at least in these materials,
a void perfusion strain can be identified at which the rate of nucleation is maxi-
mal. The void perfusion strain can be taken as e_N. Here we have not considered
the stress-controlled nucleation of voids. Equation (2.15) is the Fourier law of
heat conduction with **q** denoting the heat flux per unit deformed area, and k – the
thermal conductivity of the matrix. That the thermal conductivity of the porous
materials equals $(1 - 3/2\ f)$ times that of the matrix material is due to BUDIANSKY
[27]. In the constitutive relation (2.16) for the rate of change of internal energy,
c is the specific heat for the matrix. Nearly all of the thermophysical material pa-
rameters depend upon the temperature. However, such dependences have been
neglected for the sake of simplicity.

For a prismatic body of square cross-section, shown in Fig. 1, deformed in
plane strain tension, we presume that the deformations are symmetric about the
two centroidal axes – and study deformations of the material in the first quad-
rant. Due to the presumed symmetry of deformations, the normal component
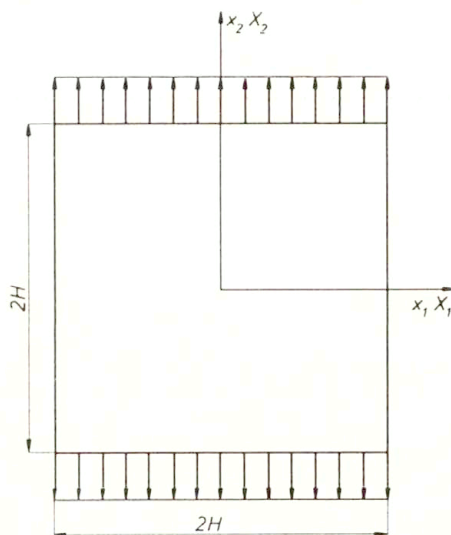
FIG. 1. A schematic sketch of the problem studied.

of velocity and tangential tractions are taken to vanish on the left-hand vertical
and bottom horizontal surfaces, the right-hand vertical surface is taken to be
traction-free, and on the top horizontal surface, zero tangential tractions and a
normal component of velocity, given below, are prescribed;

$$v_2(X_1, H, t) = v_0 t/t_r, \qquad 0 \leq t \leq t_r,$$

(2.20)

$$= v_0, \qquad t \geq t_r.$$

Thus the assigned axial speed on the top surface increases linearly from zero to

the steady value v_0 in time t_r giving an eventual nominal strain-rate of v_0/H. All the bounding surfaces of the block are taken to be thermally insulated.

Initially the block is assumed to be at rest, stress-free and at a uniform temperature θ_0. However, the initial porosity is taken to be non-uniform and given by

(2.21)
$$f(X_1, X_2, 0) = f_0 + \varepsilon(1 - r^2)^9 e^{-5r^2},$$
$$r^2 = (X_1^2 + X_2^2)/H^2.$$

The second term on the right-hand side of Eq. (2.21)$_1$ models a material defect or inhomogeneity, the value of ε is a measure of the strength of the defect.

The aforestated coupled and nonlinear partial differential equations (2.1) through (2.19) under the prescribed initial and boundary conditions are too difficult to be analyzed analytically. Therefore, we seek their numerical solution.

3. Computational considerations

In order to solve the problem numerically, we first rewrite Eq. (2.13) as

(3.1)
$$\dot{\varepsilon}_m^p = \max\left[0, \frac{1}{b}\left(\left(\frac{\sigma_m}{\sigma_0\left(\left(1 + \frac{\varepsilon_m^p}{\varepsilon_y}\right)^n (1 - \nu_s\theta)\right)}\right)^{\frac{1}{m}} - 1\right)\right].$$

Thus the equivalent plastic strain-rate is positive only when

(3.2)
$$\sigma_m > \sigma_0\left(1 + \frac{\varepsilon_m^p}{\varepsilon_y}\right)^n (1 - \nu_s\theta).$$

otherwise it equals zero implying thereby that all components of plastic strain-rate tensor at the material point under consideration and at that instant vanish identically. The value of σ_m is computed from the yield function (2.8) once $\boldsymbol{\sigma}$ or $\mathbf{s}$ has been found.

By substituting from the constitutive relations into the balance laws, we obtain evolution equations for ρ, $\mathbf{v}$ and θ which, when combined with Eqs. (2.7), (2.14) and (3.2), give a system of equations for the determination of ρ, $\mathbf{v}$, θ, $\boldsymbol{\sigma}$, f and ε_m^p at a material point and at any instant of time. We obtain a semidiscrete formulation of the problem by using the Galerkin method which results in a set of coupled and nonlinear ordinary differential equations. We employed the lumped mass matrix obtained by using the row sum technique, and evaluated various integrals over an element by using the 3-point quadrature rule. At each node

point in the mesh we have 9 unknowns, namely, ρ, $\mathbf{v}$, θ, $\boldsymbol{\sigma}$, f and ε_m^p. Thus the number of ordinary differential equations equals 9 times the number of nodes. These are integrated with respect to time t by using the subroutine LSODE incuded in the package ODEPACK. In LSODE, variables ATOL and RTOL that control the absolute and relative errors in the solution vector were each set equal to 10^{-6}. The initial discretization of the domain consisted of uniform 3-noded triangular elements, but subsequent meshes were refined adaptively with the area of the element generated being inversely proportional to the value of $\dot{\varepsilon}_m^p$ at its centroid. Thus the mesh generated had fine elements within the severely deforming region and coarse elements elsewhere. The finite element mesh was refined whenever the porosity at the block centroid increased by a preassigned amount, and the computations were stopped when the porosity at any point in the domain reached the critical value f_f. Depending upon the initial distribution of f, at most six mesh refinements had to be performed. The values of solution variables ρ, $\mathbf{v}$, θ, $\boldsymbol{\sigma}$, f and ε_m^p at the newly created nodes were computed by first ascertaining to which element in the old mesh they belonged, and then by using the interpolation method to find values at the newly generated nodes.

4. Numerical results and discussion

When computing numerical results, we assigned following values to various geometric and material parameters:

$$
\begin{aligned}
\sigma_0 &= 333\,\text{MPa}, \quad E = 210\,\text{GPa}, \quad \nu = 0.27, \quad \nu_s = 6.67 \times 10^{-4}/°\text{C}, \\
\rho_r &= 7800\,\text{kg/m}^3, \quad k = 49.2\,\text{W/m}°\text{C}, \quad c = 473\,\text{J/kg}°\text{C}, \\
b &= 10000\,\text{s}, \quad m = 0.025, \quad n = 0.02, \quad f_2 = 0.04, \quad s_2 = 0.1, \\
e_N &= 0.5, \quad \varepsilon_y = 0.017, \quad \beta_1 = 1.5, \quad \beta_2 = 1.0, \quad f_c = 0.15, \\
f_f &= 0.35, \quad f_u^* = \frac{2}{3}, \quad H = 5\,\text{mm}, \quad t_r = 0.005H/v_0.
\end{aligned}
$$
(4.1)

The aforestated values assigned to different material parameters are for a typical steel. The value of ν_s equals the reciprocal of the melting temperature, taken here to be 1500°C, of steel. For $v_0 = 25\,\text{m/s}$, the nominal strain-rate equals $5000\,\text{s}^{-1}$ and the rise time for the axial speed at the top surface to reach its steady value equals one µs.

Figure 2 depicts the effect of initial porosity distribution upon the load-displacement curve for a defect-free homogeneous specimen. The ordinate is the total axial force required to pull the specimen, and the abscissa is the average strain. In this case the deformations of the body stayed homogeneous, thus no mesh refinement was carried out. The plotted results are for a fixed mesh of 1600 uniform constant strain triangular elements. These results evince that higher values of the initial porosity facilitate plastic deformations of the body, thereby

making the system more dissipative, and oscillations in the applied load die out quicker. Subsequent to the initial peak in the load, the average load keeps on decreasing with increasing axial strain because of the softening induced due to the rise in the values of the porosity and the temperature of the body.
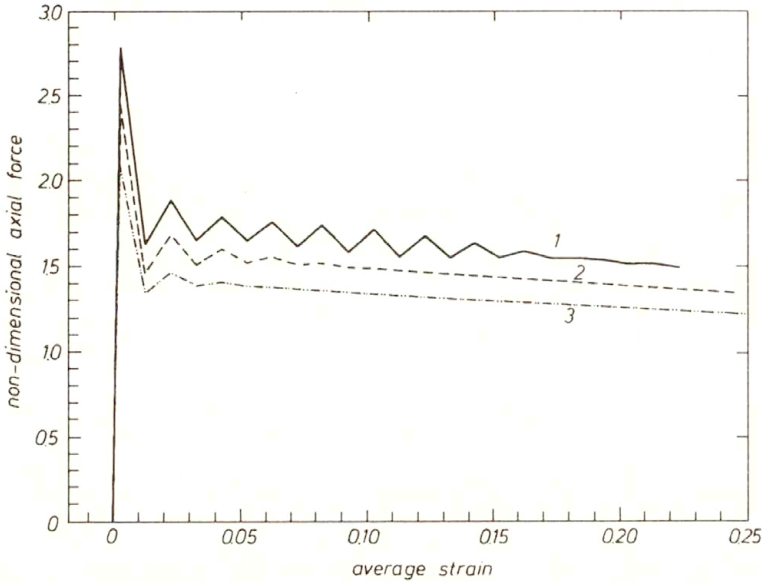

FIG. 2. Axial load vs. time for homogeneous deformations of the body at a nominal strain-rate of $5000\,\text{s}^{-1}$ and for three distributions of the initial porosity. *1* – initial porosity = 0.00, *2* – initial porosity = 0.05, *3* – initial porosity = 0.10.

4.1. Effect of nominal strain-rate and initial porosity distribution

In Fig. 3 we have plotted the history of the axial load required to pull the bar at a speed of either 5 m/s or 25 m/s and for three values of the initial porosity. In each case the initial porosity f is nonuniform with the highest value of f occurring at the block centroid, and it quickly decreases to the uniform value at a small distance from the block centroid. We attribute the oscillations of higher amplitude and longer duration at $v_0 = 25$ m/s to the predominance of inertia effects. At the lower value 5 m/s of v_0, after the initial rise in the load because of the increase in the axial speed, the load decreases gradually for each one of the three values of the initial porosity distribution. We note that for a nonporous thermoviscoplastic material Batra [33] pointed out that inertia forces start playing a noticeable role at a nominal strain-rate of $5000\,\text{s}^{-1}$. Just when the axial load began to drop suddenly, the value of f at a node point adjacent to the block centroid reached f_f and the computations were stopped. Because of this we do not see in plots of Fig. 3 the precipitous drop in the load usually associated with the initiation of the localization of the deformation. As will be shown below, the deformation does localize in a narrow band.
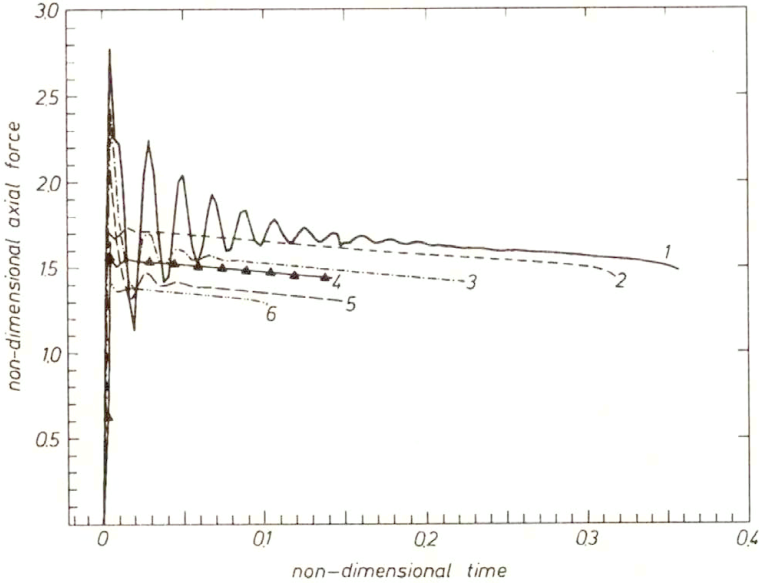
FIG. 3. Axial load vs. time for three distributions of the initial porosity and at nominal strain-rates of $500\,\mathrm{s}^{-1}$ and $5000\,\mathrm{s}^{-1}$.

$$
\begin{aligned}
&1 - \quad f = 0.025(1 - r^2)^9 \exp(-5r^2), && v_0 = 25\ \mathrm{m/s}, \\
&2 - \quad f = 0.025(1 - r^2)^9 \exp(-5r^2), && v_0 = 5\ \mathrm{m/s}, \\
&3 - \quad f = 0.05 + 0.025(1 - r^2)^9 \exp(-5r^2), && v_0 = 25\ \mathrm{m/s}, \\
&4 - \quad f = 0.05 + 0.025(1 - r^2)^9 \exp(-5r^2), && v_0 = 5\ \mathrm{m/s}, \\
&5 - \quad f = 0.1 + 0.025(1 - r^2)^9 \exp(-5r^2), && v_0 = 25\ \mathrm{m/s}, \\
&6 - \quad f = 0.1 + 0.025(1 - r^2)^9 \exp(-5r^2), && v_0 = 5\ \mathrm{m/s}.
\end{aligned}
$$

Figures 4a, 4b and 4c show, respectively, the evolution of the effective plastic strain, temperature, and porosity at the block centroid for the three different distributions of the initial porosity and two values of the axial speed. Each one of these three variables essentially evolves gradually first, and the rate of increase of these quantities picks up substantially once the deformation has begun to localize. For the same value of $f(\mathbf{x}, 0)$, the increase in the nominal strain-rate from $500\,s^{-1}$ to $5000\,s^{-1}$ delays the initiation of the localization of the deformation, primarily due to the effect of inertia forces. For a given strain-rate of $500\,s^{-1}$ or $5000\,s^{-1}$, an increase in the value of $f(\mathbf{x}, 0)$ causes the localization of the deformation to occur earlier. This is because a more porous material undergoes plastic deformation at a lower value of σ_m, thus facilitating the growth and nucleation of voids and also causing the material to heat up sooner, both of which enhance further its plastic deformations. Hence it is a self-feeding mechanism.

In order to illustrate that the deformation does localize and to depict how the finite element meshes adapt to the deformations, we show below results for the case of

$$(4.2) \qquad f(\mathbf{x}, 0) = 0.025(1 - r^2)^9 \exp(-5r^2), \qquad v_0 = 25\ \mathrm{m/s}.$$
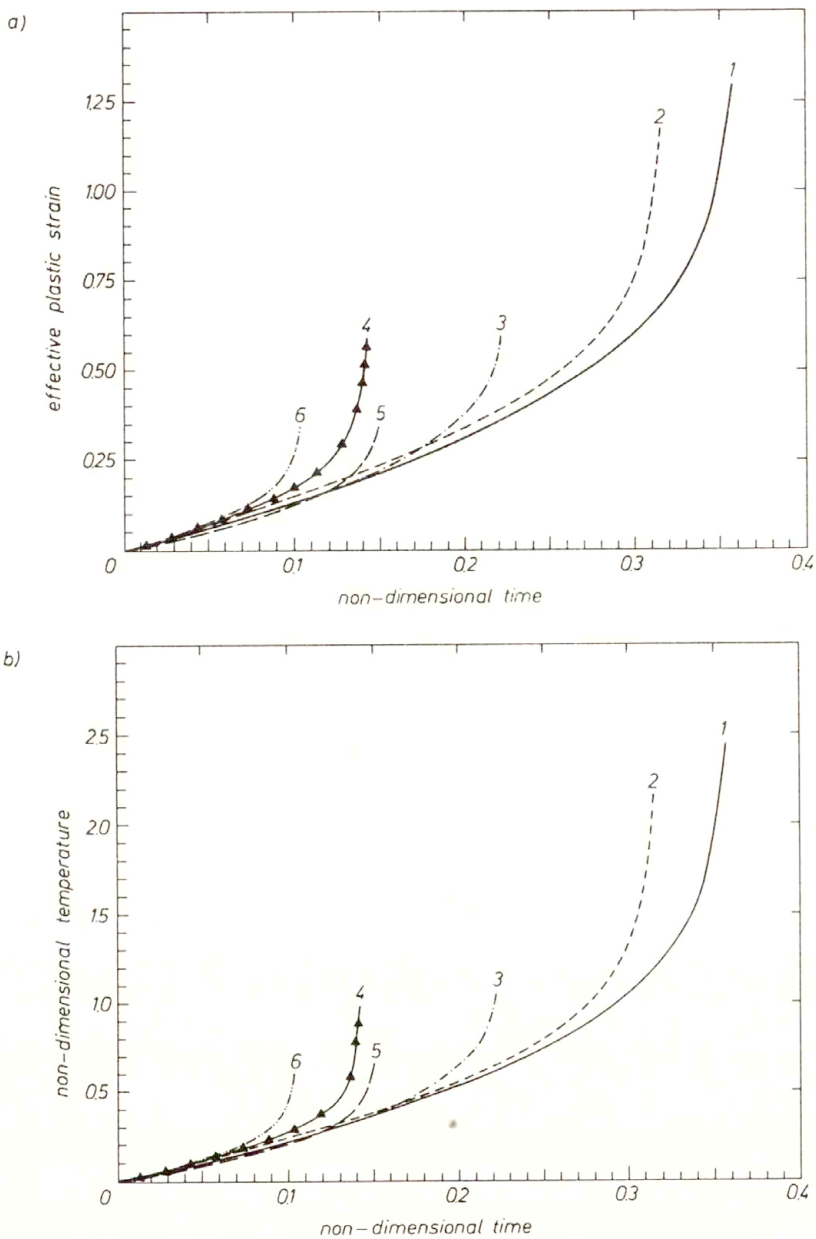
FIG. 4. Evolution at the block centroid of (a) the effective plastic strain, (b) the temperature for three distributions of the initial porosity and at nominal strain-rates of $500 \, \text{s}^{-1}$ and $5000 \, \text{s}^{-1}$.

$$1 - \quad f = 0.025(1 - r^2)^9 \exp(-5r^2), \qquad v_0 = 25 \, \text{m/s},$$
$$2 - \quad f = 0.025(1 - r^2)^9 \exp(-5r^2), \qquad v_0 = 5 \, \text{m/s},$$
$$3 - \quad f = 0.05 + 0.025(1 - r^2)^9 \exp(-5r^2), \qquad v_0 = 25 \, \text{m/s},$$
$$4 - \quad f = 0.05 + 0.025(1 - r^2)^9 \exp(-5r^2), \qquad v_0 = 5 \, \text{m/s},$$
$$5 - \quad f = 0.1 + 0.025(1 - r^2)^9 \exp(-5r^2), \qquad v_0 = 25 \, \text{m/s},$$
$$6 - \quad f = 0.1 + 0.025(1 - r^2)^9 \exp(-5r^2), \qquad v_0 = 5 \, \text{m/s}.$$

[22]
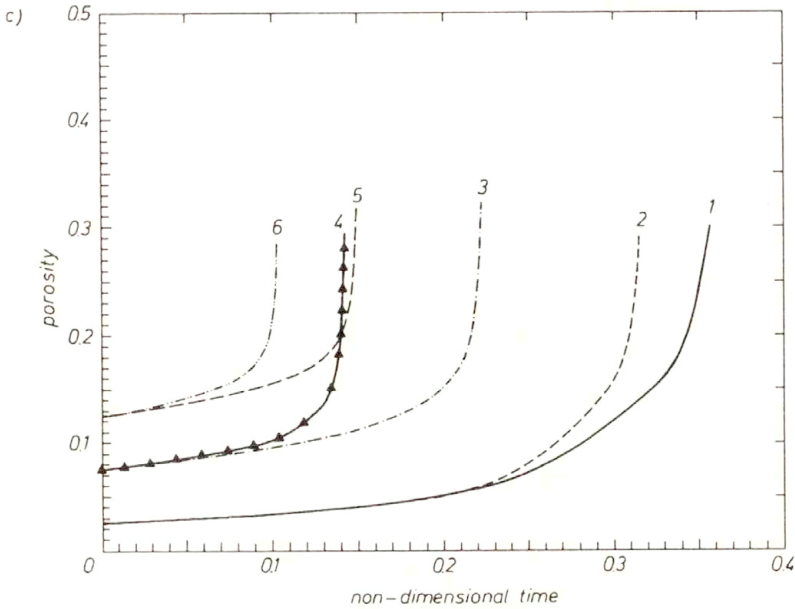
FIG. 4 [cont.]. Evolution at the block centroid of (c) the porosity for three distributions of the initial porosity and at nominal strain-rates of $500\,\mathrm{s}^{-1}$ and $5000\,\mathrm{s}^{-1}$.

$$
\begin{aligned}
&1 - \quad f = 0.025(1 - r^2)^9 \exp(-5r^2), && v_0 = 25\ \mathrm{m/s},\\
&2 - \quad f = 0.025(1 - r^2)^9 \exp(-5r^2), && v_0 = 5\ \mathrm{m/s},\\
&3 - \quad f = 0.05 + 0.025(1 - r^2)^9 \exp(-5r^2), && v_0 = 25\ \mathrm{m/s},\\
&4 - \quad f = 0.05 + 0.025(1 - r^2)^9 \exp(-5r^2), && v_0 = 5\ \mathrm{m/s},\\
&5 - \quad f = 0.1 + 0.025(1 - r^2)^9 \exp(-5r^2), && v_0 = 25\ \mathrm{m/s},\\
&6 - \quad f = 0.1 + 0.025(1 - r^2)^9 \exp(-5r^2), && v_0 = 5\ \mathrm{m/s}.
\end{aligned}
$$

Figures 5a, 5b, 5c and 5d show the finite element meshes generated at non-dimensional times $t = 0.198$, 0.285, 0.339 and 0.357. We note that the initial mesh consisted of 1600 uniform triangular elements. The finite element mesh was refined whenever the porosity f at the block centroid had increased by 0.025, a criterion chosen somewhat arbitrarily. The mesh was refined by using the code developed by BATRA and KO [34] which generates meshes such that the area of an element is inversely proportional to the value of a deformation-rate measure, here taken to be $\dot{\varepsilon}_m$, at the element centroid. It is clear then that a narrow region of the material is deforming severely at times $t = 0.339$ and 0.357. As stated earlier, computations were stopped when the porosity at any point in the deforming region reached the critical value f_f. This implies failure of the material at a point which does not necessarily result in the instantaneous failure of the block. Figures 6a, 6b, 6c and 6d evince the distribution of the velocity within the deforming region at the aforestated four values of the non-dimensional time t. Initially, because of the lateral motion of the block, the velocity component in the horizontal direction has a significant value everywhere. However, once the deformation has started to localize, the body is essentially divided into three
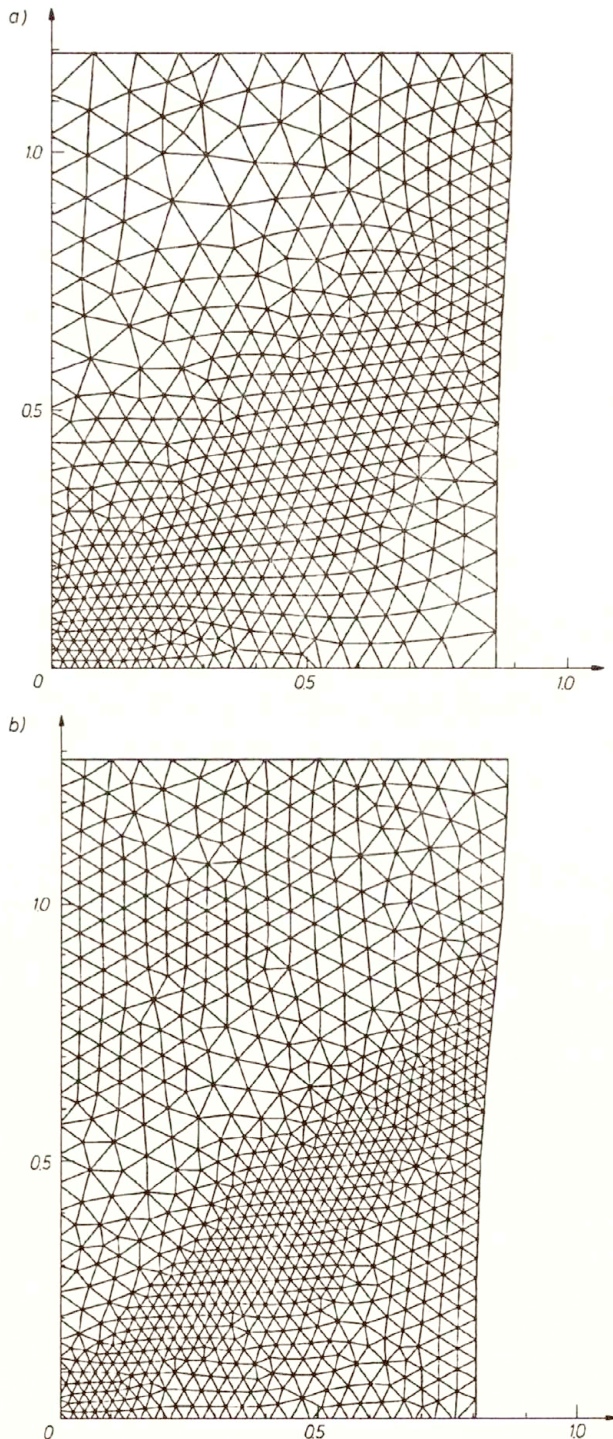
FIG. 5. Adaptively refined meshes at non-dimensional times (a) $t = 0.198$, (b) $t = 0.285$.
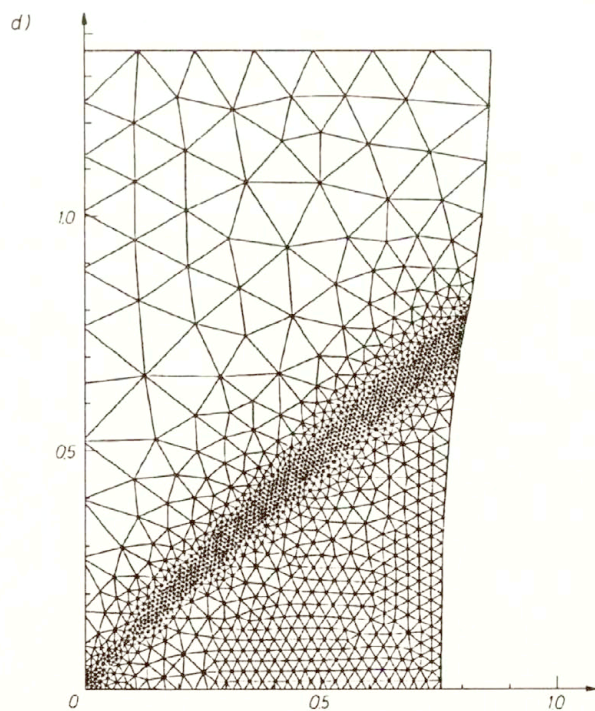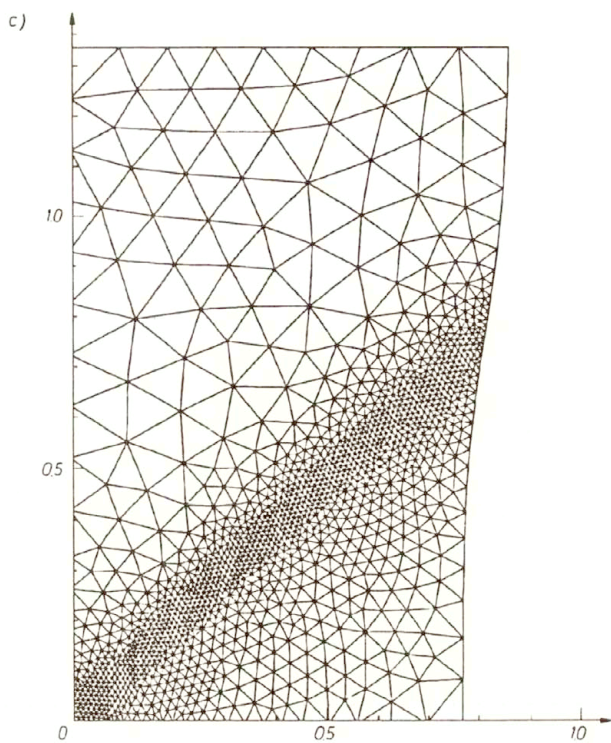
FIG. 5 [cont.]. Adaptively refined meshes at non-dimensional times (c) $t = 0.339$ and (d) $t = 0.357$.

[25]
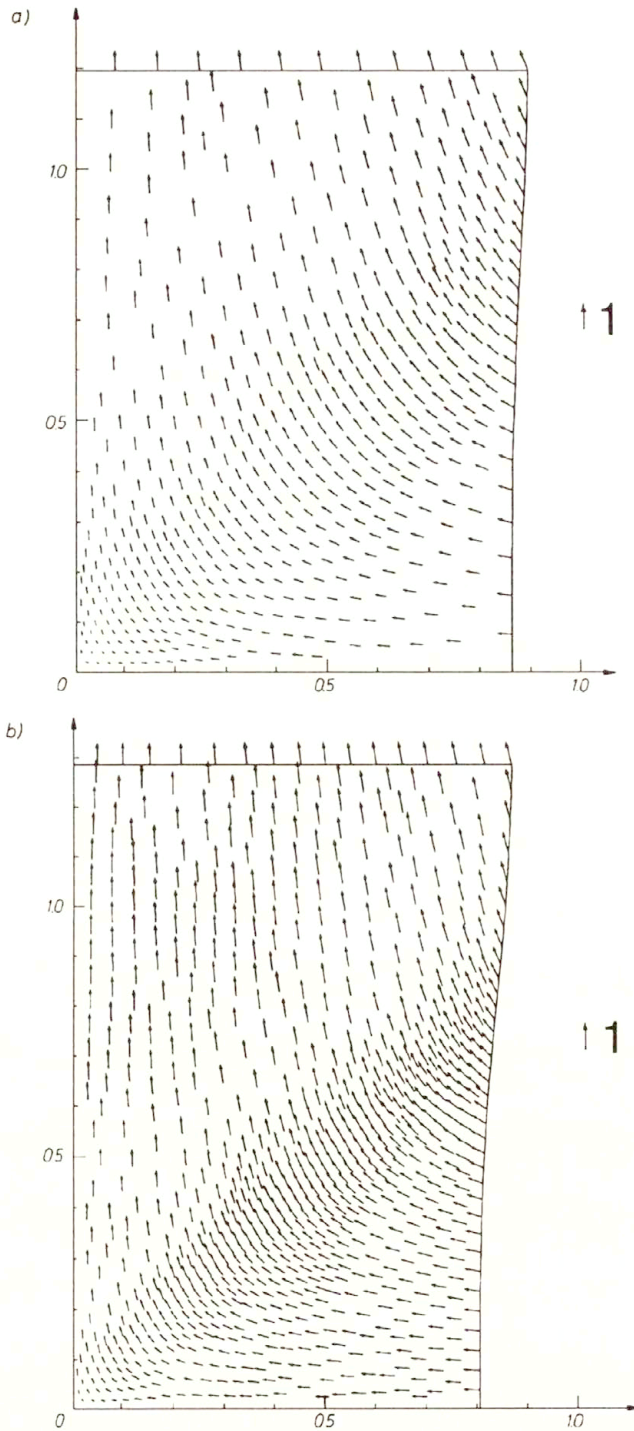
FIG. 6. Velocity distribution in the deforming region at non-dimensional times (a) $t = 0.198$, (b) $t = 0.285$.
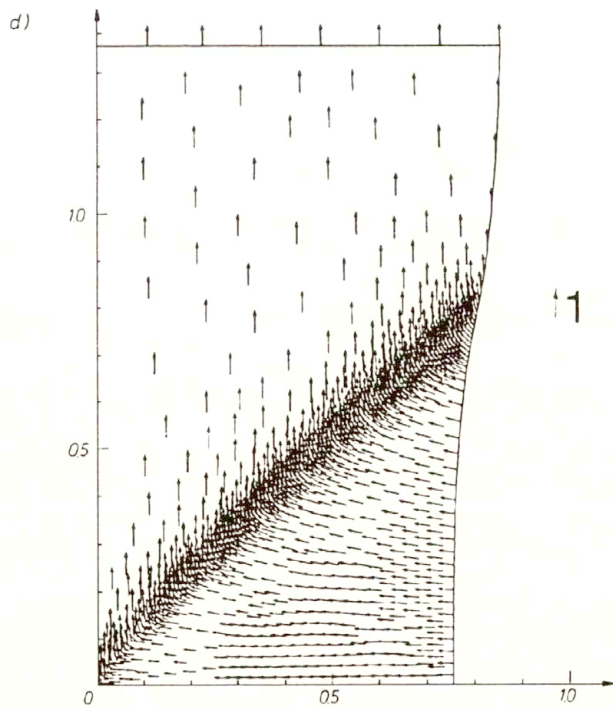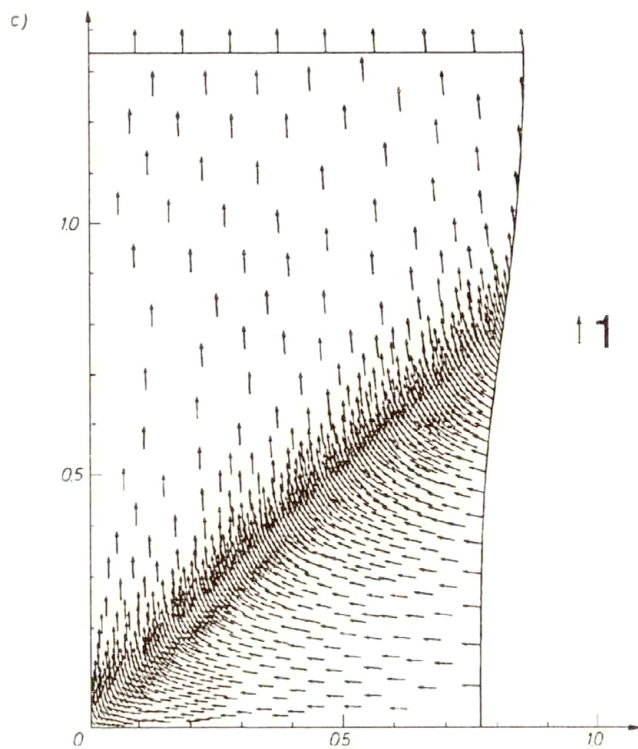
FIG. 6 [cont.] Velocity distribution in the deforming region at non-dimensional times (c) $t = 0.339$ and (d) $t = 0.357$.
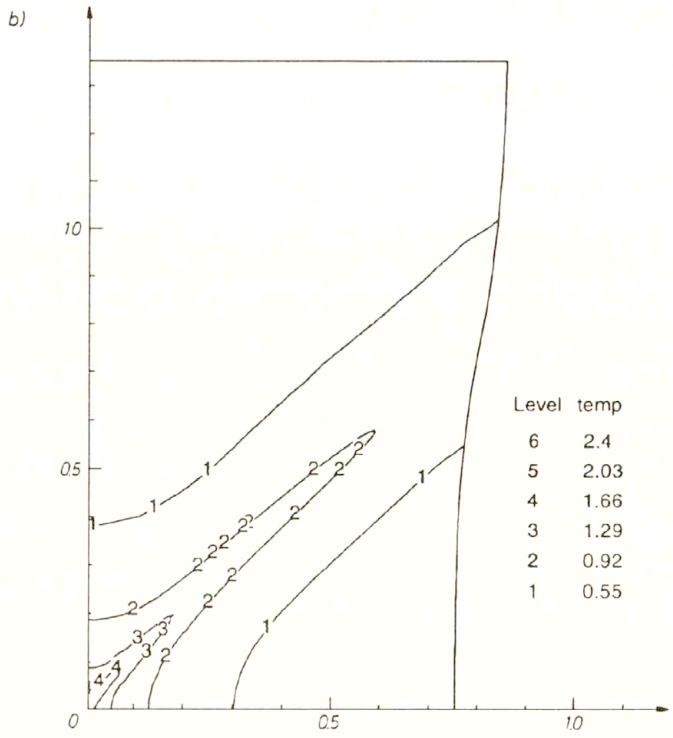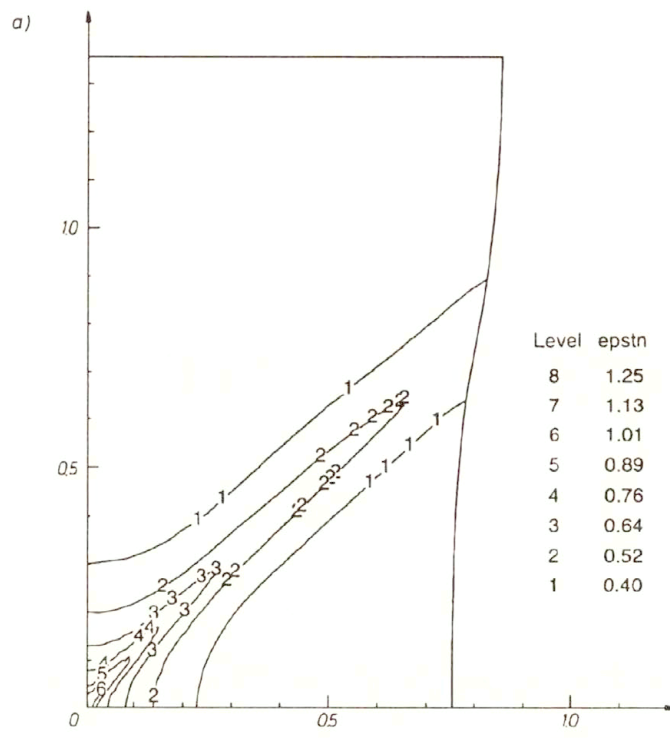
FIG. 7. Contours of (a) the effective plastic strain and (b) the temperature.

[28]
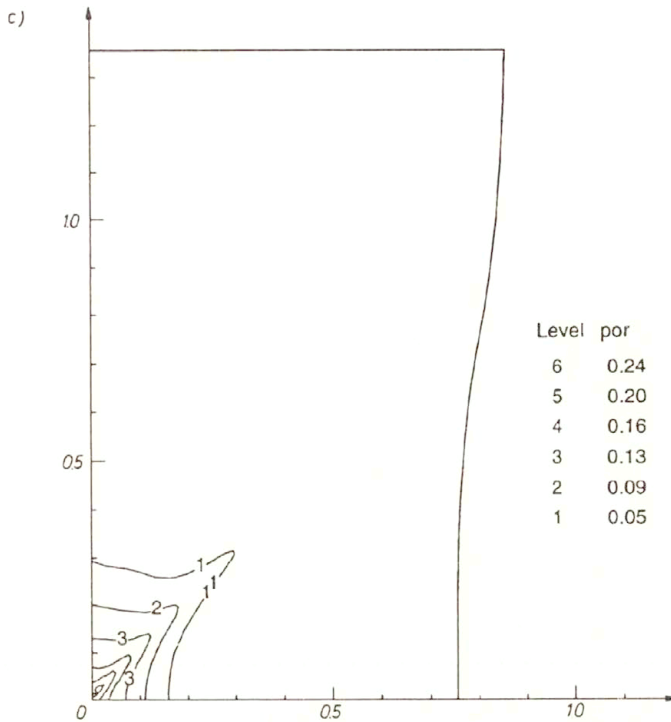
FIG. 7 [cont.]. Contours of (c) the porosity at non-dimensional time $t = 0.357$.

regions. In the region above the shear band, the material particles are moving nearly vertically, and those below the band – horizontally. Within the band, the velocity changes direction sharply.

Contours of the effective plastic strain (epstn), temperature rise, and the porosity within the deforming region at time $t = 0.357$ are shown in Figs. 7a, 7b, and 7c. It is clear that the strain near the block centroid is quite high. However, the temperature rise there is only $2.4 \times 89.8 = 216°C$, and the porosity has increased significantly only in a very narrow region surrounding the block center.

4.2. Effect of strain-induced void nucleation

In order to present the effect of the softening caused by the plastic strain-controlled nucleation of voids, we have plotted in Fig. 8 the evolution of the applied axial force at the top surface and that of temperature, effective plastic strain and porosity at the block centroid for the two cases: (i) $f_2 = 0$, and (ii) $f_2 = 0.04$. It is apparent that the consideration of strain-induced void nucleation enhances the onset of the localization of the deformation, as shown by the sharp rise in the rate of increase of the temperature, effective plastic strain and the porosity at the block centroid.

a)

non-dimensional axial force

non-dimensional time

b)

effective plastic strain

non-dimensional time
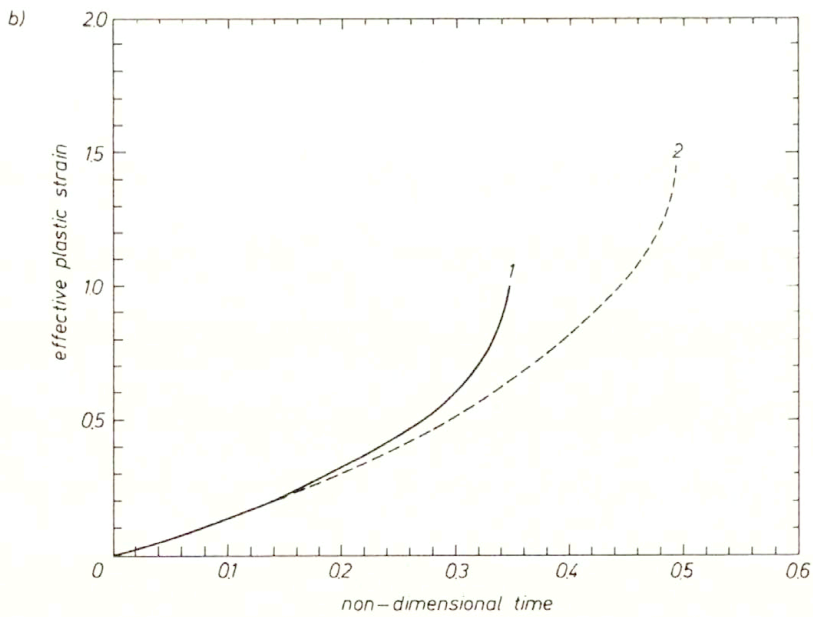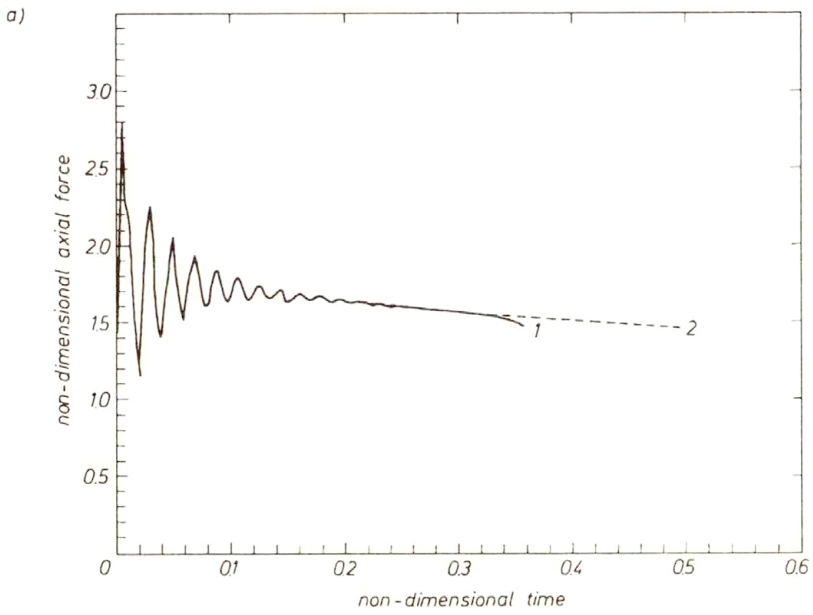
[FIG. 8 a,b]

1 – with strain-induced void nucleation, *2* – without strain-induced void nucleation.

[30]

FIG. 8. (a) Variation of the non-dimensional applied axial force with non-dimensional time, both with and without strain-induced void nucleation; (b,c,d) evolution at the block centroid of the effective plastic strain, the temperature, and the porosity with and without strain-induced void nucleation. *1* – with strain-induced void nucleation, *2* – without strain-induced void nucleation.

[31]

4.3. Thermal softening vs. softening due to porosity change

For the choice (4.1) of parameters we assessed the effect of softening caused by the rise in temperature versus that induced due to the increase in porosity by performing two sets of calculations, one with $\nu_s = 0$ and the other with $f(\mathbf{x}, t) \equiv 0$. The material defect for these computations was modelled by assuming that the yield stress $\hat{\sigma}_0$ in a quasistatic simple compression test of material particles in a small region around the block centroid was given by

$$\hat{\sigma}_0(\mathbf{X}) = \sigma_0 \left(1 - 0.1(1 - r^2)^9 e^{-5r^2}\right), \qquad r^2 \equiv (X_1^2 + X_2^2)/H^2 \leq 1,$$
$$= \sigma_0, \qquad r \geq 1.$$

In Fig. 9, we have plotted the evolution of the applied axial force, and that of the effective plastic strain and the temperature rise at the block centroid for the two cases with $v_0 = 25$ m/s. It is clear that for the parameters considered herein, the softening due to the increase in porosity is considerably higher than that caused by the rise in the temperature. Whereas a shear band initiates, as indicated by the rise in the rate of increase of the effective plastic strain and of the temperature at the block centroid at non-dimensional time $t \simeq 0.5$ when softening is caused by the change in porosity, no shear band forms till a non-dimensional time of 0.5 when the softening is induced by the temperature rise, since both the effective plastic strain and the temperature at the block centroid increase
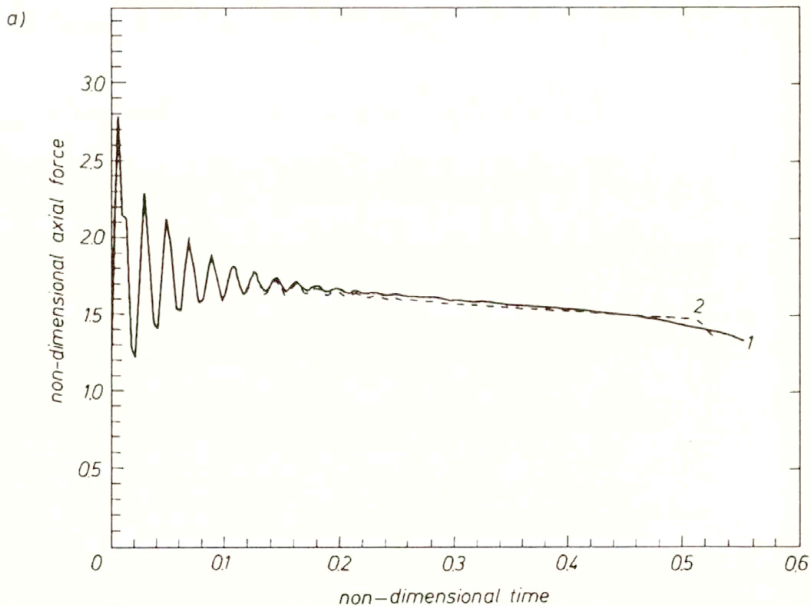
[Fig. 9 a]

1 – no thermal softening, *2* – thermal softening only.
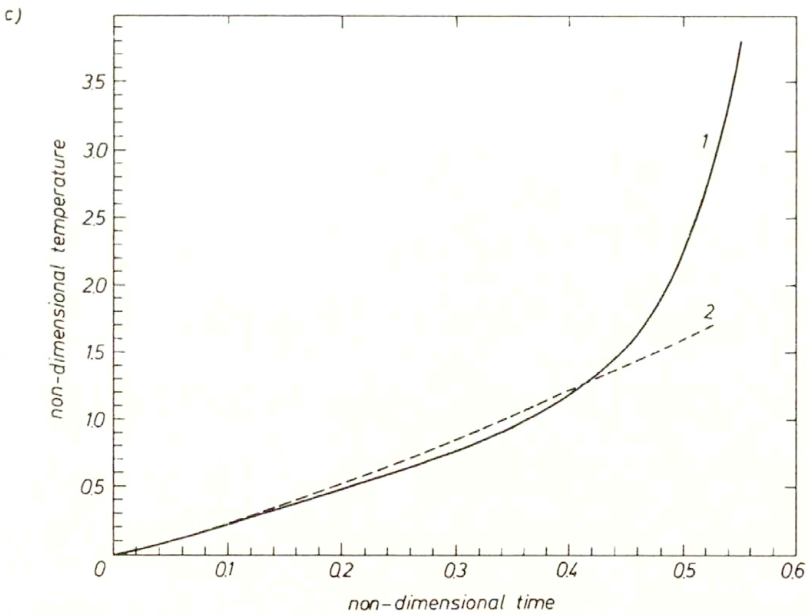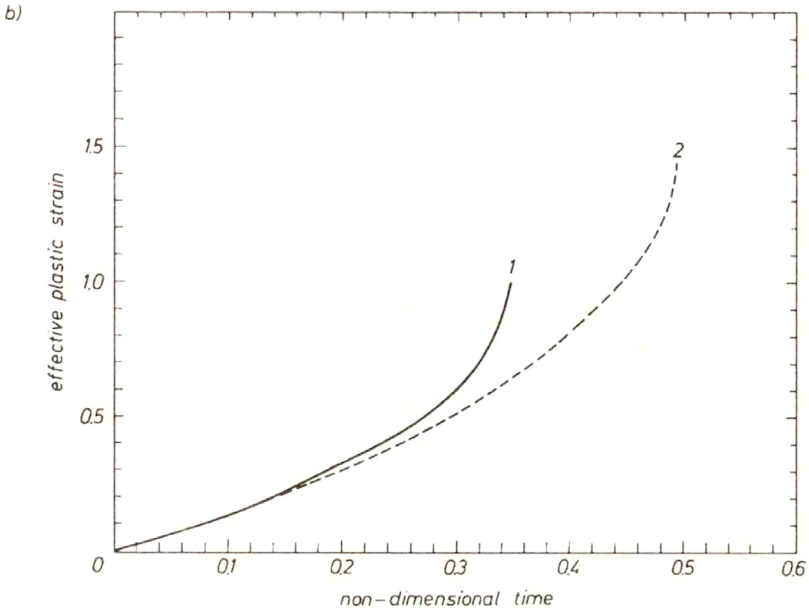
FIG. 9. Variation of (a) the non-dimensional applied axial force vs. non-dimensional time, (b) the effective plastic strain at the block centroid vs. time, 1 – with strain-induced void nucleation, 2 – without strain-induced void nucleation and (c) the temperat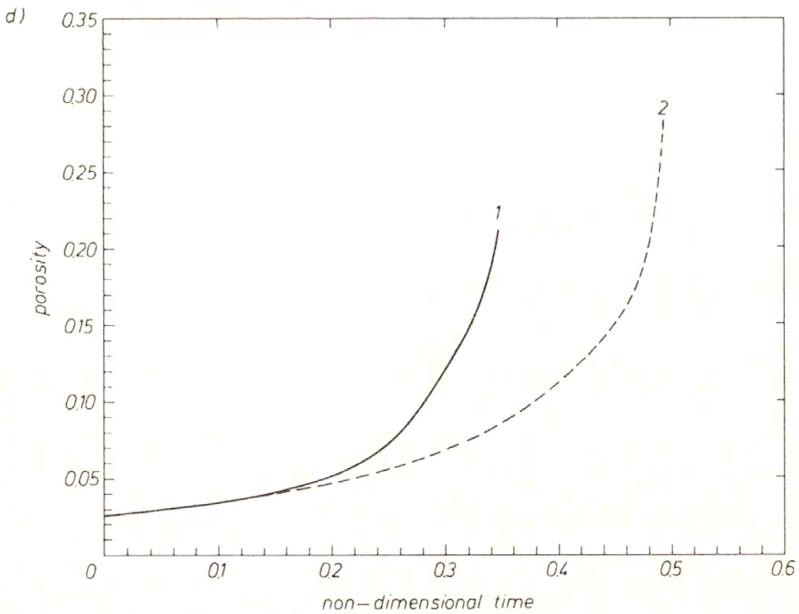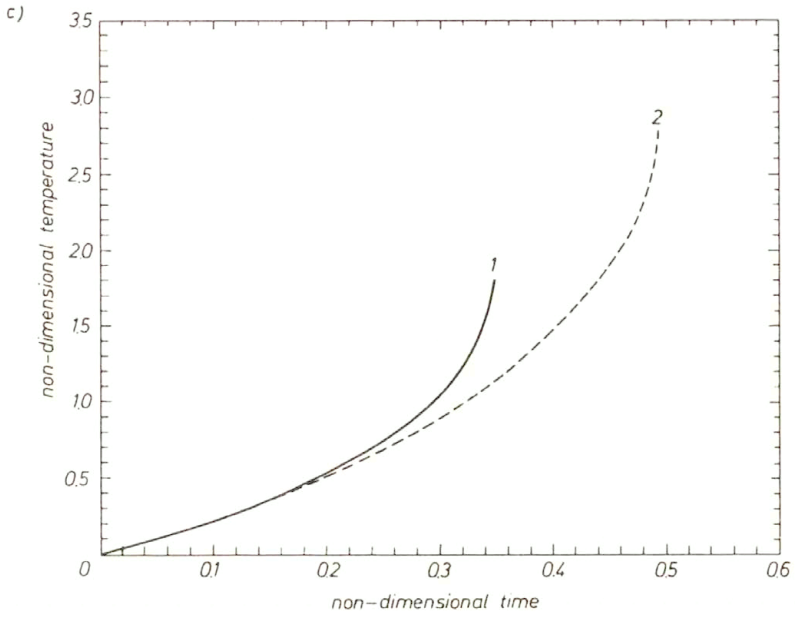ure at the block centroid vs. time, both with and without thermal softening effects considered, 1 – no thermal softening, 2 – thermal softening only.

[33]

essentially linearly with time. It is possible that a band will initiate at a later time. Thus for the values of material parameters chosen for this study, softening caused by the growth and nucleation of voids is stronger than that induced by the temperature rise.

5. Conclusions

We have studied dynamic finite plane strain thermomechanical deformations of a porous viscoplastic body deformed in tension. The material is modelled by the Gurson – Tvergaard – Needleman yield function with the flow stress for the matrix material given by a relation similar to that proposed by Batra [28]. When the dependence of material parameters upon the porosity is considered, they are assumed to be independent of temperature. The problem formulation includes the effect of inertia forces and heat conduction.

The coupled nonlinear partial differential equations governing the deformations of the body are reduced to a set of coupled nonlinear ordinary differential equations by using the Galerkin method. These are integrated with respect to time t by using the IMSL subroutine LSODE. The finite element mesh has been refined adaptively.

It is found that inertia forces play a dominant role at a nominal strain-rate $\dot{\gamma}_{avg}$ of $5000\,s^{-1}$, but a negligible role when $\dot{\gamma}_{avg} = 1000\,s^{-1}$. An increase in the initial value of the porosity makes the system more dissipative in the sense that oscillations in the applied axial force die out quickly. The shear band forms at a lower value of the nominal strain when the initial porosity is increased. Once a shear band has developed, the material above the shear band moves upwards with the velocity imposed on the top surface, and that below the band moves horizontally to the left, with the velocity changing sharply from essentially horizontal to nearly vertical on the two sides of the severely deforming region. The computations were stopped when the porosity at a point reached a critical value. The material at the center necked. The softening caused by the increase in the porosity is more than that induced by the rise in the temperature of the body, at least, for the values assigned to material parameters herein.

Acknowledgement

References

1. R.E. WINTER, Philos. Mag., **31**, 765, 1975.

2. S.P. TIMOTHY and I.M. HUTCHINGS, Acta Metall., **33**, 667, 1985.

3. H.A. GREBE, H. PAK and M.A. MEYERS, Metal. Trans., **16A**, 761, 1985.

4. L. SEAMAN, D.R. CURRAN and D.A. SHOCKEY, J. Appl. Phys., **47**, 4814, 1976.

5. A. MARCHAND, K. CHO and J. DUFFY, *The formation of adiabatic shear bands in an AISI 1018 cold-rolled steel*, Brown Univ. Report, 1988.

6. K. CHO, Y.C. CHI and J. DUFFY, *Microscopic observations of adiabatic shear bands in three different steels*, Brown Univ. Report, 1988.

7. C.F. TIPPER, *The fracture of metals*, Metallurgica, **39**, 133–138, 1949.

8. K.E. PUTTICK, *Ductile fracture in metals*, Philos. Mag., **4**, 964–969, 1959.

9. K.E. PUTTICK, *The shear component of ductile fracture*, Philos. Mag., **5**, 759–762, 1960.

10. H.C. ROGERS, *Tensile fracture of ductile metals*, Trans. TMS-AIME, **28**, 498–506, 1960.

11. C. ZENER and J.H. HOLLOMON, J. Appl. Phys., **14**, 22, 1944.

12. T.G. SHAWKI and R.J. CLIFTON, Mech. Materials, **8**, 13, 1989.

13. R.C. BATRA and Z.G. ZHU, Int. J. Solids Structures, **27**, 1829, 1991.

14. J.W. NUNZIATO and S.C. COWIN, *A nonlinear theory of elastic materials with voids*, Arch. Rational Mech. Anal., **72**, 175–201, 1979.

15. H.A. KUHN and C.L. DOWNEY, *Deformation characteristics and plasticity theory of sintered powder materials*, Int. J. Powder Metall., **7**, 15–25, 1971.

16. R.J. GREEN, *A plasticity theory for porous solids*, Int. J. Mech. Sci., **14**, 215–224, 1972.

17. A.L. GURSON, *Continuum theory of ductile rupture by void nucleation and growth. Part 1. Yield criteria and flow rules for porous ductile media*, J. Eng. Mater. Technol., **99**, 2–15, 1977.

18. S. SHIMA and M. OYANE, *Plasticity theory for ductile metals*, Int. J. Mech. Sci., **18**, 285–291, 1976.

19. V. TVERGAARD, *Influence of voids on shear band instabilities under plane strain conditions*, Int. J. Fracture, **17**, 389–407, 1981.

20. V. TVERGAARD, *On localization in ductile materials containing spherical voids*, Int. J. Fracture, **18**, 237–252, 1982.

21. V. TVERGAARD and A. NEEDLEMAN, *Analysis of the cup-cone fracture in a round tensile bar*, Acta Metall., **32**, 157–196, 1984.

22. J. PAN, M. SAJE and A. NEEDLEMAN, *Localization of deformation in rate-sensitive porous plastic solids*, Int. J. Fract., **21**, 261–278, 1983.

23. M. SAJE, J. PAN and A. NEEDLEMAN, *Void nucleation effects on shear localization in porous plastic solids*, Int. J. Fracture, **19**, 163–182, 1982.

24. H. KOBAYASHI and B. DODD, *A numerical analysis for the formation of adiabatic shear bands including void nucleation and growth*, Int. J. Impact Engng., **8**, 1–13, 1989.

25. A. ZAVALIANGOS and L. ANAND, *Thermal aspects of shear localization in microporous viscoplastic solids*, Int. J. Num. Meth. Engng., **33**, 595–634, 1992.

26. S.L. PASSMAN and R.C. BATRA, *A thermomechanical theory for a porous anisotropic elastic solid with inclusions*, Arch. Rat. Mech. Anal., **87**, 11–33, 1984.

27. B. BUDIANSKY, *Thermal and thermoelastic properties of isotropic composites*, J. Compos. Mater., **4**, 701–744, 1990.

28. R.C. BATRA, *Steady state penetration of thermoviscoplastic targets*, Computat. Mech., an Int. J., **3**, 1–11, 1988.

29. J. LITOŃSKI, Bull. Acad. Polon. Sci., **25**, 7, 1977.

30. C.C. CHU and A. NEEDLEMAN, J. Engng. Mat. and Technol., **102**, 249–256, 1980.

31. G.H. LEROY, *Large scale plastic deformation and fracture for multiaxial stress states*, Ph. D. Thesis, McMaster University, 1978.

32. J.R. FISCHER, *Void nucleation in spheroidized steels during tensile deformation*, Ph. D. Thesis, Brown University, 1980.

33. R.C. BATRA, *Effect of nominal strain-rate on the initiation and growth of adiabatic shear bands in steels*, J. Appl. Mech., **55**, 229–230, 1988.

34. R.C. BATRA and K.I. KO, *An adaptive mesh refinement technique for the analysis of shear bands in plane strain compression of a thermoviscoplastic solid*, Computat. Mech., **10**, 369–379, 1992.

DEPARTMENT OF ENGINEERING SCIENCE AND MECHANICS
VIRGINIA POLYTECHNIC INSTITUTE AND STATE UNIVERSITY, BLACKSBURG, USA.

Continuous dependence results in the nonlinear theory of elastic mixtures

R. QUINTANILLA (BARCELONA)

THIS PAPER IS CONCERNED with the nonlinear theory of binary mixtures of elastic bodies. The continuous dependence of solutions upon initial state and body forces is established. A uniqueness result is also presented.

1. Introduction

THE CONTINUUM THEORY of mixtures has been a subject of intensive study in recent years. For an extensive review of the literature on mixtures the reader is referred to the reviews by BOWEN [1], ATKIN and CRAINE [2, 3], BEDFORD and DRUMHELLER [4] and C. TRUESDELL [5]. A series of papers are devoted to the study of mixtures of elastic materials (see, e.g. [4], [6–8] and the literature cited therein). In some theories for a mixture of elastic solids (for example [9–11]) the constitutive independent variables are the displacement gradients and the relative velocities, and the spatial description is used. The first theory for a mixture of elastic solids based on the Lagrangian description has been presented by BEDFORD and STERN [12, 13]. In this theory the independent variables are the displacement gradients and the displacement fields. The theory developed in [12, 13] has been extended by POP and BOWEN [6] who established a thermodynamic theory of mixtures with a long-range spatial interactions. The model of interpenetrating solid continua was applied by TIERSTEN and JAHANMIR [17] to derive a theory of composites, where the relative displacement of the individual constituents is infinitesimal. In [8], a Lagrangian description was used to derive a theory for binary mixtures of nonsimple elastic solids where the displacement constitutive variables are the displacement fields, the first and the second displacement gradients. The asymptotic behaviour of solutions of the quations of motion in the context of the linear theory of a mixture of two homogeneous and isotropic elastic materials has been studied by DAFERMOS in [14, 15]. Uniqueness results in the linear theory of mixture of elastic solids have been presented in various papers (see e.g. [16, 17]). Recently, a uniqueness theorem for the nonlinear static problem [23] and some existence results for the linear theory [22, 21] have been obtained. Asymptotic behaviour has been studied when thermal effects are considered [22].

The present paper is concerned with the nonlinear theory for binary mixture of elastic materials. In this theory the independent constitutive variables are the displacement gradients and the relative displacement, and Lagrangian description

is used. In this paper we extend some results established by Dafermos in [18] within the classical theory of nonlinear thermoelasticity. We establish a uniqueness result and the continuous dependence of solutions upon the initial state and body forces. We introduce a distance between the states of two processes originating at neighboring states. With a view toward a treatment of continuous dependence of solutions upon the data, we study the evolution in time of this distance. Then, we derive a continuous dependence result for smooth states residing in the convexity region of internal energy.

For the case when the motion of the boundary is prescribed, a similar continuous dependence result is established under the weaker assumption that the smooth state resides in the strong ellipticity region. The boundary conditions in the theory of mixtures have been discussed in various papers (see, e.g. [2, 4, 19, 20]).

2. Preliminaries

We consider a body which, at time $t = 0$, occupies the bounded regular region B of the Euclidean three-dimensional space with the boundary surface ∂B. We assume that ∂B is sufficiently regular to assure the common laws of transformation of surface integrals and Friedrichs inequality. The configuration of the body at time $t = 0$ is taken as the reference configuration. The motion of the body is referred to the reference configuration and a fixed system of rectangular Cartesian axes. Let B be at rest with respect to the reference frame. Throughout this paper we employ the usual summation and differentiation conventions: subscripts preceded by a comma denote partial differentiation with respect to the corresponding Cartesian coordinate; a superposed dot denotes the material time derivative; $\nabla_\mathbf{x}$ is gradient operator with respect to the place $\mathbf{X}$, keeping t fixed; the symbol $|\cdot|$ denotes a norm either in an Euclidean space vector or in a tensor space, while $\|\cdot\|$ denotes an L^2-norm; summation over repeated subscripts is implied. Let N_A be the components of the outward unit normal to ∂B.

We assume that B is occupied by a binary mixture of elastic materials. A process for B is described by the following eight functions of $\mathbf{X}$ and t: the spatial position fields $\mathbf{x}$, $\mathbf{y}$; the body forces $\mathbf{f}$, $\mathbf{g}$ per unit mass, the first Piola–Kirchhoff stress tensors $\mathbf{T}$, $\mathbf{S}$; the internal body force $\mathbf{p}$ per unit volume and time, the internal energy Σ per unit of initial volume. The motions $\mathbf{x}$ and $\mathbf{y}$ determine velocities $\mathbf{v} = \dot{\mathbf{x}}$ and $\mathbf{w} = \dot{\mathbf{y}}$, the deformation gradient $\mathbf{F} = \nabla_\mathbf{x}\mathbf{x}$, $\mathbf{G} = \nabla_\mathbf{x}\mathbf{y}$ and the relative displacement $\mathbf{d} = \mathbf{x} - \mathbf{y}$. In what follows, occasionally it will be convenient to write various expressions in component form and to display vector and tensor fields by their components referred to the considered system of Cartesian axes. Thus, the components of the velocity $\mathbf{v}$ we shall denote v_i, while the components of the deformation gradient fields $\mathbf{F}$ and $\mathbf{G}$ will be denoted by F_{iA} and G_{iA}.

A process for B, defined for all $\mathbf{X}$ in B and all t in $[0, t_0]$ is called a dynamic

process in B if it is compatible with the equations of motions (see, e.g. [4])

(2.1)
$$T_{Ai,A} - p_i + \rho_1^0 f_i = \rho_1^0 \ddot{x}_i,$$
$$S_{Ai,A} + p_i + \rho_2^0 g_i = \rho_2^0 \ddot{y}_i,$$

and the energy equation

(2.2) $$\frac{d}{dt}\left[\Sigma + \frac{1}{2}(\rho_1^0 v_i v_i + \rho_2^0 w_i w_i)\right] = (T_{Ai}v_i + S_{Ai}w_i)_{,A} + \rho_1^0 f_i v_i + \rho_2^0 g_i w_i.$$

Here, ρ_1^0 and ρ_2^0 are the reference mass densities of the constituents. We assume that ρ_1^0 and ρ_2^0 are smooth and strictly positive, i.e.

(2.3) $$\rho_1^0(\mathbf{X}) \geq \tilde{\rho}_1 > 0, \qquad \rho_2^0(\mathbf{X}) \geq \tilde{\rho}_2 > 0, \qquad \mathbf{X} \in \overline{B},$$

where $\tilde{\rho}_1$ and $\tilde{\rho}_2$ are constants. The material at the point $\mathbf{X}$ is characterized by the constitutive equations

(2.4) $$\Sigma = \Sigma^*(\mathbf{F}, \mathbf{G}, \mathbf{d}), \quad \mathbf{T} = \mathbf{T}^*(\mathbf{F}, \mathbf{G}, \mathbf{d}), \quad \mathbf{S} = \mathbf{S}^*(\mathbf{F}, \mathbf{G}, \mathbf{d}), \quad \mathbf{p} = \mathbf{p}^*(\mathbf{F}, \mathbf{G}, \mathbf{d}),$$

where Σ^*, $\mathbf{T}^*$, $\mathbf{S}^*$, $\mathbf{p}^*$ are smooth functions. In particular, we assume that the partial derivative of Σ^*, $\mathbf{T}^*$, $\mathbf{S}^*$ and $\mathbf{p}^*$, at any fixed state $(\mathbf{F}, \mathbf{G}, \mathbf{d})$ are bounded functions of $(\mathbf{X}, t)$ on $\overline{B} \times [0, t_0]$. The function Σ is unaltered by superposed rigid motions, so that it must be expressible in the functional form

$$\Sigma = \hat{\Sigma}(C_{KL}, G_{KL}, D_K),$$

where

$$C_{KL} = x_{i,K} x_{i,L}, \qquad G_{KL} = x_{i,K} y_{i,L} \qquad \text{and} \qquad D_k = x_{i,K} d_i.$$

We shall say that a dynamic process is admissible if it is compatible with the constitutive equations (2.4). We say that $\mathbf{A} = (\mathbf{x}, \mathbf{y})$ is an admissible state corresponding to the loading $\Lambda = (\mathbf{f}, \mathbf{g})$ if $(\mathbf{x}, \mathbf{y}, \mathbf{f}, \mathbf{g}, \mathbf{T}, \mathbf{S}, \mathbf{p}, \Sigma)$ is an admissible dynamic process. The admissible state $\mathbf{A}$ is called smooth in B if it is such that $\mathbf{v}$, $\mathbf{w}$, $\mathbf{F}$, $\mathbf{G}$ are Lipschitz continuous, uniformly on bounded subsets of their domain. If there is no internal constraint, Eq. (2.2) implies that

(2.5) $$\mathbf{T} = \left(\frac{\partial \Sigma}{\partial \mathbf{F}}\right)^T, \qquad \mathbf{S} = \left(\frac{\partial \Sigma}{\partial \mathbf{G}}\right)^T, \qquad \mathbf{p} = \frac{\partial \Sigma}{\partial \mathbf{d}}.$$

3. Basic results

Let $\mathbf{A} = (\mathbf{x}, \mathbf{y})$ and $\overline{\mathbf{A}} = (\overline{\mathbf{x}}, \overline{\mathbf{y}})$ be two smooth admissible states on $\overline{B} \times [0, t_0]$. We define the function D on $[0, t_0]$ by

$$(3.1) \qquad D(t) = \int_B \left\{ \frac{1}{2} \left[\rho_1^0 (v_i - \overline{v}_i)(v_i - \overline{v}_i) + \rho_2^0 (w_i - \overline{w}_i)(w_i - \overline{w}_i) \right] \right.$$

$$\left. + \Sigma - \overline{\Sigma} - \overline{T}_{Ai}(F_{Ai} - \overline{F}_{Ai}) - \overline{S}_{Ai}(G_{Ai} - \overline{G}_{Ai}) - \overline{p}_i(d_i - \overline{d}_i) \right\} dV,$$

where

$$\overline{F}_{Ai} = \overline{x}_{i,A}, \qquad \overline{G}_{Ai} = \overline{y}_{i,A}, \qquad \overline{\Sigma} = \Sigma^*(\overline{\mathbf{F}}, \overline{\mathbf{G}}, \overline{\mathbf{d}}),$$

$$\overline{\mathbf{T}} = \mathbf{T}^*(\overline{\mathbf{F}}, \overline{\mathbf{G}}, \overline{\mathbf{d}}), \qquad \overline{\mathbf{S}} = \mathbf{S}^*(\overline{\mathbf{F}}, \overline{\mathbf{G}}, \overline{\mathbf{d}}), \qquad \overline{\mathbf{p}} = \mathbf{p}^*(\overline{\mathbf{F}}, \overline{\mathbf{G}}, \overline{\mathbf{d}}).$$

In order to derive continuous data dependence and uniqueness results, we first establish the evolution in time of the function D.

THEOREM 1. *If $\mathbf{A}$ and $\overline{\mathbf{A}}$ are two smooth admissible states corresponding to the loadings $\Lambda = (\mathbf{f}, \mathbf{g})$ and $\overline{\Lambda} = (\mathbf{f}, \mathbf{g})$ in $L^\infty(B \times [0, t_0])$, then*

$$(3.2) \qquad \dot{D}(t) = \int_{\partial B} \left[(T_{Ai} - \overline{T}_{Ai})(v_i - \overline{v}_i) + (S_{Ai} - \overline{S}_{Ai})(w_i - \overline{w}_i) \right] N_A \, dA$$

$$+ \int_B \left[\rho_1^0 (f_i - \overline{f}_i)(v_i - \overline{v}_i) + \rho_2^0 (g_i - \overline{g}_i)(w_i - \overline{w}_i) \right] dV$$

$$+ \int_B \left\{ \dot{F}_{iA} \left[T_{Ai} - \overline{T}_{Ai} - \frac{\partial \overline{T}_{Ai}}{\partial \overline{F}_{jB}}(F_{jB} - \overline{F}_{jB}) - \frac{\partial \overline{T}_{Ai}}{\partial \overline{G}_{jB}}(G_{jB} - \overline{G}_{jB}) \right. \right.$$

$$\left. - \frac{\partial \overline{T}_{Ai}}{\partial \overline{d}_j}(d_j - \overline{d}_j) \right] + \dot{G}_{iA} \left[S_{Ai} - \overline{S}_{Ai} - \frac{\partial \overline{S}_{Ai}}{\partial \overline{F}_{jB}}(F_{jB} - \overline{F}_{jB}) \right.$$

$$- \frac{\partial \overline{S}_{Ai}}{\partial \overline{G}_{jB}}(G_{jB} - \overline{G}_{jB}) - \frac{\partial \overline{S}_{Ai}}{\partial \overline{d}_j}(d_j - \overline{d}_j) \right] + \dot{d}_i \left[p_i - \overline{p}_i - \frac{\partial \overline{p}_i}{\partial \overline{F}_{jB}}(F_{jB} - \overline{F}_{jB}) \right.$$

$$\left. \left. - \frac{\partial \overline{p}_i}{\partial \overline{G}_{jB}}(G_{jB} - \overline{G}_{jB}) - \frac{\partial \overline{p}_i}{\partial \overline{d}_j}(d_j - \overline{d}_j) \right] \right\} dV, \qquad t \in [0, t_0].$$

Proof. From Eq. (3.1) we obtain

$$\dot{D}(t) = \int_B \left\{ \frac{d}{dt} \left[\frac{1}{2}(\rho_1^0 v_i v_i + \rho_2^0 w_i w_i) + \Sigma \right] - \frac{d}{dt} \left[\frac{1}{2}(\rho_1^0 \overline{v}_i \overline{v}_i + \rho_2^0 \overline{w}_i \overline{w}_i) + \overline{\Sigma} \right] \right.$$

$$+ 2(\rho_1^0 \overline{v}_i \dot{\overline{v}}_i + \rho_2^0 \overline{w}_i \dot{\overline{w}}_i) - \rho_1^0(\overline{v}_i \dot{v}_i + v_i \dot{\overline{v}}_i) - \rho_2^0(\overline{w}_i \dot{w}_i + w_i \dot{\overline{w}}_i)$$

$$- \dot{\overline{T}}_{Ai}(F_{iA} - \overline{F}_{iA}) - \dot{\overline{S}}_{Ai}(G_{iA} - \overline{G}_{iA}) - \dot{\overline{p}}_i(d_i - \overline{d}_i)$$

$$\left. - \overline{T}_{Ai} \dot{F}_{iA} + \overline{T}_{Ai} \dot{\overline{F}}_{iA} - \overline{S}_{Ai} \dot{G}_{iA} + \overline{S}_{Ai} \dot{\overline{G}}_{iA} - \overline{p}_i \dot{d}_i + \overline{p}_i \dot{\overline{d}}_i \right\} dV.$$

By Eqs. (2.1), (2.2) and the divergence theorem, we get

$$
(3.3) \qquad \dot{D}(t) = \int_{\partial B} \left[(T_{Ai} - \overline{T}_{Ai})(v_i - \overline{v}_i) + (S_{Ai} - \overline{S}_{Ai})(w_i - \overline{w}_i) \right] N_A \, dA
$$

$$
+ \int_B \left[\rho_1^0 (f_i - \overline{f}_i)(v_i - \overline{v}_i) + \rho_2^0 (g_i - \overline{g}_i)(w_i - \overline{w}_i) \right] dV
$$

$$
+ \int_B \left[\dot{F}_{iA} (T_{Ai} - \overline{T}_{Ai}) + \dot{G}_{iA} (S_{Ai} - \overline{S}_{Ai}) + \dot{d}_i (p_i - \overline{p}_i) \right.
$$

$$
\left. - \dot{\overline{T}}_{Ai} (F_{iA} - \overline{F}_{iA}) - \dot{\overline{S}}_{Ai} (G_{iA} - \overline{G}_{iA}) - \dot{\overline{p}}_i (d_i - \overline{d}_i) \right] dV.
$$

With the help of Eqs. (2.5), we can write

$$
\dot{\overline{T}}_{Bj} = \frac{\partial \overline{T}_{Ai}}{\partial \overline{F}_{jB}} \dot{\overline{F}}_{iA} + \frac{\partial \overline{S}_{Ai}}{\partial \overline{F}_{jB}} \dot{\overline{G}}_{iA} + \frac{\partial \overline{p}_i}{\partial \overline{F}_{jB}} \dot{\overline{d}}_i \,,
$$

$$
\dot{\overline{S}}_{Bj} = \frac{\partial \overline{T}_{Ai}}{\partial \overline{G}_{jB}} \dot{\overline{F}}_{iA} + \frac{\partial \overline{S}_{Ai}}{\partial \overline{G}_{jB}} \dot{\overline{G}}_{iA} + \frac{\partial \overline{p}_i}{\partial \overline{G}_{jB}} \dot{\overline{d}}_i \,,
$$

$$
\dot{\overline{p}}_j = \frac{\partial \overline{T}_{Ai}}{\partial \overline{d}_j} \dot{\overline{F}}_{iA} + \frac{\partial \overline{S}_{Ai}}{\partial \overline{d}_j} \dot{\overline{G}}_{iA} + \frac{\partial \overline{p}_i}{\partial \overline{d}_j} \dot{\overline{d}}_i \,.
$$

So that

$$
\dot{F}_{iA} (T_{Ai} - \overline{T}_{Ai}) + \dot{G}_{iA} (S_{Ai} - \overline{S}_{Ai}) + \dot{d}_i (p_i - \overline{p}_i)
$$

$$
- \dot{\overline{T}}_{Ai} (F_{iA} - \overline{F}_{iA}) - \dot{\overline{S}}_{Ai} (G_{iA} - \overline{G}_{iA}) - \dot{\overline{p}}_i (d_i - \overline{d}_i)
$$

$$
= \dot{F}_{iA} \left[(T_{Ai} - \overline{T}_{Ai}) - \frac{\partial \overline{T}_{Ai}}{\partial \overline{F}_{jB}} (F_{jB} - \overline{F}_{jB}) - \frac{\partial \overline{T}_{Ai}}{\partial \overline{G}_{jB}} (G_{jB} - \overline{G}_{jB}) \right.
$$

$$
\left. - \frac{\partial \overline{T}_{Ai}}{\partial \overline{d}_j} (d_j - \overline{d}_j) \right] + \dot{G}_{iA} \left[(S_{Ai} - \overline{S}_{Ai}) - \frac{\partial \overline{S}_{Ai}}{\partial \overline{F}_{jB}} (F_{jB} - \overline{F}_{jB}) \right.
$$

$$
\left. - \frac{\partial \overline{S}_{Ai}}{\partial \overline{G}_{jB}} (G_{jB} - \overline{G}_{jB}) - \frac{\partial \overline{S}_{Ai}}{\partial \overline{d}_j} (d_j - \overline{d}_j) \right]
$$

$$
+ \dot{d}_i \left[(p_i - \overline{p}_i) - \frac{\partial \overline{p}_i}{\partial \overline{F}_{jB}} (F_{jB} - \overline{F}_{jB}) \right.
$$

$$
\left. - \frac{\partial \overline{p}_i}{\partial \overline{G}_{jB}} (G_{jB} - \overline{G}_{jB}) - \frac{\partial \overline{p}_i}{\partial \overline{d}_j} (d_j - \overline{d}_j) \right].
$$

If we use the above relations, then from Eq. (3.3) we obtain the desired result.

Following Dafermos [18], we say that the smooth admissible state $\overline{A} = (\overline{x}, \overline{y})$ resides in the convexity region of the internal energy if for each $(X, t) \in \partial B \times [0, t_0]$, there exists a positive constant λ such that

$$(3.4) \quad \frac{\partial^2 \overline{\Sigma}}{\partial \overline{F}_{iA} \partial \overline{F}_{jB}} U_{iA} U_{jB} + \frac{\partial^2 \overline{\Sigma}}{\partial \overline{G}_{iA} \partial \overline{G}_{jB}} V_{iA} V_{jB} + \frac{\partial^2 \overline{\Sigma}}{\partial \overline{d}_i \partial \overline{d}_j} Z_i Z_j$$

$$+ 2 \frac{\partial^2 \overline{\Sigma}}{\partial \overline{F}_{iA} \partial \overline{G}_{jB}} U_{iA} V_{jB} + 2 \frac{\partial^2 \overline{\Sigma}}{\partial \overline{F}_{iA} \partial \overline{d}_j} U_{iA} Z_j + 2 \frac{\partial^2 \overline{\Sigma}}{\partial \overline{G}_{iA} \partial \overline{d}_j} V_{iA} Z_j$$

$$\geq \lambda \left(|U|^2 + |V|^2 + |Z|^2 \right).$$

for all U_{iA}, V_{jB}, Z_k. In the linear theory the above condition is equivalent to the positive definiteness of the energy density. A detailed discussion of the convexity of internal energy has been given in [18].

In what follows we shall need the following Gronwall-type inequality (see Dafermos [18]).

Lemma 1. Assume that the nonnegative functions $y(t) \in L^\infty[0, s]$ and $g(t) \in L^1[0, s]$ satisfy the inequality

$$(3.5) \quad y^2(\tau) \leq M^2 y^2(0) + \int_0^\tau \left[(2\alpha + 4\beta\tau) y^2(t) + 2N g(t) y(t) \right] dt, \qquad \tau \in [0, s],$$

where α, β, M and N are nonnegative constants. Then

$$y(s) \leq \left[M y(0) + N \int_0^s g(t) \, dt \right] \exp(\eta s + \beta s^2).$$

where $\eta = (\alpha + \beta)/\alpha$.

Theorem 2. *Let* $(\overline{x}, \overline{y})$ *be a smooth admissible state corresponding to the loading* $\overline{A} = (\overline{f}, \overline{g}) \in L^\infty(B \times [0, t_0])$ *and residing in the convexity region of the internal energy. Then there exist the positive constants* δ, α_1, M_1, M_2 *with the following property:*

If (x, y) *is any smooth admissible state defined on* $B \times [0, t_0]$ *corresponding to the loading* $A = (f, g) \in L^\infty(B \times [0, t_0])$, *such that*

$$(3.6) \quad |F(x, t) - \overline{F}(x, t)| + |G(x, t) - \overline{G}(x, t)| + |d(x, t) - \overline{d}(x, t)| < \delta.$$

$$(X, t) \in B \times [0, t_0].$$

$$(3.7) \quad \frac{1}{2} N_A \left[(T_{Ai} + S_{Ai}) - (\overline{T}_{Ai} + \overline{S}_{Ai}) \right] [(v_i + w_i) - (\overline{v}_i + \overline{w}_i)]$$

$$+ \frac{1}{2} N_A \left[(T_{Ai} + \overline{S}_{Ai}) - (\overline{T}_{Ai} + S_{Ai}) \right] [(v_i + \overline{w}_i) - (\overline{v}_i + w_i)]$$

$$= \left[(T_{Ai} - \overline{T}_{Ai})(v_i - \overline{v}_i) + (S_{Ai} - \overline{S}_{Ai})(w_i - \overline{w}_i) \right] N_A = 0. \quad \text{on} \quad \partial B \times [0, t_0],$$

then, for any $s \in [0, t_0]$,

$$\|(\mathbf{v} - \bar{\mathbf{v}}, \mathbf{w} - \bar{\mathbf{w}}, \mathbf{F} - \bar{\mathbf{F}}, \mathbf{G} - \bar{\mathbf{G}})(\cdot, s)\|_{L^2(B)}$$

$$\leq \left\{ M_1 \|(\mathbf{v} - \bar{\mathbf{v}}, \mathbf{w} - \bar{\mathbf{w}}, \mathbf{F} - \bar{\mathbf{F}}, \mathbf{G} - \bar{\mathbf{G}})(\cdot, 0)\|_{L^2(B)} \right.$$

$$\left. + M_2 \int_0^s \|(\mathbf{f} - \bar{\mathbf{f}}, \mathbf{g} - \bar{\mathbf{g}})\|_{L^2(B)} dt \right\} \exp(\alpha_1 s).$$

P r o o f. By (3.5), (3.7), the Schwarz inequality and (3.2), it follows that one can determine the positive constants c_1, c_2 such that, for all $t \in [0, t_0]$, one has

(3.8) $$\dot{D}(t) \leq c_1 \|(\mathbf{F} - \bar{\mathbf{F}}, \mathbf{G} - \bar{\mathbf{G}}, \mathbf{d} - \bar{\mathbf{d}})(\cdot, t)\|_{L^2(B)}^2$$

$$+ c_2 \|(\mathbf{f} - \bar{\mathbf{f}}, \mathbf{g} - \bar{\mathbf{g}})(\cdot, t)\|_{L^2(B)} \|(\mathbf{v} - \bar{\mathbf{v}}, \mathbf{w} - \bar{\mathbf{w}})(\cdot, t)\|_{L^2(B)}.$$

If we fix $s \in [0, t_0]$ and integrate (3.8) over $[0, \tau]$ (with $\tau \in [0, s]$), we obtain

(3.9) $$D(\tau) \leq D(0) + c_1 \int_0^\tau \|(\mathbf{F} - \bar{\mathbf{F}}, \mathbf{G} - \bar{\mathbf{G}}, \mathbf{d} - \bar{\mathbf{d}})(\cdot, t)\|_{L^2(B)}^2 dt$$

$$+ c_2 \int_0^\tau \|(\mathbf{f} - \bar{\mathbf{f}}, \mathbf{g} - \bar{\mathbf{g}})(\cdot, t)\|_{L^2(B)} \|(\mathbf{v} - \bar{\mathbf{v}}, \mathbf{w} - \bar{\mathbf{w}})(\cdot, t)\|_{L^2(B)} dt.$$

In view of Eqs. (2.5)

(3.10) $$\Sigma - \bar{\Sigma} - \bar{T}_{Ai}(F_{iA} - \bar{F}_{iA}) - \bar{S}_{Ai}(G_{iA} - \bar{G}_{iA}) - \bar{p}_i(d_i - \bar{d}_i)$$

$$= \frac{1}{2} \left[\frac{\partial^2 \bar{\Sigma}}{\partial \bar{F}_{iA} \partial \bar{F}_{jB}} (F_{iA} - \bar{F}_{iA})(F_{jB} - \bar{F}_{jB}) \right.$$

$$+ \frac{\partial^2 \bar{\Sigma}}{\partial \bar{G}_{iA} \partial \bar{G}_{jB}} (G_{iA} - \bar{G}_{iA})(G_{jB} - \bar{G}_{jB})$$

$$+ \frac{\partial^2 \bar{\Sigma}}{\partial \bar{d}_i \partial \bar{d}_j} (d_i - \bar{d}_i)(d_j - \bar{d}_j) + 2 \frac{\partial^2 \bar{\Sigma}}{\partial \bar{F}_{iA} \partial \bar{G}_{jB}} (F_{iA} - \bar{F}_{iA})(G_{jB} - \bar{G}_{jB})$$

$$\left. + 2 \frac{\partial^2 \bar{\Sigma}}{\partial \bar{F}_{iA} \partial \bar{d}_j} (F_{iA} - \bar{F}_{iA})(d_j - \bar{d}_j) + 2 \frac{\partial^2 \bar{\Sigma}}{\partial \bar{G}_{iA} \partial \bar{d}_j} (G_{iA} - \bar{G}_{iA})(d_j - \bar{d}_j) \right]$$

$$+ o\left(|\mathbf{F} - \bar{\mathbf{F}}|^2 + |\mathbf{G} - \bar{\mathbf{G}}|^2 + |\mathbf{d} - \bar{\mathbf{d}}|^2 \right).$$

From Eqs. (2.3), (3.1), (3.9) and (3.10) it follows that there exists a positive con-

stant δ such that, whenever Eq. (3.6) holds, we can write

$$(3.11) \qquad \tilde{\rho}_1 \|(\mathbf{v} - \bar{\mathbf{v}})(\cdot, \tau)\|^2_{L^2(B)} + \tilde{\rho}_2 \|(\mathbf{w} - \bar{\mathbf{w}})(\cdot, t)\|^2_{L^2(B)}$$

$$+ \lambda^* \|(\mathbf{F} - \bar{\mathbf{F}}, \mathbf{G} - \bar{\mathbf{G}}, \mathbf{d} - \bar{\mathbf{d}})(\cdot, \tau)\|^2_{L^2(B)}$$

$$\leq 2D(0) + 2c_1 \int_0^\tau \|(\mathbf{v} - \bar{\mathbf{v}}, \mathbf{w} - \bar{\mathbf{w}}, \mathbf{F} - \bar{\mathbf{F}}, \mathbf{G} - \bar{\mathbf{G}}, \mathbf{d} - \bar{\mathbf{d}})(\cdot, t)\|^2_{L^2(B)} dt$$

$$+ 2c_2 \int_0^\tau \|(\mathbf{f} - \bar{\mathbf{f}}, \mathbf{g} - \bar{\mathbf{g}})(\cdot, t)\|_{L^2(B)} \|(\mathbf{v} - \bar{\mathbf{v}}, \mathbf{w} - \bar{\mathbf{w}}, \mathbf{F} - \bar{\mathbf{F}}, \mathbf{G} - \bar{\mathbf{G}}, \mathbf{d} - \bar{\mathbf{d}})(\cdot, t)\|_{L^2(B)} dt.$$

If we use the estimate

$$D(0) \leq c_3 \|(\mathbf{v} - \bar{\mathbf{v}}, \mathbf{w} - \bar{\mathbf{w}}, \mathbf{F} - \bar{\mathbf{F}}, \mathbf{G} - \bar{\mathbf{G}}, \mathbf{d} - \bar{\mathbf{d}})(\cdot, 0)\|^2_{L^2(B)}$$

with $c_3 > 0$ and the notations

$$m = \min(\tilde{\rho}_1, \tilde{\rho}_2, \lambda^*), \qquad M_1^2 = 2c_3/m, \qquad \alpha_1 = c_1/m, \qquad M_2 = c_2/m.$$

then (3.11) implies that

$$\|(\mathbf{v} - \bar{\mathbf{v}}, \mathbf{w} - \bar{\mathbf{w}}, \mathbf{F} - \bar{\mathbf{F}}, \mathbf{G} - \bar{\mathbf{G}}, \mathbf{d} - \bar{\mathbf{d}})(\cdot, \tau)\|^2_{L^2(B)}$$

$$\leq M_1^2 \|(\mathbf{v} - \bar{\mathbf{v}}, \mathbf{w} - \bar{\mathbf{w}}, \mathbf{F} - \bar{\mathbf{F}}, \mathbf{G} - \bar{\mathbf{G}}, \mathbf{d} - \bar{\mathbf{d}})(\cdot, 0)\|^2_{L^2(B)}$$

$$+ \int_0^\tau \left\{ 2\alpha_1 \|(\mathbf{v} - \bar{\mathbf{v}}, \mathbf{w} - \bar{\mathbf{w}}, \mathbf{F} - \bar{\mathbf{F}}, \mathbf{d} - \bar{\mathbf{d}})(\cdot, t)\|^2_{L^2(B)} \right.$$

$$+ 2M_2 \|(\mathbf{f} - \bar{\mathbf{f}}, \mathbf{g} - \bar{\mathbf{g}})(\cdot, t)\|_{L^2(B)} \|(\mathbf{v} - \bar{\mathbf{v}}, \mathbf{w} - \bar{\mathbf{w}}, \mathbf{F} - \bar{\mathbf{F}}, \mathbf{G} - \bar{\mathbf{G}}, \mathbf{d} - \bar{\mathbf{d}})(\cdot, t)\|_{L^2(B)} \right\} dt.$$

The application of Lemma 1 leads to the desired result.

The next uniqueness theorem is a direct consequence of the Theorem 2.

THEOREM 3. *Let* $\bar{\mathbf{A}} = (\bar{\mathbf{x}}, \bar{\mathbf{y}})$ *and* $\mathbf{A} = (\mathbf{x}, \mathbf{y})$ *be two smooth admissible states residing in the convexity region of the internal energy and corresponding to the same loading and to the same initial data. If the states satisfy the boundary conditions* (3.7), *then*

$$\mathbf{x}(\mathbf{X}, t) = \bar{\mathbf{x}}(\mathbf{X}, t), \qquad \mathbf{y}(\mathbf{X}, t) = \bar{\mathbf{y}}(\mathbf{X}, t), \qquad \text{for} \quad (\mathbf{X}, t) \in \bar{B} \times [0, t_0].$$

Theorems 2 and 3 have been obtained under the assumption that the state resides in the convexity region of the internal energy. This condition can be relaxed to suppose that the state $(\bar{\mathbf{x}}, \bar{\mathbf{y}})$ resides in the strong ellipticity region, i.e.

there exist the positive constant μ with the property that for any vectors ξ_i, δ_A, η_i, λ_A, ϕ_i

$$\frac{\partial^2 \overline{\Sigma}}{\partial \overline{F}_{iA} \partial \overline{F}_{jB}} \xi_i \xi_j \delta_A \delta_B + \frac{\partial^2 \overline{\Sigma}}{\partial \overline{G}_{iA} \partial \overline{G}_{jB}} \eta_i \eta_j \lambda_A \lambda_B + \frac{\partial^2 \overline{\Sigma}}{\partial \overline{d}_i \partial \overline{d}_j} \phi_i \phi_j$$

$$+2 \frac{\partial^2 \overline{\Sigma}}{\partial \overline{F}_{iA} \partial \overline{G}_{jB}} \xi_i \delta_A \eta_i \lambda_B + 2 \frac{\partial^2 \overline{\Sigma}}{\partial \overline{F}_{iA} \partial \overline{d}_j} \xi_i \delta_A \phi_j + 2 \frac{\partial^2 \overline{\Sigma}}{\partial \overline{G}_{iA} \partial \overline{d}_j} \delta_i \lambda_A \phi_j$$

$$\geq \mu \left\{ \left(|\xi_i|^2 + |\eta_i|^2 \right) \left(|\delta_A|^2 + |\lambda_A|^2 \right) + |\phi_i|^2 \right\}.$$

THEOREM 4. *Let* $(\overline{\mathbf{x}}, \overline{\mathbf{y}})$ *be a smooth admissible state corresponding to the loading* $(\overline{\mathbf{f}}, \overline{\mathbf{g}}) \in L^\infty(B \times [0, t_0]$ *and residing in the strong ellipticity region of the internal energy. Then there exist the positive constants* δ, α_1, β, M_1, M_2 *with the following property:*

If $(\mathbf{x}, \mathbf{y})$ *is any smooth admissible state defined on* $B \times [0, t_0]$ *corresponding to the loading* $(\mathbf{f}, \mathbf{g}) \in L^\infty(B \times [0, t_0])$ *such that*

$$(3.12) \qquad |\mathbf{F}(\mathbf{x}, t) - \overline{\mathbf{F}}(\mathbf{x}, t)| + |\mathbf{G}(\mathbf{x}, t) - \overline{\mathbf{G}}(\mathbf{x}, t)| + |\mathbf{d}(\mathbf{x}, t) - \overline{\mathbf{d}}(\mathbf{x}, t)| < \delta,$$
$$(\mathbf{X}, t) \in B \times [0, t_0],$$

$$(3.13) \qquad \mathbf{x}(\mathbf{X}, t) = \overline{\mathbf{x}}(\mathbf{X}, t), \qquad \mathbf{y}(\mathbf{X}, t) = \overline{\mathbf{y}}(\mathbf{X}, t) \qquad \text{on} \quad \partial B \times [0, t_0],$$

then, for any $s \in [0, t_0]$,

$$(3.14) \qquad \|(\mathbf{v} - \overline{\mathbf{v}}, \mathbf{w} - \overline{\mathbf{w}}, \mathbf{F} - \overline{\mathbf{F}}, \mathbf{G} - \overline{\mathbf{G}})(\cdot, s)\|_{L^2(B)}$$

$$\leq \left\{ M_1 \|(\mathbf{v} - \overline{\mathbf{v}}, \mathbf{w} - \overline{\mathbf{w}}, \mathbf{F} - \overline{\mathbf{F}}, \mathbf{G} - \overline{\mathbf{G}})(\cdot, 0)\|_{L^2(B)} \right.$$

$$\left. + M_2 \int_0^s \|(\mathbf{f} - \overline{\mathbf{f}}, \mathbf{g} - \overline{\mathbf{g}})(\cdot, t)\|_{L^2(B)} dt \right\} \exp(\alpha_1 s + \beta s^2).$$

P r o o f. We recall that $\overline{\mathbf{A}} = (\overline{\mathbf{x}}, \overline{\mathbf{y}})$ resides in the strong ellipticity and $\mathbf{x} - \overline{\mathbf{x}}$, $\mathbf{y} - \overline{\mathbf{y}}$ vanish on $\partial B \times [0, t_0]$. In view of Garding inequality there exist two constants $\lambda > 0$ and κ with the property that, for any $\tau \in [0, t_0]$,

$$(3.15) \qquad \int_B \left[\frac{\partial^2 \overline{\Sigma}}{\partial \overline{F}_{iA} \partial \overline{F}_{jB}} (F_{iA} - \overline{F}_{iA})(F_{jB} - \overline{F}_{jB}) \right.$$

$$+ \frac{\partial^2 \overline{\Sigma}}{\partial \overline{G}_{iA} \partial \overline{G}_{jB}} (G_{iA} - \overline{G}_{iA})(G_{jB} - \overline{G}_{jB})$$

$$+ \frac{\partial^2 \overline{\Sigma}}{\partial \overline{d}_i \partial \overline{d}_j} (d_i - \overline{d}_i)(d_j - \overline{d}_j) + 2 \frac{\partial^2 \overline{\Sigma}}{\partial \overline{F}_{iA} \partial \overline{G}_{jB}} (F_{iA} - \overline{F}_{iA})(G_{jB} - \overline{G}_{jB})$$

$$+ 2 \frac{\partial^2 \overline{\Sigma}}{\partial \overline{F}_{iA} \partial \overline{d}_j} (F_{iA} - \overline{F}_{iA})(d_j - \overline{d}_j) + 2 \frac{\partial^2 \overline{\Sigma}}{\partial \overline{G}_{iA} \partial \overline{d}_j} (G_{iA} - \overline{G}_{iA})(d_j - \overline{d}_j) \right] dV$$

(3.15)

[cont.]

$$\geq 2\lambda \int_B \|(\mathbf{F} - \overline{\mathbf{F}}, \mathbf{G} - \overline{\mathbf{G}}, \mathbf{d} - \overline{\mathbf{d}})(\cdot, \tau)\|^2_{L^2(B)} dV$$

$$-\kappa \int_B \|(\mathbf{x} - \overline{\mathbf{x}}, \mathbf{y} - \overline{\mathbf{y}})(\cdot, \tau)\|^2_{L^2(B)} dV.$$

It follows from Eqs. (3.10) and (3.15) that there is a positive constant δ with the property that, when Eq. (3.12) is satisfied,

$$\int_B \left(\Sigma - \overline{\Sigma} - \overline{T}_{Ai}(F_{iA} - \overline{F}_{iA}) - \overline{S}_{Ai}(G_{iA} - \overline{G}_{iA}) - \overline{p}_i(d_i - \overline{d}_i) \right) dV$$

$$\geq \delta \int_B \|(\mathbf{F} - \overline{\mathbf{F}}, \mathbf{G} - \overline{\mathbf{G}}, \mathbf{d} - \overline{\mathbf{d}})(\cdot, \tau)\|^2_{L^2(B)} dV$$

$$-\kappa \int_B \|(\mathbf{x} - \overline{\mathbf{x}}, \mathbf{y} - \overline{\mathbf{y}})(\cdot, \tau)\|^2_{L^2(B)} dV.$$

By using Schwarz's inequality and the Poincaré inequality, we get

$$\|\mathbf{x}(\cdot, \tau) - \overline{\mathbf{x}}(\cdot, \tau), \mathbf{y}(\cdot, \tau) - \overline{\mathbf{y}}(\cdot, \tau)\|^2_{L^2(B)}$$

$$= \|(\mathbf{x}(\cdot, 0) - \overline{\mathbf{x}}(\cdot, 0) + \int_0^\tau (\mathbf{v}(\cdot, t) - \overline{\mathbf{v}}(\cdot, t)\, dt, \mathbf{y}(\cdot, 0) - \overline{\mathbf{y}}(\cdot, 0)$$

$$+ \int_0^\tau (\mathbf{w}(\cdot, t) - \overline{\mathbf{w}}(\cdot, t))\, dt)\|^2_{L^2(B)}$$

$$\leq 2c_5 \|(\mathbf{F}(\cdot, 0) - \overline{\mathbf{F}}(\cdot, 0), \mathbf{G}(\cdot, 0) - \overline{\mathbf{G}}(\cdot, 0))\|^2_{L^2(B)}$$

$$+ 2\tau \int_0^\tau \|(\mathbf{v}(\cdot, t) - \overline{\mathbf{v}}(\cdot, t), \mathbf{w}(\cdot, t) - \overline{\mathbf{w}}(\cdot, t))\|_{L^2(B)} dt.$$

Next we proceed as in the proof of Theorem 2. We obtain an estimate of the form (3.5) with

$$y(t) = \|(\mathbf{v} - \overline{\mathbf{v}}, \mathbf{w} - \overline{\mathbf{w}}, \mathbf{F} - \overline{\mathbf{F}}, \mathbf{G} - \overline{\mathbf{G}})(\cdot, t)\|_{L^2(B)}$$

and $g(t) = \|(\mathbf{f} - \overline{\mathbf{f}}, \mathbf{g} - \overline{\mathbf{g}})(\cdot, t)\|_{L^2(B)}$. In view of Lemma 1, we obtain the desired result.

Theorem 4 can be used to obtain a uniqueness theorem under the assumption of the strong ellipticity condition similar to Theorem 3.

References

1. R.M. BOWEN, *Theory of mixtures*, [in:] Continuum Physics, A.C. ERINGEN [ed.], vol. III, Academic Press, New York 1976.

2. R.J. ATKIN and R.E. CRAINE, *Continuum theories of mixtures: basic theory and historical development*, Quart. J. Mech. Appl. Math., **29**, 209–245, 1976.

3. R.J. ATKIN and R.E. CRAINE, *Continuum theories of mixtures: applications*, J. Int. Math. Appl., **17**, 153–207, 1976.

4. A. BEDFORD and D.S. DRUMHELLER, *Theory of immiscible and structured mixtures*, Int. J. Engng. Sci., **21**, 863–960, 1983.

5. C. TRUESDELL, *Rational thermodynamics*, [Second Ed.], Springer Verlag, New York 1984.

6. J.J. POP and R.M. BOWEN, *A theory of mixtures with a long range spatial interaction*, Acta Mech., **29**, 21–34, 1978.

7. H.F. TIERSTEN and M. JAHANMIR, *A theory of composites modelled as interpenetrating solid continua*, Arch. Rat. Mech. Anal., **65**, 153–192, 1977.

8. D. IESAN, *A theory of mixtures of nonsimple elastic bodies*, Int. J. Engng Sci., **30**, 317–328, 1992.

9. A.E. GREEN and T.R. STEEL, *Constitutive equations for interacting continua*, Int. J. Engng. Sci., **4**, 483–500, 1966.

10. T.R. STEEL, *Applications of a theory of interacting continua*, Quart. J. Mech. Appl. Math., **420**, 57–72, 1967.

11. R.M. BOWEN and J.C. WIESE, *Diffusion in mixtures of elastic materials*, Int. J. Engng. Sci., 7, 689–722, 1969.

12. A. BEDFORD and M. STERN, *A multi-continuum theory for composite elastic materials*, Acta Mech., **14**, 85–102, 1972.

13. A. BEDFORD and M. STERN, *Toward a diffusing continuum theory of composite elastic materials*, J. Appl. Mech., **38**, 8–14, 1972.

14. C.M. DAFERMOS, *Wave equations with weak damping*, SIAM J. Appl. Math., **18**, 759–767, 1970.

15. C.M. DAFERMOS, *Contraction semigroups and trend to equilibrium in continuum mechanics*, [in:] Applications of Methods of Functional Analysis to Problems in Mechanics, P. GERMAIN and B. NAYROLES [Eds.], Lectures Notes in Mathematics, vol. 503, pp. 295–306, Springer Verlag, Berlin 1976.

16. R.J. ATKIN, P. CHADWICK and T.R. STEEL, *Uniqueness theorems for linearized theories of interacting continua*, Mathematika, **14**, 27–42, 1967.

17. R.J. KNOPS and T.R. STEEL, *Uniqueness in the linear theory of two elastic solids*, Int. J. Engng. Sci., 7, 571–577, 1969.

18. C.M. DAFERMOS, *The second law of thermodynamics and stability*, Arch. Rat. Mech. Anal., **70**, 167–179, 1979.

19. K.R. RAJAGOPAL, A.S. WINEMAN and M. GANDHI, *On boundary conditions for a certain class of problems in mixture theory*, Int. J. Engng. Sci., **24**, 1453–1464, 1986.

20. K.R. RAJAGOPAL and A.S. WINEMAN, *Developments in the mechanics of interactions between a fluid and a highly elastic solid*, [in:] Recent Developments in Structured Continua, D.DEKEE and P.N. KALONI [Eds.], vol. II, Pitman Research Notes in Mathematics Series, Longman Scientific and Technical, Essex 1990.

21. D. IESAN and R. QUINTANILLA, *Existence and continuous dependence results in the theory of interacting continua* [preprint].

22. F. MARTINEZ and R. QUINTANILLA, *Some qualitative results for the linear theory of binary mixtures of thermoelastic solids* [preprint].

23. R. QUINTANILLA, *Uniqueness of equilibrium solutions in nonlinear theory of elastic mixtures* [preprint].

DEPARTAMENTO MATEMÁTICA APLICADA II
UNIVERSIDAD POLITÉCNICA DE CATALUNYA, BARCELONA, SPAIN.

A local differential geometric formulation
of dual stress-strain pairs and time derivatives

B. SVENDSEN (DARMSTADT) and CH. TSAKMAKIS (KARLSRUHE)

THE PURPOSE OF THIS WORK is to formulate, discuss and generalize, from a local differential geo-
metric point of view, the concept of "dual" stress-strain pairs and "dual" derivatives introduced by
HAUPT and TSAKMAKIS. In particular, the differential geometric represention for "line elements"
(i.e., as equivalence classes of curves) and "surfaces" (i.e., as equivalence classes of functions),
yield the corresponding families of strain tensors based on *associated* forms of the usual Green
and Piola strain tensors, respectively. Using the stress power density, two corresponding families
of stress tensors based on *associated forms* of the second Piola-Kirchoff and negative convected
stress tensors, respectively, are obtained, with the former conjugate to the Green, and the latter
to the Piola strain tensor. The other members of each family are obtained from the basic pair of
stress-strain tensors in each via the action of a group of *time-dependent* invertible linear transfor-
mations on each pair. From this point of view, each family represents the "orbit" of each basic
pair with respect to the group action in the set of all such pairs. The invariance of the stress power
density with respect to this action of the group is obtained when one takes into consideration the
fact that the group acts as well on the time derivative operator, yielding the concept of *dual* time
derivatives. We emphasize that the crucial difference between our formulation and previous work
on "objective" derivatives is the dependence of dual derivatives on the extension of the invariance
of the stress power density with respect to the action of *time-dependent* linear transformations, a
requirement that is material-independent.

1. Introduction

IT IS WELL-KNOWN that in the theory of finite deformations, stress and strain tensors
can be introduced in various ways. These various stress and strain tensors are
not initially related to each other, raising the question of whether or not there
exists a method to associate with each stress tensor, a strain tensor independent
of the material.

The theory of conjugate variables of HILL [1, 2] represents a method to asso-
ciate one strain tensor with each stress tensor independent of particular material
properties. According to this theory, a stress tensor is called conjugate to a given
deformation tensor if the inner product of the stress tensor with the material time
derivative of the deformation tensor represents the stress power. HILL's method
is formulated using mainly Lagragian variables. A modification and extension
of the method of conjugate variables to arbitrary stress-deformation pairs was
introduced by HAUPT and TSAKMAKIS [3] (hereafter HT), i.e., the method of dual
variables. In this work, we formulate this approach from a differential geometric
point of view.

After introducing basic definitions and notation in Sec. 2, we present a brief
review of basic kinematical relations for a material body used in this work (Sec. 3).

In the next three sections, we briefly review, from a local differential geometric point of view, the basic strain and stress tensors employed by HT, i.e., the (referential) Green and (spatial) Almansi strain tensors based on the deformation of "line elements" (i.e., tangent vector fields: Sec. 4), the (referential) Piola and (spatial) Finger strain tensors based on the deformation of "surfaces" (i.e., normal covectors: Sec. 5), and the (referential) second Piola – Kirchhoff and convected stress tensors as based on the Cauchy stress tensor (Sec. 6). A particular result of such a formulation for these tensors is the appearance of their *associated forms* and the explicit role of the Euclidean metric. On the basis of this representation, we analyse in Sec. 7 the pairing of these stress and strain tensors that arises in the stress power (Sec. 7), i.e., the basic "dual" stress-strain pairs, as well as their transformations. In particular, we show that these transformations can be represented as an *associated action of a group*. An important special case of this action is represented in essence by the operations of "push-forward" and "pull-back" (e.g., Marsden and Hughes [4]) of tensor fields associated with the referential and spatial configurations, respectively (Sec. 7).

As a prelude to discussing the corresponding "dual" derivatives introduced by HT, we review briefly the time derivatives of the previously-mentioned basic referential and spatial stress and strain tensors in Sec. 8. The requirement that the stress power density should be invariant with respect to action of a group of transformations yields in Sec. 9 the concept of dual derivatives of dual stress-strain tensors, representing derivatives that commute with the group action.

To maintain close contact with the work of HT, as well as "classical" continuum mechanics, we utilize in this paper a local (i.e., Euclidean-space based) representation of kinematics, stress and strain tensors, and so on. A number of results in this work (i.e., many of those to be found in Secs. 4–6 and Sec. 8) can be compared to similar results in Marsden and Hughes [4, §1.3, §1.6 and §2.2].

2. Basic mathematical definitions, concepts and notation

Let $\mathbb{R}$ and $\mathbb{R}^+ := \{a \in \mathbb{R} \mid a > 0\}$ represent, as usual, the sets of real and positive real numbers, respectively. For an arbitrary set A, let $A^n := A \times \cdots \times A$ (n times) signify the n-fold Cartesian product of A with itself.

Let $\mathrm{Map}(A, B)$ represent the set of all mappings between two sets A and B. Any $\psi \in \mathrm{Map}(A, B)$ and $\varphi \in \mathrm{Map}(A, C)$ induce $(\psi \times \varphi) \in \mathrm{Map}(A \times A, B \times C)$, defined by $(\psi \times \varphi)(p_1, p_2) := (\psi(p_1), \varphi(p_2))$ for all $p_1, p_2 \in A$. Any $\psi \in \mathrm{Map}(A \times B, C)$ induces $\psi_p \in \mathrm{Map}(B, C)$ for all $p \in A$ and $\psi_q \in \mathrm{Map}(A, C)$ for all $q \in B$, defined by $\psi_p(q) := \psi(p, q)$ for all $q \in B$ and $\psi_q(p) := \psi(p, q)$ for all $p \in A$, respectively. For any subset $U \subset A$ of a set A, the *inclusion mapping* $1_{U \subset A} \in \mathrm{Map}(U, A)$ is defined by $1_{U \subset A}(p) := p$ for all $p \in U$; in particular, $1_A := 1_{A \subset A}$ represents the *identity mapping*. In the case of a linear space $\mathcal{V}$, let $\mathbf{1}_{\mathcal{V}}$ represent the linear mapping induced by $1_{\mathcal{V}}$. Let $\mathrm{Inj}(A, B)$ and $\mathrm{Bij}(A, B)$ represent the set of all injections and

bijections between two sets A and B, respectively. For $\psi \in \mathrm{Map}(A, B)$ bijective, there exists a unique $\psi^{-1} \in \mathrm{Map}(B, A)$, called the *inverse* of $\psi \in \mathrm{Map}(A, B)$, such that $\psi \circ \psi^{-1} = 1_B$ and $\psi^{-1} \circ \psi = 1_A$.

A *group* consists of a non-empty set G on which (1) is defined, an associative binary operation

$$(2.1) \qquad \kappa : G \times G \longrightarrow G \quad | \quad (g, h) \longmapsto gh := \kappa(g, h)$$

(2), a neutral element $n \in G$ (such that $\kappa(g, n) = g = \kappa(n, g)$ for all $g \in G$) and (3), a bijective mapping

$$(2.2) \qquad \iota : G \longrightarrow G \quad | \quad g \longmapsto g^{-1} = \iota(g),$$

defined by $\kappa(g, \iota(g)) = n = \kappa(\iota(g), g) \; \forall g \in G$, assigning to each element $g \in G$ its inverse $g^{-1} \in G$. If some subset $H \subset G$ of a group G is also a *subgroup* of G, one writes $H < G$. Let A be a non-empty set and G a group. A mapping

$$(2.3) \qquad \mathfrak{a} : G \longrightarrow \mathrm{Bij}(A, A) \quad | \quad g \longmapsto \mathfrak{a}_g = \mathfrak{a}(g)$$

is called an *action* of the group G on the set A if it is a group morphism, i.e., if

$$(2.4) \qquad \kappa_{\mathrm{Bij}(A,A)} \circ (\mathfrak{a} \times \mathfrak{a}) = \mathfrak{a} \circ \kappa_G \,,$$

where $\circ$ denotes composition of mappings or operations in this work. In particular, (2.1) induces the actions

$$(2.5) \qquad \lambda : G \longrightarrow \mathrm{Bij}(G, G) \quad | \quad g \longmapsto \lambda_g = \lambda(g)$$

and

$$(2.6) \qquad \rho : G \longrightarrow \mathrm{Bij}(G, G) \quad | \quad g \longmapsto \rho_g = \rho(g)$$

of G on itself, defined by $gh := \lambda_g(h) := \kappa(g, h)$ and $hg := \rho_g(h) := \kappa(h, g)$, respectively, for all $g, h \in G$; λ_g and ρ_g are referred to as left and right *translations* of G, respectively, for all $g \in G$. With respect to the action (2.3), the subset

$$(2.7) \qquad O_p := \{q \mid q = \mathfrak{a}_g(p) \text{ for some } g \in G\}$$

of A is called the *orbit* of $p \in A$ in A, and the subgroup

$$(2.8) \qquad G_p := \{g \in G \mid \mathfrak{a}_g(p) = p\}$$

of G the *isotropy or symmetry group* of $p \in A$. Note that $G_{\mathfrak{a}_g(p)} = (\lambda_g \circ \rho_{g^{-1}})[G_p]$ for all $p \in A$ and $g \in G$.

Let V and W represent two finite-dimensional linear spaces, $\mathrm{Lin}(V, W)$ – the set of all linear mappings, $\mathrm{Lbj}(V, W) := \mathrm{Lin}(V, W) \cap \mathrm{Bij}(V, W)$ – the set of all

linear bijections (sometimes denoted Lis(V, W))), and Lbj$^+(V, W)$ – the set of all linear bijections with positive determinant, between V and W. Any $L \in Lin(V, W)$ induces a linear mapping([1])

$$(2.9) \qquad L^* : W^* \longrightarrow V^* \quad | \quad \sigma \longmapsto \sigma \circ L =: L^*\sigma$$

between the spaces $V^* := Lin(V, \mathbb{R})$ and $W^* := Lin(W, \mathbb{R})$ *dual* to V and W, respectively. $L^* \in Lin(W^*, V^*)$ is refered to as the *dual* of $L \in Lin(V, W)$. For any finite-dimensional linear space V, we have the natural identification ($\mathbf{v} \longmapsto \iota_\mathbf{v}$) $\in Lbj(V, V^{**})$ defined by $\iota_\mathbf{v}\boldsymbol{\nu} := \boldsymbol{\nu}\mathbf{v}$ for all $\boldsymbol{\nu} \in V^*$, allowing us to treat each $\mathbf{v} \in V$ as an element $\iota_\mathbf{v} \in V^{**}$, and vice-versa. Such a relationship is usually signified by writing $\iota_\mathbf{v} \cong \mathbf{v}$ and $V^{**} \cong V$; from this, further identifications follow, such as $L^{**} \cong L$ and $Lin(V^{**}, W^{**}) \cong Lin(V, W)$. In what follows, let

$$Sym(V, V^*) \quad := \quad \{M \in Lin(V, V^*) \mid M^* \cong M\}.$$

$$(2.10) \qquad Sym^+(V, V^*) \quad := \quad \{M \in Sym(V, V^*) \mid (Mv)v > 0 \quad \forall \mathbf{v} \in V \setminus \{0\}\}.$$

$$Skw(V, V^*) \quad := \quad \{M \in Lin(V, V^*) \mid M^* \cong -M\}.$$

represent the sets of all symmetric, symmetric positive-definite, and skew-symmetric, linear mappings $M \in Lin(V, V^*)$, respectively. Again, note that $M^* \in Lin(V^{**}, V^*)$ in $(2.10)_{1,3}$ can be interpreted as an element of $Lin(V, V^*)$ via $V^{**} \cong V$, i.e., $M^* \in Lin(V, V^*)$. *From now on, such identifications will be used implicitly in this work.*

Commonly, *p-contravariant, q-covariant tensors* of, or on, a linear space V (V-tensors for short) are defined as elements of the set $Lin_{p+q}(V^{*p} \times V^q, \mathbb{R})$ of all $(p + q)$-linear mappings

$$(2.11) \qquad \mu : V^{*p} \times V^q \longrightarrow \mathbb{R} \quad | \quad (\boldsymbol{\nu}_1, \ldots, \boldsymbol{\nu}_p, \mathbf{v}_1, \ldots, \mathbf{v}_q) \longmapsto$$
$$a = \mu(\boldsymbol{\nu}_1, \ldots, \boldsymbol{\nu}_p, \mathbf{v}_1, \ldots, \mathbf{v}_q)$$

of $V^{*p} \times V^q$ into $\mathbb{R}$. Of particular interest in this work are 2-covariant and 2-contravariant tensors, i.e., members of the sets $Lin_2(V^2, \mathbb{R})$ and $Lin_2(V^{*2}, \mathbb{R})$, respectively. Each 2-covariant tensor $\mu \in Lin_2(V^2, \mathbb{R})$ can be represented by a unique linear mapping $M \in Lin(V, V^*)$ (and vice-versa) defined by

$$(2.12) \qquad (M\mathbf{v}_2)\mathbf{v}_1 := \mu(\mathbf{v}_1, \mathbf{v}_2)$$

for all $\mathbf{v}_1, \mathbf{v}_2 \in V$, inducing the natural identification $Lin_2(V^2, \mathbb{R}) \cong Lin(V, V^*)$. Analogously, any 2-contravariant tensor $\mu \in Lin_2(V^{*2}, \mathbb{R})$ can be represented by a unique linear mapping $M \in Lin(V^*, V)$ (and vice-versa) defined by

$$(2.13) \qquad (M\boldsymbol{\nu}_2)\boldsymbol{\nu}_1 := \mu(\boldsymbol{\nu}_1, \boldsymbol{\nu}_2)$$

([1])The notation $L^*\sigma := L^*(\sigma)$ in (2.9) is standard for linear mappings.

for all $\boldsymbol{\nu}_1, \boldsymbol{\nu}_2 \in V^*$, inducing $\mathrm{Lin}_2(V^{*2}, \mathbb{R}) \cong \mathrm{Lin}(V^*, V^{**}) \cong \mathrm{Lin}(V^*, V)$.

A *linear group* on a finite-dimensional linear space V is by definition a closed subgroup $\mathcal{G}$ of the group $\mathrm{Lbj}(V, V)$, i.e., the so-called general linear group, of V. Any such group acts linearly on V-tensors; indeed, on the basis of (2.3), this action is of the form

$$(2.14) \qquad \mathfrak{a} : \mathcal{G} \longrightarrow \mathrm{Lbj}(\mathrm{Lin}_{p+q}(V^{*p} \times V^q, \mathbb{R}), \mathrm{Lin}_{p+q}(V^{*p} \times V^q, \mathbb{R})) \ \ |$$
$$\mathbf{L} \longmapsto \mathfrak{a}_\mathbf{L} := \mathfrak{a}(\mathbf{L}),$$

where

$$(2.15) \qquad (\mathfrak{a}_\mathbf{L}\mu)(\boldsymbol{\nu}_1, \ldots, \boldsymbol{\nu}_p, \mathbf{v}_1, \ldots, \mathbf{v}_q) := \mu(\mathbf{L}^*\boldsymbol{\nu}_1, \ldots, \mathbf{L}^*\boldsymbol{\nu}_p, \mathbf{L}^{-1}\mathbf{v}_1, \ldots, \mathbf{L}^{-1}\mathbf{v}_q)$$

for all $\mathbf{L} \in \mathcal{G}$, $\boldsymbol{\nu}_1, \ldots, \boldsymbol{\nu}_p \in V^*$ and $\mathbf{v}_1, \ldots, \mathbf{v}_q \in V$. In particular, we have $\mathfrak{a}_\mathbf{L} k = k$ for any $k \in \mathbb{R}$, $\mathfrak{a}_\mathbf{L}\mathbf{v} = \mathbf{L}\mathbf{v}$ for all $\mathbf{v} \in V \cong V^{**}$ and $\mathfrak{a}_\mathbf{L}\boldsymbol{\nu} = \mathbf{L}^{-*}\boldsymbol{\nu}$ for all $\boldsymbol{\nu} \in V^*$, from (2.15). Note that $\mathbf{L}^{-1} \in \mathcal{G}$, $\mathbf{L}^* \in \mathrm{Lbj}(V^*, V^*)$, $\mathbf{L}^{-*} := \mathbf{L}^{-1*} = \mathbf{L}^{*-1} \in \mathrm{Lbj}(V^*, V^*)$, $\mathfrak{a}_{\mathbf{L}^{-1}} = \mathfrak{a}_\mathbf{L}^{-1} \in \mathrm{Lbj}(\mathrm{Lin}_{p+q}(V^{*p} \times V^q, \mathbb{R}), \mathrm{Lin}_{p+q}(V^{*p} \times V^q, \mathbb{R}))$, $\mathfrak{a}_\mathbf{L}\mathfrak{a}_{\mathbf{L}^{-1}} = \mathfrak{a}_\mathbf{L}\mathfrak{a}_\mathbf{L}^{-1} = 1_{\mathrm{Lin}_{p+q}(V^{*p} \times V^q, \mathbb{R})}$ and $\mathfrak{a}_{\mathbf{L}^{-1}}\mathfrak{a}_\mathbf{L} = \mathfrak{a}_\mathbf{L}^{-1}\mathfrak{a}_\mathbf{L} = 1_{\mathrm{Lin}_{p+q}(V^{*p} \times V^q, \mathbb{R})}$ for all $\mathbf{L} \in \mathcal{G}$. $\mathcal{G}$ acts in particular on the sets $\mathrm{Lin}_2(V^2, \mathbb{R})$ and $\mathrm{Lin}_2(V^{*2}, \mathbb{R})$, and so via the natural identifications $\mathrm{Lin}_2(V^2, \mathbb{R}) \cong \mathrm{Lin}(V, V^*)$ and $\mathrm{Lin}_2(V^{*2}, \mathbb{R}) \cong \mathrm{Lin}(V^*, V)$, on the sets $\mathrm{Lin}(V, V^*)$ and $\mathrm{Lin}(V^*, V)$, respectively. For example, (2.15) yields

$$(2.16) \qquad (\mathfrak{a}_\mathbf{L}\mu)(\mathbf{v}_1, \mathbf{v}_2) = \mu(\mathbf{L}^{-1}\mathbf{v}_1, \mathbf{L}^{-1}\mathbf{v}_2) = (\mathbf{ML}^{-1}\mathbf{v}_2)(\mathbf{L}^{-1}\mathbf{v}_1)$$
$$= \mathbf{L}^{-*}(\mathbf{ML}^{-1}\mathbf{v}_2)\mathbf{v}_1 = ((\mathbf{L}^{-*}\mathbf{ML}^{-1})\mathbf{v}_2)\mathbf{v}_1$$

for all $\mathbf{L} \in \mathcal{G}$, $\mu \in \mathrm{Lin}_2(V^2, \mathbb{R})$ and $\mathbf{v}_1, \mathbf{v}_2 \in V$, inducing the linear bijection

$$(2.17) \qquad \mathfrak{a}_\mathbf{L} : \mathrm{Lin}(V, V^*) \longrightarrow \mathrm{Lin}(V, V^*) \ \ | \ \ \mathbf{M} \longmapsto \mathbf{L}^{-*}\mathbf{ML}^{-1} =: \mathfrak{a}_\mathbf{L}\mathbf{M}$$

on $\mathrm{Lin}(V, V^*)$ for all $\mathbf{L} \in \mathcal{G}$ (recall that $\mathfrak{a}_\mathbf{L}\mathbf{M} := \mathfrak{a}_\mathbf{L}(\mathbf{M})$ with $\mathfrak{a}_\mathbf{L}$ linear). Likewise, (2.15) implies

$$(2.18) \qquad (\mathfrak{a}_\mathbf{L}\mu)(\boldsymbol{\nu}_1, \boldsymbol{\nu}_2) = \mu(\mathbf{L}^*\boldsymbol{\nu}_1, \mathbf{L}^*\boldsymbol{\nu}_2) = (\mathbf{ML}^*\boldsymbol{\nu}_2)(\mathbf{L}^*\boldsymbol{\nu}_1)$$
$$= \mathbf{L}(\mathbf{ML}^*\boldsymbol{\nu}_2)\boldsymbol{\nu}_1 = ((\mathbf{LML}^*)\boldsymbol{\nu}_2)\boldsymbol{\nu}_1$$

for all $\mu \in \mathrm{Lin}_2(V^{*2}, \mathbb{R})$, $\mathbf{L} \in \mathcal{G}$ and $\boldsymbol{\nu}_1, \boldsymbol{\nu}_2 \in V^*$, inducing the linear bijection

$$(2.19) \qquad \mathfrak{a}_\mathbf{L} : \mathrm{Lin}(V^*, V) \longrightarrow \mathrm{Lin}(V^*, V) \ \ | \ \ \mathbf{M} \longmapsto \mathbf{LML}^* =: \mathfrak{a}_\mathbf{L}\mathbf{M}$$

on $\mathrm{Lin}(V^*, V)$ for all $\mathbf{L} \in \mathcal{G}$.

An *inner product space* is a linear space V endowed with the additional structure of a symmetric, positive-definite linear mapping $\mathbf{G} \in \mathrm{Sym}^+(V, V^*)$, which we

will call a *metric* (on V) in this work. Using $\mathbf{G} \in \mathrm{Sym}^+(V, V^*)$, one defines in the usual way the *inner product*

$$(2.20) \qquad\qquad \mathbf{u} \cdot \mathbf{w} := (\mathbf{G}\mathbf{u})\mathbf{w}$$

on V for all $\mathbf{u}, \mathbf{w} \in V$. Likewise, $\mathbf{G}^{-1} \in \mathrm{Sym}^+(V^*, V)$ can be intepreted as an inner product of covectors, i.e.,

$$(2.21) \qquad\qquad \boldsymbol{\nu} \star \boldsymbol{\sigma} := \boldsymbol{\nu}(\mathbf{G}^{-1}\boldsymbol{\sigma}) = (\mathbf{G}^{-1}\boldsymbol{\nu}) \cdot (\mathbf{G}^{-1}\boldsymbol{\sigma})$$

for all $\boldsymbol{\nu}, \boldsymbol{\sigma} \in V^*$. Any linear mapping $\mathbf{L} \in \mathrm{Lin}(V, W)$ between two such inner product spaces V and W with metrics $\mathbf{G}_V \in \mathrm{Sym}^+(V, V^*)$ and $\mathbf{G}_W \in \mathrm{Sym}^+(W, W^*)$, respectively, induces the linear mapping

$$(2.22) \qquad\qquad \mathbf{L}^\mathsf{T} := \mathbf{G}_V^{-1} \mathbf{L}^* \mathbf{G}_W \in \mathrm{Lin}(W, V)$$

called the *transpose* of $\mathbf{L} \in \mathrm{Lin}(V, W)$. A linear mapping $\mathbf{Q} \in \mathrm{Lin}(V, W)$ between two inner product spaces V and W is called *orthogonal* if $\mathbf{Q}^* \mathbf{G}_W \mathbf{Q} = \mathbf{G}_V$. As usual, let $\mathrm{Orth}(V, W)$ represent the set of all such linear mappings. From the definition (2.22) of the transpose, then, $\mathbf{Q}^* \mathbf{G}_W \mathbf{Q} = \mathbf{G}_V \mathbf{Q}^\mathsf{T}\mathbf{Q} = \mathbf{G}_V$ holds for all $\mathbf{Q} \in \mathrm{Orth}(V, W)$, implying $\mathbf{Q}^\mathsf{T}\mathbf{Q} = \mathbf{1}_V$, and in particular $\mathbf{Q}^\mathsf{T} = \mathbf{Q}^{-1}$ if $\dim V = \dim W$. As usual, let

$$
\begin{aligned}
\mathrm{Uni}^+(V, V) &:= \{\mathbf{L} \in \mathrm{Lin}(V, V) \mid \det(\mathbf{L}) = +1\}, \\
\mathrm{Sym}(V, V) &:= \{\mathbf{L} \in \mathrm{Lin}(V, V) \mid \mathbf{L}^\mathsf{T} = \mathbf{L}\}, \\
(2.23) \quad \mathrm{Sym}^+(V, V) &:= \{\mathbf{L} \in \mathrm{Sym}(V, V) \mid \mathbf{L}\mathbf{v} \cdot \mathbf{v} > 0 \quad \forall \mathbf{v} \in V \setminus \{\mathbf{0}\}\}, \\
\mathrm{Skw}(V, V) &:= \{\mathbf{L} \in \mathrm{Lin}(V, V) \mid \mathbf{L}^\mathsf{T} = -\mathbf{L}\}, \\
\mathrm{Orth}^+(V, V) &:= \mathrm{Orth}(V, V) \cap \mathrm{Uni}^+(V, V),
\end{aligned}
$$

denote the sets of all unimodular with positive determinant, symmetric, symmetric positive-definite, skew-symmetric, orthogonal, and orthogonal with positive determinant, linear mappings of V into itself, respectively.

As is well-known, a metric $\mathbf{G} \in \mathrm{Sym}^+(V, V^*)$ and its inverse $\mathbf{G}^{-1} \in \mathrm{Sym}^+(V^*, V)$ induce the operation of forming *associated tensors* (e.g., ABRAHAM *et al.* [5, §5.1]), often called "lowering and raising indices," respectively. Via linearity and duality, this operation can be extended to tensors of arbitrary order. In particular, $\mathbf{G}$ and its inverse induce the linear bijections

$$(2.24) \qquad \ell_\mathbf{G} : \mathrm{Lin}(V, V) \longrightarrow \mathrm{Lin}(V, V^*) \mid \mathbf{M} \longmapsto \mathbf{G}\mathbf{M} =: \ell_\mathbf{G}\mathbf{M},$$

$$(2.25) \qquad \ell_{\mathbf{G}^{-1}} : \mathrm{Lin}(V, V^*) \longrightarrow \mathrm{Lin}(V, V) \mid \mathbf{M} \longmapsto \mathbf{G}^{-1}\mathbf{M} =: \ell_{\mathbf{G}^{-1}}\mathbf{M},$$

$$(2.26) \qquad r_{\mathbf{G}} : \mathrm{Lin}(\mathcal{V}^*, \mathcal{V}) \longrightarrow \mathrm{Lin}(\mathcal{V}, \mathcal{V}) \quad | \quad \mathbf{M} \longmapsto \mathbf{MG} =: r_{\mathbf{G}}\mathbf{M}$$

and

$$(2.27) \qquad r_{\mathbf{G}^{-1}} : \mathrm{Lin}(\mathcal{V}, \mathcal{V}) \longrightarrow \mathrm{Lin}(\mathcal{V}^*, \mathcal{V}) \quad | \quad \mathbf{M} \longmapsto \mathbf{MG}^{-1} =: r_{\mathbf{G}^{-1}}\mathbf{M}$$

induced by $\mathbf{G}$ and $\mathbf{G}^{-1}$ on second-order $\mathcal{V}$-tensors.

The action (2.14) of $\mathcal{G}$ on $\mathcal{V}$-tensors, together with the operation of form-ing associated $\mathcal{V}$-tensors, induces various kinds of *associated actions* of $\mathcal{G}$ on $\mathcal{V}$-tensors. In particular, the actions (2.17) and (2.19), respectively, combined with the associated-tensor operations (2.24)–(2.25) and (2.26)–(2.27), respectively, in-duce two *associated actions* of $\mathcal{G}$ on $\mathrm{Lin}(\mathcal{V}, \mathcal{V})$, as follows. From (2.17), we have the induced associated action

$$(2.28) \qquad \mathfrak{a}_{\mathbf{L}}^{\ell} : \mathrm{Lin}(\mathcal{V}, \mathcal{V}) \longrightarrow \mathrm{Lin}(\mathcal{V}, \mathcal{V}) \quad | \quad \mathbf{M} \longmapsto \mathbf{G}^{-1}\mathbf{L}^{-*}(\mathbf{GM})\mathbf{L}^{-1}$$
$$= \mathbf{L}^{-\mathsf{T}}\mathbf{ML}^{-1} =: \mathfrak{a}_{\mathbf{L}}^{\ell}\mathbf{M}$$

of $\mathcal{G}$ on $\mathrm{Lin}(\mathcal{V}, \mathcal{V})$ for all $\mathbf{L} \in \mathcal{G}$ via (2.22). In terms of the associated tensor operations (2.24) and (2.25), this last action takes the form

$$(2.29) \qquad\qquad \mathfrak{a}_{\mathbf{L}}^{\ell} := \ell_{\mathbf{G}^{-1}} \circ \mathfrak{a}_{\mathbf{L}} \circ \ell_{\mathbf{G}} \, ,$$

with $\mathfrak{a}_{\mathbf{L}}$ given by (2.17).

Likewise, (2.19) induces the associated action

$$(2.30) \qquad \mathfrak{a}_{\mathbf{L}}^{r} : \mathrm{Lin}(\mathcal{V}, \mathcal{V}) \longrightarrow \mathrm{Lin}(\mathcal{V}, \mathcal{V}) \quad | \quad \mathbf{M} \longmapsto \mathbf{L}(\mathbf{MG}^{-1})\mathbf{L}^*\mathbf{G}^{-1}$$
$$= \mathbf{LML}^{\mathsf{T}} =: \mathfrak{a}_{\mathbf{L}}^{r}\mathbf{M}$$

of $\mathcal{G}$ on $\mathrm{Lin}(\mathcal{V}, \mathcal{V})$ for all $\mathbf{L} \in \mathcal{G}$, where

$$(2.31) \qquad\qquad \mathfrak{a}_{\mathbf{L}}^{r} := r_{\mathbf{G}} \circ \mathfrak{a}_{\mathbf{L}} \circ r_{\mathbf{G}^{-1}}$$

follows from (2.19), (2.26) and (2.27).

Let $\mathcal{V}$ represent 3-dimensional Euclidean translation (i.e., vector) space, and ϖ the standard volume covector of $\mathcal{V}$, i.e.,

$$(2.32) \qquad \varpi(\mathbf{v}_1, \mathbf{v}_2, \mathbf{v}_3) := (\mathbf{v}_1 \times \mathbf{v}_2) \cdot \mathbf{v}_3 = (\mathbf{G}(\mathbf{v}_1 \times \mathbf{v}_2))\mathbf{v}_3 \qquad \forall \, \mathbf{v}_1, \mathbf{v}_2, \mathbf{v}_3 \in \mathcal{V} \, .$$

In terms of the interior product operation

$$(2.33) \qquad\qquad (\iota_{\mathbf{v}}\mu)(\mathbf{v}_1, \ldots, \mathbf{v}_{q-1}) := \mu(\mathbf{v}, \mathbf{v}_1, \ldots, \mathbf{v}_{q-1})$$

for all $\mathbf{v}_1, \ldots, \mathbf{v}_{q-1}, \mathbf{v} \in \mathcal{V}$ and $\mu \in \mathrm{Lin}_q(\mathcal{V}^q, \mathbb{R})$ (e.g., ABRAHAM *et al.* [5, §6.4]), $\varpi(\mathbf{v}_1, \mathbf{v}_2, \mathbf{v}_3)$ can also be written in the form

$$(2.34) \qquad\qquad \varpi(\mathbf{v}_1, \mathbf{v}_2, \mathbf{v}_3) = \iota_{\mathbf{v}_3} \iota_{\mathbf{v}_2} \iota_{\mathbf{v}_1} \varpi = (\iota_{\mathbf{v}_2} \iota_{\mathbf{v}_1} \varpi)\mathbf{v}_3$$

for all $v_1, v_2, v_3 \in V$; note that $(\iota_{v_2} \iota_{v_1} \varpi) \in V^*$ for all $v_1, v_2 \in V$. Combining (2.32) and (2.34) yields the relation

$$(2.35) \qquad v_1 \times v_2 = G^{-1}(\iota_{v_2} \iota_{v_1} \varpi) \qquad \forall\, v_1, v_2 \in V$$

for the Euclidean cross-product used in this work. Note that $v_1 \times v_2 \in V$ and $(\iota_{v_2} \iota_{v_1} \varpi) \in V^*$ are *associated* tensors.

3. Basic kinematics

Let E represent 3-dimensional Euclidean point space with translation space V endowed with the Euclidean metric $G \in \mathrm{Sym}^+(V.V^*)$, $I \subset \mathbb{R}$ a time interval, and $B_\kappa \subset E$ the region in E occupied by a material body in some reference configuration. A motion of this body in E relative to B_κ takes the form

$$(3.1) \qquad \zeta_\kappa : I \times B_\kappa \longrightarrow E \mid (t,b) \longmapsto p = \zeta_\kappa(t,b),$$

such that the C^2 curve $\zeta_{\kappa b} := \zeta_\kappa(\cdot,b) \in C^2(I.E)$ represents the motion of $b \in B_\kappa$ in E for all $b \in B_\kappa$, and the C^k ($k \geq 1$) diffeomorphism[2] $\zeta_{\kappa t} : B_\kappa \to B_t$ – the *deformation* of $B_\kappa \subset E$ onto the region $B_t := \zeta_{\kappa t}[B_\kappa] \subset E$ in E occupied by the material body at the present time $t \in I$.

In this paper, we work with fields on both B_κ and B_t. Note that any time-dependent *referential* field

$$(3.2) \qquad \psi_\kappa : I \times B_\kappa \longrightarrow A \mid (t,b) \longmapsto \psi_\kappa(t,b)$$

with values in some set A can be represented as a time-dependent *spatial* field

$$(3.3) \qquad \psi_t : B_t \longrightarrow A \mid p \longmapsto \psi_{\kappa t}(\zeta_{\kappa t}^{-1}(p)) =: \psi_t(p).$$

i.e.,

$$(3.4) \qquad \psi_{\kappa t} = \psi_t \circ \zeta_{\kappa t}$$

for all $t \in I$ via the deformation $\zeta_{\kappa t} : B_\kappa \to B_t$. It will be useful in this work to express this last relation in the form of the operations

$$(3.5) \qquad c_{\zeta_{\kappa t}}(\psi_t) := \psi_t \circ \zeta_{\kappa t} = \psi_{\kappa t} \qquad \text{and} \qquad c_{\zeta_{\kappa t}^{-1}}(\psi_{\kappa t}) := \psi_{\kappa t} \circ \zeta_{\kappa t}^{-1} = \psi_t$$

relating $\psi_{\kappa t}$ and ψ_t.

As usual, the time-dependent vector

$$(3.6) \qquad \partial \zeta_{\kappa b} : I \longrightarrow V \mid t \longmapsto \lim_{\epsilon \to 0} \frac{1}{\epsilon}[\zeta_{\kappa b}(t+\epsilon) - \zeta_{\kappa b}(t)] =: \partial \zeta_{\kappa b}(t)$$

---

[2] Induced by the C^k injection $\zeta_{\kappa t} : B_\kappa \to E$. We use the same symbol $\zeta_{\kappa t}$ for both, for simplicity.

represents the velocity of $b \in B_\kappa$ in E for all $b \in B_\kappa$. From this, one obtains the *referential velocity*

$$(3.7) \qquad \partial \zeta_\kappa : I \times B_\kappa \longrightarrow V \quad | \quad (t,b) \longmapsto \partial \zeta_{\kappa b}(t) =: \partial \zeta_\kappa(t,b)$$

of the body, i.e., relative to B_κ. Likewise, the *spatial velocity* of the body is given, as usual, by the explicitly time-dependent vector field

$$(3.8) \qquad \mathbf{v}_t : B_t \longrightarrow V \quad | \quad p \longmapsto \partial \zeta_\kappa(t, \zeta_{\kappa t}^{-1}(p)) =: \mathbf{v}_t(p)$$

on B_t for all $t \in I$, such that $\mathbf{v}_t = (\partial \zeta_\kappa)_t \circ \zeta_{\kappa t}^{-1}$. The definition of the spatial velocity also implies the *flow relation*

$$(3.9) \qquad \partial \zeta_{\kappa t} = \mathbf{v}_t \circ \zeta_{\kappa t} : B_\kappa \longrightarrow V$$

of the body in E relative to B_κ for all $t \in I$.

The Fréchet derivative of the deformation $\zeta_{\kappa t} : B_\kappa \to B_t$ at each $t \in I$ defines the *deformation gradient*

$$(3.10) \qquad \mathbf{F}_\kappa : I \times B_\kappa \longrightarrow \mathrm{Lbj}^+(V, V) \quad | \quad (t,b) \longmapsto (D_b \zeta_{\kappa t}) =: \mathbf{F}_{\kappa t}(b) = \mathbf{F}_\kappa(t,b)$$

with respect to B_κ. In this work, we make use of the *polar decomposition*

$$(3.11) \qquad \mathbf{F}_\kappa = \mathbf{R}_\kappa \mathbf{U}_\kappa = \mathbf{V}_\kappa \mathbf{R}_\kappa$$

of $\mathbf{F}_\kappa$, where

$$(3.12) \qquad \mathbf{V}_\kappa : I \times B_\kappa \longrightarrow \mathrm{Sym}^+(V, V) \quad | \quad (t,b) \longmapsto \mathbf{V}_\kappa(t,b)$$

represents the left stretch tensor,

$$(3.13) \qquad \mathbf{U}_\kappa : I \times B_\kappa \longrightarrow \mathrm{Sym}^+(V, V) \quad | \quad (t,b) \longmapsto \mathbf{U}_\kappa(t,b)$$

the right stretch tensor, and

$$(3.14) \qquad \mathbf{R}_\kappa : I \times B_\kappa \longrightarrow \mathrm{Orth}^+(V, V) \quad | \quad (t,b) \longmapsto \mathbf{R}_\kappa(t,b)$$

the rotation. Note that the relation $\mathbf{1}_{B_t} = \zeta_{\kappa t} \circ \zeta_{\kappa t}^{-1}$ and the chain rule yield

$$(3.15) \qquad \mathbf{1}_V = [(D\zeta_{\kappa t}) \circ \zeta_{\kappa t}^{-1}](D\zeta_{\kappa t}^{-1}),$$

and so

$$(3.16) \qquad (D\zeta_{\kappa t})^{-1} = (D\zeta_{\kappa t}^{-1}) \circ \zeta_{\kappa t} \qquad \text{and} \qquad (D\zeta_{\kappa t}^{-1}) = (D\zeta_{\kappa t})^{-1} \circ \zeta_{\kappa t}^{-1}.$$

since $(D_p 1_{B_t}) = 1_V$ for all $p \in B_t$. Lastly, the time derivative of (3.10) at time $t \in I$ yields

$$(3.17) \qquad (\partial \mathbf{F}_\kappa)_t = D(\partial \zeta_\kappa)_t = D(\mathbf{v}_t \circ \zeta_{\kappa t}) = [(D\mathbf{v}_t) \circ \zeta_{\kappa t}](D\zeta_{\kappa t})$$
$$= [\mathbf{L}_t \circ \zeta_{\kappa t}] \mathbf{F}_{\kappa t} = \mathbf{L}_{\kappa t} \mathbf{F}_{\kappa t}$$

via (3.9) and the chain rule, where

$$(3.18) \qquad \mathbf{L}_t : B_t \longrightarrow \mathrm{Lin}(V, V) \quad | \quad p \longmapsto (D_p \mathbf{v}_t) =: \mathbf{L}_t(p)$$

represents the *spatial velocity gradient*, with symmetric

$$(3.19) \qquad \mathbf{D}_t : B_t \longrightarrow \mathrm{Sym}(V, V) \quad | \quad p \longmapsto \mathrm{sym}(\mathbf{L}_t(p))$$
$$:= \frac{1}{2}\{\mathbf{L}_t(p) + \mathbf{L}_t^{\mathrm{T}}(p)\} =: \mathbf{D}_t(p)$$

and skew-symmetric

$$(3.20) \qquad \mathbf{W}_t : B_t \longrightarrow \mathrm{Skw}(V, V) \quad | \quad p \longmapsto \mathrm{skw}(\mathbf{L}_t(p))$$
$$:= \frac{1}{2}\{\mathbf{L}_t(p) - \mathbf{L}_t^{\mathrm{T}}(p)\} =: \mathbf{W}_t(p)$$

parts, i.e., $\mathbf{D}_t := \mathrm{sym}(\mathbf{L}_t)$ and $\mathbf{W}_t := \mathrm{skw}(\mathbf{L}_t)$ for all $t \in I$.

4. Basic strain tensors based on line elements

The strain tensors of the first family of HT are based on the deformation of "material line elements," which represent in essence *tangent vector fields*, as we now briefly review. Let $B_\gamma \subset E$ be any configuration of a material body in E and let $C^1(\mathbb{R}, E)_p$ represent the set of all C^1 curves at the point $p \in B_\gamma$, i.e., C^1 injective mappings $c : \mathbb{N}_0 \longrightarrow E$ of some neighborhood $\mathbb{N}_0 \subset \mathbb{R}$ of $0 \in \mathbb{R}$ into E such that $c(0) = p$. Two such curves $c_1, c_2 \in C^1(\mathbb{R}, E)_p$ at $p \in B_\gamma$ are said to be *tangent at* $p \in B_\gamma$ if their tangent vectors are equal there, i.e., if $\partial_0 c_1 = \partial_0 c_2 \in V$, with $\partial_0 c_i := \partial c_i(0)$ ($i = 1,2$). Since the members of each resulting equivalence class $[c]_p$ all possess the same tangent vector $\partial_0 c \in V$ at $p \in B_\gamma$, each $[c]_p$ at $p \in B_\gamma$ is represented uniquely by $\partial_0 c \in V$. A *field* of such equivalence classes, or equivalently, their corresponding tangent vectors, on $B_\gamma \subset E$ then defines a *tangent vector field*

$$(4.1) \qquad \mathbf{u}_\gamma : B_\gamma \longrightarrow V \quad | \quad p \longmapsto \mathbf{u} = \mathbf{u}_\gamma(p)$$

on $B_\gamma \subset E$ such that $\mathbf{u}_\gamma(p) = \partial_0 c$ for some equivalence class $[c]_p$ at each $p \in B_\gamma$.

The deformation $\zeta_{\kappa t}: B_\kappa \to B_t$ of B_κ into B_t maps any C^1 curve $c \in C^1(\mathbb{R}, E)_b$ at $b = c(0) \in B_\kappa$ onto the C^1 curve $(\zeta_{\kappa t} \circ c) \in C^1(\mathbb{R}, E)_{\zeta_{\kappa t}(b)}$ at $\zeta_{\kappa t}(b) \in B_t$; consequently,

$$(4.2) \qquad \partial_0(\zeta_{\kappa t} \circ c) = (D_b\zeta_{\kappa t})\,\partial_0 c = \mathbf{F}_{\kappa t}(b)\,\partial_0 c$$

via the chain rule and (3.10). Substituting the tangent vector field relations $\partial_0(\zeta_{\kappa t} \circ c) = \mathbf{u}_{\zeta_{\kappa t}}(\zeta_{\kappa t}(b))$ and $\partial_0 c = \mathbf{u}_\kappa(b)$ into (4.2), we obtain

$$(4.3) \qquad \mathbf{u}_{\zeta_{\kappa t}}(\zeta_{\kappa t}(b)) = (D_b\zeta_{\kappa t})\,\mathbf{u}_\kappa(b) = \mathbf{F}_{\kappa t}(b)\,\mathbf{u}_\kappa(b)$$

at $b \in B_\kappa$. Letting $b \in B_\kappa$ vary yields then the field relation

$$(4.4) \qquad \mathbf{u}_{\zeta_{\kappa t}} \circ \zeta_{\kappa t} = (D\zeta_{\kappa t})\,\mathbf{u}_\kappa = \mathbf{F}_{\kappa t}\,\mathbf{u}_\kappa \,.$$

Introducing now the "push-forward"

$$(4.5) \qquad \zeta_{\kappa t*}\mu_{\kappa t} := [\mathbf{a}_{(D\zeta_{\kappa t})}\mu_\kappa] \circ \zeta_{\kappa t}^{-1}$$

and "pull-back"

$$(4.6) \qquad \zeta_{\kappa t}^*\mu_t := [\mathbf{a}_{(D\zeta_{\kappa t}^{-1})}\mu_t] \circ \zeta_{\kappa t}$$

operations[3] on referential $\mu_{\kappa t}: B_\kappa \to \mathrm{Lin}_{p+q}(V^{*p} \times V^q, \mathbb{R})$ and spatial $\mu_t: B_t \to \mathrm{Lin}_{p+q}(V^{*p} \times V^q, \mathbb{R})$ tensor fields via (2.15), (4.3) can also be written in the "push-forward"

$$(4.7) \qquad \mathbf{u}_{\zeta_{\kappa t}} = \zeta_{\kappa t*}\mathbf{u}_\kappa = [\mathbf{a}_{(D\zeta_{\kappa t})}\mathbf{u}_\kappa] \circ \zeta_{\kappa t}^{-1} = [(D\zeta_{\kappa t})\mathbf{u}_\kappa] \circ \zeta_{\kappa t}^{-1}$$

$$= (D\zeta_{\kappa t}^{-1})^{-1}(\mathbf{u}_\kappa \circ \zeta_{\kappa t}^{-1})$$

and "pull-back"

$$(4.8) \qquad \mathbf{u}_\kappa = \zeta_{\kappa t}^*\mathbf{u}_{\zeta_{\kappa t}} = [\mathbf{a}_{(D\zeta_{\kappa t}^{-1})}\mathbf{u}_{\zeta_{\kappa t}}] \circ \zeta_{\kappa t} = [(D\zeta_{\kappa t}^{-1})\mathbf{u}_{\zeta_{\kappa t}}] \circ \zeta_{\kappa t}$$

$$= (D\zeta_{\kappa t})^{-1}(\mathbf{u}_{\zeta_{\kappa t}} \circ \zeta_{\kappa t})$$

forms, where use was made of (3.16) to write the right-hand forms of (4.7) and (4.8). With the help of (3.5) and (3.10), note that (4.5) and (4.6) imply the forms

$$(4.9) \qquad \zeta_{\kappa t*} = \mathbf{c}_{\zeta_{\kappa t}^{-1}} \circ \mathbf{a}_{\mathbf{F}_{\kappa t}}$$

----

[3] Such operations on tensors fields, are in general, induced by diffeomorphism between manifolds (e.g., ABRAHAM et al. [5, §5.1]).

and

(4.10)
$$\overset{*}{\zeta}_{\kappa t} = \mathfrak{a}_{F_{\kappa t}^{-1}} \circ \mathfrak{c}_{\zeta_{\kappa t}} \, ,$$

respectively, for the push-forward $\zeta_{\kappa t *}$ and pull-back $\overset{*}{\zeta}_{\kappa t}$ operators induced by $\zeta_{\kappa t} : B_\kappa \to B_t$ on tensor fields associated with B_κ and B_t, respectively.

As usual, the *change in squared length* of any referential tangent vector field $\mathbf{u}_\kappa$ due to the deformation $\zeta_{\kappa t}$ can be represented on, or relative to, B_κ via the time-dependent function

(4.11) $$\Delta_\kappa : I \times B_\kappa \longrightarrow \mathbb{R} \quad | \quad (t, b) \longmapsto \frac{1}{2} \Big\{ \mathbf{u}_{\zeta_{\kappa t}} (\zeta_{\kappa t}(b)) \cdot \mathbf{u}_{\zeta_{\kappa t}} (\zeta_{\kappa t}(b)) $$
$$- \mathbf{u}_\kappa(b) \cdot \mathbf{u}_\kappa(b) \Big\} =: \Delta_\kappa(t, b)$$

on B_κ. By definition, then,

(4.12) $$\Delta_{\kappa t} = \frac{1}{2} \Big\{ \overset{*}{\zeta}_{\kappa t} (\mathbf{u}_{\zeta_{\kappa t}} \cdot \mathbf{u}_{\zeta_{\kappa t}}) - \mathbf{u}_\kappa \cdot \mathbf{u}_\kappa \Big\} : B_\kappa \longrightarrow \mathbb{R}$$

holds for each $t \in I$, where

(4.13) $$\overset{*}{\zeta}_{\kappa t} (\mathbf{u}_{\zeta_{\kappa t}} \cdot \mathbf{u}_{\zeta_{\kappa t}}) = (\mathbf{u}_{\zeta_{\kappa t}} \cdot \mathbf{u}_{\zeta_{\kappa t}}) \circ \zeta_{\kappa t} = (\mathbf{u}_{\zeta_{\kappa t}} \circ \zeta_{\kappa t}) \cdot (\mathbf{u}_{\zeta_{\kappa t}} \circ \zeta_{\kappa t})$$

represents the pull-back of the squared length $(\mathbf{u}_{\zeta_{\kappa t}} \cdot \mathbf{u}_{\zeta_{\kappa t}}) \in C^0(B_t, \mathbb{R}^+)$, a function on B_t, by $\zeta_{\kappa t}$. From (2.9), (2.20) and (4.3), we have

(4.14)
$$\overset{*}{\zeta}_{\kappa t} (\mathbf{u}_{\zeta_{\kappa t}} \cdot \mathbf{u}_{\zeta_{\kappa t}}) = (\mathbf{u}_{\zeta_{\kappa t}} \circ \zeta_{\kappa t}) \cdot (\mathbf{u}_{\zeta_{\kappa t}} \circ \zeta_{\kappa t}),$$
$$= [\mathbf{G}(\mathbf{u}_{\zeta_{\kappa t}} \circ \zeta_{\kappa t})](\mathbf{u}_{\zeta_{\kappa t}} \circ \zeta_{\kappa t}).$$
$$= [\mathbf{G}(D\zeta_{\kappa t})\mathbf{u}_\kappa](D\zeta_{\kappa t})\mathbf{u}_\kappa .$$
$$= [(D\zeta_{\kappa t})^* \mathbf{G}(D\zeta_{\kappa t})\mathbf{u}_\kappa]\mathbf{u}_\kappa ,$$

where $(D\zeta_{\kappa t})^*$ represents the dual of the deformation gradient $(D\zeta_{\kappa t})$ (see (2.9)). On the other hand, (2.17) and (4.6) yield

(4.15) $$\overset{*}{\zeta}_{\kappa t} \mathbf{G} = \mathfrak{a}_{F_{\kappa t}^{-1}} \mathbf{G} = \mathbf{F}_{\kappa t}^* \mathbf{G} \mathbf{F}_{\kappa t} = (D\zeta_{\kappa t})^* \mathbf{G} (D\zeta_{\kappa t})$$

(recall that $\mathbf{G} \in \mathrm{Lin}(V, V^*)$). Comparing (4.14) and (4.15), we obtain

(4.16) $$\overset{*}{\zeta}_{\kappa t} (\mathbf{u}_{\zeta_{\kappa t}} \cdot \mathbf{u}_{\zeta_{\kappa t}}) = \overset{*}{\zeta}_{\kappa t} [(\mathbf{G}\mathbf{u}_{\zeta_{\kappa t}})\mathbf{u}_{\zeta_{\kappa t}}] = [(\overset{*}{\zeta}_{\kappa t}\mathbf{G})(\overset{*}{\zeta}_{\kappa t}\mathbf{u}_{\zeta_{\kappa t}})](\overset{*}{\zeta}_{\kappa t}\mathbf{u}_{\zeta_{\kappa t}})$$
$$= [(\overset{*}{\zeta}_{\kappa t}\mathbf{G})\mathbf{u}_\kappa]\mathbf{u}_\kappa$$

via (4.8). With the help of the transposed form

$$(4.17) \qquad (D\zeta_{\kappa t})^{\mathrm{T}} := \mathbf{G}^{-1}\,(D\zeta_{\kappa t})^{*}\,\mathbf{G}$$

of $(D\zeta_{\kappa t})$ via (2.22), from which follows the relation $(D\zeta_{\kappa t})^{*}\,\mathbf{G} = \mathbf{G}\,(D\zeta_{\kappa t})^{\mathrm{T}}$, (4.15) takes the more familiar form

$$(4.18) \qquad \zeta_{\kappa t}^{*}\mathbf{G} = \mathbf{G}\,(D\zeta_{\kappa t})^{\mathrm{T}}\,(D\zeta_{\kappa t}) = \mathbf{G}\mathbf{C}_{\kappa t}\,,$$

where

$$(4.19) \qquad \mathbf{C}_{\kappa t} := (D\zeta_{\kappa t})^{\mathrm{T}}\,(D\zeta_{\kappa t}) = \mathbf{F}_{\kappa t}^{\mathrm{T}}\,\mathbf{F}_{\kappa t} = \mathbf{G}^{-1}(\zeta_{\kappa t}^{*}\mathbf{G})$$

represents the *right Cauchy – Green tensor* for all $t \in I$, i.e.,

$$(4.20) \qquad \mathbf{C}_{\kappa} : I \times B_{\kappa} \;\longrightarrow\; \mathrm{Sym}^{+}(\mathcal{V}, \mathcal{V}) \quad | \quad (t, b) \longmapsto (D_{b}\zeta_{\kappa t})^{\mathrm{T}}\,(D_{b}\zeta_{\kappa t})$$
$$= \mathbf{F}_{\kappa}^{\mathrm{T}}(t, b)\,\mathbf{F}_{\kappa}(t, b) =: \mathbf{C}_{\kappa}(t, b).$$

Clearly, (4.18) implies that $\zeta_{\kappa t}^{*}\mathbf{G}$ represents a tensor *associated* with the right Cauchy – Green tensor $\mathbf{C}_{\kappa t}$. In terms of the associated tensor operations (2.24) and (2.25), as well as the associated action (2.29) and pull-back (4.10) operations, $\mathbf{C}_{\kappa t}$ takes the form

$$(4.21) \qquad \mathbf{C}_{\kappa t} = \mathfrak{a}_{\mathbf{F}_{\kappa t}^{-1}}^{\ell}\mathbf{1}_{\mathcal{V}} = \{\ell_{\mathbf{G}^{-1}} \circ \zeta_{\kappa t}^{*} \circ \ell_{\mathbf{G}}\}\mathbf{1}_{\mathcal{V}} := \ell_{\mathbf{G}^{-1}}[\zeta_{\kappa t}^{*}(\ell_{\mathbf{G}}\mathbf{1}_{\mathcal{V}})] = \mathbf{G}^{-1}(\zeta_{\kappa t}^{*}\mathbf{G})$$

for all $t \in I$, taking (4.15) into account. Substituting (4.16)$_3$ into (4.12) yields

$$(4.22) \qquad \begin{aligned} \Delta_{\kappa t} &= \frac{1}{2}\,[(\zeta_{\kappa t}^{*}\mathbf{G} - \mathbf{G})\mathbf{u}_{\kappa}]\mathbf{u}_{\kappa}, \\[4pt] &= \frac{1}{2}\,[\mathbf{G}(\mathbf{C}_{\kappa t} - \mathbf{1}_{\mathcal{V}})\mathbf{u}_{\kappa}]\mathbf{u}_{\kappa}, \\[4pt] &= [\mathbf{G}(\mathbf{E}_{\kappa t}\mathbf{u}_{\kappa})]\mathbf{u}_{\kappa}, \\[4pt] &= \mathbf{E}_{\kappa t}\mathbf{u}_{\kappa} \cdot \mathbf{u}_{\kappa}, \end{aligned}$$

via (4.18), where

$$(4.23) \qquad \mathbf{E}_{\kappa} : I \times B_{\kappa} \;\longrightarrow\; \mathrm{Sym}(\mathcal{V}, \mathcal{V}) \quad | \quad (t, p) \longmapsto \frac{1}{2}\,(\mathbf{C}_{\kappa}(t, b) - \mathbf{1}_{\mathcal{V}}) =: \mathbf{E}_{\kappa}(t, p)$$

represents as usual the *Green strain tensor*, such that $\mathbf{E}_{\kappa t} = \frac{1}{2}\,(\mathbf{C}_{\kappa t} - \mathbf{1}_{\mathcal{V}})$ for all $t \in I$.

Pushing the strain measure $\Delta_{\kappa t}$ defined in (4.12) forward to B_t yields

$$(4.24) \qquad \Delta_t : B_t \longrightarrow \mathbb{R} \quad | \quad p \longmapsto \frac{1}{2}\Big\{\mathbf{u}_{\zeta_{\kappa t}}(p) \cdot \mathbf{u}_{\zeta_{\kappa t}}(p)$$
$$-\mathbf{u}_\kappa(\zeta_{\kappa t}^{-1}(p)) \cdot \mathbf{u}_\kappa(\zeta_{\kappa t}^{-1}(p))\Big\} =: \Delta_t(p)$$

or

$$(4.25) \qquad \Delta_t := \frac{1}{2}\Big\{\mathbf{u}_{\zeta_{\kappa t}} \cdot \mathbf{u}_{\zeta_{\kappa t}} - \zeta_{\kappa t *}(\mathbf{u}_\kappa \cdot \mathbf{u}_\kappa)\Big\} \ .$$

such that $\Delta_t = \zeta_{\kappa t *}\Delta_{\kappa t} = \Delta_{\kappa t} \circ \zeta_{\kappa t}^{-1}$ or, equivalently, $\Delta_{\kappa t} = \zeta_{\kappa t}^* \Delta_t = \Delta_t \circ \zeta_{\kappa t}$ for all $t \in I$. Analogous to (4.14),

$$(4.26) \qquad \begin{aligned} \zeta_{\kappa t *}(\mathbf{u}_\kappa \cdot \mathbf{u}_\kappa) &= (\mathbf{u}_\kappa \circ \zeta_{\kappa t}^{-1}) \cdot (\mathbf{u}_\kappa \circ \zeta_{\kappa t}^{-1}), \\ &= [\mathbf{G}(\mathbf{u}_\kappa \circ \zeta_{\kappa t}^{-1})](\mathbf{u}_\kappa \circ \zeta_{\kappa t}^{-1}), \\ &= [\mathbf{G}(D\zeta_{\kappa t}^{-1})\mathbf{u}_{\zeta_{\kappa t}}](D\zeta_{\kappa t}^{-1})\mathbf{u}_{\zeta_{\kappa t}}, \\ &= [(D\zeta_{\kappa t}^{-1})^*\mathbf{G}(D\zeta_{\kappa t}^{-1})\mathbf{u}_{\zeta_{\kappa t}}]\mathbf{u}_{\zeta_{\kappa t}}. \end{aligned}$$

holds via (2.9), (2.20) and (4.7). Comparing this last relation with the result

$$(4.27) \qquad \zeta_{\kappa t *}\mathbf{G} = \{\mathfrak{c}_{\zeta_{\kappa t}^{-1}} \circ \mathfrak{a}_{\mathbf{F}_{\kappa t}}\}\mathbf{G} = [(D\zeta_{\kappa t})^{-*}\,\mathbf{G}\,(D\zeta_{\kappa t})^{-1}] \circ \zeta_{\kappa t}^{-1}$$
$$= (D\zeta_{\kappa t}^{-1})^*\,\mathbf{G}\,(D\zeta_{\kappa t}^{-1}),$$

which follows from (2.17), (3.5)$_2$, (3.16) and (4.5), we obtain

$$(4.28) \qquad \zeta_{\kappa t *}(\mathbf{u}_\kappa \cdot \mathbf{u}_\kappa) = \zeta_{\kappa t *}[(\mathbf{G}\mathbf{u}_\kappa)\mathbf{u}_\kappa] = [(\zeta_{\kappa t *}\mathbf{G})(\zeta_{\kappa t *}\mathbf{u}_\kappa)](\zeta_{\kappa t *}\mathbf{u}_\kappa)$$
$$= [(\zeta_{\kappa t *}\mathbf{G})\mathbf{u}_{\zeta_{\kappa t}}]\mathbf{u}_{\zeta_{\kappa t}}$$

again via (4.7), and analogous to (4.16). With the relation $(D\zeta_{\kappa t})^{-*}\mathbf{G} = \mathbf{G}(D\zeta_{\kappa t})^{-\mathrm{T}}$ obtained from (4.17),

$$(4.29) \qquad \zeta_{\kappa t *}\mathbf{G} = \mathbf{G}[(D\zeta_{\kappa t})^{-\mathrm{T}}(D\zeta_{\kappa t})^{-1}] \circ \zeta_{\kappa t}^{-1} = \mathbf{G}\mathbf{B}_t^{-1}$$

follows from (4.27) for the push-forward of $\mathbf{G}$ by $\zeta_{\kappa t}$, where

$$(4.30) \qquad \mathbf{B}_t := [(D\zeta_{\kappa t})^{-\mathrm{T}}(D\zeta_{\kappa t})^{-1}] \circ \zeta_{\kappa t}^{-1} = (\zeta_{\kappa t *}\mathbf{G}^{-1})\mathbf{G}$$

represents the *left Cauchy-Green tensor* for all $t \in I$. As a field on B_κ, $\mathbf{B}_t$ is given by

$$(4.31) \qquad \mathbf{B}_{\kappa t} := \mathbf{B}_t \circ \zeta_{\kappa t} = (D\zeta_{\kappa t})(D\zeta_{\kappa t})^{\mathrm{T}} = \mathbf{F}_{\kappa t}\,\mathbf{F}_{\kappa t}^{\mathrm{T}}$$

for all $t \in I$, i.e.,

$$(4.32) \qquad \mathbf{B}_\kappa : I \times B_\kappa \longrightarrow \mathrm{Sym}^+(\mathcal{V}, \mathcal{V}) \quad | \quad (t, b) \longmapsto (D_b \zeta_{\kappa t})(D_b \zeta_{\kappa t})^\mathsf{T}$$
$$= \mathbf{F}_\kappa(t, b)\, \mathbf{F}_\kappa^\mathsf{T}(t, b) =: \mathbf{B}_\kappa(t, b).$$

In terms of the associated action (2.31), the operation $(3.5)_2$ and push-forward (4.9), $\mathbf{B}_t$ takes the form

$$(4.33) \qquad \mathbf{B}_t = \{\mathfrak{c}_{\zeta_{\kappa t}^{-1}} \circ \mathfrak{a}_{\mathbf{F}_{\kappa t}}^\mathsf{T}\} \mathbf{1}_{\mathcal{V}} = \{r_\mathbf{G} \circ \zeta_{\kappa t *} \circ r_{\mathbf{G}^{-1}}\} \mathbf{1}_{\mathcal{V}} = r_\mathbf{G}[\zeta_{\kappa t *}(r_{\mathbf{G}^{-1}} \mathbf{1}_{\mathcal{V}})]$$
$$= (\zeta_{\kappa t *} \mathbf{G}^{-1})\mathbf{G}$$

for all $t \in I$ via (4.27). Analogous to $\zeta_{\kappa t}^* \mathbf{G}$ and $\mathbf{C}_{\kappa t}$, the result (4.29) shows that $\zeta_{\kappa t *} \mathbf{G}$ and $\mathbf{B}_t^{-1}$ are associated tensors. Note that (4.18) and (4.29) imply $\mathbf{C}_{\kappa t} = \zeta_{\kappa t}^* \mathbf{B}_t$, or equivalently $\mathbf{B}_t = \zeta_{\kappa t *} \mathbf{C}_{\kappa t}$ for all $t \in I$. Substituting (4.28) into (4.25), it takes the form

$$
\begin{aligned}
\Delta_t &= \frac{1}{2}[(\mathbf{G} - \zeta_{\kappa t *}\mathbf{G})\mathbf{u}_{\zeta_{\kappa t}}]\mathbf{u}_{\zeta_{\kappa t}} \, . \\[4pt]
&= \frac{1}{2}[\mathbf{G}(\mathbf{1}_{\mathcal{V}} - \mathbf{B}_t^{-1})\mathbf{u}_{\zeta_{\kappa t}}]\mathbf{u}_{\zeta_{\kappa t}} \, . \\[4pt]
&= (\mathbf{G}\mathbf{A}_t \mathbf{u}_{\zeta_{\kappa t}})\mathbf{u}_{\zeta_{\kappa t}} \, . \\[4pt]
&= \mathbf{A}_t \mathbf{u}_{\zeta_{\kappa t}} \cdot \mathbf{u}_{\zeta_{\kappa t}} \, .
\end{aligned}
$$

(4.34)

via (4.29), where $\mathbf{A}_t = \frac{1}{2}(\mathbf{1}_{\mathcal{V}} - \mathbf{B}_t^{-1})$ represents the *Almansi strain tensor* for all $t \in I$, i.e.,

$$(4.35) \qquad \mathbf{A}_t : B_t \longrightarrow \mathrm{Sym}(\mathcal{V}, \mathcal{V}) \quad | \quad p \longmapsto \frac{1}{2}(\mathbf{1}_{\mathcal{V}} - \mathbf{B}_t^{-1}(p)) =: \mathbf{A}_t(p) \, .$$

Note that, from (4.18) and the pull-back of (4.29), it follows that

$$(4.36) \qquad \zeta_{\kappa t}^*(\mathbf{G}\mathbf{A}_t) = \frac{1}{2}(\zeta_{\kappa t}^*\mathbf{G} - \zeta_{\kappa t}^*(\mathbf{G}\mathbf{B}_t^{-1})) = \frac{1}{2}(\mathbf{G}\mathbf{C}_{\kappa t} - \mathbf{G}) = \mathbf{G}\mathbf{E}_{\kappa t}$$

for all $t \in I$. In terms of the action (2.17), the operation $(3.5)_1$, and (4.6), the last result becomes

$$(4.37) \qquad \mathbf{G}\mathbf{E}_{\kappa t} = \zeta_{\kappa t}^*(\mathbf{G}\mathbf{A}_t) = \left\{\mathfrak{a}_{\mathbf{F}_{\kappa t}^{-1}} \circ \mathfrak{c}_{\zeta_{\kappa t}}\right\}(\mathbf{G}\mathbf{A}_t) = \mathbf{F}_{\kappa t}^* \mathbf{G}\,(\mathbf{A}_t \circ \zeta_{\kappa t})\, \mathbf{F}_{\kappa t} \, .$$

Alternatively, (4.36) can be rewritten in the forms

$$(4.38)
\begin{array}{ccc}
\mathbf{E}_{\kappa t} = \{\ell_{\mathbf{G}^{-1}} \circ \zeta_{\kappa t}^* \circ \ell_\mathbf{G}\}\mathbf{A}_t & & \mathbf{A}_t = \{\ell_{\mathbf{G}^{-1}} \circ \zeta_{\kappa t *} \circ \ell_\mathbf{G}\}\mathbf{E}_{\kappa t} \\[6pt]
& \text{or} & \\[6pt]
= \{\mathfrak{a}_{\mathbf{F}_{\kappa t}^{-1}}^\ell \circ \mathfrak{c}_{\zeta_{\kappa t}}\}\mathbf{A}_t & & = \{\mathfrak{c}_{\zeta_{\kappa t}^{-1}} \circ \mathfrak{a}_{\mathbf{F}_{\kappa t}}^\ell\}\mathbf{E}_{\kappa t}
\end{array}$$

in terms of the associated tensor operations (2.24) and (2.25), as well as the associated action (2.29), at each $t \in I$.

5. Basic strain tensors based on material surfaces

The strain tensors of the second family of HT are based on the deformation of "material surfaces", which represent geometric objects "dual" to "material line elements" in the following sense. Let $B_\gamma \subset E$ again be any region in E occupied by the material body. The mapping "dual" to a curve $c \in C^1(\mathbb{R}, E)_p$ at $p \in B_\gamma$ is a C^1 function $f \in C_p^1(E, \mathbb{R})$ at $p \in B_\gamma$, i.e., a C^1 mapping of some neighbourhood $N_p \subset E$ of p in E into $\mathbb{R}$. Analogous to equivalent (i.e., tangent) curves at p, two such functions $f_1, f_2 \in C_p^1(E, \mathbb{R})$ are *equivalent* at $p \in B_\gamma$ if their (Fréchet) derivatives there are equal, i.e., $D_p f_1 = D_p f_2$. As with curves and their tangent vectors, any resulting equivalence class $[f]_p$ of such functions is then uniquely represented by their common covector $(D_p f) \in V^*$ at $p \in B_\gamma$. A field of such covectors on B_γ comprises then a *covector field*

$$(5.1) \qquad \boldsymbol{\nu}_\gamma : B_\gamma \longrightarrow V^* \quad | \quad p \longmapsto \nu = \boldsymbol{\nu}_\gamma(p)$$

on the configuration B_γ such that $\boldsymbol{\nu}_\gamma(p) = (D_p f)$ for some equivalence class $[f]_p$ at each $p \in B_\gamma$.

To make contact with the notion of a "material surface", we first note that any covector field such as (5.1) defines a 2-dimensional subspace $S_{\boldsymbol{\nu}_\gamma(p)} :=$ $\{\mathbf{v} \in V \mid \boldsymbol{\nu}_\gamma(p)\mathbf{v} = 0\}$ of V at each $p \in B_\gamma$. The unit vector field

$$(5.2) \qquad \mathbf{n}_\gamma : B_\gamma \longrightarrow V \quad | \quad p \longmapsto \frac{\mathbf{G}^{-1}\boldsymbol{\nu}_\gamma(p)}{|\mathbf{G}^{-1}\boldsymbol{\nu}_\gamma(p)|} =: \mathbf{n}_\gamma(p)$$

associated with $\boldsymbol{\nu}_\gamma$ then represents the *unit normal* of the corresponding *material surface* $S_{\boldsymbol{\nu}_\gamma(p)}$ at each $p \in B_\gamma$. In particular, if the composition $f_\gamma \circ c \in C^1(\mathbb{N}_0, \mathbb{R})$ of a C^1 function $f_\gamma \in C^1(B_\gamma, \mathbb{R})$ and any curve $c \in C^1(\mathbb{N}_0, B_\gamma)$ represents a *constant* map, then one has $\partial_s(f_\gamma \circ c) = 0$ for all $s \in \mathbb{N}_0$, and so $(D_p f_\gamma)\mathbf{u}_\gamma(p) = 0$ for all $p \in c[\mathbb{N}_0]$ with $\partial c = \mathbf{u}_\gamma \circ c$. Clearly, each equivalence class $[f]_p$ of C^1 functions $f \in C_p^1(E, \mathbb{R})$ at $p \in E$ can be associated with a material surface at $p \in E$ as represented by the unit normal (5.2).

In a fashion dual to curves, the deformation $\zeta_{\kappa t} : B_\kappa \longrightarrow B_t$ maps any C^1 spatial function $f_{\zeta_{\kappa t}} \in C^1_{\zeta_{\kappa t}(b)}(E, \mathbb{R})$ to the C^1 referential function $\zeta_{\kappa t}^* f_{\zeta_{\kappa t}} =$ $f_{\zeta_{\kappa t}} \circ \zeta_{\kappa t} \in C_b^1(E, \mathbb{R})$, such that

$$(5.3) \qquad D_b(\zeta_{\kappa t}^* f_{\zeta_{\kappa t}}) = D_b(f_{\zeta_{\kappa t}} \circ \zeta_{\kappa t}) = (D_{\zeta_{\kappa t}(b)} f_{\zeta_{\kappa t}})(D_b \zeta_{\kappa t})$$

$$= (D_b \zeta_{\kappa t})^* (D_{\zeta_{\kappa t}(b)} f_{\zeta_{\kappa t}})$$

via (2.9). Substituting the corresponding covector fields $\boldsymbol{\nu}_{\zeta_{\kappa t}}(\zeta_{\kappa t}(b)) = (D_{\zeta_{\kappa t}(b)} f_{\zeta_{\kappa t}})$

and $\boldsymbol{\nu}_\kappa(b) = D_b(\zeta^*_{\kappa t} f_{\zeta_{\kappa t}})$ into the last result, we obtain

(5.4) $$\boldsymbol{\nu}_\kappa(b) = (D_b \zeta_{\kappa t})^* \boldsymbol{\nu}_{\zeta_{\kappa t}}(\zeta_{\kappa t}(b)) = \mathbf{F}^*_{\kappa t}(b) \boldsymbol{\nu}_{\zeta_{\kappa t}}(\zeta_{\kappa t}(b))$$

at $b \in B_\kappa$. Letting $b \in B_\kappa$ vary, (5.4) becomes

(5.5) $$\boldsymbol{\nu}_\kappa = (D\zeta_{\kappa t})^* (\boldsymbol{\nu}_{\zeta_{\kappa t}} \circ \zeta_{\kappa t}) = \mathbf{F}^*_{\kappa t} (\boldsymbol{\nu}_{\zeta_{\kappa t}} \circ \zeta_{\kappa t}) .$$

The last relation can also be written in the pull-back

(5.6) $$\boldsymbol{\nu}_\kappa = \zeta^*_{\kappa t} \boldsymbol{\nu}_{\zeta_{\kappa t}} = [\mathfrak{a}_{(D\zeta_{\kappa t}^{-1})} \boldsymbol{\nu}_{\zeta_{\kappa t}}] \circ \zeta_{\kappa t} = [(D\zeta_{\kappa t}^{-1})^{-*} \boldsymbol{\nu}_{\zeta_{\kappa t}}] \circ \zeta_{\kappa t}$$
$$= (D\zeta_{\kappa t})^* (\boldsymbol{\nu}_{\zeta_{\kappa t}} \circ \zeta_{\kappa t})$$

and push-forward

(5.7) $$\boldsymbol{\nu}_{\zeta_{\kappa t}} = \zeta_{\kappa t *} \boldsymbol{\nu}_\kappa = [\mathfrak{a}_{(D\zeta_{\kappa t})} \boldsymbol{\nu}_\kappa] \circ \zeta_{\kappa t}^{-1} = [(D\zeta_{\kappa t})^{-*} \boldsymbol{\nu}_\kappa] \circ \zeta_{\kappa t}^{-1}$$
$$= (D\zeta_{\kappa t}^{-1})^* (\boldsymbol{\nu}_\kappa \circ \zeta_{\kappa t}^{-1})$$

forms via (4.6), (4.5) and (3.16). In terms of the associated vector fields $\mathbf{G}^{-1}\boldsymbol{\nu}_\kappa$ and $\mathbf{G}^{-1}\boldsymbol{\nu}_{\zeta_{\kappa t}}$, (5.5) takes the more familiar form

(5.8) $$\mathbf{G}^{-1}\boldsymbol{\nu}_\kappa = \mathbf{G}^{-1} \mathbf{F}^*_{\kappa t}(\boldsymbol{\nu}_{\zeta_{\kappa t}} \circ \zeta_{\kappa t}) = \mathbf{F}^{\mathrm{T}}_{\kappa t}[(\mathbf{G}^{-1}\boldsymbol{\nu}_{\zeta_{\kappa t}}) \circ \zeta_{\kappa t}]$$

via the definition (2.22) of the transpose of a linear mapping.

Using the inner product induced by $\mathbf{G}^{-1} \in \mathrm{Sym}^+(V^*, V)$ on covectors, i.e., (2.21), one can define, similarly to (4.11), the change in squared length

(5.9) $$\delta_\kappa : I \times B_\kappa \longrightarrow \mathbb{R} \mid (t, b) \longmapsto \frac{1}{2} \{ \boldsymbol{\nu}_{\zeta_{\kappa t}}(\zeta_{\kappa t}(t, b)) \star \boldsymbol{\nu}_{\zeta_{\kappa t}}(\zeta_{\kappa t}(t, b))$$
$$-\boldsymbol{\nu}_\kappa(b) \star \boldsymbol{\nu}_\kappa(b) \} =: \delta_\kappa(t, b)$$

of the "normal" covector field $\boldsymbol{\nu}_\kappa$ on B_κ. By definition, then,

(5.10) $$\delta_{\kappa t} := \frac{1}{2} \{ \zeta^*_{\kappa t}(\boldsymbol{\nu}_{\zeta_{\kappa t}} \star \boldsymbol{\nu}_{\zeta_{\kappa t}}) - \boldsymbol{\nu}_\kappa \star \boldsymbol{\nu}_\kappa \} : B_\kappa \longrightarrow \mathbb{R}$$

for all $t \in I$, where

(5.11) $$\zeta^*_{\kappa t}(\boldsymbol{\nu}_{\zeta_{\kappa t}} \star \boldsymbol{\nu}_{\zeta_{\kappa t}}) = (\boldsymbol{\nu}_{\zeta_{\kappa t}} \star \boldsymbol{\nu}_{\zeta_{\kappa t}}) \circ \zeta_{\kappa t} = (\boldsymbol{\nu}_{\zeta_{\kappa t}} \circ \zeta_{\kappa t}) \star (\boldsymbol{\nu}_{\zeta_{\kappa t}} \circ \zeta_{\kappa t})$$

represents the pull-back of the squared length $(\boldsymbol{\nu}_{\zeta_{\kappa t}} \star \boldsymbol{\nu}_{\zeta_{\kappa t}}) : B_t \longrightarrow \mathbb{R}^+$ of the deformed normal covector $\boldsymbol{\nu}_{\zeta_{\kappa t}}$ to B_κ by $\zeta_{\kappa t}$. Analogous to (4.14),

(5.12)
$$
\begin{aligned}
\zeta_{\kappa t}^*(\boldsymbol{\nu}_{\zeta_{\kappa t}} \star \boldsymbol{\nu}_{\zeta_{\kappa t}}) &= (\boldsymbol{\nu}_{\zeta_{\kappa t}} \circ \zeta_{\kappa t}) \star (\boldsymbol{\nu}_{\zeta_{\kappa t}} \circ \zeta_{\kappa t}), \\
&= (\boldsymbol{\nu}_{\zeta_{\kappa t}} \circ \zeta_{\kappa t})[\mathbf{G}^{-1}(\boldsymbol{\nu}_{\zeta_{\kappa t}} \circ \zeta_{\kappa t})], \\
&= [(D\zeta_{\kappa t})^{-*}\boldsymbol{\nu}_\kappa][\mathbf{G}^{-1}(D\zeta_{\kappa t})^{-*}\boldsymbol{\nu}_\kappa], \\
&= \boldsymbol{\nu}_\kappa[(D\zeta_{\kappa t})^{-1}\mathbf{G}^{-1}(D\zeta_{\kappa t})^{-*}\boldsymbol{\nu}_\kappa],
\end{aligned}
$$

follows from (2.9), $(D\zeta_{\kappa t})^{-**} \cong (D\zeta_{\kappa t})^{-1}$ (see Sec. 2) and (5.6). Combining the last result with

(5.13)
$$
\zeta_{\kappa t}^*\mathbf{G}^{-1} = \mathfrak{a}_{\mathbf{F}_{\kappa t}^{-1}}\mathbf{G}^{-1} = (D\zeta_{\kappa t})^{-1}\,\mathbf{G}^{-1}\,(D\zeta_{\kappa t})^{-*}
$$

(recall that $\mathbf{G}^{-1} \in \mathrm{Lin}(V^*, V)$) from (2.19) and (4.6) yield

(5.14)
$$
\zeta_{\kappa t}^*(\boldsymbol{\nu}_{\zeta_{\kappa t}} \star \boldsymbol{\nu}_{\zeta_{\kappa t}}) = \zeta_{\kappa t}^*[\boldsymbol{\nu}_{\zeta_{\kappa t}}(\mathbf{G}^{-1}\boldsymbol{\nu}_{\zeta_{\kappa t}})] = (\zeta_{\kappa t}^*\boldsymbol{\nu}_{\zeta_{\kappa t}})[(\zeta_{\kappa t}^*\mathbf{G}^{-1})(\zeta_{\kappa t}^*\boldsymbol{\nu}_{\zeta_{\kappa t}})]
$$
$$
= \boldsymbol{\nu}_\kappa[(\zeta_{\kappa t}^*\mathbf{G}^{-1})\boldsymbol{\nu}_\kappa]
$$

via (5.6), analogous to (5.14). Substituting the relation $(D\zeta_{\kappa t})^{-\mathrm{T}}\mathbf{G}^{-1} = \mathbf{G}^{-1}(D\zeta_{\kappa t})^{-*}$ obtained from (4.17) into (5.13), it takes the more familiar form

(5.15)
$$
\zeta_{\kappa t}^*\mathbf{G}^{-1} = (D\zeta_{\kappa t})^{-1}\,(D\zeta_{\kappa t})^{-\mathrm{T}}\,\mathbf{G}^{-1} = \mathbf{C}_{\kappa t}^{-1}\mathbf{G}^{-1}\ .
$$

To proceed further, we substitute (5.14) into (5.10) to obtain

(5.16)
$$
\begin{aligned}
\delta_{\kappa t} &= \frac{1}{2}\boldsymbol{\nu}_\kappa[(\zeta_{\kappa t}^*\mathbf{G}^{-1} - \mathbf{G}^{-1})\boldsymbol{\nu}_\kappa], \\
&= \frac{1}{2}\boldsymbol{\nu}_\kappa[(\mathbf{C}_{\kappa t}^{-1} - \mathbf{1}_V)\mathbf{G}^{-1}\boldsymbol{\nu}_\kappa], \\
&= \boldsymbol{\nu}_\kappa[(\boldsymbol{\varepsilon}_{\kappa t}\mathbf{G}^{-1})\boldsymbol{\nu}_\kappa], \\
&= \boldsymbol{\varepsilon}_{\kappa t}(\mathbf{G}^{-1}\boldsymbol{\nu}_\kappa) \cdot (\mathbf{G}^{-1}\boldsymbol{\nu}_\kappa),
\end{aligned}
$$

via (5.15), where $\boldsymbol{\varepsilon}_{\kappa t} := \frac{1}{2}(\mathbf{C}_{\kappa t}^{-1} - \mathbf{1}_V)$ represents the *Piola strain tensor* for all $t \in I$, i.e.,

(5.17)
$$
\boldsymbol{\varepsilon}_\kappa : I \times B_\kappa \longrightarrow \mathrm{Sym}(V, V) \quad | \quad (t, b) \longmapsto \frac{1}{2}(\mathbf{C}_\kappa^{-1}(t, b) - \mathbf{1}_V) =: \boldsymbol{\varepsilon}_\kappa(t, b).
$$

The definitions (4.23) and (5.17) yield the relation

(5.18)
$$
\mathbf{E}_\kappa = -\mathbf{C}_\kappa\,\boldsymbol{\varepsilon}_\kappa
$$

between the Green and Piola strain tensors.

Pushing the strain measure (5.9) forward to B_t yields

$$(5.19) \qquad \delta_t : B_t \longrightarrow \mathbb{R} \quad | \quad p \longmapsto \frac{1}{2}\left\{\boldsymbol{\nu}_{\zeta_{\kappa t}}(p) \star \boldsymbol{\nu}_{\zeta_{\kappa t}}(p)\right.$$
$$\left. -\boldsymbol{\nu}_{\kappa}(\zeta_{\kappa t}^{-1}(p)) \star \boldsymbol{\nu}_{\kappa}(\zeta_{\kappa t}^{-1}(p))\right\} =: \delta_t(p),$$

or

$$(5.20) \qquad \delta_t := \frac{1}{2}\left\{\boldsymbol{\nu}_{\zeta_{\kappa t}} \star \boldsymbol{\nu}_{\zeta_{\kappa t}} - \zeta_{\kappa t \star}(\boldsymbol{\nu}_{\kappa} \star \boldsymbol{\nu}_{\kappa})\right\} : B_t \longrightarrow \mathbb{R}$$

for each $t \in I$, such that $\delta_t = \zeta_{\kappa t \star}\delta_{\kappa t}$ and $\delta_{\kappa t} = \zeta_{\kappa t}^{\star}\delta_t$. Analogous to (4.26),

$$(5.21) \qquad \begin{aligned} \zeta_{\kappa t \star}(\boldsymbol{\nu}_{\kappa} \star \boldsymbol{\nu}_{\kappa}) &= (\boldsymbol{\nu}_{\kappa} \circ \zeta_{\kappa t}^{-1}) \star (\boldsymbol{\nu}_{\kappa} \circ \zeta_{\kappa t}^{-1}), \\ &= (\boldsymbol{\nu}_{\kappa} \circ \zeta_{\kappa t}^{-1})[\mathbf{G}^{-1}(\boldsymbol{\nu}_{\kappa} \circ \zeta_{\kappa t}^{-1})], \\ &= [(D\zeta_{\kappa t}^{-1})^{-\star}\boldsymbol{\nu}_{\zeta_{\kappa t}}][\mathbf{G}^{-1}(D\zeta_{\kappa t}^{-1})^{-\star}\boldsymbol{\nu}_{\zeta_{\kappa t}}], \\ &= \boldsymbol{\nu}_{\zeta_{\kappa t}}[(D\zeta_{\kappa t}^{-1})^{-1}\mathbf{G}^{-1}(D\zeta_{\kappa t}^{-1})^{-\star}\boldsymbol{\nu}_{\zeta_{\kappa t}}]. \end{aligned}$$

holds via (2.9), $(D\zeta_{\kappa t}^{-1})^{-\star\star} \cong (D\zeta_{\kappa t}^{-1})^{-1}$ and (5.7). Together with

$$(5.22) \qquad \zeta_{\kappa t \star}\mathbf{G}^{-1} = \{\mathfrak{c}_{\zeta_{\kappa t}^{-1}} \circ \mathbf{a}_{\mathbf{F}_{\kappa t}}\}\mathbf{G}^{-1} = (D\zeta_{\kappa t}^{-1})^{-1}\,\mathbf{G}^{-1}\,(D\zeta_{\kappa t}^{-1})^{-\star}$$

from (2.19) and (4.5), $(5.21)_4$ implies

$$(5.23) \qquad \begin{aligned} \zeta_{\kappa t \star}(\boldsymbol{\nu}_{\kappa} \star \boldsymbol{\nu}_{\kappa}) = \zeta_{\kappa t \star}[\boldsymbol{\nu}_{\kappa}(\mathbf{G}^{-1}\boldsymbol{\nu}_{\kappa})] &= (\zeta_{\kappa t \star}\boldsymbol{\nu}_{\kappa})[(\zeta_{\kappa t \star}\mathbf{G}^{-1})(\zeta_{\kappa t \star}\boldsymbol{\nu}_{\kappa})] \\ &= \boldsymbol{\nu}_{\zeta_{\kappa t}}[(\zeta_{\kappa t \star}\mathbf{G}^{-1})\boldsymbol{\nu}_{\zeta_{\kappa t}}] \end{aligned}$$

via (5.7). With the relation $\mathbf{G}^{-1}(D\zeta_{\kappa t})^{\star} = (D\zeta_{\kappa t})^{\mathsf{T}}\,\mathbf{G}^{-1}$ from (4.17), (5.22) takes the form

$$(5.24) \qquad \begin{aligned} \zeta_{\kappa t \star}\mathbf{G}^{-1} &= [(D\zeta_{\kappa t})\,\mathbf{G}^{-1}\,(D\zeta_{\kappa t})^{\star}] \circ \zeta_{\kappa t}^{-1} \\ &= \{[(D\zeta_{\kappa t})\,(D\zeta_{\kappa t})^{\mathsf{T}}] \circ \zeta_{\kappa t}^{-1}\}\,\mathbf{G}^{-1} = \mathbf{B}_t\mathbf{G}^{-1} \end{aligned}$$

via (4.31). Substituting (5.23) into (5.20), we obtain

$$(5.25) \qquad \begin{aligned} \delta_t &= \frac{1}{2}\boldsymbol{\nu}_{\zeta_{\kappa t}}[(\mathbf{G}^{-1} - \zeta_{\kappa t \star}\mathbf{G}^{-1})\boldsymbol{\nu}_{\zeta_{\kappa t}}], \\ &= \frac{1}{2}\boldsymbol{\nu}_{\zeta_{\kappa t}}[(\mathbf{1}_V - \mathbf{B}_t)\mathbf{G}^{-1}\boldsymbol{\nu}_{\zeta_{\kappa t}}], \\ &= \boldsymbol{\nu}_{\zeta_{\kappa t}}[(\boldsymbol{\alpha}_t\mathbf{G}^{-1})\boldsymbol{\nu}_{\zeta_{\kappa t}}], \\ &= \boldsymbol{\alpha}_t(\mathbf{G}^{-1}\boldsymbol{\nu}_{\zeta_{\kappa t}}) \cdot (\mathbf{G}^{-1}\boldsymbol{\nu}_{\zeta_{\kappa t}}). \end{aligned}$$

via (5.24), where $\boldsymbol{\alpha}_t := \frac{1}{2}(\mathbf{1}_V - \mathbf{B}_t)$ represents the *Finger strain tensor* for all $t \in I$, i.e.,

$$(5.26) \qquad \boldsymbol{\alpha}_t : B_t \longrightarrow \mathrm{Sym}(\mathcal{V}, \mathcal{V}) \quad | \quad p \longmapsto \frac{1}{2}(\mathbf{1}_V - \mathbf{B}_t(p)) =: \boldsymbol{\alpha}_t(p) \,.$$

The definitions (4.35) and (5.26) of the Almansi and Finger strain tensors, respectively, yield

$$(5.27) \qquad\qquad\qquad \boldsymbol{\alpha}_t = -\mathbf{B}_t \mathbf{A}_t \,.$$

analogous to (5.18). Using (5.15) and the result $\mathbf{G}^{-1} = \zeta_{\kappa t}^*(\mathbf{B}_t \mathbf{G}^{-1})$ from (4.30), we obtain

$$(5.28) \quad \zeta_{\kappa t}^*(\boldsymbol{\alpha}_t \mathbf{G}^{-1}) = \frac{1}{2}(\zeta_{\kappa t}^* \mathbf{G}^{-1} - \zeta_{\kappa t}^*(\mathbf{B}_t \mathbf{G}^{-1})) = \frac{1}{2}(\mathbf{C}_{\kappa t}^{-1}\mathbf{G}^{-1} - \mathbf{G}^{-1}) = \boldsymbol{\varepsilon}_{\kappa t}\mathbf{G}^{-1}$$

for all $t \in I$. Analogous to (4.37),

$$(5.29) \quad \boldsymbol{\varepsilon}_{\kappa t}\mathbf{G}^{-1} = \zeta_{\kappa t}^*(\boldsymbol{\alpha}_t \mathbf{G}^{-1}) = \{\mathfrak{a}_{\mathbf{F}_{\kappa t}^{-1}} \circ \mathfrak{c}_{\zeta_{\kappa t}}\}(\boldsymbol{\alpha}_t \mathbf{G}^{-1}) = \mathbf{F}_{\kappa t}^{-1}[(\boldsymbol{\alpha}_t \mathbf{G}^{-1}) \circ \zeta_{\kappa t}] \mathbf{F}_{\kappa t}^{-*}$$

follows from (2.19), (3.5) and (4.6). The associated-tensor operations (2.26) and (2.27), as well as the associated action (2.31), imply then the operator forms

$$(5.30) \qquad
\begin{aligned}
\boldsymbol{\varepsilon}_{\kappa t} &= \{{}^r\mathbf{G} \circ \zeta_{\kappa t}^* \circ {}^r\mathbf{G}^{-1}\}\boldsymbol{\alpha}_t \\
&= \{\mathfrak{a}_{\mathbf{F}_{\kappa t}^{-1}}^r \circ \mathfrak{c}_{\zeta_{\kappa t}}\}\boldsymbol{\alpha}_t
\end{aligned}
\qquad \text{or} \qquad
\begin{aligned}
\boldsymbol{\alpha}_t &= \{{}^r\mathbf{G} \circ \zeta_{\kappa t*} \circ {}^r\mathbf{G}^{-1}\}\boldsymbol{\varepsilon}_{\kappa t} \\
&= \{\mathfrak{c}_{\zeta_{\kappa t}^{-1}} \circ \mathfrak{a}_{\mathbf{F}_{\kappa t}}^r\}\boldsymbol{\varepsilon}_{\kappa t}
\end{aligned}$$

from (5.29) for the transformation between $\boldsymbol{\varepsilon}_{\kappa t}$ and $\boldsymbol{\alpha}_t$ for all $t \in I$.

6. Basic stress tensors

We begin with a brief review of area elements, with respect to which stress tensors are defined. Let $\mathbf{u}_\gamma$ and $\mathbf{w}_\gamma$ represent two linearly independent tangent vector fields on $B_\gamma \subset E$. Each such pair $(\mathbf{u}_\gamma, \mathbf{w}_\gamma)$ defines an *area element* $\mathbf{u}_\gamma \times \mathbf{w}_\gamma$ on B_γ with direction

$$(6.1) \qquad\qquad\qquad \mathbf{n}_\gamma := \frac{\mathbf{u}_\gamma \times \mathbf{w}_\gamma}{|\mathbf{u}_\gamma \times \mathbf{w}_\gamma|}$$

and magnitude

$$(6.2) \qquad\qquad\qquad da_\gamma := |\mathbf{u}_\gamma \times \mathbf{w}_\gamma| \,.$$

Now, from the relation (2.35) for the Euclidean cross-product, we obtain the expression

$$(6.3) \qquad \mathbf{n}_\gamma \, da_\gamma = \mathbf{u}_\gamma \times \mathbf{w}_\gamma = \mathbf{G}^{-1}(\imath_{\mathbf{w}_\gamma} \imath_{\mathbf{u}_\gamma} \varpi)$$

for the area element $\mathbf{n}_\gamma \, da_\gamma$. Note that the last relation can be written in the alternative form

$$(6.4) \qquad (\mathbf{G}\mathbf{n}_\gamma) \, da_\gamma = \mathbf{G}(\mathbf{u}_\gamma \times \mathbf{w}_\gamma) = \imath_{\mathbf{w}_\gamma} \imath_{\mathbf{u}_\gamma} \varpi \, .$$

implying that the "normal" covector field $\imath_{\mathbf{w}_\gamma} \imath_{\mathbf{u}_\gamma} \varpi$ is *associated* with the area element $\mathbf{n}_\gamma \, da_\gamma$.

Let $\mathbf{u}_{\zeta_{\kappa t}}$ and $\mathbf{w}_{\zeta_{\kappa t}}$ be two such vector fields on B_t, and

$$(6.5) \qquad (\mathbf{G}\mathbf{n}_{\zeta_{\kappa t}}) \, da_{\zeta_{\kappa t}} = \mathbf{G}(\mathbf{u}_{\zeta_{\kappa t}} \times \mathbf{w}_{\zeta_{\kappa t}}) = \imath_{\mathbf{w}_{\zeta_{\kappa t}}} \imath_{\mathbf{u}_{\zeta_{\kappa t}}} \varpi$$

– the associated normal covector field from (6.4). Pulling this normal covector field on B_t back to B_κ yields the result

$$(6.6) \qquad \zeta^*_{\kappa t}(\imath_{\mathbf{w}_{\zeta_{\kappa t}}} \imath_{\mathbf{u}_{\zeta_{\kappa t}}} \varpi) = (D\zeta_{\kappa t})^* [(\imath_{\mathbf{w}_{\zeta_{\kappa t}}} \imath_{\mathbf{u}_{\zeta_{\kappa t}}} \varpi) \circ \zeta_{\kappa t}] \, .$$

On the other hand, one also has

$$(6.7) \qquad \zeta^*_{\kappa t}(\imath_{\mathbf{w}_{\zeta_{\kappa t}}} \imath_{\mathbf{u}_{\zeta_{\kappa t}}} \varpi) = (\imath_{\zeta^*_{\kappa t}\mathbf{w}_{\zeta_{\kappa t}}} \imath_{\zeta^*_{\kappa t}\mathbf{u}_{\zeta_{\kappa t}}} \zeta^*_{\kappa t}\varpi) = \det(D\zeta_{\kappa t}) \, (\imath_{\mathbf{w}_\kappa} \imath_{\mathbf{u}_\kappa} \varpi) \, .$$

with $\mathbf{u}_\kappa = \zeta^*_{\kappa t}\mathbf{u}_{\zeta_{\kappa t}}$, $\mathbf{w}_\kappa = \zeta^*_{\kappa t}\mathbf{w}_{\zeta_{\kappa t}}$ (see (4.8)), and $\zeta^*_{\kappa t}\varpi = \det(D\zeta_{\kappa t}) \varpi$, i.e.,

$$(6.8) \qquad (\zeta^*_{\kappa t}\varpi)(\mathbf{v}_1, \mathbf{v}_2, \mathbf{v}_3) := \varpi((D\zeta_{\kappa t})\mathbf{v}_1, (D\zeta_{\kappa t})\mathbf{v}_2, (D\zeta_{\kappa t})\mathbf{v}_3)$$
$$= \det(D\zeta_{\kappa t}) \, \varpi(\mathbf{v}_1, \mathbf{v}_2, \mathbf{v}_3)$$

for all $\mathbf{v}_1, \mathbf{v}_2, \mathbf{v}_3 \in \mathcal{V}$. Together, (6.6) and (6.7) imply

$$(6.9) \qquad (\imath_{\mathbf{w}_{\zeta_{\kappa t}}} \imath_{\mathbf{u}_{\zeta_{\kappa t}}} \varpi) \circ \zeta_{\kappa t} = \det(D\zeta_{\kappa t}) \, (D\zeta_{\kappa t})^{-*}(\imath_{\mathbf{w}_\kappa} \imath_{\mathbf{u}_\kappa} \varpi) \, .$$

The usual form of this result is its *associated* form, i.e.,

$$(6.10) \qquad (\mathbf{n}_{\zeta_{\kappa t}} \, da_{\zeta_{\kappa t}}) \circ \zeta_{\kappa t} = \det(D\zeta_{\kappa t}) \, (D\zeta_{\kappa t})^{-\mathsf{T}} \mathbf{n}_\kappa \, da_\kappa$$

which follows from (6.3) and (4.17).

On the basis of the spatial area element (6.3) for B_t, the standard spatial contact force "element" takes the form

$$(6.11) \qquad \mathbf{T}_t \mathbf{n}_{\zeta_{\kappa t}} \, da_{\zeta_{\kappa t}} = \mathbf{T}_t \mathbf{G}^{-1}(\imath_{\mathbf{w}_{\zeta_{\kappa t}}} \imath_{\mathbf{u}_{\zeta_{\kappa t}}} \varpi) \, ,$$

where the explicitly time-dependent spatial tensor field

$$(6.12) \qquad \mathbf{T}_t : B_t \longrightarrow \mathrm{Sym}(\mathcal{V}, \mathcal{V}) \quad | \quad p \longmapsto \mathbf{T}_t(p)$$

represents, as usual, the Cauchy stress tensor([4]), and

$$(6.13) \qquad \mathbf{T}_t\,\mathbf{G}^{-1} : B_t \longrightarrow \mathrm{Sym}(\mathcal{V}^*, \mathcal{V}) \quad | \quad p \longmapsto \mathbf{T}_t(p)\,\mathbf{G}^{-1}$$

represents a spatial tensor field *associated* with $\mathbf{T}_t$. Introducing now the *weighted Cauchy stress tensor*

$$(6.14) \qquad \mathbf{S}_t : B_t \longrightarrow \mathrm{Sym}(\mathcal{V}, \mathcal{V}) \quad | \quad p \longmapsto \det\{(D_{\zeta_{\kappa t}^{-1}(p)}\zeta_{\kappa t})\}\,\mathbf{T}_t(p) =: \mathbf{S}_t(p)\,,$$

i.e., $\mathbf{S}_t := [\det(D\zeta_{\kappa t}) \circ \zeta_{\kappa t}^{-1}]\,\mathbf{T}_t$ for all $t \in I$, pull-back of (6.11) to B_κ leads to

$$(6.15) \qquad
\begin{aligned}
\zeta_{\kappa t}^* (\mathbf{T}_t \mathbf{n}_{\zeta_{\kappa t}} da_{\zeta_{\kappa t}}) &= \zeta_{\kappa t}^* (\mathbf{T}_t \mathbf{G}^{-1})[\zeta_{\kappa t}^*({}^l\mathbf{w}_{\zeta_{\kappa t}}\,{}^l\mathbf{u}_{\zeta_{\kappa t}}\, \varpi)], \\
&= (D\zeta_{\kappa t})^{-1}[(\mathbf{T}_t \mathbf{G}^{-1}) \circ \zeta_{\kappa t}](D\zeta_{\kappa t})^{-*}[\det(D\zeta_{\kappa t})({}^l\mathbf{w}_\kappa\,{}^l\mathbf{u}_\kappa \varpi)], \\
&= (D\zeta_{\kappa t})^{-1} (\mathbf{S}_t \circ \zeta_{\kappa t})(D\zeta_{\kappa t})^{-\mathrm{T}} \mathbf{G}^{-1} ({}^l\mathbf{w}_\kappa\,{}^l\mathbf{u}_\kappa\, \varpi). \\
&= (D\zeta_{\kappa t})^{-1} (\mathbf{S}_t \circ \zeta_{\kappa t})(D\zeta_{\kappa t})^{-\mathrm{T}} \mathbf{n}_\kappa\, da_\kappa\,,
\end{aligned}$$

via (4.17), (6.3), (6.9), and the pull-back

$$(6.16) \qquad
\begin{aligned}
\zeta_{\kappa t}^* (\mathbf{T}_t\,\mathbf{G}^{-1}) &= (D\zeta_{\kappa t})^{-1}[(\mathbf{T}_t\,\mathbf{G}^{-1}) \circ \zeta_{\kappa t}](D\zeta_{\kappa t})^{-*} \\
&= [(D\zeta_{\kappa t})^{-1} (\mathbf{T}_t \circ \zeta_{\kappa t})(D\zeta_{\kappa t})^{-\mathrm{T}}]\mathbf{G}^{-1}
\end{aligned}$$

of the associated Cauchy stress tensor $\mathbf{T}_t\,\mathbf{G}^{-1}$. In terms of the *second Piola–Kirchhoff stress tensor*

$$(6.17) \qquad \tilde{\mathbf{T}}_\kappa : I \times B_\kappa \longrightarrow \mathrm{Sym}(\mathcal{V}, \mathcal{V}) \quad | \quad (t, b) \longmapsto (D_b\zeta_{\kappa t})^{-1}\,\mathbf{S}(t, \zeta_\kappa(t, b))$$
$$\times (D_b\zeta_{\kappa t})^{-\mathrm{T}} =: \tilde{\mathbf{T}}_\kappa(t, b),$$

i.e.,

$$(6.18) \qquad \tilde{\mathbf{T}}_{\kappa t} := (D\zeta_{\kappa t})^{-1} (\mathbf{S}_t \circ \zeta_{\kappa t})(D\zeta_{\kappa t})^{-\mathrm{T}} : B_\kappa \longrightarrow \mathrm{Sym}(\mathcal{V}, \mathcal{V})$$

for all $t \in I$, (6.15) takes the usual form

$$(6.19) \qquad
\begin{aligned}
\zeta_{\kappa t}^* (\mathbf{T}_t\, \mathbf{n}_{\zeta_{\kappa t}}\, da_{\zeta_{\kappa t}}) &= \tilde{\mathbf{T}}_{\kappa t}\, \mathbf{G}^{-1} ({}^l\mathbf{w}_\kappa\,{}^l\mathbf{u}_\kappa\, \varpi). \\
&= \tilde{\mathbf{T}}_{\kappa t}\, \mathbf{n}_\kappa\, da_\kappa\,.
\end{aligned}$$

---

[4]We assume the material body is non-polar, i.e., that the Cauchy stress tensor is symmetric, in this work.

Analogous to (6.16),

$$(6.20) \qquad \zeta_{\kappa t}^*(\mathbf{S}_t\,\mathbf{G}^{-1}) = (D\zeta_{\kappa t})^{-1}\,[(\mathbf{S}_t\,\mathbf{G}^{-1})\circ\zeta_{\kappa t}]\,(D\zeta_{\kappa t})^{-*}$$
$$= [(D\zeta_{\kappa t})^{-1}\,(\mathbf{S}_t\circ\zeta_{\kappa t})\,(D\zeta_{\kappa t})^{-\mathrm{T}}]\mathbf{G}^{-1} = \tilde{\mathbf{T}}_{\kappa t}\,\mathbf{G}^{-1}$$

follows for the pull-back of $\mathbf{S}_t\,\mathbf{G}^{-1}$ from (6.18). In terms of the operations (2.26), (2.27), (2.31), (4.9) and (4.10), the last result is given by

$$(6.21)\qquad
\begin{aligned}
\tilde{\mathbf{T}}_{\kappa t} &= \{r_{\mathbf{G}}\circ\zeta_{\kappa t}^*\circ r_{\mathbf{G}-1}\}\mathbf{S}_t & \qquad \mathbf{S}_t &= \{r_{\mathbf{G}}\circ\zeta_{\kappa t*}\circ r_{\mathbf{G}-1}\}\tilde{\mathbf{T}}_{\kappa t}\\
& \qquad\qquad\text{or} \\
&= \{\mathfrak{a}^r_{\mathbf{F}_{\kappa t}^{-1}}\circ\mathfrak{c}_{\zeta_{\kappa t}}\}\mathbf{S}_t & &= \{\mathfrak{c}_{\zeta_{\kappa t}^{-1}}\circ\mathfrak{a}^r_{\mathbf{F}_{\kappa t}}\}\tilde{\mathbf{T}}_{\kappa t}
\end{aligned}$$

which is analogous to (5.30).

Another associated form of $\mathbf{T}_t$ is given by

$$(6.22)\qquad \mathbf{G}\,\mathbf{T}_t : B_t \longrightarrow \mathrm{Sym}(\mathcal{V},\mathcal{V}^*) \quad | \quad p \longmapsto \mathbf{G}\mathbf{T}_t(p)\,.$$

Pulling this back to B_κ yields

$$(6.23)\qquad
\begin{aligned}
\zeta_{\kappa t}^*\,(\mathbf{G}\,\mathbf{T}_t) &= (D\zeta_{\kappa t})^*\,[(\mathbf{G}\,\mathbf{T}_t)\circ\zeta_{\kappa t}]\,(D\zeta_{\kappa t}), \\
&= (D\zeta_{\kappa t})^*\,\mathbf{G}\,(\mathbf{T}_t\circ\zeta_{\kappa t})\,(D\zeta_{\kappa t}), \\
&= \mathbf{G}\,(D\zeta_{\kappa t})^{\mathrm{T}}\,(\mathbf{T}_t\circ\zeta_{\kappa t})\,(D\zeta_{\kappa t}),
\end{aligned}$$

by analogy with (4.18), such that

$$(6.24)\qquad (D\zeta_{\kappa t})^{\mathrm{T}}\,(\mathbf{T}_t\circ\zeta_{\kappa t})\,(D\zeta_{\kappa t}) = \mathbf{G}^{-1}\,\zeta_{\kappa t}^*\,(\mathbf{G}\mathbf{T}_t)\,.$$

In an analogous fashion, we obtain

$$(6.25)\qquad
\begin{aligned}
\zeta_{\kappa t}^*\,(\mathbf{G}\mathbf{S}_t) &= (D\zeta_{\kappa t})^*\,[(\mathbf{G}\mathbf{S}_t)\circ\zeta_{\kappa t}]\,(D\zeta_{\kappa t}), \\
&= (D\zeta_{\kappa t})^*\,\mathbf{G}\,(\mathbf{S}_t\circ\zeta_{\kappa t})\,(D\zeta_{\kappa t}), \\
&= \mathbf{G}\,(D\zeta_{\kappa t})^{\mathrm{T}}\,(\mathbf{S}_t\circ\zeta_{\kappa t})\,(D\zeta_{\kappa t}), \\
&= \mathbf{G}\,\overline{\mathbf{T}}_{\kappa t}
\end{aligned}$$

for the pull-back of $\mathbf{G}\mathbf{S}_t$, in which the "convected" stress tensor

$$(6.26)\qquad \overline{\mathbf{T}}_\kappa : I\times B_\kappa \longrightarrow \mathrm{Sym}(\mathcal{V},\mathcal{V}) \quad | \quad (t,b) \longmapsto (D_b\zeta_{\kappa t})^{\mathrm{T}}\,\mathbf{S}_t(\zeta_\kappa(t,b))\,(D_b\zeta_{\kappa t})$$
$$=: \overline{\mathbf{T}}_\kappa(t,b)$$

appears, such that

$$(6.27)\qquad \overline{\mathbf{T}}_{\kappa t} := (D\zeta_{\kappa t})^{\mathrm{T}}\,(\mathbf{S}_t\circ\zeta_{\kappa t})\,(D\zeta_{\kappa t}) = \mathbf{G}^{-1}\,\zeta_{\kappa t}^*\,(\mathbf{G}\mathbf{S}_t) : B_\kappa \longrightarrow \mathrm{Sym}(\mathcal{V},\mathcal{V})$$

for all $t \in I$. With the help of the operations (2.24), (2.25), (2.29), (4.9) and (4.10), (6.25) can be expressed in the form

(6.28)
$$\overline{T}_{\kappa t} = \{\ell_{G^{-1}} \circ \overset{*}{\zeta}_{\kappa t} \circ \ell_G\} S_t \qquad\qquad S_t = \{\ell_{G^{-1}} \circ \zeta_{\kappa t*} \circ \ell_G\} \overline{T}_{\kappa t}$$
$$\text{or}$$
$$= \{a^\ell_{F_{\kappa t}^{-1}} \circ c_{\zeta_{\kappa t}}\} S_t \qquad\qquad = \{c_{\zeta_{\kappa t}^{-1}} \circ a^\ell_{F_{\kappa t}}\} \overline{T}_{\kappa t}$$

analogous to (4.38). Lastly, we have the relation

(6.29)
$$\overline{T}_\kappa = a^\ell_{F_\kappa^{-1}} S_\kappa = a^\ell_{F_\kappa^{-1}} a^r_{F_\kappa} \tilde{T}_\kappa = F_\kappa^T[F_\kappa \tilde{T}_\kappa F_\kappa^T]F_\kappa = C_\kappa \tilde{T}_\kappa C_\kappa$$

between the second Piola–Kirchhoff $\tilde{T}_\kappa$ and convected $\overline{T}_\kappa$ stress tensors from (4.20), (6.21) and (6.28).

This completes the formulation of the basic strain and stress tensors involved in the formulation of the concept of dual stress-strain tensor pairs, and dual derivatives, to which we now return.

7. The stress power and the two families

The two families of "dual" stress-strain tensors introduced by HT are based on the pairs $(\tilde{T}_{\kappa t}, E_{\kappa t})$ and $(\tilde{\tau}_{\kappa t}, \varepsilon_{\kappa t})$, where

(7.1)
$$\tilde{\tau}_{\kappa t} := -\overline{T}_{\kappa t}$$

represents the negative of the convected stress tensor $\overline{T}_{\kappa t}$. These pairings arise when one expresses the spatial stress power "element"

(7.2)
$$\varrho_t \pi_t \varpi = (T_t \cdot L_t) \varpi$$

relative to the reference configuration B_κ, where the time-dependent function

(7.3)
$$\varrho_t \pi_t := T_t \cdot L_t := \operatorname{tr}_V(T_t L_t^T) = T_t \cdot D_t : B_t \longrightarrow \mathbb{R}$$

represents the spatial stress power density, and π_t the specific spatial stress power. In terms of the associated stress tensors introduced above, the spatial stress power density takes the form

(7.4)
$$\varrho_t \pi_t = \operatorname{tr}_V(T_t L_t^T) = \begin{cases} \operatorname{tr}_V\{(T_t G^{-1})(L_t^* G)\}. \\[2mm] \operatorname{tr}_{V^*}\{(G T_t)(L_t^T G^{-1})\}. \end{cases}$$

Pulling (7.2) back to B_κ and using the associated forms (7.4) for the stress power density yields

(7.5)
$$\overset{*}{\zeta}_{\kappa t}(\varrho_t \pi_t \varpi) = \operatorname{tr}_V\{\tilde{T}_{\kappa t} (\partial F_{\kappa t})^T F_{\kappa t}\} \varpi$$

in the case of the first family via (3.17), (6.8), (6.14) and (6.20), and

(7.6) $$\zeta_{\kappa t}^{*}(\varrho_t\,\pi_t\,\varpi) = \mathrm{tr}_V\{\tilde{\mathbf{T}}_{\kappa t}\,\mathbf{F}_{\kappa t}^{-1}(\partial\mathbf{F}_{\kappa t}^{-\mathrm{T}})\}\,\varpi$$

in the case of the second family via (3.17), (6.8), (6.14), (6.25), (7.1), and the relation $\mathbf{F}_{\kappa t}^{-\mathrm{T}}(\partial\mathbf{F}_{\kappa t}^{\mathrm{T}}) = -(\partial\mathbf{F}_{\kappa t}^{-\mathrm{T}})\,\mathbf{F}_{\kappa t}^{\mathrm{T}}$, which follows from the identity $\mathbf{F}_{\kappa t}^{-\mathrm{T}}\mathbf{F}_{\kappa t}^{\mathrm{T}} = \mathbf{1}_\kappa$.
Pulling back the stress power element itself, we obtain

(7.7)
$$\begin{aligned}\zeta_{\kappa t}^{*}(\varrho_t\,\pi_t\,\varpi) &= (\zeta_{\kappa t}^{*}\varrho_t)\,(\zeta_{\kappa t}^{*}\pi_t)\,(\zeta_{\kappa t}^{*}\varpi),\\ &= \varrho_{\kappa t}\pi_{\kappa t}\,\det(\mathbf{F}_{\kappa t})\,\varpi\,,\\ &= \varrho_\kappa\pi_{\kappa t}\,\varpi\,,\end{aligned}$$

via (6.8), where $\varrho_\kappa := \varrho_{\kappa t}\,\det(\mathbf{F}_{\kappa t})$ is constant in time via mass balance as usual.
Combining (7.5)–(7.7), we have

(7.8)
$$\varrho_\kappa\,\pi_{\kappa t} = \begin{cases} \tilde{\mathbf{T}}_{\kappa t}\cdot(\partial\mathbf{E}_{\kappa t}),\\[6pt] \tilde{\mathbf{\tau}}_{\kappa t}\cdot(\partial\mathbf{\epsilon}_{\kappa t}) \end{cases}$$

for the referential stress power density $\varrho_\kappa\,\pi_{\kappa t}$, where

(7.9) $$\partial\mathbf{E}_{\kappa t} = \frac{1}{2}\,(\partial\mathbf{C}_{\kappa t}) = \mathrm{sym}\{(\partial\mathbf{F}_{\kappa t}^{\mathrm{T}})\mathbf{F}_{\kappa t}\} = \mathrm{sym}\{\mathbf{F}_{\kappa t}^{\mathrm{T}}(\partial\mathbf{F}_{\kappa t})\} = \mathbf{F}_{\kappa t}^{\mathrm{T}}\,\mathbf{D}_{\kappa t}\,\mathbf{F}_{\kappa t}$$

follows from (4.20) and (4.23), and

(7.10) $$\partial\mathbf{\epsilon}_{\kappa t} = \frac{1}{2}\,(\partial\mathbf{C}_{\kappa t}^{-1}) = \mathrm{sym}\{(\partial\mathbf{F}_{\kappa t}^{-1})\mathbf{F}_{\kappa t}^{-\mathrm{T}}\} = \mathrm{sym}\{\mathbf{F}_{\kappa t}^{-1}(\partial\mathbf{F}_{\kappa t}^{-\mathrm{T}})\}$$
$$= -\mathbf{F}_{\kappa t}^{-1}\,\mathbf{D}_{\kappa t}\,\mathbf{F}_{\kappa t}^{-\mathrm{T}}$$

from (4.20) and (5.17). Note that

(7.11) $$\mathbf{F}_{\kappa t}^{\mathrm{T}}\,\mathbf{D}_{\kappa t}\,\mathbf{F}_{\kappa t} = \{\mathfrak{a}_{\mathbf{F}_{\kappa t}^{-1}}^{\ell}\circ\mathfrak{c}_{\zeta_{\kappa t}}\}\mathbf{D}_t \quad\text{and}\quad \mathbf{F}_{\kappa t}^{-1}\,\mathbf{D}_{\kappa t}\,\mathbf{F}_{\kappa t}^{-\mathrm{T}} = \{\mathfrak{a}_{\mathbf{F}_{\kappa t}}^{r}\circ\mathfrak{c}_{\zeta_{\kappa t}}\}\mathbf{D}_t$$

hold via (2.28) and (2.30), respectively.
To obtain the other members of each family from the corresponding pair, HT introduced the "affine" transformations

(7.12)
$$\begin{aligned}\Pi_\kappa &:= \mathsf{L}[\mathbf{E}_\kappa] := \Psi_\kappa^{-\mathrm{T}}\mathbf{E}_\kappa\,\Psi_\kappa^{-1} & \Sigma_\kappa &:= \mathsf{L}^{-\mathrm{T}}[\tilde{\mathbf{T}}_\kappa] := \Psi_\kappa\,\tilde{\mathbf{T}}_\kappa\,\Psi_\kappa^{\mathrm{T}}\\ \pi_\kappa &:= \mathsf{M}[\mathbf{\epsilon}_\kappa] := \Psi_\kappa\,\mathbf{\epsilon}_\kappa\,\Psi_\kappa^{\mathrm{T}} & \sigma_\kappa &:= \mathsf{M}^{-\mathrm{T}}[\tilde{\mathbf{\tau}}_\kappa] := \Psi_\kappa^{-\mathrm{T}}\tilde{\mathbf{\tau}}_\kappa\,\Psi_\kappa^{-1}\end{aligned}$$

of the basic tensors as based on an explicitly time-dependent referential field

(7.13) $$\Psi_\kappa : I\times B_\kappa \longrightarrow \mathrm{Lbj}(V,V)\ \mid\ (t,b)\longmapsto \Psi_\kappa(t,b)\,.$$

Special cases of $\boldsymbol{\Psi}_\kappa$ considered by HT are summarized in the following table:

Table 1. Specific stress-strain tensor transformations.

	$\boldsymbol{\Psi}_\kappa$	:	$I \times B_\kappa$	——	$\mathrm{Lbj}(\mathcal{V}, \mathcal{V})$
Identity	$\mathbf{1}_\kappa$	:	$I \times B_\kappa$	——	$\{\mathbf{1}_\mathcal{V}\}$
Right stretch	$\mathbf{U}_\kappa$	:	$I \times B_\kappa$	——	$\mathrm{Sym}^+(\mathcal{V}, \mathcal{V})$
Polar decomposition rotation	$\mathbf{R}_\kappa$	:	$I \times B_\kappa$	——	$\mathrm{Orth}^+(\mathcal{V}, \mathcal{V})$
Deformation gradient	$\mathbf{F}_\kappa$	:	$I \times B_\kappa$	——	$\mathrm{Lbj}^+(\mathcal{V}, \mathcal{V})$
Material spin rotation	$\mathbf{P}_\kappa$	:	$I \times B_\kappa$	——	$\mathrm{Orth}^+(\mathcal{V}, \mathcal{V})$

where

(7.14) $\mathbf{P}_\kappa : I \times B_\kappa \;\longrightarrow\; \mathrm{Orth}^+(\mathcal{V}, \mathcal{V}) \;\mid\; (t, b) \longmapsto \mathbf{P}_\kappa(t, b)$

is defined by

(7.15) $\partial \mathbf{P}_\kappa = \mathbf{W}_\kappa \mathbf{P}_\kappa \;.$

Note that $\mathbf{1}_\kappa$ is a *constant* map. We note in passing that HT also considered the case when $\boldsymbol{\Psi}_\kappa$ is given by the plastic part $\mathbf{F}_\kappa^{\mathrm{p}}$ of the deformation gradient $\mathbf{F}_\kappa$ in the usual multiplicative elastoplastic decomposition $\mathbf{F}_\kappa = \mathbf{F}_\kappa^{\mathrm{E}}\mathbf{F}_\kappa^{\mathrm{p}}$ of $\mathbf{F}_\kappa$. In contrast to the polar decomposition of $\mathbf{F}_\kappa$, of course, this elastoplastic decomposition is of a *physical* nature, and as such, a subject to interpretation. The detailed discussion of the formulation and interpretation of such "physical" decompositions of $\mathbf{F}_\kappa$ in a differential geometric setting is an issue in itself, requiring in fact concepts which go beyond the scope of this work, and as such, will be dealt with in future work. It suffices here to note that the results for $\mathbf{F}_\kappa^{\mathrm{p}}$ are analogous to those given for $\mathbf{F}_\kappa$ in what follows. Another possibility arises when $\boldsymbol{\Psi}_\kappa$ takes values in $\mathrm{Uni}^+(\mathcal{V}, \mathcal{V})$, e.g., $\boldsymbol{\Psi}_\kappa := \mathbf{F}_\kappa / [\det(\mathbf{F}_\kappa)]^{1/3}$ or $\boldsymbol{\Psi}_\kappa := \mathbf{U}_\kappa / [\det(\mathbf{U}_\kappa)]^{1/3}$. In what follows, let

(7.16) $\mathfrak{G}_\kappa := \{\boldsymbol{\Psi}_\kappa \mid \boldsymbol{\Psi}_\kappa : I \times B_\kappa \longrightarrow \mathrm{Lbj}(\mathcal{V}, \mathcal{V})\}$

represent a "group" of such transformations, including the ones just discussed. Note that all of these mappings have in common the feature that they map vector fields associated with B_κ to vector fields associated with certain "intermediate configurations" of the material body; in particular, of course, $\mathbf{F}_{\kappa t}$ maps such fields to vector fields associated with B_κ to B_t, as discussed in Sec. 4.

In this section, we want to show that the "affine" transformations (7.12) introduced by HT, are, like the transformations in (4.38), (5.30), (6.21) and

(6.28), based on (1), the formation of associated tensors via the Euclidean metric $\mathbf{G} \in \mathrm{Sym}^{+}(V, V^{*})$, and (2), the *action* (2.14) of elements of $\mathfrak{G}_{\kappa}$ on V-tensor-valued time-dependent fields. Starting with the associated Green strain tensor $\mathbf{GE}_{\kappa} : I \times B_{\kappa} \to \mathrm{Sym}(V, V^{*})$, we note that it represents a field of linear transformations of the kind considered in (2.17). Consequently,

$$
\begin{aligned}
\mathfrak{a}_{\Psi_{\kappa}}(\mathbf{GE}_{\kappa}) &= \Psi_{\kappa}^{-*}\,\mathbf{GE}_{\kappa}\,\Psi_{\kappa}^{-1}, \\
&= \mathbf{G}\,[\Psi_{\kappa}^{-\mathrm{T}}\,\mathbf{E}_{\kappa}\,\Psi_{\kappa}^{-1}], \\
&= \mathbf{G}\,\mathbf{L}[\mathbf{E}_{\kappa}]
\end{aligned}
$$

(7.17)

from $(7.12)_1$, implying that

(7.18) $\qquad \mathbf{E}_{\Psi_{\kappa}} := \mathbf{L}[\mathbf{E}_{\kappa}] := \Psi_{\kappa}^{-\mathrm{T}}\,\mathbf{E}_{\kappa}\,\Psi_{\kappa}^{-1} = \mathbf{G}^{-1}\,\mathfrak{a}_{\Psi_{\kappa}}(\mathbf{GE}_{\kappa}) = \mathfrak{a}_{\Psi_{\kappa}}^{\ell}\,\mathbf{E}_{\kappa}$

via (2.29), i.e., $\mathbf{L} = \mathfrak{a}_{\Psi_{\kappa}}^{\ell}$. Consequently, the "affine" transformation $\mathbf{L}$ introduced by HT represents an *associated action* of $\mathfrak{G}_{\kappa}$ on $\mathbf{E}_{\kappa} : I \times B_{\kappa} \to \mathrm{Sym}(V, V)$. Note that (4.38) represents a particular case of (7.18), i.e.,

(7.19) $\qquad \mathbf{A}_{\kappa t} = \mathfrak{c}_{\zeta_{\kappa t}}\mathbf{A}_{t} = \mathbf{A}_{t} \circ \zeta_{\kappa t} = \mathbf{E}_{\mathbf{F}_{\kappa t}} = \mathfrak{a}_{\mathbf{F}_{\kappa t}}^{\ell}\,\mathbf{E}_{\kappa t}$

can be obtained from (7.18) with $\Psi_{\kappa} = \mathbf{F}_{\kappa}$. From Table 1 and (7.18), we have then the following strain tensors of the first family:

Table 2. Particular strain tensors of the first family.

Ψ_{κ} $\mathbf{E}_{\Psi_{\kappa}} = \mathfrak{a}_{\Psi_{\kappa}}^{\ell}\,\mathbf{E}_{\kappa} = \Psi_{\kappa}^{-\mathrm{T}}\mathbf{E}_{\kappa}\Psi_{\kappa}^{-1}$		Strain tensor
$\mathbf{1}_{\kappa}$ $\mathbf{E}_{\mathbf{1}_{\kappa}} = \mathfrak{a}_{\mathbf{1}_{\kappa}}^{\ell}\,\mathbf{E}_{\kappa} = \mathbf{1}_{\kappa}^{-\mathrm{T}}\mathbf{E}_{\kappa}\mathbf{1}_{\kappa}^{-1}$	$= \frac{1}{2}\,(\mathbf{U}_{\kappa}^{\mathrm{T}}\mathbf{U}_{\kappa} - \mathbf{1}_{\kappa})$	Green
$\mathbf{U}_{\kappa}$ $\mathbf{E}_{\mathbf{U}_{\kappa}} = \mathfrak{a}_{\mathbf{U}_{\kappa}}^{\ell}\,\mathbf{E}_{\kappa} = \mathbf{U}_{\kappa}^{-\mathrm{T}}\mathbf{E}_{\kappa}\mathbf{U}_{\kappa}^{-1}$	$= \frac{1}{2}\,(\mathbf{1}_{\kappa} - \mathbf{U}_{\kappa}^{-\mathrm{T}}\mathbf{U}_{\kappa}^{-1})$	referential Karni–Reiner
$\mathbf{R}_{\kappa}$ $\mathbf{E}_{\mathbf{R}_{\kappa}} = \mathfrak{a}_{\mathbf{R}_{\kappa}}^{\ell}\,\mathbf{E}_{\kappa} = \mathbf{R}_{\kappa}^{-\mathrm{T}}\mathbf{E}_{\kappa}\mathbf{R}_{\kappa}^{-1}$	$= \frac{1}{2}\,(\mathbf{V}_{\kappa}^{\mathrm{T}}\mathbf{V}_{\kappa} - \mathbf{1}_{\kappa})$	spatial Karni–Reiner
$\mathbf{F}_{\kappa}$ $\mathbf{E}_{\mathbf{F}_{\kappa}} = \mathfrak{a}_{\mathbf{F}_{\kappa}}^{\ell}\,\mathbf{E}_{\kappa} = \mathbf{F}_{\kappa}^{-\mathrm{T}}\mathbf{E}_{\kappa}\mathbf{F}_{\kappa}^{-1}$	$= \frac{1}{2}\,(\mathbf{1}_{\kappa} - \mathbf{V}_{\kappa}^{-\mathrm{T}}\mathbf{V}_{\kappa}^{-1})$	Almansi
$\mathbf{P}_{\kappa}$ $\mathbf{E}_{\mathbf{P}_{\kappa}} = \mathfrak{a}_{\mathbf{P}_{\kappa}}^{\ell}\,\mathbf{E}_{\kappa} = \mathbf{P}_{\kappa}^{-\mathrm{T}}\mathbf{E}_{\kappa}\mathbf{P}_{\kappa}^{-1}$		Jaumann

All of these strain tensors of the first family are elements of the "orbit" $O_{\mathbf{E}_{\kappa}}$ of $\mathbf{E}_{\kappa}$ in $\mathrm{Map}(I \times B_{\kappa}, \mathrm{Sym}(V, V))$ with respect to $\mathfrak{G}_{\kappa}$. Clearly, all elements of

$O_{\mathbf{E}_\kappa}$ represent strain tensors having the same physical interpretation as $\mathbf{E}_\kappa$, i.e., deformation of tangent vector fields.

Turning now to the associated Piola strain tensor $\varepsilon_\kappa \mathbf{G}^{-1} : I \times B_\kappa \rightarrow \text{Sym}(\mathcal{V}^*, \mathcal{V})$, we note that it represents a field of linear transformations of the kind represented in (2.19). Consequently,

$$\mathfrak{a}_{\Psi_\kappa}(\varepsilon_\kappa \mathbf{G}^{-1}) = \Psi_\kappa \varepsilon_\kappa \mathbf{G}^{-1} \Psi_\kappa^* .$$

(7.20)
$$= [\Psi_\kappa \varepsilon_\kappa \Psi_\kappa^{\mathrm{T}}] \mathbf{G}^{-1} ,$$

$$= \mathsf{M}[\varepsilon_\kappa] \mathbf{G}^{-1}$$

from (7.12)$_3$, implying that

(7.21) $\qquad \varepsilon_{\Psi_\kappa} := \mathsf{M}[\varepsilon_\kappa] := \Psi_\kappa \varepsilon_\kappa \Psi_\kappa^{\mathrm{T}} = \mathfrak{a}_{\Psi_\kappa}(\varepsilon_\kappa \mathbf{G}^{-1}) \mathbf{G} = \mathfrak{a}_{\Psi_\kappa}^r \varepsilon_\kappa$

via (2.31), i.e., $\mathsf{M} = \mathfrak{a}_{\Psi_\kappa}^r$. As above, then, the "affine" transformation M introduced by HT represents a second associated action of $\mathfrak{G}_\kappa$ via $\Psi_\kappa \in \mathfrak{G}_\kappa$ on $\varepsilon_\kappa : I \times B_\kappa \rightarrow \text{Sym}(\mathcal{V}, \mathcal{V})$. With $\Psi_\kappa = \mathbf{F}_\kappa$, (7.21) yields in particular

(7.22) $\qquad \alpha_{\kappa t} = \mathfrak{c}_{\zeta_{\kappa t}} \alpha_t = \alpha_t \circ \zeta_{\kappa t} = \varepsilon_{\mathbf{F}_{\kappa t}} = \mathfrak{a}_{\mathbf{F}_{\kappa t}}^r \varepsilon_{\kappa t} .$

i.e., (5.30), for all $t \in I$. From Table 1 and (7.21), then, we have the following strain tensors of the second family:

Table 3. Particular strain tensors of the second family.

Ψ_κ	$\varepsilon_{\Psi_\kappa} = \mathfrak{a}_{\Psi_\kappa}^r \varepsilon_\kappa = \Psi_\kappa \varepsilon_\kappa \Psi_\kappa^{\mathrm{T}}$			Strain tensor
$\mathbf{1}_\kappa$	$\varepsilon_{\mathbf{1}_\kappa} = \mathfrak{a}_{\mathbf{1}_\kappa}^r \varepsilon_\kappa$	$= \mathbf{1}_\kappa \varepsilon_\kappa \mathbf{1}_\kappa^{\mathrm{T}}$	$= \frac{1}{2}(\mathbf{U}_\kappa^{-1}\mathbf{U}_\kappa^{-\mathrm{T}} - \mathbf{1}_\kappa)$	Piola
$\mathbf{U}_\kappa$	$\varepsilon_{\mathbf{U}_\kappa} = \mathfrak{a}_{\mathbf{U}_\kappa}^r \varepsilon_\kappa$	$= \mathbf{U}_\kappa \varepsilon_\kappa \mathbf{U}_\kappa^{\mathrm{T}}$	$= \frac{1}{2}(\mathbf{1}_\kappa - \mathbf{U}_\kappa \mathbf{U}_\kappa^{\mathrm{T}})$	negative Green
$\mathbf{R}_\kappa$	$\varepsilon_{\mathbf{R}_\kappa} = \mathfrak{a}_{\mathbf{R}_\kappa}^r \varepsilon_\kappa$	$= \mathbf{R}_\kappa \varepsilon_\kappa \mathbf{R}_\kappa^{\mathrm{T}}$	$= \frac{1}{2}(\mathbf{V}_\kappa^{-1}\mathbf{V}_\kappa^{-\mathrm{T}} - \mathbf{1}_\kappa)$	negative Almansi
$\mathbf{F}_\kappa$	$\varepsilon_{\mathbf{F}_\kappa} = \mathfrak{a}_{\mathbf{F}_\kappa}^r \varepsilon_\kappa$	$= \mathbf{F}_\kappa \varepsilon_\kappa \mathbf{F}_\kappa^{\mathrm{T}}$	$= \frac{1}{2}(\mathbf{1}_\kappa - \mathbf{V}_\kappa \mathbf{V}_\kappa^{\mathrm{T}})$	Finger
$\mathbf{P}_\kappa$	$\varepsilon_{\mathbf{P}_\kappa} = \mathfrak{a}_{\mathbf{P}_\kappa}^r \varepsilon_\kappa$	$= \mathbf{P}_\kappa \varepsilon_\kappa \mathbf{P}_\kappa^{\mathrm{T}}$		rotated Piola

As with the first family based on $\mathbf{E}_\kappa$, all of the strain tensors in Table 2 are elements of the orbit O_{ε_κ} of ε_κ in $\text{Map}(I \times B_\kappa, \text{Sym}(\mathcal{V}, \mathcal{V}))$ with respect to $\mathfrak{G}_\kappa$. Note that (5.18), (7.18) and (7.21) imply that $\mathbf{E}_\kappa$ and ε_κ are in different associated $\mathfrak{G}_\kappa$-orbits in $\text{Map}(I \times B_\kappa, \text{Sym}(\mathcal{V}, \mathcal{V}))$.

Following the same procedure for the associated second Piola – Kirchhoff stress tensor $\tilde{\mathbf{T}}_\kappa \mathbf{G}^{-1} : I \times B_\kappa \to \mathrm{Sym}(V^*, V)$, we have from (2.19) the result

$$
\begin{aligned}
\mathfrak{a}_{\Psi_\kappa}(\tilde{\mathbf{T}}_\kappa \mathbf{G}^{-1}) &= \Psi_\kappa \tilde{\mathbf{T}}_\kappa \mathbf{G}^{-1} \Psi_\kappa^*, \\
(7.23) \qquad\qquad &= [\Psi_\kappa \tilde{\mathbf{T}}_\kappa \Psi_\kappa^\mathrm{T}] \mathbf{G}^{-1}, \\
&= \mathbf{L}^{-\mathrm{T}}[\tilde{\mathbf{T}}_\kappa] \mathbf{G}^{-1},
\end{aligned}
$$

where

$$
(7.24) \qquad \tilde{\mathbf{T}}_{\Psi_\kappa} := \mathbf{L}^{-\mathrm{T}}[\tilde{\mathbf{T}}_\kappa] := \Psi_\kappa \tilde{\mathbf{T}}_\kappa \Psi_\kappa^\mathrm{T} = \mathfrak{a}_{\Psi_\kappa}(\tilde{\mathbf{T}}_\kappa \mathbf{G}^{-1}) \mathbf{G} = \mathfrak{a}_{\Psi_\kappa}^r \tilde{\mathbf{T}}_\kappa
$$

from $(7.12)_2$ such that $\mathbf{L}^{-\mathrm{T}} = \mathfrak{a}_{\Psi_\kappa}^r$. Note from (7.21) and (7.24) that stress tensors of the first family, as based on $\tilde{\mathbf{T}}_\kappa$ (i.e., on $\tilde{\mathbf{T}}_\kappa \mathbf{G}^{-1}$), transform in the same way as strain tensors of the second family, as based on ε_κ (i.e., on $\varepsilon_\kappa \mathbf{G}^{-1}$). Again, the choice $\Psi_\kappa = \mathbf{F}_\kappa$ in (7.24) yields

$$
(7.25) \qquad \mathbf{S}_{\kappa t} = \mathfrak{c}_{\zeta_{\kappa t}} \mathbf{S}_t = \mathbf{S}_t \circ \zeta_{\kappa t} = \tilde{\mathbf{T}}_{\mathbf{F}_{\kappa t}} = \mathfrak{a}_{\mathbf{F}_{\kappa t}}^r \tilde{\mathbf{T}}_{\kappa t},
$$

i.e., (6.21), for all $t \in I$. Table 1 and (7.24) yield in particular the following stress tensors of the first family:

Table 4. Particular stress tensors of the first family.

Ψ_κ	$\tilde{\mathbf{T}}_{\Psi_\kappa} = \mathfrak{a}_{\Psi_\kappa}^r \tilde{\mathbf{T}}_\kappa = \Psi_\kappa \tilde{\mathbf{T}}_\kappa \Psi_\kappa^\mathrm{T}$			Stress tensor
$\mathbf{1}_\kappa$	$\tilde{\mathbf{T}}_{\mathbf{1}_\kappa} = \mathfrak{a}_{\mathbf{1}_\kappa}^r \tilde{\mathbf{T}}_\kappa$	$= \mathbf{1}_\kappa \tilde{\mathbf{T}}_\kappa \mathbf{1}_\kappa^\mathrm{T}$	$= \mathfrak{a}_{\mathbf{F}_\kappa^{-1}}^r \mathbf{S}_\kappa$	2$^{\mathrm{nd}}$ Piola – Kirchoff
$\mathbf{U}_\kappa$	$\tilde{\mathbf{T}}_{\mathbf{U}_\kappa} = \mathfrak{a}_{\mathbf{U}_\kappa}^r \tilde{\mathbf{T}}_\kappa$	$= \mathbf{U}_\kappa \tilde{\mathbf{T}}_\kappa \mathbf{U}_\kappa^\mathrm{T}$	$= \mathfrak{a}_{\mathbf{R}_\kappa^{-1}}^r \mathbf{S}_\kappa$	
$\mathbf{R}_\kappa$	$\tilde{\mathbf{T}}_{\mathbf{R}_\kappa} = \mathfrak{a}_{\mathbf{R}_\kappa}^r \tilde{\mathbf{T}}_\kappa$	$= \mathbf{R}_\kappa \tilde{\mathbf{T}}_\kappa \mathbf{R}_\kappa^\mathrm{T}$	$= \mathfrak{a}_{\mathbf{V}_\kappa^{-1}}^r \mathbf{S}_\kappa$	
$\mathbf{F}_\kappa$	$\tilde{\mathbf{T}}_{\mathbf{F}_\kappa} = \mathfrak{a}_{\mathbf{F}_\kappa}^r \tilde{\mathbf{T}}_\kappa$	$= \mathbf{F}_\kappa \tilde{\mathbf{T}}_\kappa \mathbf{F}_\kappa^\mathrm{T}$	$= \mathfrak{a}_{\mathbf{1}_\kappa^{-1}}^r \mathbf{S}_\kappa$	weighted Cauchy
$\mathbf{P}_\kappa$	$\tilde{\mathbf{T}}_{\mathbf{P}_\kappa} = \mathfrak{a}_{\mathbf{P}_\kappa}^r \tilde{\mathbf{T}}_\kappa$	$= \mathbf{P}_\kappa \tilde{\mathbf{T}}_\kappa \mathbf{P}_\kappa^\mathrm{T}$		rotated 2$^{\mathrm{nd}}$ Piola – Kirchhoff

Again, we emphasize that all of these stress tensors are equivalent to $\tilde{\mathbf{T}}_\kappa$ in the sense that they are all elements of the orbit $O_{\tilde{\mathbf{T}}_\kappa}$ of $\tilde{\mathbf{T}}_\kappa$ in $\mathrm{Map}(I \times B_\kappa, \mathrm{Sym}(V, V))$ with respect to $\mathfrak{G}_\kappa$, and possess consequently the same physical interpretation.

Lastly, for the associated convected stress tensor $G\tilde{\tau}_\kappa : I \times B_\kappa \to \mathrm{Sym}(V, V^*)$, we obtain

$$
\begin{aligned}
\mathfrak{a}_{\Psi_\kappa}(G\tilde{\tau}_\kappa) &= \Psi_\kappa^{-*} G\tilde{\tau}_\kappa \Psi_\kappa^{-1}, \\
\text{(7.26)} \qquad &= G\,[\Psi_\kappa^{-T} \tilde{\tau}_\kappa \Psi_\kappa^{-1}], \\
&= G\,M^{-T}[\tilde{\tau}_\kappa]
\end{aligned}
$$

from (2.17), where

$$
\text{(7.27)} \qquad \tilde{\tau}_{\Psi_\kappa} := M^{-T}[\tilde{\tau}_\kappa] := \Psi_\kappa^{-T} \tilde{\tau}_\kappa \Psi_\kappa^{-1} = G^{-1}\,\mathfrak{a}_{\Psi_\kappa}(G\tilde{\tau}_\kappa) = \mathfrak{a}_{\Psi_\kappa}^\ell \tilde{\tau}_\kappa
$$

from $(7.12)_2$ such that $M^{-T} = \mathfrak{a}_{\Psi_\kappa}^\ell$. Comparing (7.18) and (7.27), we see that stress tensors of the second family, being based on $\tilde{\tau}_\kappa$ (i.e., on $G\tilde{\tau}_\kappa$), transform in the same fashion as do the strain tensors of the first family based on E_κ (i.e., on GE_κ). Again, note the particular case of (7.27):

$$
\text{(7.28)} \qquad s_{\kappa t} := -S_{\kappa t} = \tilde{\tau}_{F_\kappa} = \mathfrak{a}_{F_\kappa}^\ell \tilde{\tau}_{\kappa t}.
$$

i.e., (6.28) follows from (7.27) for the choice $\Psi_\kappa = F_\kappa$. Combining the elements of $\mathfrak{G}_\kappa$ in Table 1 with (7.27) yields the following particular stress tensors of the second family:

Table 5. Particular stress tensors of the second family.

Ψ_κ	$\tilde{\tau}$	$= \mathfrak{a}_{\Psi_\kappa}^\ell \tilde{\tau}_\kappa$	$= \Psi_\kappa^{-T}\tilde{\tau}_\kappa\Psi_\kappa^{-1}$		Stress tensor
1_κ	$\tilde{\tau}_{1_\kappa}$	$= \mathfrak{a}_{1_\kappa}^\ell \tilde{\tau}_\kappa$	$= 1_\kappa^{-T}\tilde{\tau}_\kappa 1_\kappa^{-1}$	$= \mathfrak{a}_{F_\kappa^{-1}}^\ell s_\kappa$	negative convected
U_κ	$\tilde{\tau}_{U_\kappa}$	$= \mathfrak{a}_{U_\kappa}^\ell \tilde{\tau}_\kappa$	$= U_\kappa^{-T}\tilde{\tau}_\kappa U_\kappa^{-1}$	$= \mathfrak{a}_{R_\kappa^{-1}}^\ell s_\kappa$	
R_κ	$\tilde{\tau}_{R_\kappa}$	$= \mathfrak{a}_{R_\kappa}^\ell \tilde{\tau}_\kappa$	$= R_\kappa^{-T}\tilde{\tau}_\kappa R_\kappa^{-1}$	$= \mathfrak{a}_{V_\kappa^{-1}}^\ell s_\kappa$	
F_κ	$\tilde{\tau}_{F_\kappa}$	$= \mathfrak{a}_{F_\kappa}^\ell \tilde{\tau}_\kappa$	$= F_\kappa^{-T}\tilde{\tau}_\kappa F_\kappa^{-1}$	$= \mathfrak{a}_{1_\kappa}^\ell s_\kappa$	negative weighted Cauchy
P_κ	$\tilde{\tau}_{P_\kappa}$	$= \mathfrak{a}_{P_\kappa}^\ell \tilde{\tau}_\kappa$	$= P_\kappa^{-T}\tilde{\tau}_\kappa P_\kappa^{-1}$		rotated negative convected

Like E_κ and ε_κ, the associated $\mathfrak{G}_\kappa$-orbits $O_{\tilde{T}_\kappa}$ and $O_{\tilde{\tau}_\kappa}$ of $\tilde{T}_\kappa$ and $\tilde{\tau}_\kappa$ in $\mathrm{Map}(I \times B_\kappa, \mathrm{Sym}(V, V))$ are clearly different.

We close this section by deriving relations between some of the strain and stress tensors of each family induced by multiplicative decomposition of the deformation gradient (e.g., polar decomposition (3.11)). To do this, we first consider the left translation

$$(7.29) \qquad \Phi_\kappa = Z_\kappa \Psi_\kappa = \lambda_{Z_\kappa} \Psi_\kappa$$

of $\Psi_\kappa \in \mathfrak{G}_\kappa$ to $\Phi_\kappa \in \mathfrak{G}_\kappa$ by $Z_\kappa \in \mathfrak{G}_\kappa$. Particular cases of (7.29) include the polar decomposition (3.11) of F_κ (i.e., with $\Phi_\kappa = F_\kappa$, $Z_\kappa = R_\kappa$ and $\Psi_\kappa = U_\kappa$, or $Z_\kappa = V_\kappa$ and $\Psi_\kappa = R_\kappa$), or the multiplicative decomposition of F_κ in finite elastoplasticity (i.e., with $\Phi_\kappa = F_\kappa$, $Z_\kappa = F_\kappa^E$ and $\Psi_\kappa = F_\kappa^P$). Let Υ_κ be any time-dependent $\mathcal{V}$-tensor-valued referential field, and define $\Upsilon_{\Psi_\kappa} := \mathfrak{a}_{\Psi_\kappa} \Upsilon_\kappa$ for any $\Psi_\kappa \in \mathfrak{G}_\kappa$; in particular, we then have $\Upsilon_{1_\kappa} = \Upsilon_\kappa$. The left translation (7.29) induces then the transformation

$$(7.30) \qquad \Upsilon_{\Phi_\kappa} = \mathfrak{a}_{\Phi_\kappa} \Upsilon_\kappa = \mathfrak{a}_{\Phi_\kappa} \mathfrak{a}_{\Psi_\kappa^{-1}} \Upsilon_{\Psi_\kappa} = \mathfrak{a}_{\Phi_\kappa \Psi_\kappa^{-1}} \Upsilon_{\Psi_\kappa} = \mathfrak{a}_{Z_\kappa} \Upsilon_{\Psi_\kappa}$$

of Υ_{Ψ_κ} to Υ_{Φ_κ}. Such a transformation is induced, for example, by the polar decompositions (3.11); in particular, with $\Upsilon_{\Psi_\kappa} = \mathfrak{a}^\ell_{\Psi_\kappa} \Upsilon_{1_\kappa} = \mathfrak{a}^\ell_{\Psi_\kappa} \Upsilon_\kappa$, we have

$$(7.31) \qquad \Upsilon_{F_\kappa} = \mathfrak{a}^\ell_{F_\kappa} \Upsilon_{1_\kappa} = \begin{cases} \mathfrak{a}^\ell_{R_\kappa} \Upsilon_{U_\kappa}, \\ \mathfrak{a}^\ell_{V_\kappa} \Upsilon_{R_\kappa}, \end{cases}$$

which imply

$$\Upsilon_{U_\kappa} = \begin{cases} \mathfrak{a}^\ell_{U_\kappa} \Upsilon_{1_\kappa} = U_\kappa^{-T} \Upsilon_{1_\kappa} U_\kappa^{-1}, \\ \mathfrak{a}^\ell_{R_\kappa^{-1}} \Upsilon_{F_\kappa} = R_\kappa^T \Upsilon_{F_\kappa} R_\kappa. \end{cases}$$

$$(7.32) \qquad \text{and}$$

$$\Upsilon_{R_\kappa} = \begin{cases} \mathfrak{a}^\ell_{R_\kappa} \Upsilon_{1_\kappa} = R_\kappa^{-T} \Upsilon_{1_\kappa} R_\kappa^{-1}, \\ \mathfrak{a}^\ell_{V_\kappa^{-1}} \Upsilon_{F_\kappa} = V_\kappa^T \Upsilon_{F_\kappa} V_\kappa. \end{cases}$$

In particular, (7.32) hold for $\Upsilon_\kappa = E_\kappa$ and $\Upsilon_\kappa = \tilde{\tau}_\kappa$. Similarly, with $\Upsilon_{\Psi_\kappa} = \mathfrak{a}^r_{\Psi_\kappa} \Upsilon_{1_\kappa} = \mathfrak{a}^r_{\Psi_\kappa} \Upsilon_\kappa$, (3.11) induces

$$(7.33) \qquad \Upsilon_{F_\kappa} = \mathfrak{a}^r_{F_\kappa} \Upsilon_{1_\kappa} = \begin{cases} \mathfrak{a}^r_{R_\kappa} \Upsilon_{U_\kappa}, \\ \mathfrak{a}^r_{V_\kappa} \Upsilon_{R_\kappa}. \end{cases}$$

such that

$$
\Upsilon_{U_\kappa} = \begin{cases} a^{\tau}_{U_\kappa} \Upsilon_{1_\kappa} = U_\kappa \Upsilon_{1_\kappa} U_\kappa^{\tau}, \\ a^{\tau}_{R_\kappa^{-1}} \Upsilon_{F_\kappa} = R_\kappa^{-1} \Upsilon_{F_\kappa} R_\kappa^{-\tau}, \end{cases}
$$

(7.34)   and

$$
\Upsilon_{R_\kappa} = \begin{cases} a^{\tau}_{R_\kappa} \Upsilon_{1_\kappa} = R_\kappa \Upsilon_{1_\kappa} R_\kappa^{\tau}, \\ a^{\tau}_{V_\kappa^{-1}} \Upsilon_{F_\kappa} = V_\kappa^{-1} \Upsilon_{F_\kappa} V_\kappa^{-\tau}. \end{cases}
$$

In particular, these hold for $\Upsilon_\kappa = \varepsilon_\kappa$ and $\Upsilon_\kappa = \tilde{T}_\kappa$. Analogous relations are induced by the elastoplastic decomposition $F_\kappa = F_\kappa^E F_\kappa^P$ of F_κ. Note also that $a^{\ell}_{R_\kappa} \Upsilon_\kappa = a^{r}_{R_\kappa} \Upsilon_\kappa$.

8. Time derivatives of the basic strain and stress tensors

As a prelude to discussing the "dual" derivatives introduced by HT, we consider in this section various common time derivatives of the basic stress and strain tensors discussed in Secs. 4–6. To begin, consider the relation (3.4) between the referential $\psi_{\kappa t}: B_\kappa - A$ and spatial $\psi_t: B_t - A$ forms of some field $\psi_{\kappa t} = \psi_t \circ \zeta_{\kappa t}$, with A representing now some normed linear space. The time derivative of this relation takes the form

(8.1) $$\partial \psi_{\kappa t} := (\partial \psi_\kappa)_t = (\mathcal{M}_{v_t} \psi_t) \circ \zeta_{\kappa t} .$$

for all $t \in I$ via the chain rule and the flow relation (3.9), where

(8.2) $$\mathcal{M}_{v_t} \psi_t = \dot{\psi}_t := \partial \psi_t + (D\psi_t)v_t$$

represents as usual the *material time derivative* of ψ_t. If ψ_t is in fact not explicitly time-dependent, then naturally $\partial \psi_t$ vanishes and $\mathcal{M}_{v_t} \psi_t = (D\psi_t)v_t$. Note that we have the commutation relation

(8.3) $$\partial \circ c_{\zeta_{\kappa t}} = c_{\zeta_{\kappa t}} \circ \mathcal{M}_{v_t}$$

using (3.5), as well as the operator form

(8.4) $$\mathcal{M}_{v_t} = c_{\zeta_{\kappa t}^{-1}} \circ \partial \circ c_{\zeta_{\kappa t}}$$

for the material time derivative.

A second type of time derivative arises when we consider a time-dependent spatial $\mu_t \colon B_t \to \mathrm{Lin}_{p+q}(V^{*p} \times V^q, \mathbb{R})$ tensor field and its pull-back $\zeta_{\kappa t}^* \mu_t$ defined in (4.6). Taking the time derivative of $\zeta_{\kappa t}^* \mu_t$ yields

(8.5)
$$\partial(\zeta_{\kappa t}^* \mu_t) = \zeta_{\kappa t}^* (\mathcal{L}_{\mathbf{v}_t} \mu_t) \,,$$

where

(8.6)
$$\mathcal{L}_{\mathbf{v}_t} \mu_t := \partial \mu_t + \mathcal{L}_{\mathbf{v}_t} \mu_t$$

represents the *dynamic Lie derivative*, and $\mathcal{L}_{\mathbf{v}_t} \mu_t$ the *autonomous Lie derivative*, of $\mu_t \colon B_t \to \mathrm{Lin}_{p+q}(V^{*p} \times V^q, \mathbb{R})$ with respect to $\mathbf{v}_t$ (e.g., ABRAHAM *et al.* [5, §§5.3–5.4]). Rather than give the general definition of $\mathcal{L}_{\mathbf{v}_t} \mu_t$, we will obtain it directly in the cases of interest below. The result (8.5) contains the commutation relation

(8.7)
$$\partial \circ \zeta_{\kappa t}^* = \zeta_{\kappa t}^* \circ \mathcal{L}_{\mathbf{v}_t}$$

analogous to (8.3), implying the operator form

(8.8)
$$\mathcal{L}_{\mathbf{v}_t} = \zeta_{\kappa t *} \circ \partial \circ \zeta_{\kappa t}^*$$

for $\mathcal{L}_{\mathbf{v}_t}$ analogous to (8.4) for $\mathcal{M}_{\mathbf{v}_t}$. Via (4.9) and (4.10), (8.7) and (8.8) take the forms

(8.9)
$$\partial \circ \mathbf{a}_{\mathbf{F}_{\kappa t}^{-1}} \circ \mathbf{c}_{\zeta_{\kappa t}} = \partial \circ \zeta_{\kappa t}^* = \zeta_{\kappa t}^* \circ \mathcal{L}_{\mathbf{v}_t} = \mathbf{a}_{\mathbf{F}_{\kappa t}^{-1}} \circ \mathbf{c}_{\zeta_{\kappa t}} \circ \mathcal{L}_{\mathbf{v}_t}$$

and

(8.10)
$$\mathcal{L}_{\mathbf{v}_t} = \zeta_{\kappa t *} \circ \partial \circ \zeta_{\kappa t}^* = \mathbf{c}_{\zeta_{\kappa t}^{-1}} \circ \mathbf{a}_{\mathbf{F}_{\kappa t}} \circ \partial \circ \mathbf{a}_{\mathbf{F}_{\kappa t}^{-1}} \circ \mathbf{c}_{\zeta_{\kappa t}} \,.$$

respectively, in terms of $\mathbf{a}_{\mathbf{F}_{\kappa t}}$, $\mathbf{a}_{\mathbf{F}_{\kappa t}^{-1}}$ and ∂. The structure $\mathbf{a}_{\mathbf{F}_{\kappa t}} \circ \partial \circ \mathbf{a}_{\mathbf{F}_{\kappa t}^{-1}}$ present in the operator form (8.10) for $\mathcal{L}_{\mathbf{v}_t}$ is characteristic of all "objective" time derivatives considered in this work.

We turn now to the stress and strain tensor relations obtained in the previous sections. Via the relations $\partial(D\zeta_{\kappa t}) = \mathbf{L}_{\kappa t}(D\zeta_{\kappa t})$ and $\partial(D\zeta_{\kappa t})^* = [\partial(D\zeta_{\kappa t})]^* = (D\zeta_{\kappa t})^* \mathbf{L}_{\kappa t}^*$ from (3.17), the time derivative of (4.18) yields

(8.11)
$$\partial(\mathbf{G}\mathbf{C}_{\kappa t}) = \partial(\zeta_{\kappa t}^* \mathbf{G}) = \zeta_{\kappa t}^*[\mathbf{L}_t^* \mathbf{G} + \mathbf{G}\mathbf{L}_t]$$

since $\mathbf{G}$ is constant, such that $\partial \mathbf{G}$ vanishes. On the other hand, (8.5) and (8.6) imply

(8.12)
$$\partial(\mathbf{G}\mathbf{C}_{\kappa t}) = \partial(\zeta_{\kappa t}^* \mathbf{G}) = \zeta_{\kappa t}^*(\mathcal{L}_{\mathbf{v}_t} \mathbf{G}) \,.$$

where

$$(8.13) \qquad \mathcal{L}_{\mathbf{v}_t}\mathbf{G} = \partial\mathbf{G} + (D\mathbf{G})\mathbf{v}_t + \mathbf{L}_t^*\mathbf{G} + \mathbf{G}\mathbf{L}_t = \mathbf{L}_t^*\mathbf{G} + \mathbf{G}\mathbf{L}_t = \mathbf{G}[\mathbf{L}_t^{\mathsf{T}} + \mathbf{L}_t] = 2\,\mathbf{G}\mathbf{D}_t$$

represents the dynamic Lie derivative of $\mathbf{G}$ with respect $\mathbf{v}_t$, with $\partial\mathbf{G}$ and $D\mathbf{G}$ vanishing since $\mathbf{G}$ is constant. The result (8.12) can also be written in the form

$$(8.14) \qquad \partial\mathbf{C}_{\kappa t} = \mathbf{G}^{-1}\,\zeta_{\kappa t}^*(\mathcal{L}_{\mathbf{v}_t}\mathbf{G}) = \{\ell_{\mathbf{G}^{-1}} \circ \zeta_{\kappa t}^* \circ \mathcal{L}_{\mathbf{v}_t} \circ \ell_{\mathbf{G}}\}\mathbf{1}_V$$

using (2.24) and (2.25). Combining the definition (4.23) of $\mathbf{E}_{\kappa t}$ with (8.13), we have

$$(8.15) \qquad \partial\mathbf{E}_{\kappa t} = \mathbf{G}^{-1}\,\zeta_{\kappa t}^*(\mathbf{G}\mathbf{D}_t) = \{\ell_{\mathbf{G}^{-1}} \circ \zeta_{\kappa t}^* \circ \ell_{\mathbf{G}}\}\mathbf{D}_t = \{\mathfrak{a}_{\mathbf{F}_\kappa^{-1}}^\ell \circ \mathfrak{c}_{\zeta_{\kappa t}}\}\,\mathbf{D}_t$$

for the time derivative of the Green strain tensor at each $t \in I$ via (2.29) and (4.10).

Taking the time derivative of (4.36), we obtain

$$(8.16) \qquad \partial(\mathbf{G}\mathbf{E}_{\kappa t}) = \partial[\zeta_{\kappa t}^*(\mathbf{G}\mathbf{A}_t)] = \zeta_{\kappa t}^*[\partial(\mathbf{G}\mathbf{A}_t) + (D(\mathbf{G}\mathbf{A}_t))\mathbf{v}_t$$
$$+\mathbf{L}_t^*(\mathbf{G}\mathbf{A}_t) + (\mathbf{G}\mathbf{A}_t)\mathbf{L}_t],$$

where again we have used $\partial(D\zeta_{\kappa t}) = \mathbf{L}_{\kappa t}(D\zeta_{\kappa t})$ and $\partial(D\zeta_{\kappa t})^* = (D\zeta_{\kappa t})^*\mathbf{L}_{\kappa t}^*$ from (3.17). With $\mu_t = \mathbf{G}\mathbf{A}_t$, (8.5), (8.6) and (8.16) yield the expression

$$(8.17) \qquad \begin{aligned} \mathcal{L}_{\mathbf{v}_t}(\mathbf{G}\mathbf{A}_t) &= (D(\mathbf{G}\mathbf{A}_t))\mathbf{v}_t + \mathbf{L}_t^*(\mathbf{G}\mathbf{A}_t) + (\mathbf{G}\mathbf{A}_t)\mathbf{L}_t, \\ &= \mathbf{G}[(D\mathbf{A}_t)\mathbf{v}_t + \mathbf{L}_t^{\mathsf{T}}\mathbf{A}_t + \mathbf{A}_t\mathbf{L}_t] \end{aligned}$$

for the autonomous Lie derivative of $\mathbf{G}\mathbf{A}_t$ with respect to $\mathbf{v}_t$, as well as that

$$(8.18) \qquad \mathcal{L}_{\mathbf{v}_t}(\mathbf{G}\mathbf{A}_t) = \partial(\mathbf{G}\mathbf{A}_t) + \mathcal{L}_{\mathbf{v}_t}(\mathbf{G}\mathbf{A}_t) = \mathcal{M}_{\mathbf{v}_t}(\mathbf{G}\mathbf{A}_t) + \mathbf{L}_t^*(\mathbf{G}\mathbf{A}_t) + (\mathbf{G}\mathbf{A}_t)\mathbf{L}_t$$

for its dynamic Lie derivative with respect to $\mathbf{v}_t$ via (8.2). In this case, (8.16) becomes

$$(8.19) \qquad \partial(\mathbf{G}\mathbf{E}_{\kappa t}) = \partial[\zeta_{\kappa t}^*(\mathbf{G}\mathbf{A}_t)] = \zeta_{\kappa t}^*[\mathcal{L}_{\mathbf{v}_t}(\mathbf{G}\mathbf{A}_t)] .$$

or equivalently

$$(8.20) \qquad \partial\mathbf{E}_{\kappa t} = \mathbf{G}^{-1}\,\zeta_{\kappa t}^*[\mathcal{L}_{\mathbf{v}_t}(\mathbf{G}\mathbf{A}_t)] .$$

Note that the associated form $\mathbf{G}^{-1}\mathcal{L}_{\mathbf{v}_t}(\mathbf{G}\mathbf{A}_t)$ of the dynamic Lie derivative $\mathcal{L}_{\mathbf{v}_t}(\mathbf{G}\mathbf{A}_t)$ of $\mathbf{G}\mathbf{A}_t$ represents the so-called "upper" Oldroyd time derivative of the Almansi strain tensor $\mathbf{A}_t$, i.e.,

$$(8.21) \qquad \begin{aligned} \mathbf{G}^{-1}\mathcal{L}_{\mathbf{v}_t}(\mathbf{G}\mathbf{A}_t) &= \mathcal{M}_{\mathbf{v}_t}\mathbf{A}_t + \mathbf{L}_t^{\mathsf{T}}\mathbf{A}_t + \mathbf{A}_t\mathbf{L}_t \\ &= \{\ell_{\mathbf{G}^{-1}} \circ \mathfrak{c}_{\zeta_{\kappa t}^{-1}} \circ \mathfrak{a}_{\mathbf{F}_{\kappa t}} \circ \partial \circ \mathfrak{a}_{\mathbf{F}_{\kappa t}^{-1}} \circ \mathfrak{c}_{\zeta_{\kappa t}} \circ \ell_{\mathbf{G}}\}\mathbf{A}_t \end{aligned}$$

from (8.17) and (8.18), where $(8.21)_2$ follows from (2.24), (2.25) and (8.10). A comparison of (8.15) and (8.20) yields the well-known result $\mathbf{D}_t = \mathbf{G}^{-1}\mathcal{L}_{\mathbf{v}_t}(\mathbf{GA}_t)$. Notice that the transformation between $\partial\mathbf{E}_{\kappa t}$ and $\mathbf{G}^{-1}\mathcal{L}_{\mathbf{v}_t}(\mathbf{GA}_t)$ is the same as that between $\mathbf{E}_{\kappa t}$ and $\mathbf{A}_t$, i.e.,

(8.22)
$$\mathbf{E}_{\kappa t} = \{\mathbf{a}^{\ell}_{\mathbf{F}_{\kappa t}^{-1}} \circ \mathbf{c}_{\zeta_{\kappa t}}\}\mathbf{A}_t,$$
$$\partial\mathbf{E}_{\kappa t} = \{\mathbf{a}^{\ell}_{\mathbf{F}_{\kappa t}^{-1}} \circ \mathbf{c}_{\zeta_{\kappa t}}\}[\mathbf{G}^{-1}\mathcal{L}_{\mathbf{v}_t}(\mathbf{GA}_t)]$$

from $(4.38)_1$ and (8.20), respectively, using (2.29) and (4.10).

With the help of the relations

$$\partial[(D\zeta_{\kappa t})^{-1}] = -(D\zeta_{\kappa t})^{-1}\mathbf{L}_{\kappa t}$$

and

$$\partial[(D\zeta_{\kappa t})^{-*}] = -\mathbf{L}^{*}_{\kappa t}(D\zeta_{\kappa t})^{-*},$$

the time derivative of (5.28) takes the form

(8.23) $\quad \partial(\mathbf{\epsilon}_{\kappa t}\mathbf{G}^{-1}) = \zeta^{*}_{\kappa t}[\partial(\mathbf{\alpha}_t\mathbf{G}^{-1}) + (D(\mathbf{\alpha}_t\mathbf{G}^{-1}))\mathbf{v}_t - \mathbf{L}_t(\mathbf{\alpha}_t\mathbf{G}^{-1}) - (\mathbf{\alpha}_t\mathbf{G}^{-1})\mathbf{L}^{*}_t],$

or equivalently

(8.24)
$$\partial\mathbf{\epsilon}_{\kappa t} = \zeta^{*}_{\kappa t}[\mathcal{L}_{\mathbf{v}_t}(\mathbf{\alpha}_t\mathbf{G}^{-1})]\mathbf{G}$$

via (8.5) and (8.6) for $\mu_t = \mathbf{\alpha}_t\mathbf{G}^{-1}$, where

(8.25)
$$\mathcal{L}_{\mathbf{v}_t}(\mathbf{\alpha}_t\mathbf{G}^{-1}) = \partial(\mathbf{\alpha}_t\mathbf{G}^{-1}) + \pounds_{\mathbf{v}_t}(\mathbf{\alpha}_t\mathbf{G}^{-1})$$

and

(8.26)
$$\pounds_{\mathbf{v}_t}(\mathbf{\alpha}_t\mathbf{G}^{-1}) = (D(\mathbf{\alpha}_t\mathbf{G}^{-1}))\mathbf{v}_t - \mathbf{L}_t(\mathbf{\alpha}_t\mathbf{G}^{-1}) - (\mathbf{\alpha}_t\mathbf{G}^{-1})\mathbf{L}^{*}_t,$$
$$= [(D\mathbf{\alpha}_t)\mathbf{v}_t - \mathbf{L}_t\mathbf{\alpha}_t - \mathbf{\alpha}_t\mathbf{L}^{\mathsf{T}}_t]\mathbf{G}^{-1}.$$

Together, (8.25) and (8.26) yield

(8.27) $\quad \mathcal{L}_{\mathbf{v}_t}(\mathbf{\alpha}_t\mathbf{G}^{-1})\mathbf{G} = \mathcal{M}_{\mathbf{v}_t}\mathbf{\alpha}_t - \mathbf{L}_t\mathbf{\alpha}_t - \mathbf{\alpha}_t\mathbf{L}^{\mathsf{T}}_t$

$$= \{r_{\mathbf{G}} \circ \mathbf{c}_{\zeta_{\kappa t}^{-1}} \circ \mathbf{a}_{\mathbf{F}_{\kappa t}} \circ \partial \circ \mathbf{a}_{\mathbf{F}_{\kappa t}^{-1}} \circ \mathbf{c}_{\zeta_{\kappa t}} \circ r_{\mathbf{G}^{-1}}\}\mathbf{\alpha}_t,$$

representing the so-called "lower" Oldroyd time derivative of the Finger strain tensor $\mathbf{\alpha}_t$, where $(8.27)_2$ follows from (2.26), (2.27) and (8.10). As in the case

of $\mathbf{E}_{\kappa t}$, $\mathbf{A}_t$, $\partial\mathbf{E}_{\kappa t}$ and $\mathbf{G}^{-1}\mathcal{L}_{\mathbf{v}_t}(\mathbf{GA}_t)$ in (8.22), the transformation between $\boldsymbol{\varepsilon}_{\kappa t}$ and $\boldsymbol{\alpha}_t$ is the same as that between $\partial\boldsymbol{\varepsilon}_{\kappa t}$ and $\mathcal{L}_{\mathbf{v}_t}(\boldsymbol{\alpha}_t\mathbf{G}^{-1})\mathbf{G}$, i.e.,

$$
\begin{aligned}
\boldsymbol{\varepsilon}_{\kappa t} &= \{\mathfrak{a}^r_{\mathbf{F}_{\kappa t}^{-1}} \circ \mathfrak{c}_{\zeta_{\kappa t}}\}\boldsymbol{\alpha}_t, \\
\partial\boldsymbol{\varepsilon}_{\kappa t} &= \{\mathfrak{a}^r_{\mathbf{F}_{\kappa t}^{-1}} \circ \mathfrak{c}_{\zeta_{\kappa t}}\}[\mathcal{L}_{\mathbf{v}_t}(\boldsymbol{\alpha}_t\mathbf{G}^{-1})\mathbf{G}]
\end{aligned}
$$

(8.28)

from $(5.30)_1$ and (8.24), respectively, using (2.31) and (4.9).

We turn now to the time derivatives of the basic stress tensors. Beginning with the first family, (6.20), (8.5) and (8.6) with $\mu_t = \mathbf{S}_t\mathbf{G}^{-1}$ imply

(8.29) $$\partial(\tilde{\mathbf{T}}_{\kappa t}\mathbf{G}^{-1}) = \partial[\zeta^*_{\kappa t}(\mathbf{S}_t\mathbf{G}^{-1})] = \zeta^*_{\kappa t}[\mathcal{L}_{\mathbf{v}_t}(\mathbf{S}_t\mathbf{G}^{-1})].$$

with

(8.30) $$\mathcal{L}_{\mathbf{v}_t}(\mathbf{S}_t\mathbf{G}^{-1}) = \partial(\mathbf{S}_t\mathbf{G}^{-1}) + \pounds_{\mathbf{v}_t}(\mathbf{S}_t\mathbf{G}^{-1})$$

and

(8.31) $$\pounds_{\mathbf{v}_t}(\mathbf{S}_t\mathbf{G}^{-1}) = [(D\mathbf{S}_t)\mathbf{v}_t - \mathbf{L}_t\mathbf{S}_t - \mathbf{S}_t\mathbf{L}_t^{\mathsf{T}}]\mathbf{G}^{-1};$$

the form of $\pounds_{\mathbf{v}_t}(\mathbf{S}_t\mathbf{G}^{-1})$ follows from (8.26) since $\mathbf{S}_t\mathbf{G}^{-1}$ is of the same tensorial type as $\boldsymbol{\alpha}_t\mathbf{G}^{-1}$. Combining (8.30) and (8.31) yields the form

(8.32) $$\mathcal{L}_{\mathbf{v}_t}(\mathbf{S}_t\mathbf{G}^{-1}) = [\mathcal{M}_{\mathbf{v}_t}\mathbf{S}_t - \mathbf{L}_t\mathbf{S}_t - \mathbf{S}_t\mathbf{L}_t^{\mathsf{T}}]\mathbf{G}^{-1}$$

for the dynamic Lie derivative of $\mathbf{S}_t\mathbf{G}^{-1}$ with respect to $\mathbf{v}_t$. From (8.29), we have then

(8.33) $$\partial\tilde{\mathbf{T}}_{\kappa t} = \zeta^*_{\kappa t}[\mathcal{L}_{\mathbf{v}_t}(\mathbf{S}_t\mathbf{G}^{-1})]\mathbf{G} = \{\mathfrak{a}^r_{\mathbf{F}_{\kappa t}^{-1}} \circ \mathfrak{c}_{\zeta_{\kappa t}}\}[\mathcal{L}_{\mathbf{v}_t}(\mathbf{S}_t\mathbf{G}^{-1})\mathbf{G}]$$

for the time derivative of the second Piola–Kirchhoff stress tensor $\tilde{\mathbf{T}}_{\kappa t}$; $(8.33)_2$ follows from (2.26), (2.27), (2.31) and (8.10). A comparison of $(6.21)_1$ and (8.33), i.e.,

$$
\begin{aligned}
\tilde{\mathbf{T}}_{\kappa t} &= \{\mathfrak{a}^r_{\mathbf{F}_{\kappa t}^{-1}} \circ \mathfrak{c}_{\zeta_{\kappa t}}\}\mathbf{S}_t, \\
\partial\tilde{\mathbf{T}}_{\kappa t} &= \{\mathfrak{a}^r_{\mathbf{F}_{\kappa t}^{-1}} \circ \mathfrak{c}_{\zeta_{\kappa t}}\}[\mathcal{L}_{\mathbf{v}_t}(\mathbf{S}_t\mathbf{G}^{-1})\mathbf{G}].
\end{aligned}
$$

(8.34)

shows that $\tilde{\mathbf{T}}_{\kappa t}$ and $\mathbf{S}_t$ transform in the same way as $\partial\tilde{\mathbf{T}}_{\kappa t}$ and $\mathcal{L}_{\mathbf{v}_t}(\mathbf{S}_t\mathbf{G}^{-1})\mathbf{G}$, analogous to (8.28).

In a similar fashion, (6.25), (7.1) and (7.28) imply

(8.35) $$\partial(\mathbf{G}\tilde{\boldsymbol{\tau}}_{\kappa t}) = \zeta^*_{\kappa t}[\mathcal{L}_{\mathbf{v}_t}(\mathbf{G}\mathbf{s}_t)]$$

via (8.5) and (8.6) with $\mu_t = \mathbf{G}\mathbf{s}_t$, where

$$(8.36) \qquad \mathcal{L}_{\mathbf{v}_t}(\mathbf{G}\mathbf{s}_t) = \partial(\mathbf{G}\mathbf{s}_t) + \mathcal{L}_{\mathbf{v}_t}(\mathbf{G}\mathbf{s}_t)$$

as usual, and

$$(8.37) \qquad \mathcal{L}_{\mathbf{v}_t}(\mathbf{G}\mathbf{s}_t) = \mathbf{G}[(D\mathbf{s}_t)\mathbf{v}_t + \mathbf{L}_t^{\mathsf{T}}\mathbf{s}_t + \mathbf{s}_t\,\mathbf{L}_t]$$

from (8.17) since $\mathbf{G}\mathbf{s}_t$ and $\mathbf{G}\mathbf{A}_t$ are of the same tensorial type. Together, (8.36) and (8.37) yield

$$(8.38) \qquad \mathcal{L}_{\mathbf{v}_t}(\mathbf{G}\mathbf{s}_t) = \mathbf{G}[\mathcal{M}_{\mathbf{v}_t}\mathbf{s}_t + \mathbf{L}_t^{\mathsf{T}}\mathbf{s}_t + \mathbf{s}_t\,\mathbf{L}_t]$$

via (8.2). Combining (8.35) and (8.38), we obtain

$$(8.39) \qquad \partial\tilde{\tau}_{\kappa t} = \mathbf{G}^{-1}\,\zeta_{\kappa t}^*[\mathcal{L}_{\mathbf{v}_t}(\mathbf{G}\mathbf{s}_t)]\ .$$

Lastly, the relations $(6.28)_1$, (7.1), (7.28) and (8.39) imply

$$(8.40) \qquad
\begin{aligned}
\tilde{\tau}_{\kappa t} &= \{\mathfrak{a}^{\ell}_{\mathbf{F}_{\kappa t}^{-1}} \circ \mathfrak{c}_{\zeta_{\kappa t}}\}\mathbf{s}_t\,, \\
\partial\tilde{\tau}_{\kappa t} &= \{\mathfrak{a}^{\ell}_{\mathbf{F}_{\kappa t}^{-1}} \circ \mathfrak{c}_{\zeta_{\kappa t}}\}[\mathbf{G}^{-1}\,\mathcal{L}_{\mathbf{v}_t}(\mathbf{G}\mathbf{s}_t)],
\end{aligned}$$

i.e., that the transformation between $\partial\tilde{\tau}_{\kappa t}$ and $\mathbf{G}^{-1}\mathcal{L}_{\mathbf{v}_t}(\mathbf{G}\mathbf{s}_t)$ is the same as that between $\tilde{\tau}_{\kappa t}$ and $\mathbf{s}_t$. Note that (8.40) is analogous to (8.22).

9. Induced action and dual derivatives

The transformations (7.17), (7.20), (7.23) and (7.26) between the basic stress and strain tensors and corresponding arbitrary tensors of each family induce an action on the referential stress power density $\varrho_\kappa\pi_\kappa : I \times B_\kappa \to \mathbb{R}$. From the point of view that $\varrho_\kappa\pi_\kappa$ is a time-dependent *scalar function*, one would expect that the action of any $\Psi_\kappa \in \mathfrak{G}_\kappa$ on $\varrho_\kappa\pi_\kappa$ would leave it *invariant*, i.e., $\mathfrak{a}_{\Psi_\kappa}(\varrho_\kappa\pi_\kappa) = \varrho_\kappa\pi_\kappa$, such that $\mathfrak{G}_\kappa$ is a "symmetry group" for $\varrho_\kappa\pi_\kappa$ (see Sec. 2). The question is, what form does this action take? One possibility would be simply to substitute naively $\mathfrak{a}_{\Psi_\kappa}(\tilde{\mathbf{T}}_\kappa\mathbf{G}^{-1})$ for $\tilde{\mathbf{T}}_\kappa\mathbf{G}^{-1}$, and so on, into $\varrho_\kappa\pi_\kappa$, yielding

$$(9.1) \qquad (\varrho_\kappa\pi_\kappa)_{\Psi_\kappa} :=
\begin{cases}
\operatorname{tr}_V\{\mathfrak{a}_{\Psi_\kappa}(\tilde{\mathbf{T}}_\kappa\mathbf{G}^{-1})\,\partial[\mathfrak{a}_{\Psi_\kappa}(\mathbf{G}\mathbf{E}_\kappa)]\} = \operatorname{tr}_V\{\tilde{\mathbf{T}}_{\Psi_\kappa}(\partial\mathbf{E}_{\Psi_\kappa})\}. \\[6pt]
\operatorname{tr}_{V^*}\{\mathfrak{a}_{\Psi_\kappa}(\mathbf{G}\tilde{\tau}_\kappa)\,\partial[\mathfrak{a}_{\Psi_\kappa}(\varepsilon_\kappa\mathbf{G}^{-1})]\} = \operatorname{tr}_V\{\tilde{\tau}_{\Psi_\kappa}(\partial\varepsilon_{\Psi_\kappa})\}.
\end{cases}$$

Unfortunately, since the time dependence of Ψ_κ implies that $\partial \circ \mathfrak{a}_{\Psi_\kappa} \neq \mathfrak{a}_{\Psi_\kappa} \circ \partial$, i.e., that the operations of time differentiation ∂ and the action $\mathfrak{a}_{\Psi_\kappa}$ do not commute,

$(\varrho_\kappa \pi_\kappa)_{\Psi_\kappa} \neq \varrho_\kappa \pi_\kappa$ holds *in general*. Consequently, the choice (9.1) does not fulfill the requirement that the action leaves $\varrho_\kappa \pi_\kappa$ invariant. Of course, if ∂ and $\mathfrak{a}_{\Psi_\kappa}$ did in fact commute, i.e., if Ψ_κ was in fact *time-independent*, then we would have, for example,

$$
\begin{aligned}
(\varrho_\kappa \pi_\kappa)_{\Psi_\kappa} &= \mathrm{tr}_V\{\mathfrak{a}_{\Psi_\kappa}(\tilde{\mathbf{T}}_\kappa \mathbf{G}^{-1})\,\partial[\mathfrak{a}_{\Psi_\kappa}(\mathbf{G}\mathbf{E}_\kappa)]\}, \\
&= \mathrm{tr}_V\{\mathfrak{a}_{\Psi_\kappa}(\tilde{\mathbf{T}}_\kappa \mathbf{G}^{-1})\,\mathfrak{a}_{\Psi_\kappa}[\partial(\mathbf{G}\mathbf{E}_\kappa)]\}, \\
&= \mathrm{tr}_V\{\Psi_\kappa^{-1}(\tilde{\mathbf{T}}_\kappa \mathbf{G}^{-1})\Psi_\kappa^{-*}\,\Psi_\kappa^*[\partial(\mathbf{G}\mathbf{E}_\kappa)]\Psi_\kappa\}, \\
&= \mathrm{tr}_V\{(\tilde{\mathbf{T}}_\kappa \mathbf{G}^{-1})\,\partial(\mathbf{G}\mathbf{E}_\kappa)\}, \\
&= \varrho_\kappa \pi_\kappa,
\end{aligned}
$$

(9.2)

via (2.17) and (2.19), i.e., $\varrho_\kappa \pi_\kappa$ invariant. The same would be true, of course, for $\varrho_\kappa \pi_\kappa$ in terms of $\tilde{\tau}_\kappa$ and ε_κ. Clearly, $\mathrm{Lbj}(\mathcal{V}, \mathcal{V})$ represents a symmetry group for $\varrho_\kappa \pi_\kappa$ via (9.1), in essence the "subgroup" of $\mathfrak{G}_\kappa$ containing all of its *constant* elements. Since the elements of $\mathfrak{G}_\kappa$, however, are in general time-dependent, $\varrho_\kappa \pi_\kappa$ is not invariant with respect to the action of $\mathfrak{G}_\kappa$ as represented in (9.1), $(\varrho_\kappa \pi_\kappa)_{\Psi_\kappa} \neq \varrho_\kappa \pi_\kappa$. This result contradicts the fact that the elements of each family, being in the orbit of the corresponding basic strain or stress tensor, are simply different representations of the same physical entity.

The problem here is that, in (9.1), we have tacitly assumed that *the time derivative operator ∂ is invariant with respect to the action of $\mathfrak{G}_\kappa$*, something that is clearly true only for *time-independent* $\Psi_\kappa \in \mathfrak{G}_\kappa$. Since the elements of $\mathfrak{G}_\kappa$ are, however, in general time-dependent, ∂ loses its "absoluteness," i.e., invariance with respect to $\mathfrak{G}_\kappa$ and its action. From this point of view, the "true" action of $\mathfrak{G}_\kappa$ on the stress power density takes the form

(9.3)
$$
\mathfrak{a}_{\Psi_\kappa}(\varrho_\kappa \pi_\kappa) := \begin{cases} \mathrm{tr}_V\{\mathfrak{a}_{\Psi_\kappa}(\tilde{\mathbf{T}}_\kappa \mathbf{G}^{-1})\,\partial_{\Psi_\kappa}[\mathfrak{a}_{\Psi_\kappa}(\mathbf{G}\mathbf{E}_\kappa)]\}. \\ \mathrm{tr}_{V^*}\{\mathfrak{a}_{\Psi_\kappa}(\mathbf{G}\tilde{\tau}_\kappa)\,\partial_{\Psi_\kappa}[\mathfrak{a}_{\Psi_\kappa}(\varepsilon_\kappa \mathbf{G}^{-1})]\}, \end{cases}
$$

where ∂_{Ψ_κ} represents ∂ after being acted upon by the (in general time-dependent) element Ψ_κ of $\mathfrak{G}_\kappa$. The form of ∂_{Ψ_κ} is then determined, on the basis of the above discussion, by *the requirement that* $\mathfrak{a}_{\Psi_\kappa}(\varrho_\kappa \pi_\kappa) = \varrho_\kappa \pi_\kappa$ hold. In this case, we obtain

(9.4)
$$
\partial_{\Psi_\kappa} = \mathfrak{a}_{\Psi_\kappa} \circ \partial \circ \mathfrak{a}_{\Psi_\kappa^{-1}},
$$

representing a Ψ_κ-dependent time derivative, such that the commutation relation

(9.5)
$$
\partial_{\Psi_\kappa} \circ \mathfrak{a}_{\Psi_\kappa} = \mathfrak{a}_{\Psi_\kappa} \circ \partial
$$

holds. Substituting (9.5) into (9.3)$_1$, for example, we see immediately that

$$(9.6) \qquad \mathrm{tr}_{\mathcal{V}}\{\mathfrak{a}_{\Psi_\kappa}(\tilde{\mathbf{T}}_\kappa \mathbf{G}^{-1})\, \partial_{\Psi_\kappa}[\mathfrak{a}_{\Psi_\kappa}(\mathbf{GE}_\kappa)]\} = \mathrm{tr}_{\mathcal{V}}\{\tilde{\mathbf{T}}_\kappa(\partial \mathbf{E}_\kappa)\}\,,$$

i.e., $\mathfrak{a}_{\Psi_\kappa}(\varrho_\kappa \pi_\kappa) = \varrho_\kappa \pi_\kappa$. This also holds, of course, for $\varrho_\kappa \pi_\kappa$ in terms of $\tilde{\tau}_\kappa$ and ε_κ. The form (9.3) represents a generalization of (9.1) in the sense that, if Ψ_κ is in fact time-independent, then (9.3) reduces to (9.1), i.e.,

$$(9.7) \qquad \partial_{\Psi_\kappa} = \mathfrak{a}_{\Psi_\kappa} \circ \partial \circ \mathfrak{a}_{\Psi_\kappa^{-1}} = \mathfrak{a}_{\Psi_\kappa} \circ \mathfrak{a}_{\Psi_\kappa^{-1}} \circ \partial = \partial$$

from (9.4). Note that the usual form of the referential stress power density $\varrho_\kappa \pi_\kappa$ is implicitly based on the identity $\mathbf{1}_\kappa \in \mathfrak{G}_\kappa$ and its induced derivative, i.e., $\partial_{\mathbf{1}_\kappa} = \mathfrak{a}_{\mathbf{1}_\kappa} \circ \partial \circ \mathfrak{a}_{\mathbf{1}_\kappa^{-1}} = \partial$ from (9.4) with $\Psi_\kappa = \mathbf{1}_\kappa$.

To begin our investigation of the properties of the derivative ∂_{Ψ_κ} induced by elements $\Psi_\kappa \in \mathfrak{G}_\kappa$ of $\mathfrak{G}_\kappa$, we first show how the "dual" derivatives discussed by HT can be obtained from it. To do this, we require the time-dependent referential field

$$(9.8) \qquad \Lambda_{\Psi_\kappa} : I \times B_\kappa \longrightarrow \mathrm{Lin}(\mathcal{V}, \mathcal{V}) \quad | \quad (t,b) \longmapsto (\partial \Psi_\kappa)(t,b)\, \Psi_\kappa^{-1}(t,b)$$

$$=: \Lambda_{\Psi_\kappa}(t,b),$$

such that

$$(9.9) \qquad \partial \Psi_\kappa = \Lambda_{\Psi_\kappa} \Psi_\kappa\,.$$

For the particular elements of $\mathfrak{G}_\kappa$ given in Table 1, the last field (9.8) takes the following forms:

Table 6. Specific derivatives.

Ψ_κ	$\Lambda_{\Psi_\kappa} = (\partial \Psi_\kappa)\Psi_\kappa^{-1}$	$: I \times B_\kappa \longrightarrow \mathrm{Lin}(\mathcal{V}, \mathcal{V})$	Derivative
$\mathbf{1}_\kappa$	$\Lambda_{\mathbf{1}_\kappa} = \mathbf{0}_\kappa$	$: I \times B_\kappa \longrightarrow \{\mathbf{0}_{\mathrm{Lin}(\mathcal{V},\mathcal{V})}\}$	Material
$\mathbf{U}_\kappa$	$\Lambda_{\mathbf{U}_\kappa} = (\partial \mathbf{U}_\kappa)\mathbf{U}_\kappa^{-1}$	$: I \times B_\kappa \longrightarrow \mathrm{Lin}(\mathcal{V}, \mathcal{V})$	
$\mathbf{R}_\kappa$	$\Lambda_{\mathbf{R}_\kappa} = (\partial \mathbf{R}_\kappa)\mathbf{R}_\kappa^{-1}$	$: I \times B_\kappa \longrightarrow \mathrm{Skw}(\mathcal{V}, \mathcal{V})$	Green – MacInnis – Dienes
$\mathbf{F}_\kappa$	$\Lambda_{\mathbf{F}_\kappa} = (\partial \mathbf{F}_\kappa)\mathbf{F}_\kappa^{-1}$	$: I \times B_\kappa \longrightarrow \mathrm{Lin}(\mathcal{V}, \mathcal{V})$	Oldroyd
$\mathbf{P}_\kappa$	$\Lambda_{\mathbf{P}_\kappa} = (\partial \mathbf{P}_\kappa)\mathbf{P}_\kappa^{-1}$	$: I \times B_\kappa \longrightarrow \mathrm{Skw}(\mathcal{V}, \mathcal{V})$	Zaremba – Jaumann

Note again that $\mathbf{L}_\kappa = (\partial \mathbf{F}_\kappa)\mathbf{F}_\kappa^{-1}$ and $\mathbf{W}_\kappa = (\partial \mathbf{P}_\kappa)\mathbf{P}_\kappa^{-1}$. Using (9.8), we have

(9.10) $$\partial_{\Psi_\kappa}[\mathfrak{a}_{\Psi_\kappa}(\mathbf{G}\mathbf{E}_\kappa)] = \mathbf{G}(\partial^\ell_{\Psi_\kappa}\mathbf{E}_{\Psi_\kappa})$$

via (2.17), (7.18) and (9.4), where

(9.11) $$\partial^\ell_{\Psi_\kappa}\mathbf{E}_{\Psi_\kappa} := \{\ell_{\mathbf{G}^{-1}} \circ \partial_{\Psi_\kappa} \circ \ell_\mathbf{G}\}\mathbf{E}_{\Psi_\kappa} = \partial\mathbf{E}_{\Psi_\kappa} + \Lambda^\mathrm{T}_{\Psi_\kappa}\mathbf{E}_{\Psi_\kappa} + \mathbf{E}_{\Psi_\kappa}\Lambda_{\Psi_\kappa}$$

is equivalent to the first of two Ψ_κ-dependent dual derivatives introduced by HT, who used the notation Π for $\mathbf{E}_{\Psi_\kappa}$, Λ for Λ_{Ψ_κ}, and $\overset{\triangle}{\Pi}$ for $\partial^\ell_{\Psi_\kappa}\mathbf{E}_{\Psi_\kappa}$. With the choice $\Psi_\kappa = \mathbf{F}_\kappa$, such that $\Lambda_{\Psi_\kappa} = \Lambda_{\mathbf{F}_\kappa} = \mathbf{L}_\kappa$, (9.11) represents in particular a referential version of the upper Oldroyd derivative (8.21) of the Almansi strain tensor $\mathbf{A}_\kappa$, i.e.,

(9.12) $$\partial^\ell_{\mathbf{F}_{\kappa t}}\mathbf{E}_{\mathbf{F}_{\kappa t}} = \partial\mathbf{A}_{\kappa t} + \mathbf{L}^\mathrm{T}_{\kappa t}\mathbf{A}_{\kappa t} + \mathbf{A}_{\kappa t}\mathbf{L}_{\kappa t}$$

for all $t \in I$. Turning now to the second dual derivative, we have a result analogous to (9.10), i.e.,

(9.13) $$\partial_{\Psi_\kappa}[\mathfrak{a}_{\Psi_\kappa}(\mathbf{\varepsilon}_\kappa \mathbf{G}^{-1})] = (\partial^r_{\Psi_\kappa}\mathbf{\varepsilon}_{\Psi_\kappa})\mathbf{G}^{-1}$$

for the Piola strain tensor using (2.19), (7.21) and (9.4), where

(9.14) $$\partial^r_{\Psi_\kappa}\mathbf{\varepsilon}_{\Psi_\kappa} := \{r_\mathbf{G} \circ \partial_{\Psi_\kappa} \circ r_{\mathbf{G}^{-1}}\}\mathbf{\varepsilon}_{\Psi_\kappa} = \partial\mathbf{\varepsilon}_{\Psi_\kappa} - \Lambda_{\Psi_\kappa}\mathbf{\varepsilon}_{\Psi_\kappa} - \mathbf{\varepsilon}_{\Psi_\kappa}\Lambda^\mathrm{T}_{\Psi_\kappa}$$

is equivalent to the other Ψ_κ-dependent derivative introduced by HT, who used the notation π for $\mathbf{\varepsilon}_{\Psi_\kappa}$, and $\overset{\triangle}{\pi}$ for $\partial^r_{\Psi_\kappa}\mathbf{\varepsilon}_{\Psi_\kappa}$. For the case $\Psi_\kappa = \mathbf{F}_\kappa$, (9.14) represents, in particular, a referential version of the lower Oldroyd derivative (8.27) of the Finger strain tensor α_κ, i.e.,

(9.15) $$\partial^r_{\mathbf{F}_{\kappa t}}\mathbf{\varepsilon}_{\mathbf{F}_{\kappa t}} = \partial\alpha_{\kappa t} - \mathbf{L}_{\kappa t}\alpha_{\kappa t} - \alpha_{\kappa t}\mathbf{L}^\mathrm{T}_{\kappa t}$$

for all $t \in I$.

Note that, from (8.10) and (9.4), with $\Psi_{\kappa t} = \mathbf{F}_{\kappa t}$, we have

(9.16) $$\mathcal{L}_{\mathbf{v}_t} = \mathfrak{c}_{\zeta_{\kappa t}^{-1}} \circ \partial_{\mathbf{F}_{\kappa t}} \circ \mathfrak{c}_{\zeta_{\kappa t}}.$$

implying that the Lie derivative of spatial tensor fields with respect to $\mathbf{v}_t$ is a special case of the derivative (9.4). Comparing the forms of (3.9) and (9.9), i.e.

(9.17) $$\partial\zeta_{\kappa t} = \mathbf{v}_t \circ \zeta_{\kappa t} \quad \text{and} \quad \partial\Psi_\kappa = \Lambda_{\Psi_\kappa}\Psi_\kappa.$$

however, we see that $\Psi_\kappa \in \mathfrak{G}_\kappa$ could be interpreted as a sort of "local" motion on $\mathrm{Lbj}(V, V)$ with "spatial" velocity Λ_{Ψ_κ}, or similarly the "flow" of the vector field Λ_{Ψ_κ} on $\mathrm{Lbj}(V, V)$. On the basis of (9.17), then, we could interpret ∂_{Ψ_κ} as a type of Lie derivative based on the flow (9.9), in which case the notation $\mathcal{L}_{\Lambda_{\Psi_\kappa}}$ for ∂_{Ψ_κ} would perhaps be more appropriate. For simplicity, however, we retain the notation ∂_{Ψ_κ} in this work.

As in the case of the stress power, we have the induced action

(9.18)
$$\mathfrak{a}_{\Psi_\kappa}(\varrho_\kappa \Delta\pi_\kappa) = \mathrm{tr}_V\{\partial_{\Psi_\kappa}(\tilde{\mathbf{T}}_{\Psi_\kappa}\mathbf{G}^{-1})\partial_{\Psi_\kappa}(\mathbf{G}\mathbf{E}_{\Psi_\kappa})\}$$
$$= \mathrm{tr}_V\{(\partial^r_{\Psi_\kappa}\tilde{\mathbf{T}}_{\Psi_\kappa})(\partial^\ell_{\Psi_\kappa}\mathbf{E}_{\Psi_\kappa})\} = \varrho_\kappa \Delta\pi_\kappa,$$

$$\mathfrak{a}_{\Psi_\kappa}(\varrho_\kappa \delta\pi_\kappa) = \mathrm{tr}_{V^*}\{\partial_{\Psi_\kappa}(\mathbf{G}\tilde{\tau}_{\Psi_\kappa})\partial_{\Psi_\kappa}(\varepsilon_{\Psi_\kappa}\mathbf{G}^{-1})\}$$
$$= \mathrm{tr}_V\{(\partial^\ell_{\Psi_\kappa}\tilde{\tau}_{\Psi_\kappa})(\partial^r_{\Psi_\kappa}\varepsilon_{\Psi_\kappa})\} = \varrho_\kappa \delta\pi_\kappa,$$

of $\mathfrak{G}_\kappa$ via Ψ_κ on the "incremental" forms

(9.19)
$$\varrho_\kappa \Delta\pi_\kappa := \mathrm{tr}_V\{\partial(\tilde{\mathbf{T}}_\kappa\mathbf{G}^{-1})\partial(\mathbf{G}\mathbf{E}_\kappa)\},$$
$$\varrho_\kappa \delta\pi_\kappa := \mathrm{tr}_{V^*}\{\partial(\mathbf{G}\tilde{\tau}_\kappa)\partial(\varepsilon_\kappa\mathbf{G}^{-1})\}.$$

of the referential stress power density with respect to each family, in which appear the derivatives $\partial^\ell_{\Psi_\kappa}\tilde{\tau}_{\Psi_\kappa}$ and $\partial^r_{\Psi_\kappa}\tilde{\mathbf{T}}_{\Psi_\kappa}$ of $\tilde{\tau}_{\Psi_\kappa}$ and $\tilde{\mathbf{T}}_{\Psi_\kappa}$, analogous to (9.11) and (9.14), respectively. In this way, the *presumed* invariance of the "incremental" forms (9.19) of the referential stress power *determines*, for a given choice $\Psi_\kappa \in \mathfrak{G}_\kappa$, the corresponding appropriate dual derivatives of the transformed dual stress-strain pair *within* each family. Note that the stress power is invariant in both families, while the incremental form (9.19) is invariant only within each family.

We turn now to the transformation properties of the derivative (9.4). The left translation of $\mathfrak{G}_\kappa$ onto itself, e.g.(7.29), induces, via the properties of the action (2.14) and the relation (9.4), the transformation

(9.20)
$$\partial_{\Phi_\kappa} = \mathfrak{a}_{\Phi_\kappa} \circ \partial \circ \mathfrak{a}_{\Phi_\kappa^{-1}},$$
$$= \mathfrak{a}_{Z_\kappa \Psi_\kappa} \circ \partial \circ \mathfrak{a}_{\Psi_\kappa^{-1} Z_\kappa^{-1}},$$
$$= \mathfrak{a}_{Z_\kappa} \circ \mathfrak{a}_{\Psi_\kappa} \circ \partial \circ \mathfrak{a}_{\Psi_\kappa^{-1}} \circ \mathfrak{a}_{Z_\kappa^{-1}},$$
$$= \mathfrak{a}_{Z_\kappa} \circ \partial_{\Psi_\kappa} \circ \mathfrak{a}_{Z_\kappa^{-1}},$$
$$= \mathfrak{a}\mathfrak{d}_{Z_\kappa}(\partial_{\Psi_\kappa}).$$

of ∂_{Ψ_κ}, where

(9.21) $\mathfrak{a}\mathfrak{b} : \mathfrak{G}_\kappa \longrightarrow \mathrm{Bij}(\mathcal{D}_\kappa, \mathcal{D}_\kappa) \mid Z_\kappa \longmapsto \mathfrak{a}\mathfrak{b}_{Z_\kappa} := \mathfrak{a}\mathfrak{b}(Z_\kappa)$.

defined by

(9.22) $\mathfrak{a}\mathfrak{b}_{Z_\kappa} : \mathcal{D}_\kappa \longrightarrow \mathcal{D}_\kappa \mid \partial_{\Psi_\kappa} \longmapsto \partial_{Z_\kappa \Psi_\kappa} = \mathfrak{a}_{Z_\kappa} \circ \partial_{\Psi_\kappa} \circ \mathfrak{a}_{Z_\kappa^{-1}} =: \mathfrak{a}\mathfrak{b}_{Z_\kappa}(\partial_{\Psi_\kappa})$

represents a linear *adjoint action* of $\mathfrak{G}_\kappa$ on the set $\mathcal{D}_\kappa$ of all such derivatives induced by elements of $\mathfrak{G}_\kappa$. Note that the form of this transformation is "tensorial" as it must be if the referential stress power density (9.3) is to be invariant with respect to the action of $\mathfrak{G}_\kappa$. The tensorial nature of (9.20) is due in essence to the non-tensorial nature of that

(9.23) $\Lambda_{\Phi_\kappa} = \Lambda_{Z_\kappa} + Z_\kappa \Lambda_{\Psi_\kappa} Z_\kappa^{-1}$

for the transformation Λ_{Ψ_κ} defined in (9.8) induced by $\Psi_\kappa \in \mathfrak{G}_\kappa$, which follows from (7.29) and the definition (9.8). In fact, the non-tensorial nature of (9.23) implies that it represents in some fashion the transformation of a *connection*.

Another consequence of (9.20) is given by

$$
\begin{aligned}
\partial_{\Phi_\kappa} \circ \partial_{\Phi_\kappa} &= \partial_{\Phi_\kappa} \circ \mathfrak{a}_{Z_\kappa} \circ \partial_{\Psi_\kappa} \circ \mathfrak{a}_{Z_\kappa^{-1}} , \\
&= \mathfrak{a}_{Z_\kappa} \circ \partial_{\Psi_\kappa} \circ \partial_{\Psi_\kappa} \circ \mathfrak{a}_{Z_\kappa^{-1}} , \\
&= \mathfrak{a}\mathfrak{b}_{Z_\kappa}(\partial_{\Psi_\kappa} \circ \partial_{\Psi_\kappa}).
\end{aligned}
$$

(9.24)

i.e., the second-order derivative $\partial_{\Phi_\kappa}^2 := \partial_{\Phi_\kappa} \circ \partial_{\Phi_\kappa}$ transforms tensorially as well. By induction, then, $\partial_{\Phi_\kappa}^k = \mathfrak{a}\mathfrak{b}_{Z_\kappa}(\partial_{\Psi_\kappa}^k)$, where $\partial_{\Phi_\kappa}^k := \partial_{\Phi_\kappa} \circ \partial_{\Phi_\kappa}^{k-1}$ represents the kth order derivative. This result might be useful in higher-order constitutive relations of the rate type.

As at the end of Sec. 7, let Υ_κ again be any time-dependent V-tensor-valued referential field, and define $\Upsilon_{\Psi_\kappa} := \mathfrak{a}_{\Psi_\kappa} \Upsilon_\kappa$ for any $\Psi_\kappa \in \mathfrak{G}_\kappa$. Analogous to (7.30), the left translation (e.g., (7.29)) of $\mathfrak{G}_\kappa$ onto itself induces the transformation

(9.25) $\partial_{\Phi_\kappa} \Upsilon_{\Phi_\kappa} = \mathfrak{a}\mathfrak{b}_{Z_\kappa}(\partial_{\Psi_\kappa})\mathfrak{a}_{Z_\kappa} \Upsilon_{\Psi_\kappa} = \{\mathfrak{a}_{Z_\kappa} \circ \partial_{\Psi_\kappa}\}\Upsilon_{\Psi_\kappa} = \mathfrak{a}_{Z_\kappa}(\partial_{\Psi_\kappa} \Upsilon_{\Psi_\kappa})$

of the derivative $\partial_{\Psi_\kappa} \Upsilon_{\Psi_\kappa}$ corresponding to Υ_{Ψ_κ} via (7.30) and (9.22). Note that both Υ_{Ψ_κ}, as shown in (7.30), and its corresponding derivative $\partial_{\Psi_\kappa} \Upsilon_{\Psi_\kappa}$, as shown in (9.25), transform in the *same* fashion. Not suprisingly, this is also the characterizing feature of the dual derivatives of HT. In particular, for $\Upsilon_{\Psi_\kappa} = \mathfrak{a}_{\Psi_\kappa}^\ell \Upsilon_{1_\kappa}$

$= \mathfrak{a}^{\ell}_{\Psi_\kappa} \Upsilon_\kappa$, we have the transformations

$$(9.26) \qquad \partial^{\ell}_{F_\kappa} \Upsilon_{F_\kappa} = \mathfrak{a}^{\ell}_{F_\kappa}(\partial^{\ell}_{1_\kappa} \Upsilon_{1_\kappa}) = \begin{cases} \mathfrak{a}^{\ell}_{R_\kappa U_\kappa}(\partial^{\ell}_{1_\kappa} \Upsilon_{1_\kappa}) = \mathfrak{a}^{\ell}_{R_\kappa}(\partial^{\ell}_{U_\kappa} \Upsilon_{U_\kappa}), \\[2mm] \mathfrak{a}^{\ell}_{V_\kappa R_\kappa}(\partial^{\ell}_{1_\kappa} \Upsilon_{1_\kappa}) = \mathfrak{a}^{\ell}_{V_\kappa}(\partial^{\ell}_{R_\kappa} \Upsilon_{R_\kappa}) \end{cases}$$

induced by, similarly to (7.31), the polar decompositions (3.11), such that

$$(9.27) \qquad \partial^{\ell}_{U_\kappa} \Upsilon_{U_\kappa} = \begin{cases} \mathfrak{a}^{\ell}_{U_\kappa}(\partial^{\ell}_{1_\kappa} \Upsilon_{1_\kappa}), \\[2mm] \mathfrak{a}^{\ell}_{R_\kappa^{-1}}(\partial^{\ell}_{F_\kappa} \Upsilon_{F_\kappa}) \end{cases} \quad \text{and} \quad \partial^{\ell}_{R_\kappa} \Upsilon_{R_\kappa} = \begin{cases} \mathfrak{a}^{\ell}_{R_\kappa}(\partial^{\ell}_{1_\kappa} \Upsilon_{1_\kappa}), \\[2mm] \mathfrak{a}^{\ell}_{V_\kappa^{-1}}(\partial^{\ell}_{F_\kappa} \Upsilon_{F_\kappa}), \end{cases}$$

analogous to (7.32). As with (7.31) and (7.32), (9.26) and (9.27) hold in particular for $\Upsilon_\kappa = E_\kappa$ and $\Upsilon_\kappa = \tilde{\tau}_\kappa$. Likewise, with $\Upsilon_{\Psi_\kappa} = \mathfrak{a}^r_{\Psi_\kappa} \Upsilon_{1_\kappa} = \mathfrak{a}^r_{\Psi_\kappa} \Upsilon_\kappa$, we have

$$(9.28) \qquad \partial^r_{F_\kappa} \Upsilon_{F_\kappa} = \mathfrak{a}^r_{F_\kappa}(\partial^r_{1_\kappa} \Upsilon_{1_\kappa}) = \begin{cases} \mathfrak{a}^r_{R_\kappa U_\kappa}(\partial^r_{1_\kappa} \Upsilon_{1_\kappa}) = \mathfrak{a}^r_{R_\kappa}(\partial^r_{U_\kappa} \Upsilon_{U_\kappa}) \\[2mm] \mathfrak{a}^r_{V_\kappa R_\kappa}(\partial^r_{1_\kappa} \Upsilon_{1_\kappa}) = \mathfrak{a}^r_{V_\kappa}(\partial^r_{R_\kappa} \Upsilon_{R_\kappa}) \end{cases}$$

and so

$$(9.29) \qquad \partial^r_{U_\kappa} \Upsilon_{U_\kappa} = \begin{cases} \mathfrak{a}^r_{U_\kappa}(\partial^r_{1_\kappa} \Upsilon_{1_\kappa}) \\[2mm] \mathfrak{a}^r_{R_\kappa^{-1}}(\partial^r_{F_\kappa} \Upsilon_{F_\kappa}) \end{cases} \quad \text{and} \quad \partial^r_{R_\kappa} \Upsilon_{R_\kappa} = \begin{cases} \mathfrak{a}^r_{R_\kappa}(\partial^r_{1_\kappa} \Upsilon_{1_\kappa}) \\[2mm] \mathfrak{a}^r_{V_\kappa^{-1}}(\partial^r_{F_\kappa} \Upsilon_{F_\kappa}) \end{cases}$$

analogous to (7.33) and (7.34), respectively, which hold in particular for $\Upsilon_\kappa = \varepsilon_\kappa$ and $\Upsilon_\kappa = \tilde{T}_\kappa$. Again, note that such relations are also induced by the elastoplastic decomposition $F_\kappa = F^E_\kappa F^P_\kappa$ of F_κ.

References

1. R. HILL, *On constitutive inequalities for simple materials*, Int. J. Mech. Phys. Solids, 16, 229–242, 1968.
2. R. HILL, *Aspects of invariance in solid mechanics*, [in:] Advances in Appl. Mech., 18, 1–75, C.-S. YIH [Ed.], Academic Press 1978.
3. P. HAUPT and Ch. TSAKMAKIS, *On the application of dual variables in continuum mechanics*, Continuum Mech. Thermodyn., 1, 165–196, 1989.
4. J.E. MARSDEN, T.J.R. HUGHES, *Mathematical theory of elasticity*, Prentice–Hall, 1983.
5. R. ABRAHAM, J.E. MARSDEN, T. RATIU, *Manifolds, tensor analysis, and applications*, Applied Mathematical Sciences, 75, Springer–Verlag, 1988.

TECHNISCHE HOCHSCHULE DARMSTADT,
FACHBEREICH 6, MECHANIK III, DARMSTADT, GERMANY
and
KERNFORSCHUNGSZENTRUM KARLSRUHE,
INSTITUT FÜR MATERIALFORSCHUNG II, KARLSRUHE, GERMANY.

One-way extension of a plane crack
due to tensile pre-stress and dilatational waves

A. N. DAS (DARJEELING)

IN AN INFINITE elastic medium, initially in a state of uniform tensile pre-stress, the problem of one-way extension of an infinitesimal flaw into a plane crack due to two identical linearly varying plane dilatational waves with non-parallel wave fronts has been analyzed. Fracture is assumed to initiate at a point a finite time after the waves intersect there, and one of its edges is assumed to extend along the trace of the wave intersection. Following CHEREPANOV [12], and CHEREPANOV and AFANAS'EV [13], the general solution of the problem has been derived in terms of an analytic function of complex variable. The results include the expressions for the stress intensity factors at the crack tips.

1. Introduction

BROBERG [1] first considered the problem of symmetric extension of a crack at a constant velocity under the condition of plane stress or strain in a homogeneous isotropic elastic medium. Using the method of homogeneous function, CRAGGS [2] also solved the same problem, while the corresponding anti-plane problem was solved by ACHENBACH and BROCK [3]. All the anti-plane problems mentioned above are, however, self-similar ones with index (0, 0), and are concerned with symmetric extension of a crack.

Problems involving non-symmetric extension of cracks under uniform loading along the crack surface have also been investigated in recent years. Following the method of homogeneous functions developed by CRAGGS [2], the problem of non-symmetric extension of a small flaw into a plane crack under loading of polynomial form was solved by BROCK [4]. BROCK [5] also solved the problem of non-symmetric extension of a crack due to incidence of plane dilatational waves. An integral equation approach has been developed by GEORGIADIS [6]. He considered the elastodynamic problem of an expanding crack under homogeneous polynomial form of loading and reduced it to the solution of a Cauchy integral equation. Recently, DAS and GHOSH [7, 8] and DAS [9–11] have solved the problems of non-symmetric extension of a crack in an infinite elastic medium.

This paper presents the analysis of the problem of one-way extension of an infinitesimal flaw into a plane crack due to the action of two identical, linearly varying plane dilatational waves, which have non-parallel wave fronts and propagate towards each other in an infinite elastic medium which is initially in a state of uniform tensile pre-stress. A finite time after the crossing of the plane wave fronts, a fracture is assumed to initiate along the line where the wave fronts crossed, and one of its edges is assumed to extend along the trace of the wave

intersection. Superposition considerations allow the original problem to be separated into three self-similar problems with $(0, 0)$, $(0, 1)$ and $(1, 0)$ as the indices of similarity. Following CHEREPANOV [12] and CHEREPANOV and AFANAS'EV [13], the mentioned self-similar problems have all been formulated as some Riemann and Hilbert problems, which can be easily solved. The results include the analytical expressions for the stress intensity factors at the crack tips. It may be mentioned that the anti-plane strain problem of one-way extension of a crack due to two non-parallel plane SH-waves has been solved by DAS [14].

2. Formulation of the problem

Let two identical dilatational waves be defined by

$$(2.1) \qquad \sigma_{yy} = A_0 W_\pm H(W_\pm), \qquad \sigma_{xx} = (1 - 2m^2) A_0 W_\pm H(W_\pm), \qquad \sigma_{xy} = 0$$

referred to the coordinate system (x, y, z), with

$$W_\pm = c_1 t \pm y \sin \theta_0 + x \cos \theta_0, \qquad 0 \le \theta_0 \le \pi/2, \qquad m = c_2/c_1,$$

where c_1, c_2 are the velocities of longitudinal and transversal waves, respectively, and $H()$ is Heaviside's unit function; the waves propagate through an infinite solid which is pre-stressed, so that

$$(2.2) \qquad\qquad \sigma_{yy} = \sigma_{xx} = \sigma, \qquad \sigma_{xy} = 0.$$

Let us assume that at $t = 0$ the non-parallel plane waves intersect at $x = y = 0$. A micro-crack is assumed to appear at $t = t_0$ at $x = y = 0$ and one of its edges starts to extend along the trace of the wave intersection with velocity c, where c is constant and smaller than the Rayleigh wave speed. The expanding crack, the circular wave fronts associated with its motion and the plane wave fronts are shown in Fig. 1.

Using the symmetry and superposition conditions, solution to this problem can be obtained by considering an initially undisturbed half-plane $y \ge 0$ satisfying the boundary conditions for $y = 0$, $0 < x < ct'$:

$$(2.3) \qquad \sigma_{yy} = -\sigma - 2A_0 c_1 t_0 - 2A_0(c_1 t' + x \cos \theta_0), \qquad \sigma_{xy} = 0,$$

and for $y = 0$, $x \le 0$ or $x \ge ct'$:

$$(2.4) \qquad\qquad \sigma_{xy} = u_y = 0.$$

Here $t' = t - t_0$ and u_y is the displacement in y-direction.

Equation $(2.3)_1$ shows that by applying the superposition principle, the problem exposed can be divided into three separate problems of a constant normal stress, a normal stress varying linearly with time, and a normal stress linearly varying with distance measured along the crack plane.
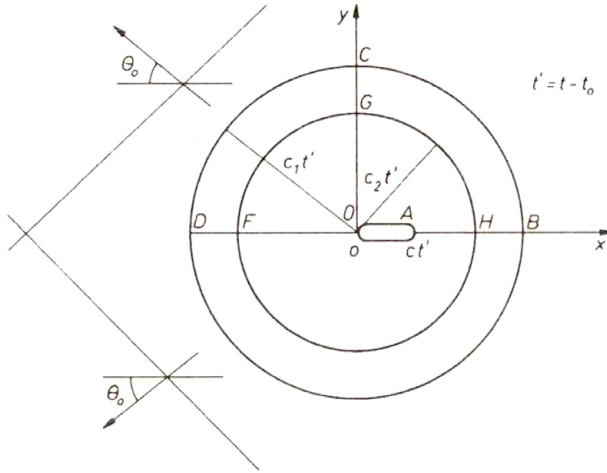
FIG. 1. The $x - y$ plane.

3. Constant normal stress on the crack faces

The wave motion generated by constant normal stress on the faces of the crack defined by $y = 0, 0 < x < ct$ has been considered; for simplicity, t instead of t' has been used. The boundary conditions at $y = 0$ are

(3.1)
$$\sigma_{yy} = -p_0 \qquad \text{for} \quad 0 < x < ct,$$
$$u_y = 0 \qquad \text{for} \quad x \leq 0 \quad \text{and} \quad x \geq ct,$$

where

$$p_0 = \sigma + 2A_0 c_1 t_0.$$

Now from [13] we obtain

(3.2)
$$\text{at} \quad y = 0, \qquad \frac{\partial u_y}{\partial t} = \text{Re} \, \phi_0(z),$$

$$\text{at} \quad y = 0, \qquad \frac{\partial \sigma_{yy}}{\partial t} = -\mu c_2^2 t^{-1} \text{Re} \left[\frac{z S(z)}{\sqrt{c_1^{-2} - z^2}} \phi_0'(z) \right],$$

where

(3.3)
$$S(z) = (c_2^{-2} - 2z^2)^2 + 4z^2 \sqrt{(c_1^{-2} - z^2)(c_2^{-2} - z^2)},$$
$$z = z_1 = z_2 = t/x \qquad \text{at} \quad y = 0$$

with

(3.4)
$$z_k = \frac{xt - iy\sqrt{t^2 - c_k^{-2}(x^2 + y^2)}}{x^2 + y^2} \qquad (k = 1, 2).$$

The transformations given by Eq. (3.4) map the semi-circular regions of the cylindrical regions in the upper half-plane of the $x - y$ plane into the lower half of the complex z_k-planes, as shown in the Fig. 2 and Fig. 3.
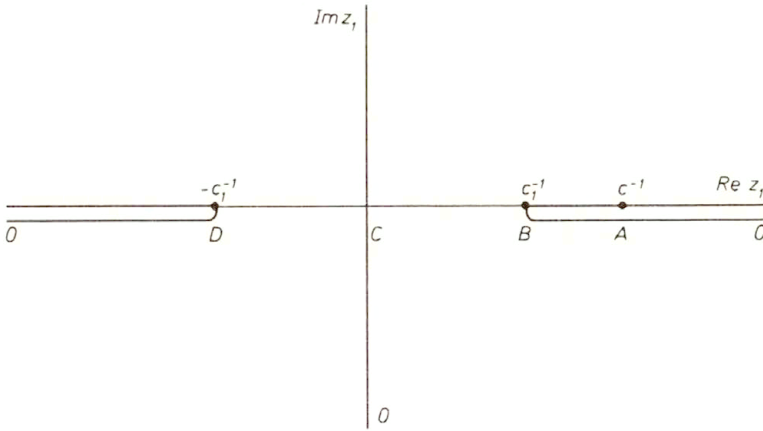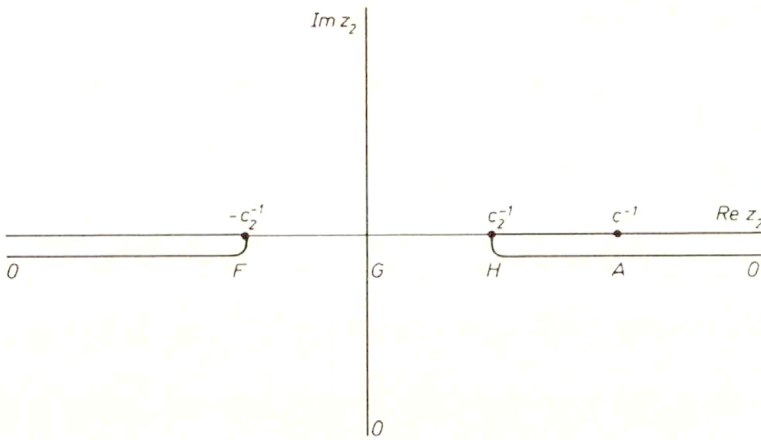

FIG. 2. The complex z_1-plane.

FIG. 3. The complex z_2-plane.

Therefore the boundary conditions given by Eqs. (3.1) are converted to the following conditions in the z-plane:

(3.5)
$$\text{Im}\, z = 0, \qquad \text{Re}\, z < c^{-1}, \qquad \text{Re}\, \phi_0(z) = 0,$$
$$\text{Im}\, z = 0, \qquad \text{Re}\, z > c^{-1}, \qquad \text{Im}\, \phi_0'(z) = 0.$$

In order to determine the analytic function $\phi_0(z)$ subject to the conditions (3.5) it is necessary to know the behaviour of the function $\phi_0(z)$ when $z \to 0$, c^{-1}. The zero point of the z-plane corresponds to the point $x = 0$, $y = c_1 t$ in the physical plane where $\partial u_y / \partial t$ is zero.

Hence, taking the representation $(3.2)_1$ into account, we obtain

(3.6) $$\text{Re}\,\phi_0(0) = 0.$$

Further, the condition $(3.5)_2$ may be put after integration in the form

(3.7) $$\text{Im}\,z = 0, \qquad \text{Re}\,z > c^{-1}, \qquad \text{Im}\,\phi_0(z) = 0.$$

Moreover, the displacement derivative $\partial u_y/\partial t$ at the moving crack tip $x = ct$, $y = 0$ should exhibit square root singularity, so that at $z \to c^{-1}$

(3.8) $$\phi_0(z) = 0\left[(z - c^{-1})^{-1/2}\right].$$

The boundary conditions given by Eqs. $(3.5)_1$, (3.7), together with the conditions (3.6) and (3.8), suggest that

(3.9) $$\phi_0(z) = A_1(z - c^{-1})^{-1/2},$$

where the unknown constant A_1 is to be determined from the condition $(3.1)_1$.
Integrating Eq. $(3.2)_2$ with respect to t, it can be easily shown that for $x > 0$

(3.10)
$$\sigma_{yy}(x,0,t) = \mu A_1 c_2^2 \,\text{Re} \int_{c_1^{-1}}^{t/x} \frac{S(z)\,dz}{2\sqrt{(c_1^{-2} - z^2)(z - c^{-1})^3}},$$

$$\sigma_{yy}(-x,0,t) = \mu A_1 c_2^2 \,\text{Re} \int_{-c_1^{-1}}^{-t/x} \frac{S(z)\,dz}{2\sqrt{(c_1^{-2} - z^2)(z - c^{-1})^3}}.$$

Next, using the boundary condition $(3.1)_1$ in $(3.10)_1$ we obtain, after some algebraic manipulations, the result

$$A_1 = \frac{-p_0\sqrt{c^{-1} + c_1^{-1}}}{\mu c_2^2 I},$$

with

$$I = I_2 E(p) - I_1 F(p) + I_3 F(p') + I_4 E(p'),$$

where

$$I_1 = \frac{8}{5}(c^{-1} + c_1^{-1})\left\{D_- + c_1^{-1}(3c^{-1} - c_1^{-1})\right\},$$

$$I_2 = \frac{8}{5}(c^{-1} + c_1^{-1})\left\{D_+ + (3c^{-2} - c_1^{-2})\right\}.$$

$$I_3 = \frac{8}{5}(2c^{-1} + c_2^{-1})(4c^{-1} - c_2^{-1})c_1^{-1}\sqrt{\frac{c^{-1} + c_1^{-1}}{c^{-1} + c_2^{-1}}},$$

$$I_4 = \frac{8}{5}(c^{-1} + c_2^{-1})(c_2^{-2} - 8c^{-2})\sqrt{\frac{c^{-1} + c_1^{-1}}{c^{-1} + c_2^{-1}}},$$

$$D_\pm = \frac{8}{5}\left[\frac{(c_2^{-2} - 2c^{-2})^2}{c^{-2} - c_1^{-2}} \pm 4\left(c_1^{-2} + c^{-2} - c_2^{-2}\right)\frac{c^{-1} \pm c_1^{-1}}{c^{-1} + c_1^{-1}}\right].$$

Here

(3.11) $$p = \sqrt{\frac{c^{-1} - c_1^{-1}}{c^{-1} + c_1^{-1}}}, \qquad p' = \sqrt{\frac{c^{-1} - c_2^{-1}}{c^{-1} + c_2^{-1}}},$$

and $F(\ )$, $E(\ )$ are complete elliptic integrals of the first and second kind, respectively.

Performing the integration $(3.10)_1$, the following result has been used:

$$\mathrm{Re}\int_{c_1^{-1}}^{M} \frac{dz}{(c_1^{-2} - z^2)(z - c^{-1})^3} = \frac{1}{c^{-2} - c_1^{-2}}\,\mathrm{Re}\int_{c_1^{-1}}^{M} \sqrt{\frac{z - c^{-1}}{c_1^{-2} - z^2}}dz \qquad (c^{-1} < M \le \infty).$$

The stress intensity factors at the crack tips $x = ct,\ y = 0$ and $x = y = 0$ defined by

$$N_{01} = \mathop{\mathrm{Lt}}_{x \to ct+} \sqrt{x - ct}\,\sigma_{yy}(x, 0, t),$$

$$N_{02} = \mathop{\mathrm{Lt}}_{x \to 0+} \sqrt{x}\,\sigma_{yy}(-x, 0, t),$$

respectively, are obtained by the results $(3.10)_{1-2}$,

(3.12) $$N_{01} = -4\mu A_1\sqrt{(1 - n^2)t},$$

$$N_{02} = -4\mu A_1\sqrt{t},$$

where $n = c/c_1$ is the non-dimensional crack tip velocity.

4. Problem of normal stress increasing linearly with time on the crack faces

For the case of normal stress on the faces of the crack increasing linearly with time, the boundary conditions are

(4.1) $$\sigma_{yy} = -p_1 t \qquad \text{for} \quad 0 < x < ct,$$

$$u_y = 0 \qquad \text{for} \quad x \le 0 \quad \text{and} \quad x \ge ct.$$

where
$$p_1 = 2A_0c_1.$$

The second order derivative $\partial^2 u_y/\partial t^2$ can be assumed to be the real part of an analytic function $\phi_1(z)$, so that

at $y = 0$

(4.2)
$$\frac{\partial^2 u_y}{\partial t^2} = \operatorname{Re} \phi_1(z);$$

this implies

at $y = 0$

(4.3)
$$\frac{\partial^2 \sigma_{yy}}{\partial t^2} = -\mu c_2^2 t^{-1} \operatorname{Re} \left[\frac{zS(z)}{\sqrt{c_1^{-2} - z^2}} \phi_1'(z) \right],$$

where $\phi_1(z)$ satisfies the conditions

(4.4) $\operatorname{Im} z = 0,$ $\operatorname{Re} z < c^{-1},$ $\operatorname{Re} \phi_1(z) = 0.$

(4.5) $\operatorname{Im} z = 0,$ $\operatorname{Re} z > c^{-1},$ $\operatorname{Im} \phi_1'(z) = 0.$

From Eq. (4.2) we see that

(4.6)
$$\operatorname{Re} \phi_1(z) = \frac{d}{dz} \left[\frac{1}{x} \frac{\partial u_y}{\partial t} \right].$$

Taking into account the facts that near the moving crack tip $x = ct$, $y = 0$ the displacement derivative $\partial u_y/\partial t$ is inversely proportional to the factor $\sqrt{ct - x}$ and that $\operatorname{Re} \phi_1(0) = 0$, in view of the conditions (4.4), (4.5) and Eq. (4.6), we obtain the result

(4.7)
$$\phi_1(z) = \frac{d}{dz} \left[\frac{A_2 z}{\sqrt{z - c^{-1}}} \right],$$

where the real constant A_2 is to be determined from the condition that on the crack surface stress $\sigma_{yy} = -p_1 t$.

From Eq. (4.3), after integration, we obtain for $x > 0$

(4.8)
$$\sigma_{yy}(x, 0, t) = -\mu A_2 c_2^2 t \operatorname{Re} \int_{c_1^{-1}}^{t/x} \frac{S(z)}{4\sqrt{(c_1^{-2} - z^2)}}$$

$$\times \left[\frac{3c^{-1}}{\sqrt{(z - c^{-1})^5}} - \frac{1}{\sqrt{(z - c^{-1})^3}} \right] dz,$$

(4.8)
[cont.]

$$\sigma_{yy}(-x, 0, t) = -\mu A_2 c_2^2 t \operatorname{Re} \int\limits_{-c_1^{-1}}^{-t/x} \frac{S(z)}{4\sqrt{(c_1^{-2} - z^2)}}$$

$$\times \left[\frac{3c^{-1}}{\sqrt{(z - c^{-1})^5}} - \frac{1}{\sqrt{(z - c^{-1})^3}} \right] dz.$$

Therefore, using the boundary condition $(4.1)_1$ in $(4.8)_1$ we obtain after simplification

$$A_2 = 2\frac{p_1\sqrt{c^{-1} + c_1^{-1}}}{\mu c_2^2 J},$$

with

$$J = J_1 F(p) - J_2 E(p) + J_3 F(p') - J_4 E(p')$$

and

$$J_1 = c^{-1}\left\{ \left(\frac{c_2^{-2} - 2c^{-2}}{c_1^{-1} - c^{-1}}\right)^2 \left(\frac{c_1^{-1} + 3c^{-1}}{c_1^{-1} + c^{-1}}\right) - 8c_1^{-1}(c_1^{-1} + c^{-1}) \right.$$

$$\left. + \frac{12}{c_1^{-1} - c^{-1}} \left(c_1^{-1}(5c^{-2} + c_1^{-2} - c_2^{-2}) - c^{-1}(3c_1^{-2} + c_2^{-2} - c^{-2})\right) \right\} + I_1,$$

(4.9) $$J_2 = c^{-1}\left\{ \left(\frac{c_2^{-2} - 2c^{-2}}{c_1^{-1} - c^{-1}}\right)^2 \left(\frac{c_1^{-1} - c^{-1}}{c_1^{-1} + c^{-1}}\right) - 8c^{-1}(c_1^{-1} + c^{-1}) \right.$$

$$\left. -6(c_1^{-2} + c_2^{-2} - 3c^{-2}) \right\} + I_2,$$

$$J_3 = \left\{ \sqrt{\frac{c^{-1} + c_1^{-1}}{c^{-1} + c_2^{-1}}} \frac{2c_1^{-1}c^{-1}}{c_2^{-1} - c^{-1}} (c_2^{-2} + 24c^{-1}c_2^{-1} - 29c^{-2}) - I_3 \right\}.$$

$$J_4 = \left\{ \sqrt{\frac{c^{-1} + c_1^{-1}}{c^{-1} + c_2^{-1}}} \frac{2c^{-2}}{c_2^{-1} - c^{-1}} (25c_2^{-2} - 29c^{-2}) + I_4 \right\}.$$

To perform the integration $(4.8)_1$, the following result has been used:

$$\operatorname{Re} \int\limits_{c_1^{-1}}^{M} \frac{dz}{\sqrt{(c_1^{-2} - z^2)}(z - c^{-1})^5} = \frac{1}{3(c_1^{-2} - c^{-2})} \operatorname{Re} \left[\int\limits_{c_1^{-1}}^{M} \frac{dz}{\sqrt{(c_1^{-2} - z^2)}(z - c^{-1})} \right.$$

$$\left. - \frac{2c^{-1}}{c_1^{-2} - c^{-2}} \int\limits_{c_1^{-1}}^{M} \sqrt{\frac{z - c^{-1}}{c_1^{-2} - z^2}} dz \right] \quad (c^{-1} < M \le \infty).$$

In this case, the stress intensity factors are obtained,

(4.10)
$$N_{11} = \underset{x \to ct+}{\mathrm{Lt}} \sqrt{x - ct}\,\sigma_{yy}(x, 0, t) = -2\mu A_2 t\sqrt{(1 - n^2)t}\,,$$

$$N_{12} = \underset{x \to 0+}{\mathrm{Lt}} \sqrt{x}\,\sigma_{yy}(-x, 0, t) = -2\mu A_2 t^{3/2}\,.$$

5. Problem of normal stress increasing linearly with the distance along the crack faces

Consider the initially undisturbed half-space $y \geq 0$ subject to the normal stress $-p_2 x$ over $y = 0$, $0 < x < ct$. The boundary conditions are

(5.1)
$$\sigma_{yy} = -p_2 x, \qquad 0 < x < ct,$$

$$u_y = 0, \qquad x \leq 0, \qquad x \geq ct,$$

where

$$p_2 = 2A_0 \cos\theta_0.$$

In this case, $\partial^2 u_y/\partial x \partial t$ shows dynamic similarity. So we take at $y = 0$

$$\frac{\partial^2 u_y}{\partial x \partial t} = \mathrm{Re}\,\phi_2(z)$$

with
at $y = 0$

(5.2)
$$\frac{\partial^2 \sigma_{yy}}{\partial x \partial t} = -\mu c_2^2 t^{-1} \mathrm{Re}\left[\frac{z S(z)}{\sqrt{c_1^{-2} - z^2}}\phi_2'(z)\right],$$

where $\phi_2(z)$ satisfies the conditions

(5.3)
$$\mathrm{Im}\,z = 0, \qquad \mathrm{Re}\,z < c^{-1}, \qquad \mathrm{Re}\,\phi_2(z) = 0,$$

$$\mathrm{Im}\,z = 0, \qquad \mathrm{Re}\,z > c^{-1}, \qquad \mathrm{Im}\,\phi_2'(z) = 0.$$

From Eq. (5.2)$_1$, after integration, it is found that

(5.3')
$$\mathrm{Re}\,\phi_1(z) = -z^2 \frac{d}{dz}\left[\frac{1}{t}\frac{\partial u_y}{\partial t}\right].$$

Since near the moving crack tip $x = ct$, $y = 0$ the displacement derivative $\partial u_y/\partial t$ should exhibit a square root singularity, and also since $\mathrm{Re}\,\phi_2(0) = 0$, we have, in view of the conditions (5.3), the result

(5.4)
$$\phi_2(z) = z^2 \frac{d}{dz}\left[\frac{A_3}{z\sqrt{z - c^{-1}}}\right],$$

where the real constant A_3 is to be determined from Eq. (5.1)$_1$.

Equation $(5.2)_2$ can be integrated to obtain for $x > 0$

$$\sigma_{yy}(x,0,t) = -3\mu A_3 c_2^2 x \,\mathrm{Re} \int_{c_1^{-1}}^{t/x} \frac{S(z)}{4\sqrt{(c_1^{-2} - z^2)}}$$

(5.5)
$$\times \left[\frac{c^{-1}}{\sqrt{(z - c^{-1})^5}} + \frac{1}{\sqrt{(z - c^{-1})^3}} \right] dz,$$

$$\sigma_{yy}(-x,0,t) = 3\mu A_3 c_2^2 x \,\mathrm{Re} \int_{-c_1^{-1}}^{-t/x} \frac{S(z)}{4\sqrt{(c_1^{-2} - z^2)}}$$

$$\times \left[\frac{c^{-1}}{\sqrt{(z - c^{-1})^5}} + \frac{1}{\sqrt{(z - c^{-1})^3}} \right] dz.$$

So, using the condition $(5.1)_1$ in $(5.5)_1$, we obtain

$$A_3 = 2 \frac{p_2 \sqrt{c^{-1} + c_1^{-1}}}{\mu c_2^2 L},$$

where

$$L = L_1 F(p) - L_2 E(p) + L_3 F(p') - L_4 E(p')$$

with the notations

(5.6)
$$\begin{aligned}
L_1 &= J_1 - 4I_1, \\
L_2 &= J_2 - 4I_2, \\
L_3 &= 3\left(J_3 + \frac{3}{2} I_3 \right), \\
L_4 &= 3\left(J_4 - \frac{3}{2} I_4 \right).
\end{aligned}$$

The stress intensity factors at the crack tips are obtained from the formulae

(5.7)
$$\begin{aligned}
N_{21} &= \underset{x \to ct+}{\mathrm{Lt}} \sqrt{x - ct}\,\sigma_{yy}(x,0,t) = 4\mu A_3 ct \sqrt{(1 - n^2)t}\,. \\
N_{22} &= \underset{x \to 0+}{\mathrm{Lt}} \sqrt{x}\,\sigma_{yy}(-x,0,t) = 0.
\end{aligned}$$

6. Discussion

The solution of the original crack problem is obtained by taking $p_0 = \sigma + 2A_0 c_1 t_0$, $p_1 = 2A_0 c_1$ and $p_2 = 2A_0 \cos\theta_0$ and superposing the results obtained in

Secs. 3–5 over the stress fields given by Eqs. (2.1) and (2.2). Putting together the results obtained in the Secs. 3–5, it is possible to write the stress intensity factors at the crack edges in the form

$$S_1 = \frac{N_{01} + N_{11} + N_{21}}{\sigma\sqrt{c_1 t_0}} = -\frac{4\mu}{\sqrt{c}}\left[\frac{1+\Delta}{p_0}A_1 + \frac{\Delta\tau}{2p_1}A_2\right.$$

(6.1)
$$\left. - \frac{\tau m \Delta \cos\theta_0}{p_2}A_3\right]\sqrt{(1-n^2)n\tau} \ ,$$

$$S_2 = \frac{N_{02} + N_{12} + N_{22}}{\sigma\sqrt{c_1 t_0}} = -\frac{4\mu}{\sqrt{c}}\left[\frac{1+\Delta}{p_0}A_1 + \frac{\Delta\tau}{2p_1}A_2\right]\sqrt{n\tau}.$$

Here $\tau = (t/t_0) - 1$ is the dimensionless time after crack initiation, and $\Delta = 2A_0 c_1 t_0/\sigma$ is the ratio (at $x = y = 0$) at initiation of the crack plane stress due to the plane waves and the pre-stress.

The expressions for the stress intensity factors and constants A_1, A_2 and A_3 given in Secs. 3–5 are very simple. One may easily obtain information about the stresses in the crack line and their intensities for each problem, as well as for the original problem considered in this paper.

7. Conclusions

Chaplygin's technique is, at the present, the simplest and most descriptive formulation of all the similarity techniques and it has been employed in several elastodynamic problems [2–6, 8–10] concerning crack extension. This technique has also some disadvantages, especially in the plane stress and strain cases, during the final steps of the analysis, when appropriate forms of the complex functions are sought for. However, the method of determining the complex function presented in this paper is correct and leads to the correct solution of the problem.

References

1. K.B. BROBERG, *The propagation of a brittle crack*, Archiv. Physik, **18**, 159, 1960.

2. J.W. CRAGGS, *Fracture of solids*, J. Wiley and Sons, New York 1963.

3. J.D. ACHENBACH and L.M. BROCK, *Rapid extension of a crack*, J. Elast., **1**, 51, 1971.

4. L.M. BROCK, *Non-uniform extension of a small flaw into a plane crack at a constant rate under polynomial form loading*, Int. J. Engng. Sci., **14**, 181, 1976.

5. L.M. BROCK, *Non-symmetric extension of a plane crack due to tensile pre-stress and dilatational waves*, Int. J. Engng. Sci., **13**, 951, 1975.

6. H.G. GEORGIADIS, *An integral equation approach to self-similar plane elastodynamic crack problem*, J. Elast., **25**, 17, 1991.

7. A.N. DAS and M.L. GHOSH, *Non-symmetric extension of a plane crack due to plane SH-waves in a pre-stressed infinite elastic medium*, Int. J. Fract., **61**, 361, 1993.

8. A.N. DAS and M.L. GHOSH, *Extension of a crack due to plane SH-waves in a pre-stressed infinite elastic medium*, Int. J. Engng. Sci., [in press, Ms. No. 6009, 1994].

9. A.N. DAS, *Extension of a plane crack in a pre-stressed infinite elastic medium*, Engng. Frac. Mech., **46**, 4, 543, 1993.

10. A.N. DAS, *Non-symmetric extension of a crack in an infinite elastic medium under anti-plane shear stress*, Int. J. Engng. Sci., [in press, Ms. No. 6032, 1994].

11. A.N. DAS, *Non-symmetric extension of a crack*, Acta Mech., [in press, 1994].

12. G.P. CHEREPANOV, *Mechanics of brittle fracture*, Mc-Graw Hill, 1979.

13. G.P. CHEREPANOV, E.F. AFANAS'EV, *Some dynamic problems of the theory of elasticity – a review*, Int. J. Engng. Sci., **12**, 665, 1974.

14. A.N. DAS, *Extension of a plane crack due to plane SH-waves in a pre-stressed infinite elastic medium*, Arch. Mech., **45**, 2, 183, 1993.

DEPARTMENT OF MATHEMATICS
NORTH BENGAL UNIVERSITY, DARJEELING, WEST BENGAL, INDIA.

Invariant description of symmetric conservative systems

S. PIEKARSKI (WARSZAWA)

IN CONTINUUM MECHANICS, one often considers the systems of conservation laws consistent with the additional conservation equation and, in particular, the symmetric conservative systems. In thermomechanics, additional conservation equation implied by such systems is often interpreted as the entropy balance. In this paper, the theory of the systems of conservation laws consistent with the additional conservation law is equivalently formulated in terms of the properties of the systems of conservation laws possesing nontrivially different conservative forms. Such formulation enables one to generalize the results on the subject of the relations between the systems of conservation laws and the symmetric systems published before (S. PIEKARSKI, *On the uniqueness of symmetric algebraic consequences implied by a system of conservation laws consistent with the additional conservation law*, to be published in Cont. Mech. Thermod.) and is more general than that of Friedrichs (K.O. FRIEDRICHS, *On the laws of relativistic electro-magneto-fluid dynamics*, Comm. Pure Appl. Math., **27**, 1974). The description of the possible transformations between the alternative symmetric conservative forms of a given system of p.d.e. occurs naturally as a special case. Such transformations are involved in the problem of finding a symmetric conservative form of a given system of conservation laws.

1. Introduction

IN CONTINUUM MECHANICS, one often considers the systems of conservation laws consistent with the additional conservation equation and, in particular, the symmetric conservative systems. In thermomechanics, the additional conservation equation related with such systems is often interpreted as the entropy balance [1–7].

In this paper, the theory of the systems of conservation laws consistent with the additional conservation equation is equivalently formulated in terms of the properties of the systems of conservation laws possessing nontrivially different conservative forms. Such formulation explicitly shows the most general class of transformations relating equivalent systems of conservation laws consistent with the additional conservation equation. Two applications of such an approach seem to be interesting; the first concerns the relations between the systems of conservation laws consistent with the additional conservation equation and the symmetric systems. Some results on this subject were given in [14]; however, the class of equivalent transformations between the systems of conservation laws, discussed there, was restricted to a certain distinguished family of transformations and was not as general as possible. In this paper we discuss all possible transformations and it is possible to show that the results formulated in [14] remain valid also for the general case.

The second application of our approach concerns the symmetric conservative systems since it makes it possible to discuss the transformations involved in the transition between the equivalent symmetric conservative systems subjected to

the most general transformations. Such a discussion is of interest since it shows the class of transformations involved in the problem of writing a given system of p.d.e. in the symmetric conservative form. One of the well-known problems related with the transformations of the systems of conservation laws is that the number of possible coordinate systems is infinite. Therefore, it is convenient to use the invariant description which does not depend on the choice of a coordinate system, and the standard approach is that of Cartan (see [8, 9] and the literature cited therein). However, the "dual" approach initiated by Peradzyński [10–12] seems to be more convenient for the problems discussed here and, therefore, all our discussion is held in the dual language.

In order to maintain the self-consistency of presentation, all necessary definitions are given at the beginning of Sec. 2. A discussion presented in this paper is restricted to the case of such systems of conservation laws consistent with the additional conservation equation which do not possess nontrivially different additional conservation equations; however, the general case can be discussed in a similar manner.

For simplicity, we assume that the source terms in the discussed equations vanish; it can be easily checked that all results remain valid also in the case of non-vanishing production terms. The invariant properties of the systems of conservation laws consistent with the additional conservation equation and of the symmetric conservative systems are discussed in Secs. 2 and 3, correspondingly. Final remarks are given in Sec. 4; in particular, in Sec. 4 we compare our approach with that of Friedrichs [15].

In principle, throughout this paper we apply Einstein's notation assuming summation with respect to repeated indices; however, in some cases, in order to make the structure of the discussed expressions clearer, some sums are written explicitly.

2. Invariant description of the systems of conservation laws consistent with the additional conservation equation

In the invariant description of the systems of conservation laws [7, 10–14], in the space of the dependent variables we allow "arbitrary" (i.e. diffeomorphic) changes of coordinates, whereas the allowed coordinate transformations in the space of the independent variables are the affine transformations. As a consequence, we can interpret the space of the dependent variables as a manifold (which shall be denoted by Q) and, in turn, the space of the independent variables can be interpreted as the affine space (which shall be denoted by A). The vector space composed of the vectors tangent to A will be denoted by T_A.

We assume, that the dimensions of Q and A are m and n, correspondingly. The affine coordinate systems on A have the following form

$$(2.1) \qquad \mathbb{R}^n \ni (x_1, \ldots, x_n) \to \nu + x_i \mathbf{e}_i \in A.$$

where $\mathbb{R}$ denotes the set of real numbers, ν is the arbitrary point of A, and $\mathbf{e}_1$, $\ldots$, $\mathbf{e}_n$ is a basis in T_A. The important property of the coordinate systems of the form (2.1) is that the vectors $\partial_{x_1}, \ldots, \partial_{x_n}$ tangent to its coordinate lines can be identified with the corresponding vectors $\mathbf{e}_1, \ldots, \mathbf{e}_n$ tangent to T_A. In turn, the natural base forms $dx^1, \ldots, dx^n$ of the coordinate system (2.1) can be identified with the corresponding forms $F^1, \ldots, F^n$ from the linear space dual to T_A; the space dual to T_A shall be denoted as T_A^* and the vectors $\mathbf{e}_1, \ldots, \mathbf{e}_n$ are related to the forms $F^1, \ldots, F^n$ via the relations (2.2)

$$(2.2) \qquad \left\langle \mathbf{e}_i, F^{i'} \right\rangle = \delta_i^{i'}, \qquad i, i' = 1, \ldots, n,$$

where $\langle , \rangle$ denotes the action of a form on a vector and $\delta_i^{i'}$ stands for Kronecker's symbol. Let (q_j), $j = 1, \ldots, m$ be a certain local coordinate system on the manifold of the dependent variables Q. The system of conservation laws

$$(2.3) \qquad \frac{\partial}{\partial x_i} U^{I,i}(q_j) = 0, \qquad i = 1, \ldots, n, \qquad j = 1, \ldots, m$$

can be interpreted as the system of equations for the function f acting from the affine space of the independent variables A into the manifold of the dependent variables Q; the functions

$$(2.4) \qquad q_j = f_j(x_i)$$

solving Eq. (2.3) are then the coordinate representation of the function f. The derivative f_* of f, understood in the sense of the derivative of the mapping between manifolds A and Q, is given by

$$(2.5) \qquad f_* = \partial_{q_j} \frac{\partial q_j}{\partial x_i} \otimes dx_i,$$

where ∂_{q_j}, $j = 1, \ldots, m$ are the natural base vectors of the coordinate system (q_j), $j = 1, \ldots, m$ on Q.

From the above mentioned identification of $dx^1, \ldots, dx^n$ and $F^1, \ldots, F^n$ it follows that the derivative (2.5) can be written in the following equivalent form:

$$(2.6) \qquad f_* = \partial_{q_j} \frac{\partial q_j}{\partial x_i} \otimes dx^i = \partial_{q_j} \frac{\partial q_j}{\partial x_i} \otimes F^i.$$

Let us define the fields of the two-point tensors $w^1, \ldots, w^m$ by the following rule

$$(2.7) \qquad w^I := \frac{\partial U^{I,i}}{\partial q_j} \otimes dq_j \otimes \mathbf{e}_i,$$

where dq_j, $j = 1, \ldots, m$ are the natural base forms of the coordinate system (q_j), $j = 1, \ldots, m$ on Q. As it has been discussed in literature [7, 10–14], the whole

system (2.3) can be written in terms of the corresponding contractions of $w^1, \ldots,$ w^m with f_*;

$$
(2.8) \qquad \left\langle w^I, f_* \right\rangle = \left\langle \frac{\partial U^{I,i}}{\partial q_j} dq^j \otimes e_i, \, \partial_{q_{j'}} \frac{\partial q_{j'}}{\partial x_{i'}} \otimes F^{i'} \right\rangle = \frac{\partial U^{I,i}}{\partial q_j} \frac{\partial q_{j'}}{\partial x_{i'}} \delta_j^{j'} \delta_i^{i'}
$$

$$
= \frac{\partial q^{I,i}}{\partial q_j} \frac{\partial q_j}{\partial x_i} = \frac{\partial}{\partial x_i} \left(U^{I,i} \right) = 0.
$$

The important fact is that the fields of the two-point tensors $w^1, \ldots, w^m$ are the differentials of the vector functions $\mathbf{U}^1, \ldots, \mathbf{U}^m$ on Q with values in T_A which are defined as

$$
(2.9) \qquad \mathbf{U}^I = U^{I,i} e_i, \qquad I = 1, \ldots, m, \qquad i = 1, \ldots, n\,.
$$

since

$$
(2.10) \qquad w^I = d\mathbf{U}^I, \qquad I = 1, \ldots, m
$$

and therefore the system (2.3) can be written as

$$
(2.11) \qquad \left\langle d\mathbf{U}^I, f_* \right\rangle = 0, \qquad I = 1, \ldots, m.
$$

For the expression $\left\langle d\mathbf{U}^I, f_* \right\rangle$ we shall apply also the alternative notation $\operatorname{div} \mathbf{U}^I$. The vector fields $\mathbf{U}^1, \ldots, \mathbf{U}^m$ are treated in Eq. (2.10) as the vector-valued differential 0-forms with values in T_A. However, since in that notation for conservation laws one does not distinguish between "the time derivative" and "the divergence of the flux", the vector fields $\mathbf{U}^1, \ldots, \mathbf{U}^m$ shall be sometimes called the "four-fluxes" (of course, this terminology cannot be interpreted in a strict sense since, in general, A is not the Minkowski space of special relativity). We shall assume that the system (2.3) is determined, that is, for each $q \in Q$ the differentials $d\mathbf{U}^1(q), \ldots, d\mathbf{U}^m(q)$ are linearly independent [7, 10].

Let $\lambda_1, \ldots, \lambda_m$ be smooth, real functions on Q. Then the vector-valued differential 1-form given by

$$
(2.12) \qquad \Omega := \sum_I \lambda_I d\mathbf{U}^I
$$

defines the quasilinear partial differential equation which is implied by the discussed set of conservation laws

$$
(2.13) \qquad \langle \Omega, f_* \rangle = \sum_I \lambda_I \left\langle d\mathbf{U}^I, f_* \right\rangle = \sum_I \lambda_I \operatorname{div} \mathbf{U}^I = 0.
$$

If the 1-form Ω is closed, that is, if

(2.14) $$0 = d\Omega = \sum_{I=1}^{m} d\lambda_I \wedge d\mathbf{U}^I.$$

then locally it possesses the potential $\mathbf{S}$, $\mathbf{S} : Q \to T_A$

(2.15) $$\Omega = d\mathbf{S} = \sum_I \lambda_I d\mathbf{U}^I$$

and the Eq. (2.13) becomes the conservation law [7, 13]

(2.16) $$\langle d\mathbf{S}, f_* \rangle = \operatorname{div} \mathbf{S} = \sum_I \lambda_I \operatorname{div} \mathbf{U}^I = 0.$$

We shall say that the system (2.3) implies the additional conservation equation (2.16) if Eq. (2.14) has a nontrivial solution in the sense that not all λ_I are constant [7,13]. The additional balance equation is usually called the entropy balance and the functions λ_I, $I = 1, \ldots, m$ are called the Lagrange – Liu multipliers. If we add to all the Lagrange – Liu multipliers arbitrary real constants, then we obtain another admissible set of Lagrange – Liu multipliers what, in turn, modifies the entropy balance by adding to it the corresponding linear combination of equations from the system (2.3).

Now we shall discuss such systems of conservation laws which possess nontrivially different conservative forms and we shall see that for the system of conservation laws the property of "possessing nontrivially different conservative forms" is equivalent to the property of "implying an additional balance equation".

Let us multiply the equations from the system of conservation laws (2.3) by a real, nondegenerate, $m \times m$ matrix M_I^J defined on Q; that leads to the equivalent system of p.d.e.

(2.17) $$M_I^J \operatorname{div} \mathbf{U}^I = 0, \qquad I, J = 1, \ldots, m.$$

which can be geometrically written by means of the contractions of f_* with the vector-valued 1-forms $\omega^1, \ldots, \omega^m$

(2.18)
$$\omega^J := \sum_{I=1}^{m} M_I^J d\mathbf{U}^I,$$
$$\langle \omega^J, f_* \rangle = M_I^J \operatorname{div} \mathbf{U}^I = 0, \qquad J, I = 1, \ldots, m.$$

The condition that the transformed system (2.17), (2.18)$_2$ is also of a conservative form is equivalent to the condition that the 1-forms ω^J, $J = 1, \ldots, m$ are closed [7],

(2.19) $$d\omega^J = \sum_{I=1}^{m} dM_I^J \wedge d\mathbf{U}^I = 0, \qquad J = 1, \ldots, m.$$

If condition (2.19) is satisfied, then the 1-forms ω^J, $J = 1, \ldots, m$ have local potentials $\mathbf{V}^J$, $\mathbf{V}^J : Q - T_A$, which are such that

$$(2.20) \qquad \omega^J = d\mathbf{V}^J$$

and the system $(2.18)_2$ can be written in the form

$$(2.21) \qquad \left\langle \omega^J, f_* \right\rangle = \left\langle d\mathbf{V}^J, f_* \right\rangle = \operatorname{div} \mathbf{V}^J = 0, \qquad J = 1, \ldots, m.$$

We shall say that the system (2.3) possesses nontrivially different conservative forms if and only if the system of Eqs. (2.19) has a solution for the matrix M_I^J which is nondegenerate and is not constant (in the sense that at least one of its elements has a non-vanishing differential).

Let the values of indices (J_0, I_0) correspond to such an element of the matrix M_I^J that $dM_{I_0}^{J_0}$ is different from zero.

Taking in Eq. (2.19) $J = J_0$ we obtain the equation

$$(2.22) \qquad \sum_{I=1}^{m} dM_I^{J_0} \bigwedge d\mathbf{U}^I = 0$$

which is identical with the condition (2.14) ensuring the existence of the additional conservation law.

In turn, let us consider the system of conservation laws consistent with the additional conservation law (2.16). Let C_I^J be a real $m \times m$ matrix and let C^J, $J = 1, \ldots, m$ denote arbitrary real numbers. Let us define the set of 1-forms L^J, $J = 1, \ldots, m$

$$(2.23) \qquad L^J := \sum_{I=1}^{m} C_I^J d\mathbf{U}^I + C^J ds = \sum_{I=1}^{m} C_I^J d\mathbf{U}^I + C^J \sum_{I=1}^{m} \lambda_I d\mathbf{U}^I$$

$$= \sum_{I=1}^{m} \left(C_I^J + C^J \lambda_I \right) d\mathbf{U}^I.$$

On account of Eq. (2.14) L^J, $J = 1, \ldots, m$ are closed and therefore the contractions of L^J with f_* define the system of conservation laws which is equivalent to the system

$$(2.24) \qquad \operatorname{div} \mathbf{U}^I = 0, \qquad I = 1, \ldots, m$$

if and only if the matrix

$$(2.25) \qquad K_I^J(q) := C_I^J + C^J \lambda_I$$

is nondegenerate.

For example, the matrix (2.25) is locally nondegenerate if the matrix C_I^J is nondegenerate and $C^{.J}$, $J = 1,\ldots, m$ are sufficiently small. Therefore, for the system of conservation laws consistent with additional conservation equation we can always find nontrivially equivalent system of conservation laws. As a consequence, we see that for the systems of conservation laws the property of "implying an additional balance equation" is equivalent to the property of "possessing nontrivially equivalent conservative forms". We shall say that the system of conservation laws (2.3) consistent with additional conservation equation (2.16) implies only one independent additional conservation equation if the difference of any entropy balances implied by Eq. (2.3) is equal to the sum of equations from the system (2.3) taken with the constant, real coefficients. Let us consider the two nontrivially different conservative forms

$$(2.26) \qquad \operatorname{div} \mathbf{U}^I = 0, \qquad I = 1,\ldots, m$$

and

$$(2.27) \qquad \operatorname{div} \mathbf{V}^J = 0, \qquad J = 1,\ldots, m$$

of a system of conservation laws which implies only one independent additional conservation law, and let

$$(2.28) \qquad \operatorname{div} \mathbf{S} = \sum_I \lambda_I \operatorname{div} \mathbf{U}^I = \langle d\mathbf{S}, f_* \rangle$$

and

$$(2.29) \qquad \operatorname{div} \mathbf{R} = \sum_J \Lambda_J \operatorname{div} \mathbf{V}^J = \langle d\mathbf{R}, f_* \rangle$$

be the additional conservation laws consistent with Eqs. (2.26) and (2.27), respectively; $\mathbf{S}$ and $\mathbf{R}$ are the entropy four-fluxes corresponding to Eqs. (2.26) and (2.27). The real functions λ_I, $I = 1,\ldots, m$ and Λ_J, $J = 1,\ldots, m$ are the Lagrange–Liu multipliers relating Eqs. (2.26) with (2.28) and (2.27) with Eqs. (2.29). Let

$$(2.30) \qquad \operatorname{div} \boldsymbol{\xi} = \langle d\boldsymbol{\xi}, f_* \rangle = 0$$

be any conservation equation algebraically implied by the system (2.26) (or, what is equivalent, by Eq. (2.27)); the vector field $\boldsymbol{\xi}$, $\boldsymbol{\xi} : Q - T_A$ is the "four-vector" corresponding to the conservation equation (2.30). From the assumption that only one independent entropy balance exists it follows that $d\boldsymbol{\xi}$ can be expressed in the following form

$$(2.31) \qquad d\xi = \sum_I G_I d\mathbf{U}^I + g d\mathbf{S} = \sum_J H_J d\mathbf{V}^J + h\, d\mathbf{R}.$$

where $g, h, G_I, H_J, I, J = 1, \ldots, m$ are the real numbers. If g is different from
zero, then Eq. (2.31) is an additional conservation law for the system (2.26) and,
similarly, if h is different from zero, then (2.31) is the additional conservation
law for the system (2.27). In particular, the differentials $d\mathbf{U}^I$, $I = 1, \ldots, m$
corresponding to the conservation laws from the system (2.26) can be written in
the form

$$(2.32) \qquad d\mathbf{U}^I = \sum_J \left(B_J^I + b^I A_J \right) d\mathbf{V}^J,$$

where the determinant of the matrix N_J^I,

$$(2.33) \qquad N_J^I = B_J^I + b^I A_J$$

is different from zero and $B_J^I, b^I, I, J = 1, \ldots, m$ are the real numbers. After
inserting Eq. (2.32) into Eq. (2.31) we obtain the identity

$$(2.34) \qquad \sum_I G_I d\mathbf{U}^I + g \sum_I \lambda_I d\mathbf{U}^I = \sum_I (G_I + g\lambda_I) d\mathbf{U}^I$$

$$= \sum_{I,J} (G_I + g\lambda_I) N_J^I d\mathbf{V}^J = \sum_{I,J} (G_I + g\lambda_I) \left(B_J^I + b^I A_J \right) d\mathbf{V}^J$$

$$= \sum_J H_J d\mathbf{V}^J + h \, d\mathbf{R} = \sum_J (H_J + h A_J) d\mathbf{V}^J.$$

From the linear independence of $d\mathbf{V}^J$, $J = 1, \ldots, m$ it follows that

$$(2.35) \qquad H_J + h A_J = \sum_I (G_I + g\lambda_I) \left(B_J^I + b^I A_J \right)$$

and therefore

$$(2.36) \qquad A_J \left[h - \sum_I (G_I + g\lambda_I) b^I \right] = \sum_I B_J^I (G_I + g\lambda_I) - H_J.$$

what shows that in the domain where

$$(2.37) \qquad h - \sum_I (G_I + g\lambda_I) b^I \neq 0,$$

the multipliers A_J, $J = 1, \ldots, m$ can be explicitly written as the functions of the
multipliers λ_I, $I = 1, \ldots, m$

$$(2.38) \qquad A_J = \frac{1}{\left[h - \sum_I (G_I + g\lambda_I) b^I \right]} \left[-H_J + \sum_I B_J^I (G_I + g\lambda_I) \right].$$

From Eq. (2.35) we can also obtain the identity relating the differentials of the multipliers

$$(2.39) \qquad d\Lambda_J = \left[h - \sum_I b^I (G_I + g\lambda_I) \right]^{-1} \sum_I \left(B_J^I + b^I \lambda_J \right) d\lambda_I$$

$$= \left[h - \sum_I b^I (G_I + g\lambda_I) \right]^{-1} \sum_I N_J^I d\lambda_I.$$

Identity Eq. (2.39) shows that the dimension of the space spanned by the differentials of the Lagrange–Liu multipliers remains invariant under the transition between nontrivially different conservative forms (this follows from the fact that the matrix N_J^I, given by Eq. (2.33), is nondegenerate).

The dimension of the space spanned by the differentials of the multipliers is an important invariant which, in particular, allows one to classify the "canonical" forms of the systems of conservation laws consistent with the additional conservation equation [7, 14]. However, here we generalize this observation to the case of more general transformations.

3. Invariant description of symmetric conservative systems

As it is well-known (see, for example [13]), the system of conservation laws consistent with the additional balance equation can be written in the symmetric conservative form if and only if the Lagrange–Liu multipliers form a local coordinate system on Q, what, in turn, is equivalent to the condition that the dimension of the vector space spanned by the differentials of the Lagrange–Liu multipliers is equal to $m = \dim Q$. As it has been mentioned in Sec. 3, the transformations between the equivalent conservative forms (2.26) and (2.27) preserve the dimension of the space spanned by the differentials of the Lagrange–Liu multipliers and therefore, the possibility of writing the system of conservation laws possessing nontrivially equivalent conservative forms as the symmetric conservative system does not depend on the transformation between the nontrivially different conservative forms. In this section we shall discuss the symmetric conservative systems and therefore, we shall assume that the dimension of the vector space spanned by the differentials of the Lagrange-Liu multipliers is equal to $m = \dim Q$. The fact that the system of conservation laws can be written in the symmetric conservative form with respect to the Lagrange–Liu multipliers λ_I, $I = 1, \ldots, m$ means that there exists such a function $\mathcal{F}$, $\mathcal{F} : Q - T_A$ (called the vector potential) that the "four-fluxes" $\mathbf{U}^I$, $I = 1, \ldots, m$ defining this system are given by the derivatives of $\mathcal{F}$:

$$(3.1) \qquad \mathbf{U}^I = \frac{\partial \mathcal{F}}{\partial \lambda_I}, \qquad I = 1, \ldots, m.$$

The symmetric conservative form of a discussed system of conservation laws is given by

$$(3.2) \qquad \text{div}\left(\frac{\partial \mathcal{F}}{\partial \lambda_I}\right) = 0, \qquad I = 1, \ldots, m.$$

Let us write the vector potential $\mathcal{F}$ in the basis $\mathbf{e}_1, \ldots, \mathbf{e}_n$ of T_A

$$(3.3) \qquad \mathcal{F} = \mathcal{F}^i \mathbf{e}_i.$$

After inserting Eq. (3.3) into Eq. (3.2) we arrive at the explicit form of a symmetric conservative system

$$(3.4) \qquad \frac{\partial}{\partial x_i}\left(\frac{\partial \mathcal{F}^i}{\partial \lambda_I}\right) = 0, \qquad I = 1, \ldots, m.$$

Let us subject the coordinates of the coordinate system λ_I, $I = 1, \ldots, m$ to the affine transformation

$$(3.5) \qquad \lambda'_{I'} = A^I_{I'}\lambda_I + a^I, \qquad I, I' = 1, \ldots, m,$$

where $A^I_{I'}$ is a nondegenerate, constant, real $m \times m$ matrix and a^I, $I = 1, \ldots, m$ are arbitrary real numbers. The functions $\partial \mathcal{F}/\partial \lambda'_{I'}$, $I' = 1, \ldots, m$ define the set of four-fluxes which correspond to the system of conservation laws

$$(3.6) \qquad \text{div}\left(\frac{\partial \mathcal{F}}{\partial \lambda'_{I'}}\right) = 0, \qquad I' = 1, \ldots, m.$$

From the relations

$$(3.7) \qquad \frac{\partial \mathcal{F}}{\partial \lambda_I} = \frac{\partial \mathcal{F}}{\partial \lambda'_{I'}}\frac{\partial \lambda'_{I'}}{\partial \lambda_I} = A^I_{I'}\frac{\partial \mathcal{F}}{\partial \lambda_I}$$

it follows that the systems (3.4) and (3.6) are trivially equivalent, that is, they can be transformed one into another after multiplying by a constant, nondegenerate, real matrix $A^I_{I'}$. Therefore, the symmetric conservative form remains preserved under the transformations (3.5) of the Lagrange – Liu multipliers and such transformations change one symmetric conservative system into the other, trivially equivalent symmetric conservative system. All coordinate systems which are related by means of the affine transformation (3.5) have the important property that their natural base vectors $\partial_{\lambda'_{I'}}$, $I' = 1, \ldots, m$ and ∂_{λ_I}, $I = 1, \ldots, m$ are related by the constant, nondegenerate matrix $A^I_{I'}$:

$$(3.8) \qquad \partial_{\lambda_I} = \frac{\partial \lambda'_{I'}}{\partial \lambda_I}\partial_{\lambda'_{I'}} = A^I_{I'}\partial_{\lambda'_{I'}}.$$

Also the inverse relation holds: if there exist a coordinate system (y_J), $J = 1, \ldots, m$ which is such that its natural base vectors ∂_{y_J}, $J = 1, \ldots, m$ are related to the natural base vectors ∂_{λ_I}, $I = 1, \ldots, m$ of the coordinate system (λ_I), $I = 1, \ldots, m$ by a real, nondegenerate, constant $m \times m$ matrix D_J^I:

$$(3.9) \qquad\qquad \partial_{\lambda_I} = D_J^I \partial_{y_J}$$

then the coordinate functions of the coordinate system (y_J), $J = 1, \ldots, m$ are related with the coordinates of the coordinate system λ_I, $I = 1, \ldots, m$ by the relations

$$(3.10) \qquad\qquad y_J = D_J^I \lambda_I + k^J ,$$

where k^J, $J = 1, \ldots, m$ are the arbitrary real constants. Therefore, the whole class of coordinate systems which are mutually related by affine transformations (3.5) can be determined by specifying the set of natural base vectors corresponding to any coordinate system from that class. For example, as such a set of natural base vectors we can take ∂_{λ_I}, $I = 1, \ldots, m$. All other affinely related coordinate systems can be obtained in the manner described by Eqs. (3.9) and (3.10) (that is, after taking all nondegenerate, constant, real $m \times m$ matrices, inserting them into Eq. (3.9) and integrating Eq. (3.9) in order to obtain the coordinate transformations of the form (3.10)). The important fact is that the transition between the affinely related coordinate systems, which transforms one symmetric conservative system of p.d.e into another, trivially equivalent symmetric conservative system, does not change the vector potential $\mathcal{F}$ (however, it is worth to stress that such a transition modifies the entropy law; see a more detailed discussion of this aspect given in [13]). As it has been already mentioned, the possibility of writing the discussed system of p.d.e in the symmetric conservative form does not depend on the transition between the nontrivially equivalent conservative forms. Therefore, we can consider the two symmetric conservative systems corresponding to the nontrivially equivalent systems of conservation laws;

$$(3.11) \qquad \operatorname{div} U^I = \operatorname{div} \left(\frac{\partial \mathcal{F}}{\partial \lambda_I} \right) = 0, \qquad I = 1, \ldots, m$$

and

$$(3.12) \qquad \operatorname{div} V^J = \operatorname{div} \left(\frac{\partial \mathcal{F}'}{\partial \lambda_J} \right) = 0, \qquad J = 1, \ldots, m .$$

The transformation rules between the multipliers λ_I, $I = 1, \ldots, m$ and Λ_J, $J = 1, \ldots, m$ in Eqs. (3.11) and (3.12) were discussed in Sec. 2, and from the results of Sec. 2 we could derive the corresponding transformation rules for the vector potentials $\mathcal{F}$ and $\mathcal{F}'$ in Eqs. (3.11) and (3.12). However, instead of doing that, we

shall show that the transition between Eqs. (3.11) and (3.12) is trivial in the sense that both systems correspond to the same symmetric system. Let W denote the tensor field defined via the relation

$$(3.13) \qquad W := \sum_I d\lambda_I \otimes d\left(\frac{\partial \mathcal{F}}{\partial \lambda_I}\right).$$

The system (3.1) can be alternatively represented by the following contraction of W and f_*

$$(3.14) \qquad \underset{(2.4)\,(3.5)}{\mathrm{Tr}\ \mathrm{Tr}}\ W \otimes f_* = \underset{(2.4)\,(3.5)}{\mathrm{Tr}\ \mathrm{Tr}}\left[\sum_I d\lambda_I \otimes d\left(\frac{\partial \mathcal{F}}{\partial \lambda_I}\right)\right] \otimes f_*$$

$$= \underset{(2.4)\,(3.5)}{\mathrm{Tr}\ \mathrm{Tr}}\left[\sum_{I,J,i} d\lambda_I \otimes \frac{\partial \mathcal{F}^i}{\partial \lambda_I \partial \lambda_J} d\lambda_J \otimes e_i\right] \otimes \left[\sum_{i',I'} \partial_{\lambda_{I'}} \frac{\partial \lambda_{I'}}{\partial x_{i'}} \otimes F^{i'}\right]$$

$$= \sum_{\substack{I,J,i \\ i',I'}} d\lambda_I \frac{\partial \mathcal{F}^i}{\partial \lambda_I \partial \lambda_J} \frac{\partial \lambda_{I'}}{\partial x_{i'}} \delta^J_{I'} \delta^{i'}_i = d\lambda_I \frac{\partial \mathcal{F}^i}{\partial \lambda_I \partial \lambda_J} \frac{\partial \lambda_J}{\partial x_i} = d\lambda_I \left(\frac{\partial}{\partial x_i} \frac{\partial \mathcal{F}^i}{\partial \lambda_I}\right) = 0,$$

where Tr denoted the trace operation taken with respect to the indices listed below, and the equivalence of Eqs. (3.11) and (3.14) follows from the fact that the differentials $d\lambda_I$, $I = 1. \ldots, m$ in Eq. (3.14) are linearly independent.

The definition (3.14) is formulated invariantly, that is, it does not depend on the choice of the coordinate system, and the fact that the system (3.14) is symmetric is exhibited in the property that the tensor W given by Eq. (3.13) is symmetric in the first two indices [13, 14].

In turn, the system (3.12) can be represented by the tensor field W',

$$(3.15) \qquad W' := \sum_J dA_J \otimes d\left(\frac{\partial \mathcal{F}'}{\partial A_J}\right)$$

in the manner analogous to the representation of the system (3.4) by the tensor field W (given by Eq. (3.13)). The relation between the system (3.11) and (3.12) is a special case of the relation between Eqs. (2.26) and (2.27); therefore, from Eqs. (2.32), (2.33), (2.39) we obtain the identities

$$(3.16) \qquad d\left(\frac{\partial \mathcal{F}}{\partial \lambda_I}\right) = N^I_J d\left(\frac{\partial \mathcal{F}'}{\partial A_J}\right).$$

$$(3.17) \qquad dA_J = \left[h - \sum_I b^I (G_I + g\lambda_I)\right]^{-1} \sum_I N^I_J d\lambda_I.$$

After inserting Eq. (3.16) into Eqs. (3.13) and Eq. (3.17) into Eq. (3.15) we see that

$$(3.18) \qquad W = \sum_{I,J} N_J^I d\lambda_I \otimes d\left(\frac{\partial \mathcal{F}'}{\partial \Lambda_J}\right)$$

and

$$(3.19) \qquad W' = \sum_J d\Lambda_J \otimes d\left(\frac{\partial \mathcal{F}'}{\partial \Lambda_J}\right)$$

$$= \left[h - \sum_I b^I (G_I + g\lambda_I)\right]^{-1} \sum_{I,J} N_J^I d\lambda_I \otimes d\left(\frac{\partial \mathcal{F}'}{\partial \Lambda_J}\right).$$

From the comparison of Eqs. (3.18) and (3.19) we see that in the domain of the transformation (2.38) the tensor fields W and W' are identical up to the multiplication by a scalar function of the dependent variables. However, this means that they define the same symmetric system since the symmetric systems which can be transformed one into another after multiplication by a scalar function of the dependent variables can be considered as undistinguishable. As a consequence, the transformations between the nontrivially equivalent symmetric systems do not modify the structure of the discussed system of p.d.e. in the sense that their action is equivalent to the change of variables in the same symmetric system.

4. Final remarks

As it is well-known, in the theory of p.d.e. one distinguishes between the invariant definition of a system of p.d.e. (which is identified with a corresponding subset of a jet space – see [9] and the literature cited therein) and the "form" of a system (by the "form" one means a choice of a set of "independent" equations which represent the system, see [9, 10]). Some properties (like, for example, symmetries) are related with the "invariant" aspect of a system of p.d.e. while other, like the properties of "being expressible in a conservative form" or "being expressible in a Cauchy form" characterize the admissible forms of a system.

Any system of conservation laws, after multiplying by a real, constant, nondegenerate matrix, can be transformed into the other system of conservation laws which is equivalent to the initial one. However, sometimes a system of p.d.e. can possess different equivalent conservative forms which are not trivially equivalent; in such a case, different equivalent conservative forms can be transformed one into another after multiplying by a matrix which depends on the dependent variables. In this paper we discuss such determined systems of the first order p.d.e. which admit nontrivially equivalent conservative forms. It can be easily seen that,

for such systems, the property of "possessing nontrivially equivalent conservative forms" is equivalent to the property of "implying additional conservation equation". For simplicity, only the systems of conservation laws possessing one independent additional conservation equation are discussed in detail. For such systems, the most important result is that the dimension of the space spanned by the differentials of the Lagrange – Liu multipliers does not depend on the choice of a conservative form of a discussed system.

This fact has the following implications:

a. The classification based on the dimension of this space and discussed in [7] (see also [14]) does not depend on the choice of a particular conservative form of a system.

b. The possibility of writing the discussed system of p.d.e. in a symmetric conservative form does not depend on the choice of a conservative form.

c. The different symmetric conservative forms are trivially equivalent in the sense that they correspond to the same symmetric system (see a discussion of trivial and nontrivial equivalencies of symmetric systems given in [16]).

d. In [14] it has been shown that every system of conservation laws admitting additional conservation equation implies the symmetric system; it can be easily shown that the symmetric system obtained in that manner does not depend on the choice of a particular conservative form of a discussed system of p.d.e. (in order to check that, one has to repeat the reasoning given in Sec. 3 but without assuming that the dimension of the vector space spanned by the differentials of the Lagrange – Liu multipliers is equal to $m = \dim Q$).

The systems of conservation laws consistent with the additional conservation equation were described by FRIEDRICHS [15] in a manner which was, to some extent, independent of the choice of a particular conservative form of the discussed system of p.d.e. However, he has not taken into account all possible conservative forms of the discussed system of p.d.e. and, therefore, the approach presented in this paper, in which we construct all possible conservative forms explicitly, is more general than that of Friedrichs. Another important difference between our approach and that of Friedrichs is that our approach does not depend on the choice of a particular coordinate system.

It can be also checked that our results can be generalized to the case of systems of conservation laws admitting arbitrary number (i.e., finite or infinite number of arbitrary cardinality) of additional conservation equations. In such a case, the most important result is the following:

Let $\tilde{S}$ denote the set of conservation equations algebraically implied by a given system of conservation laws. Let $\tilde{s}$ denote the arbitrary conservation law from $\tilde{S}$. Among all conservative forms of a discussed system we can distinguish such conservative forms for which $\tilde{s}$ is the additional conservation equation; let us denote such a set of conservative forms by $C(\tilde{s})$. Then the dimension of the space spanned by the differentials of the Lagrange – Liu multipliers does not depend on

the choice of a particular conservative form from $C(\tilde{s})$. As a consequence, a discussion presented in this paper can be generalized to the case of an arbitrary system of conservation laws and, in particular, it is possible to classify all admissible symmetric conservative forms of a given system.

All observations mentioned above, describe the properties of the conservative systems of the first order partial differential equations. However, in phenomenological thermodynamics one sometimes considers field equations which have a structure of systems of conservations laws of the order higher than one. The additional balance equation implied by such systems is interpreted as the balance of entropy (in general, for such systems the entropy balance can be described by the conservation law of the order higher than one). The systems of conservation laws of the order higher than one can also possess nontrivially equivalent conservative forms, and the relations between the properties of "possessing nontrivially equivalent conservative forms" and "implying additional balance equation" can be discussed in a manner similar to that presented in this paper. The only difference is that, for the systems of conservation laws of the order higher than one, it is necessary to take into account not only the algebraic, but also the differential consequences of the discussed system (for the systems of the first order conservation laws it is sufficient to consider only the algebraic consequences).

Our results can be useful also for classification of weak solutions of the systems of conservation laws.

Acknowledgement

References

1. I-SHIU LIU, I. MULLER, *Extended thermodynamics of classical and degenerate gases*, Arch. Rat. Mech. Anal., **83**, 285, 1983.

2. I-SHIU LIU, *Method of Lagrange multipliers for exploitation of the entropy principle*, Arch. Rat. Mech. Anal., **46**, 131, 1973.

3. С.К. ГОДУНОВ, *Интересный класс квазилинейных систем*, Докл. Акад. Наук СССР, **139**, 521, 1961.

4. С.К. ГОДУНОВ, *Проблема обобщенного решения в теории квазилинейных уравнений и в газовой динамике*, Усп. Мат. Наук., **17**, 147, 1962.

5. T. RUGGERI, *Entropy principle, symmetric hyperbolic systems and shock wave phenomena*, [in:] Modern Theory and Applications, C. ROGERS and T.B. MOODIE [Eds.], North Holland Mathematical Studies, **97**, 211, 1984.

6. T. RUGGERI, A. STRUMIA, *Main field and convex covariant density for quasilinear hyperbolic systems*, Ann. Inst. H. Poincaré, **34**, 65, 1981.

7. S. PIEKARSKI, *On integration of constraints imposed on a system of conservation laws by the second law of thermodynamics*, Continuum Mech. Thermodyn., **4**, 109, 1992.

8. H.H. JOHNSON, *The absolute invariants of conservation laws*, Pacific J. of Math., **144**, 51, 1990.

9. A.M. VINOGRADOV, I.S. KRASILSHCHIK and V.V. LICHAGIN, *Introduction to geometry of nonlinear differential equations*, [in Russian], Moscow Science, 1986.

10. Z. Peradzyński, *Geometry of nonlinear interactions in partial differential equations*, [in Polish], Habilitation Thesis, Warszawa 1981.

11. Z. Peradzyński, *Geometry of interactions of Riemann waves*, [in:] Advances in Nonlinear Waves, L. Debneth [Ed.], Pitman, 244, 1985.

12. Z. Peradzyński, *Riemann invariants in nonlinear interactions of waves. Applications in dynamics of gases*, [in Polish], Doctoral Thesis, Warsaw 1973.

13. S. Piekarski, *Geometrical aspect of symmetric conservative systems of partial differential equations*, Arch. Mech., **44**, 603, 1992.

14. S. Piekarski, *On the uniqueness of symmetric algebraic consequences implied by a system of conservation laws consistent with the additional conservation equation*, [to be published in Cont. Mech. Thermod.].

15. K.O. Friedrichs, *On the laws of relativistic electro-magneto-fluid dynamics*, Comm. Pure. Appl. Math., 27, 1974.

16. S. Piekarski, *Geometrical aspect of symmetrization of quasi-linear systems of the first order partial differential equations*, Arch. Mech., **45**, 371, 1993.

Excitation, waveguiding and scattering of EM and elastic waves by a periodic system of in-plane strips or cracks

E. DANICKI (WARSZAWA)

A COMMON METHOD is applied to the analysis of two different waves, electromagnetic (EM) and elastic. This method allows us to analyze the phenomena of scattering, detection and excitation of waves by periodic systems of in-plane obstacles, such like perfectly conducting strips (in EM case) or cracks (in elastic wave case). New 3-dimesional inhomogeneous boundary problems for strips are formulated and solved. Numerical results are presented for elastic waves guided and Bragg-scattered by cracks. Isotropic media are considered in detail, and cases of arbitrary anisotropic and layered media are discussed briefly.

1. Introduction

IN THIS PAPER a common method is applied to the analysis of two different waves, electromagnetic (EM) and elastic waves. This method allows us to analyze scattering, detection and excitation of waves by periodic systems of in-plane obstacles, such like perfectly conducting strips (in EM case) or cracks (in elastic wave case). We consider isotropic media only, but the method can be applied for analyzing the waves in arbitrary anisotropic bodies. Generally, the method can be applied to solving boundary-value problems which are formulated with the help of a "planar Green's function" that possesses certain asymptotic properties in spectral domain. Formally, the applied method is similar to that called "orthogonalized-plane-wave method" and "the augmented plane wave method" in solid state physics [1]. It exploits a properly chosen system of functions satisfying boundary conditions and having suitable asymptotic properties for large values of the spectral variable. The system allows us to represent the solution in the form of a short series. Coefficients of this expansion are chosen to satisfy the equations (in spectral domain) for small values of spectral variable only.

In the problems considered, we deal with a set of two functions which are a complementary pair of the solutions of certain electrostatic (elastostatic) problem for periodic strips (cracks). The pair describes the electric field and electric charge distributions in the plane of strips. The method has been introduced in the literature by C-M. CHU [2], R.M. WHITE et al. [3] and K. BLØTEKJÆR et al. in two excellent papers [4,5] on the analysis of surface acoustic waves (SAW) in piezoelectrics covered by periodic conducting strips. It was further generalized in [6,7] for obliquely propagating SAW and for certain inhomogeneous problem where some strips possessed given electric potentials. Application of this method to analysis of the (i) EM wave scattering by conducting strips is presented in [8],

and (ii) certain elastostatic problem for plates with cracks – in [9]. In this paper the method is exploited to analyze certain inhomogeneous problems of excitation of EM waves by strips, and of scattering and waveguiding of elastic waves by cracks.

The advantage of the method is that the analysis of a "short-wave" case is formally as easy as that of a "long-wave" case, however the resulting systems of equations have different dimensions. Particularly, in a long-wave case we deal with at most two equations, and twice as much in the case of first-order Bragg reflection. Another advantage over the well-known Wiener–Hopf theory [10] is that the method can easily be adopted to the analysis of waves in arbitrary anisotropic media and waves in layered systems with strips (cracks) having different periods and orientations between layers. Full advantage of the method is apparent in Sec. 5 of this paper where an analysis of a certain 3-dimensional inhomogeneous boundary problem is carried out.

The paper is organized in five sections as follows. Next section presents the formulation of scattering problem for EM waves, which is the simplest problem suitable for presentation of the method exploited in this paper. A formal solution will be presented only, some numerical examples can be found in [10, 11]. Basing on the derived relations, in the last section we consider the excitation of EM waves by strips which are supplied by the external potential and current sources. Transadmittance relations for strips are derived which describe the mutual influence of the strips by means of the excited EM waves. The considered boundary problem is fully 3-dimensional, the electric forces applied to the strips depend on both x and z in the plane of strips.

In next Secs. 3 and 4 we deal with elastic waves. The corresponding scattering problem and homogeneous problem of waveguiding of elastic waves by cracks are analyzed. Some numerical examples are presented.

In the Appendices, auxiliary relations and derivations are presented. Some Green's functions (in spectral domain) are given which can be exploited in the analysis of certain wave problems by the method presented. A system of complementary functions is also presented which generalizes the method to the cases of periodic systems of groups of strips (cracks).

2. EM wave scattering by periodic strips

2.1. Formulation of the problem

Let us consider an infinite periodic system of infinitesimally thin and perfectly conducting strips arranged on $y = 0$ plane. The infinite (along the z-axis) strips are w wide, their period is $\varLambda$ (Fig. 1). An incident EM harmonic wave of arbitrary polarization and propagation direction is characterized by its angular frequency ω, wave-vector (r_I, s_I, τ), and complex amplitudes of electric and magnetic fields $\mathbf{E}^I$ and $\mathbf{H}^I$, correspondingly. Below, we consider EM waves in isotropic media (in

vacuum), the incident wave is sufficiently characterized by two vector-components of either the electric field in $y = 0$ plane, that is by $\mathbf{E}^I = (E_x^I, E_z^I)$, or by the corresponding magnetic field $\mathbf{H}^I = (H_x^I, H_z^I)$ only.
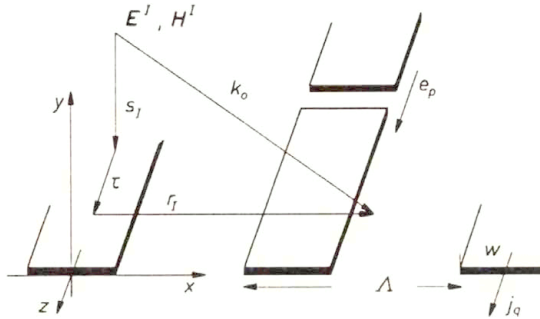

FIG. 1. Scattering of EM waves by periodic strips.

We shall use the following notations:
$K = 2\pi/\Lambda$ a strip wavenumber,
$\Delta = \pi w/\Lambda$ a parameter describing the strip width,
ε, μ electric and magnetic permittivity of the media,
$k_o = \omega\sqrt{\varepsilon\mu}$ EM wave-number in the media,
$r_I = r + IK$, where I is an integer chosen to obtain $0 \leq r < K$.

The harmonic incident wave propagating from the infinity in the upper half-space $(y > 0)$ is

(2.1)
$$e^{-jr_Ix}e^{js_Iy}e^{-j\tau z}e^{j\omega t},$$

where $s_I = \sqrt{k_o^2 - r_I^2 - \tau^2}$. In what follows, the dependence on time will be neglected.

We seek the solution to the electric and magnetic scattered fields, $\mathbf{E}^s$ and $\mathbf{H}^s$, which are parts of the full electromagnetic field $\mathbf{E}$ and $\mathbf{H}$,

(2.2)
$$\mathbf{E} = \mathbf{E}^s + \mathbf{E}^I, \qquad \mathbf{H} = \mathbf{H}^s + \mathbf{H}^I,$$

governed by Maxwell equations. In this paper we use the Maxwell equations indirectly. They will be used to obtain a matrix "planar Green's function" in spectral domain $(r, \tau; \omega)$ which describes the dependence between the tangential vector components of the EM field in the $y = 0$ plane (these field components are involved in boundary conditions at the $y = 0$ plane in the problem considered).

The solutions for $\mathbf{E}^s$, $\mathbf{H}^s$ are subject to the following constraints:

• they must obey the radiation conditions, which state that the scattered field must either carry out the EM energy from the scatterer, or must vanish at infinity,

• and they must satisfy the boundary conditions at the $y = 0$ plane, which are

(2.3)
$$[H_i] = H_i(y = +0) - H_i(y = -0) = 0, \quad i = x, z, \quad \text{between strips,}$$
$$E_i = 0, \quad i = x, z, \quad \text{on strips.}$$

It is well known, that some vector components of the electric and magnetic fields are square-root singular at the strip edges [12], and some other are not. However their x-derivatives are singular. According to the method applied in this paper, we deal with the square-root singular functions only. For this reason we seek a solution for the following functions defined on the $y = 0$ plane

$$(2.4) \qquad \frac{\partial}{\partial x} J_x = \frac{\partial}{\partial x}[H_z], \qquad J_z = -[H_x], \quad E_x, \quad \frac{\partial}{\partial x} E_z,$$

which are all square-root singular at the strip edges. Note that E_i, H_i are full EM fields, including the incident and scattered waves.

Boundary conditions at the $y = 0$ plane can be rewritten in the form

$$(2.5) \qquad \begin{aligned} \frac{\partial}{\partial x} J_x(x, z) &= 0, \qquad J_z(x, z) = 0, \quad \text{between strips,} \\ E_x(x, z) &= 0, \qquad \frac{\partial}{\partial x} E_z(x, z) = 0, \quad \text{on strips,} \end{aligned}$$

with the following additional one-point constraints

$$(2.6) \qquad \begin{aligned} J_x\left(\frac{\Lambda}{2} + p\Lambda, z\right) &= J_{p+1/2} e^{-j\tau z}, \\ E_z(p\Lambda, z) &= e_p e^{-j\tau z}. \end{aligned}$$

In the scattering problem, $J_{p+1/2} = 0$ and $e_p = 0$ (the generalized boundary conditions including $J_{p+1/2}$ and e_p will be exploited in Sec. 5).

2.2. Method of solution

The scattering obstacles are periodic, thus the Floquet theorem allows us to expand the EM field at $y = 0$ plane and, in particular, the functions presented in Eqs. (2.4), into the series

$$J_z(x, z) = \sum_{n=-\infty}^{\infty} J_z^{(n)} e^{-jr_n x} e^{-j\tau z},$$

$$\frac{\partial}{\partial x} J_x(x, z) = \sum_n J_{x,x}^{(n)} e^{-jr_n x} e^{-j\tau z},$$

$$(2.7) \qquad E_x(x, z) = \sum_n E_x^{(n)} e^{-jr_n x} e^{-j\tau z},$$

$$\frac{\partial}{\partial x} E_z(x, z) = \sum_n E_{z,x}^{(n)} e^{-jr_n x} e^{-j\tau z}.$$

where $r_n = r + nK$, and $J_z^{(n)}$, $J_{x,x}^{(n)}$, $E_x^{(n)}$, $E_{z,x}^{(n)}$ denote complex amplitudes of the corresponding Fourier components.

The scattered EM field in the media can be uniquely expressed by the above functions. Generally, the field is expressed in the form of a series analogous to the above ones, with additional terms $\exp(-js_n y)$ (for $y > 0$), or $\exp(+js_n y)$ (for $y < 0$). To satify the radiation conditions at $y \to \pm\infty$, we choose

$$(2.8) \qquad s_n = \begin{cases} \sqrt{k_o^2 - r_n^2 - \tau^2}, & k_n = \sqrt{r_n^2 + \tau^2} < k_o, \\ -j\sqrt{r_n^2 + \tau^2 - k_o^2}, & k_n > k_o. \end{cases}$$

It is convenient to consider a slightly lossy media, characterized by the EM wave number $k_o = k_o' - j\varepsilon'$, $\varepsilon' > 0$, $\varepsilon' \approx 0$. In this case the square-root s_n is a single-valued complex variable on the complex plane r, with cuts from a branch point k_o down to $-j\infty$, and from $-k_o$ up to $j\infty$.

Maxwell equations result in the following relations between the complex amplitudes of the wave components included in Eqs.(2.7) (see Appendix A)

$$(2.9) \qquad \mathbf{g}_\infty^{-1} \begin{bmatrix} J_{x,x}^{(n)} \\ J_z^{(n)} \end{bmatrix} = \frac{2}{\omega\mu}\bar{\mathbf{g}}_n \begin{bmatrix} E_x^{(n)} \\ E_{z,x}^{(n)} \end{bmatrix} - \frac{2}{\omega\mu}\bar{\mathbf{g}}_n \begin{bmatrix} E_x^I \\ -j(r + nK)E_z^I \end{bmatrix} \delta_{nI} .$$

where Kronecker delta δ_{nI} selects the proper harmonic component of the incident wave.

$$(2.10) \qquad \mathbf{g}_\infty = \begin{bmatrix} k_o^2 - \tau^2 & j\tau \\ j\tau & 1 \end{bmatrix}, \qquad \bar{\mathbf{g}}_n = \begin{bmatrix} -jr_n/s_n & \tau/(r_n s_n) \\ 0 & s_n/(-jr_n) \end{bmatrix}.$$

To simplify the notations, let us introduce

$$(2.11) \qquad \mathbf{C}_n = \frac{\omega\mu}{2}\mathbf{g}_\infty^{-1}\left[J_{x,x}^{(n)}, J_z^{(n)}\right]^T, \qquad \mathbf{F}_n = \left[E_x^{(n)}, E_{z,x}^{(n)}\right]^T.$$

which, applied to Eqs. (2.9), yield

$$(2.12) \qquad \mathbf{C}_n = \bar{\mathbf{g}}_n \mathbf{F}_n - \bar{\mathbf{g}}_n \mathbf{F}^I \delta_{nI}.$$

We leave this equation for a moment, and we will try to guess the solution satisfying boundary conditions (2.5), or the equivalent ones,

$$(2.13) \qquad \begin{aligned} \sum_n \mathbf{C}_n e^{-jr_n x} &= 0, & \text{between strips,} \quad w/2 < |x| < \Lambda/2. \\ \sum_n \mathbf{F}_n e^{-jr_n x} &= 0, & \text{on strips,} \quad |x| < w/2. \end{aligned}$$

Taking into account Eqs. (B.2) we conclude, that Eqs. (2.13) will be satisfied by solution (2.7) provided that the corresponding amplitudes $\mathbf{C}_n$ and $\mathbf{F}_n$ are expanded

into series

(2.14)

$$\mathbf{C}_n = \sum_m \mathbf{c}^{(m)} P_{n-m}(\cos \varDelta),$$

$$\mathbf{F}_n = \sum_m \mathbf{f}^{(m)} S_{m-m} P_{n-m}(\cos \varDelta),$$

where coefficients $\mathbf{c}^{(m)}$, $\mathbf{f}^{(m)}$ are unknown as yet.

Following Eq. (2.7) and Appendix B, these coefficients appear in the expansion of EM field on $y = 0$ plane, e.g.

$(2.15) \qquad E_x(x,z) = -jS_\theta \dfrac{\sum_m f_1^{(m)} e^{-jm\theta}}{\sqrt{\cos \varDelta - \cos \theta}} \sqrt{2} e^{j\theta/2} e^{-j\tau z}, \qquad \theta = Kx.$

This shows that the coefficients $\mathbf{c}^{(m)}$ and $\mathbf{f}^{(m)}$ are coefficients of Fourier expansion of a certain smooth analytical function being the numerator of the square-root singular function (we deal with square-root singular functions only, like E_x above). Thus, applying finite series over m within sufficiently large limits, we can meet the required accuracy of representation of the EM field. Independently of the limits, the square-root singularity of the solution is always preserved.

2.3. Selfconsistency

We make the initial assumption that the summation with respect to m in Eqs. (2.14) is carried out over some finite limits

$(2.16) \qquad\qquad\qquad M^- \le m \le M^+.$

In a few steps described below we shall show that $\mathbf{c}^{(m)}$ and $\mathbf{f}^{(m)}$ depend on each other. Indeed, let us note that for $|n| \to \infty$ ($|n|$ large and $|n| > |I|$)

$(2.17) \qquad\qquad s_n = -j\sqrt{r_n^2 + \tau^2 - k_o^2} \to -j|r_n|, \qquad \mathbf{\bar{g}}_n \to S_n \mathbf{I}.$

Thus Eqs. (2.12) yield an infinite number of conditions ($|n|$ large)

$(2.18) \qquad \sum_m \mathbf{c}^{(m)} P_{n-m}(\cos \varDelta) = \sum_m S_n \mathbf{f}_m S_{n-m} P_{n-m}(\cos \varDelta)$

for a finite number of unknowns $\mathbf{c}^{(m)}$ and $\mathbf{f}^{(m)}$. There is only one solution

$(2.19) \qquad\qquad\qquad \mathbf{c}^{(m)} = \mathbf{f}^{(m)}$

which, substituted in Eqs. (2.12), results in the equations

$(2.20) \qquad \sum_m [\mathbf{I} - S_{n-m}\mathbf{\bar{g}}_n] \, \mathbf{c}^{(m)} P_{n-m}(\cos \varDelta) = -\mathbf{\bar{g}}_n \mathbf{F}^I \delta_{nI}$

which, according to the Maxwell equations satisfied in the media, must be satisfied for any $n \in (-\infty, \infty)$.

2.4. Approximation to Green's function

So far we have not used any substantial approximations. At this step of analysis we must apply one that allows us to solve efficiently the infinite system of Eqs. (2.20). In agreement with the previously used asymptotic property of $\bar{\mathbf{g}}_n$, we apply the approximation

$$(2.21) \qquad \bar{\mathbf{g}}_n = S_n \mathbf{I}, \quad \text{if} \quad \begin{cases} n < N^- \leq 0, \\ n > N^+ \geq 0, \end{cases}$$

where $N^\pm$ are sufficiently large, and $N^- \leq I \leq N^+$.

Considering Eq. (2.10) we conclude, that $\bar{\mathbf{g}}_n \to S_n \mathbf{I}$ as fast as n^{-2}, and that there are indeed certain large integers $N^\pm$ for which $\bar{\mathbf{g}}_n$ differs from $S_n \mathbf{I}$ by a negligibly small matrix. Instead of a rigorous mathematical proof of convergence properties of the approximation, we present here the following physical discussion of the problem.

Consider a case of layered media with layers parallel to the $y = 0$ plane. We can derive the corresponding Green's function in spectral domain, and the matrix analogous to $\bar{\mathbf{g}}_n$ which will be a certain complicated function of n. However, for large n, the corresponding harmonic wave-field $\exp(-j(r + nh) - js_n y - j\tau z)$ penetrates only the layer closest to $y = 0$ plane (if n is sufficiently large, the wave-field decays at the shorter distance from the plane $y = 0$ than the layer thickness). Thus for large n, $\bar{\mathbf{g}}_n$ is that derived in Appendix A for a halfspace, however with different ε, μ. It is evident that the approximation to $\bar{\mathbf{g}}_n$ corresponds to the introduction of thin dielectric layers on both sides of the $y = 0$ plane. Their properties are close to those of the considered media, because the difference between $\bar{\mathbf{g}}_n$ and $S_n \mathbf{I}$ is small, depending on $(N^\pm)^{-2}$.

A small change in the dieletric property of a thin layer around the conducting strips cannot influence much the scattered EM field. This justifies physically the introduced approximation of $\bar{\mathbf{g}}_n$. Anyway, the discussed method of analysis should be considered as a numerical one. Results are obtained by numerical solution of certain system of equations. The above considerations help us to apply proper truncation of the infinite system of Eqs. (2.20).

As a result of the applied approximation (2.21), it is easy to prove by inspection that Eqs. (2.20) will be satisfied automatically for all n outside the domain $[N^-, N^+]$, if we apply

$$(2.22) \qquad N^- \leq m \leq N^+ + 1,$$

that is

$$(2.23) \qquad M^- = N^-, \qquad M^+ = N^+ + 1$$

(note that $S_k = 1$ for $k \geq 0$ and -1 otherwise, note also that $N^- \leq I \leq N^+$).

There are $2(N^+ - N^- + 1)$ equations ($n \in [N^-, N^+]$) for $2(N^+ - N^- + 2)$ unknowns $c_1^{(m)}$ and $c_2^{(m)}$ in Eqs. (2.20). A sample matrix of the resulting system

of equations is shown below

$$\begin{bmatrix} \cdot & & & & & & & \\ \cdot & \cdot & \cdot & & & & & \\ \cdot & \cdot & \cdot & \cdot & \cdot & \cdot & \cdot & \\ \cdot & \cdot & \cdot & \cdot & \cdot & \cdot & \cdot & \cdot \\ & \cdot & \cdot & \cdot & \cdot & \cdot & \cdot & \cdot \\ & & & & & & & \cdot \end{bmatrix}.$$

Apparently, the domain $[N^-, N^+]$ can be chosen narrower by 3 in this example (the corresponding changes in $M^\pm$ follow from Eq. (2.23)).

The remaining pair of equations are those resulting from Eqs. (2.6). They are evaluated in Appendix C in the forms

$$J_x|_{x=A/2} = \frac{jAe^{-jr\frac{A}{2}-j\tau z}}{\omega\mu\sin r\frac{A}{2}} \sum_{m=M^-}^{M^+} \left[(k_o^2 - \tau^2)c_1^{(m)} + j\tau c_2^{(m)}\right]$$

(2.24)
$$\times P_{-m-r/K}(\cos \varDelta) = 0,$$

$$E_z|_{x=0} = \frac{jAe^{-j\tau z}}{2\sin r\frac{A}{2}} \sum_m (-1)^m c_2^{(m)} P_{-m-r/K}(-\cos \varDelta) = 0.$$

Thus the closed system of equations consists of the set of Eqs. (2.20) taken for $N^- \le n \le N^+$, and Eqs. (2.24).

Summarizing, we have solved the scattering problem in the following steps:

• choosing the limits for $M^\pm$ appropriate for the assumed accuracy of expansions (2.7), (2.14), and determination of $N^\pm$ from Eqs. (2.23). The resulting limits must satisfy Eq. (2.21),

• evaluation of all $c^{(m)}$ except $c^{(0)}$, by F^I and $c^{(0)}$, on the basis of Eqs. (2.20), taken for $n \in [N^-, N^+]$,

• evaluation of c_0 by means of Eqs. (2.24),

• and, finally, evaluation of EM field on the $y = 0$ plane, and in the media. This can be done by means of relations used in Appendix A. This concludes the solution of the diffraction problem.

2.5. Detection of EM waves by strips

There is some interest, particularly in the theory of leaky-wave antenna [13] in evaluation of the total current j flowing along the strips, and the difference of strip potentials U defined as follows:

$$j = \int_{-w/2}^{w/2} J_z(x,z)\, dx = \int_{-A/2}^{A/2} J_z(x,z)\, dx,$$

(2.25)
$$U = -\int_{w/2}^{A-w/2} E_x\, dx = -\int_0^A E_x\, dx.$$

The integration and subsequent summation over n can be explicitly evaluated with the help of identities given in Appendix B (see also Appendix C). We obtain

(2.26)
$$j = \frac{2\Lambda}{\omega\mu} \sum_m \left(j\tau c_1^{(m)} + c_2^{(m)} \right) P_{-m-r/K}(\cos \Delta) e^{-j\tau z},$$

$$U = -\Lambda \sum_m (-1)^m f_1^{(m)} P_{-m-r/K}(-\cos \Delta) e^{-j\tau z};$$

the strip current and the voltage difference between strips can be used in detection of the incident EM field. To generalize these results to a nonplanar incident wave, one should apply a 2-dimensional Fourier transformation with spectral variables r_l and τ, as discussed in last section of this paper.

3. Scattering of elastic waves by cracks

Below we consider briefly the problem of elastic wave scattering by in-plane periodic array of cracks in an isotropic body. Te problem was analyzed previously in the literature [14, 15]. In this paper we shall show how the presented method of analysis works in this case. The incident wave of arbitrary polarization and propagation direction is characterized by either the stress tensor components $(T_{yx}^I, T_{yy}^I, T_{yz}^I) = \mathbf{T}^I$ or the particle displacement vector $\mathbf{u}^I$ at the $y = 0$ plane, where cracks are included. The incident wave propagates in the upper halfspace from infinity, the projection of its wave-vector on $y = 0$ plane is (r_l, τ), $r_l = r + IK$, $0 < r < K$. Crack width is $w = \Delta\Lambda/\pi$ and period $\Lambda = 2\pi/K$.

Scattered field in the upper halfspace is $\mathbf{u}^+$, $\mathbf{T}^+$, and $\mathbf{u}^-$, $\mathbf{T}^-$ in the lower one ($y < 0$). The relations between them (in the spectral domain) is given in Appendix A. Full elastic field at $y = +0$ plane is

(3.1)
$$\mathbf{u} = \mathbf{u}^+ + \mathbf{u}^I, \qquad \mathbf{T} = \mathbf{T}^+ + \mathbf{T}^I.$$

The boundary conditions are (see Fig. 2)

(3.2)
$$\mathbf{T} = \mathbf{T}^- = \mathbf{T}^+,$$
$$\mathbf{T} = 0, \qquad \text{on cracks},$$
$$\mathbf{V} = \partial_x[\mathbf{u} - \mathbf{u}^-] = 0, \qquad \text{between cracks},$$
$$\mathbf{u} - \mathbf{u}^- = 0, \qquad \text{somewhere between cracks, e.g. at } x = 0.$$

The above *additional* one-point constraint is imposed because we must have not only $\mathbf{V}(x, z) = 0$ between the cracks but $\mathbf{u} - \mathbf{u}^- = 0$ as well.

Similarly to the EM case, we deal with a square-root singular functions $\mathbf{V}(x, z)$ $(-jr(\mathbf{u} - \mathbf{u}^-)$ in spectral domain) and $\mathbf{T}(x, z)$. A relation analogous to Eq. (A.8) is in this case (see Appendix A)

(3.3)
$$\mathbf{V} = \mathbf{gT} + 2(-jr)\mathbf{u}^I.$$
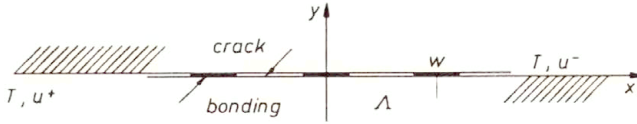
FIG. 2. Waveguiding of elastic waves by periodic cracks.

We seek the solution for $\mathbf{T}(x, z)$ and $\mathbf{V}(x, z)$ in the form

$$(3.4) \qquad \sum_{n=\infty}^{\infty} \begin{pmatrix} \mathbf{T}_n \\ \mathbf{V}_n \end{pmatrix} e^{-jr_n x - j\tau z}, \qquad r_n = r + nK$$

satisfying the boundary conditions

$$(3.5) \qquad \begin{aligned} \sum_n \mathbf{T}_n e^{-jr_n x} &= 0, & \text{on strips, } \ pA + w/2 < x < (p+1)A - w/2, \\ \sum_n \mathbf{V}_n^{-jr_n x} &= 0. & \text{between strips } \ pA - w/2 < x < pA + w/2 \end{aligned}$$

and, additionally, the condition resulting from the one-point constraint

$$(3.6) \qquad \sum_n \frac{\mathbf{V}_n}{-jr_n} = 0.$$

Conditions (3.5) will be satisfied if we apply

$$(3.7) \qquad \mathbf{T}_n = \sum_m \mathbf{t}_m P_{n-m}(\cos \Delta), \qquad \mathbf{V}_n = \sum_m \mathbf{v}_m S_{n-m} P_{n-m}(\cos \Delta),$$

where the sums with respect to m are assumed to be finite. Eqs. (3.3) yield

$$(3.8) \qquad \sum_m (S_{n-m}\mathbf{v}_m - \mathbf{g}_n \mathbf{t}_m)P_{n-m} = -j2r\mathbf{u}^I \delta_{nI}, \qquad \mathbf{g}_n = \mathbf{g}(r_n).$$

Now we apply the approximation that the value of a "planar Green's matrix function" $\mathbf{g}(r_n)$ is $S_r \mathbf{g}_\infty = \mathbf{g}(r_n - \pm\infty)$ if n is outside the limits $N^- \leq n \leq N^+$, where $N^- \leq I \leq N^+$. This yields the selfconsistency condition, and ultimately the closed system of equations

$$(3.9) \qquad \begin{aligned} \mathbf{v}_m &= \mathbf{g}_\infty \mathbf{t}_m, \\ \sum_{m=N^-}^{N^++1} (S_{n-m}\mathbf{g}_\infty - \mathbf{g}_n)\mathbf{t}_m P_{n-m}(\cos \Delta) &= -jr_I \mathbf{u}^I \delta_{nI}, \qquad N^- \leq n \leq N^+, \\ \sum_{m=N^-}^{N^++1} (-1)^m \mathbf{v}_m P_{-r/K-m}(-\cos \Delta) &= 0. \end{aligned}$$

This concludes the solution of the problem of scattering of elastic waves by a periodic system of in-plane cracks. Analogously to the EM case, problems for layered media with cracks between the layers having different periods and orientations can also be solved by the method presented. The fields resulting in a given plane from the solution on the other plane (see Eqs. (A.11), for instance), should be included in the equations for the fields at the given plane, such like the incident waves in Eq. (2.9), with specific value of Λ for that plane.

4. Waveguiding of elastic waves by cracks

4.1. Formulation of an eigenvalue boundary problem

Let us consider a 2-dimensional problem for an elastic isotropic body including periodic in-plane cracks in the $y = 0$ plane (Fig. 2). If cracks are wide, in the limit equal to the crack period Λ, we have two separated elastic halfspaces. In this case Rayleigh wave exists. Below we shall show that a guided wave exists for quite narrow cracks. The wave is trapped at the $y = 0$ plane so that the wave-motion decays for larger $|y|$, the decay coefficient and the wave velocity depend on Λ, w and on the elastic properties of the body. The analysis is presented for a plane wave propagating along the $y = 0$ plane prependicularly to the cracks, which are infinite in the direction z (elastic field does not depend on z). However, the presented analysis can be applied, without major difficulties, to a general case of a wave propagating obliquely with respect to the cracks.

Formulation of an eigenvalue problem is the following. Apply the solution in the $y = 0$ plane as represented by series (3.4) and (3.7), which satisfies boundary conditions (3.5), and find a nontrivial solution to the homogeneous equations resulting from the equations of motion of an elastic body, and *additional* one-point constraint on $\mathbf{u} - \mathbf{u}^-$ between the cracks (3.6)

(4.1)
$$\sum_{m=N^-}^{N^++1} (S_{n-m}\mathbf{g}_\infty - \mathbf{g}_n)\mathbf{t}_m P_{n-m}(\cos \Delta) = 0,$$
$$\sum_{m=N^-}^{N^++1} (-1)^m \mathbf{v}_m P_{-r/K-m}(-\cos \Delta) = 0, \qquad \mathbf{v}_m = \mathbf{g}_\infty \mathbf{t}_m.$$

The known condition of nontrivial solution of a system of homogeneous linear equation allows us to evaluate the guided wave wave-number r.

4.2. Sample solutions

4.2.1. Dense system of cracks.
We consider a dense system of cracks, dense as compared to the wavelength of the solution sought, $r/K \ll 1$, and wave-motion in the sagittal plane only, $u_z = 0$. In that case we can put $N^- = N^+ = 0$, and

Eqs. (4.1) are reduced to very simple forms. They are separated into two cases, ($T_1 = T_{yx} = 0$, $V_x = 0$), and ($T_2 = T_{yy} = 0$, $V_y = 0$). Their solutions are

$$(4.2) \qquad \sqrt{r^2 - k_i^2} = \frac{w(r)}{2r(k_t^2 - k_i^2)} \frac{P_{-r/K}(-\cos \Delta) - P_{r/K}(-\cos \Delta)}{P_{-r/K}(-\cos \Delta) + P_{r/K}(-\cos \Delta)} \,.$$

where $i = l, t$. It is evident that the value of the right-hand side of Eq. (4.2) is small and positive. The Rayleigh determinant $w(r)$ (see Eq. (A.16)) is positive if $k_t < r < k_R$, where k_R is the Rayleigh wave-number. Thus the left-hand side of Eq. (4.2) should be real-valued and small. This is possible only for $i = t$. That is the case where $T_{yy} = 0$ and $V_y = 0$. In conclusion, there is a guided wave solution, with wave-number close to the shear wave wave-number, $r \approx k_t$. Moreover, the wave-motion includes matched displacements perpendicular to the cracks on both sides of $y = 0$, $u_y^+ = u_y^-$, and there are no normal stress in the plane of cracks, $T_{yy} = 0$.

If the cracks are wider, in the limit $\cos \Delta - 1$, the fraction including Legendre functions on the right-hand side of (4.2) becomes positive infinite (see Appendix B). The solution exists at $w(r) = 0$. This is a Rayleigh wave solution $r = k_R$ as it should be for halfspaces separated by wide cracks. In case of narrow cracks, $\cos \Delta \to -1$, the fraction value becomes zero (small positive), and the solution is $r \to k_t$, as it should be for a homogeneous body without cracks.

4.2.2. Waveguiding and Bragg reflection by cracks. Below we analyze the case $K \approx 2k_t$ and $T_{yy} = 0$, $V_y = u_y^+ - u_y^- = 0$, in agreement with the previous result ($u_z = 0$). We must now apply wider limits for n and m in Eqs. (4.1), because $\mathbf{g}_n \neq \pm\mathbf{g}_\infty$ at small n. However, for simplicity of the analysis here, in a rough approximation we apply $N^- = -1$, $N^+ = 0$. These are the narrowest limits allowing us to analyze the Bragg reflection of waves.

Equations (4.1) yield for $n = -1$. 0 ($R = r - K$, other notations are given below)

$$t_{-1}\left(\frac{Rs_{-1}}{w_{-1}} + 1\right) + t_0\left(\frac{Rs_{-1}}{w_{-1}} - 1\right) + t_1\left(\frac{Rs_{-1}}{w_{-1}} - 1\right)\cos \Delta = 0.$$

$$t_{-1}\left(\frac{rs_0}{w_0} + 1\right)\cos \Delta + t_0\left(\frac{rs_0}{w_0} + 1\right) + t_1\left(\frac{rs_0}{w_0} - 1\right) = 0.$$

$$(4.3) \qquad -t_{-1}P_{1-r/K}(-\cos \Delta) + t_0 P_{-r/K}(-\cos \Delta) - t_1 P_{r/K}(-\cos\Delta) = 0.$$

$$s_0 = \sqrt{r^2 - k_t^2}, \quad s_{-1} = \sqrt{(r - K)^2 - k_t^2}, \quad w_n = \frac{1}{2}w(r + nK)/(k_t^2 - k_l^2).$$

The solution (for $\lambda = 0$) concerning wavenumber r is shown in Fig. 3, where $(r - k_t)/k_t$ is plotted versus the relative frequency $2k_t/K$.

There is a complex solution for r in a certain frequency band where $2k_t \approx K$. It is a stopband, where the Bragg reflection takes place, which is a synchronous
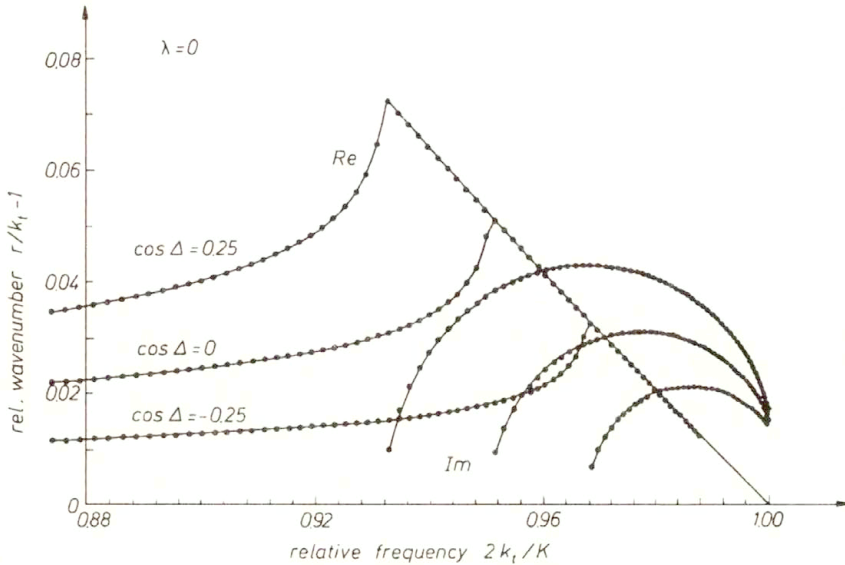
FIG. 3. Bragg reflection of guided waves.

reflection of a wave from the cracks. It can be important for applications, that the stopband is quite wide and a maximum imaginary value of r is quite large. This can help to make a "mirror" for guided waves like that applied in the SAW devices [7].

5. 3-dimensional inhomogeneous problem

In this section we consider a periodic system of strips which have infinitely dense and infinitely thin cuts across each strip, the cuts being parallel to x-axis (i.e. perpendicular to the strip axis z, Fig. 1). In Sec. 2, where the problem of scattering was analyzed, we have assumed that the strips have "short-circuited" cuts, so that electric current could flow along the strips without any resistance and electric field E_z was zero. In this section we assume that in each cut an electric field $E_z = e_p$ (for p-th strip) is applied coming from an external source, and current $J_z = j_p$ (in j-th strip) (which flows from one part of strip to the other) flows through that external source. Let us note, however, that $E_x = 0$ is still valid, and that the external source does not influence the distribution of the current across the strip (in x-direction). The source "sees" only the total current flowing along the strip.

There is another generalization of the boundary conditions for the strips. Suppose that there exist infinitely thin and perfect electric connections between the neighbouring strips. In this case, the current J_x is different from zero in the spacing between the strips but constant across the spacing, that is $\partial_x J_x = 0$. Let us stress that the condition $J_z = 0$ between strips is still assumed. Like in

the previous case, we assume that there are external sources delivering currents into the system, and that there is a certain difference of potentials $U_{p+1/2}$ of the neighbouring (p and $p + 1$) strips resulting from these currents ($J_{p+1/2}$, see the rigorous definitions in Appendix C).

Summarizing, in this section we analyze strands of infinitely dense perfectly conducting but isolated infinitesimally narrow "sub-strips," which are arranged in place of the previously considered solid strips. There can be "external" electric connections between the neighbouring sub-strips in the same strand, as well as between the corresponding sub-strips of neighbouring strands. The above physical considerations are closed in the boundary conditions on strips formulated in advance in Eqs.(2.6) in Sec. 2.

It is worth noticing that the boundary conditions (2.5) and the resulting Eqs. (2.20) are still assumed in the current analysis. These equations allow us to evaluate all the expansion coefficients included in Eqs. (2.14), that is $\mathbf{f}^{(m)}$ and $\mathbf{c}^{(m)}$ by $\mathbf{f}^{(0)}$ and $\mathbf{c}^{(0)}$ (here, we deal with a homogeneous system of Eqs. (2.12), thus the right-hand side of Eqs. (2.20) is zero). Moreover, the selfconsistency condition (2.19) enables us to evaluate $\mathbf{f}^{(0)}$ by $\mathbf{c}^{(0)}$. In conclusion, we have only two unknown scalars, $c_1^{(0)}$ and $c_2^{(0)}$. We introduce the notations

$$\bar{\mathbf{f}}^{(m)} = \left[f_1^{(m)}/f_1^{(0)}, f_2^{(m)}/f_2^{(0)} \right]^T, \qquad \bar{\mathbf{c}}^{(m)} = \left[c_1^{(m)}/c_1^{(0)}, c_2^{(m)}/c_2^{(0)} \right]^T.$$

and we admit that $\mathbf{c}^{(0)}$ and $\mathbf{f}^{(0)}$ are functions of r and τ.

Below we deal with discrete functions like the strip current j_p, the voltage and current between the strips $U_{q+1/2}$ and $J_{p+1/2}$, and an electric field along the strip e_q. Following Appendix D, we introduce inverse Fourier transforms to these discrete functions, defined by

(5.1)
$$x_n(\tau) = \frac{1}{K} \int_0^K X(r,\tau) e^{-jrn\Lambda} dr.$$

where $X(r,\tau)$ are U, J, e, j, the functions of r, τ presented in Appendix C.
Explicitly,

(5.2)
$$J_{p+1/2}(\tau) = j\frac{\Lambda}{\omega\mu}\frac{1}{K}\int_0^K \frac{e^{-jr(p+1/2)\Lambda}}{\sin \pi r/K}$$
$$\times \left[c_1^{(0)}(r,\tau)(k_o^2 - \tau^2)\bar{c}_1^{(m)} + j\tau c_2^{(0)}(r,\tau)\bar{c}_2^{(m)} \right] P_{-m-r/K}(\cos\Lambda)\,dr,$$

$$U_{q+1/2}(\tau) = -\Lambda\frac{1}{K}\int_0^K (-1)^m f_1^{(0)}(r,\tau)\bar{f}_1^{(m)}$$
$$\times P_{-m-r/K}(-\cos\Lambda)e^{-jr(q+1/2)\Lambda}dr,$$

(5.2)
[cont.]
$$e_q(\tau) = j\frac{\Lambda}{2}\frac{1}{K}\int_0^K \frac{E^{-jrq\Lambda}}{\sin \pi r/K}(-1)^m f_2^{(0)}(r,\tau)\overline{f}_2^{(m)}P_{-m-r/K}(-\cos \Delta)\,dr,$$

$$j_p(\tau) = \frac{2\Lambda}{\omega\mu}\frac{1}{K}\int_0^K \left[jr c_1^{(0)}(r,\tau)\overline{c}_1^{(m)} + c_2^{(0)}(r,\tau)\overline{c}_2^{(m)} \right]$$

$$\times P_{-m-r/K}(\cos \Delta)e^{-jp\Lambda}\,dr,$$

where we marked the dependence on r and τ only in $\mathbf{c}^{(0)}$ and $\mathbf{f}^{(0)}$, however $\overline{\mathbf{c}}^{(m)}$ and $\overline{\mathbf{f}}^{(m)}$ are also functions of r, τ. To simplify the notations we dropped the summation symbols over m.

As it was shown above, $J_{p+1/2}$ and e_q are known. This allows us to determine the unknown functions $c_i^{(0)} = f_i^{(0)}$, the two unknowns for $i = 1, 2$. Indeeed, in order to obtain

(5.3)
$$\frac{1}{K}\int_0^K c(r)e^{-jp\Lambda}\,dr = e_q\delta_{pq}\,.$$

we must apply

(5.4)
$$f_2^{(0)}(r,\tau) = -j\frac{2}{\Lambda}\frac{e_q e^{jrq\Lambda}\sin \pi r/K}{\sum_m (-1)^m \overline{f}_2^{(m)} P_{-m-r/K}(-\cos \Delta)}$$

what is easy to prove by inspection. Similarly, from the given $J_{p+1/2}$ and

(5.5)
$$J_{p+1/2} = \frac{1}{K}\int_0^K J(r,\tau)e^{-jr(p+1/2)\Lambda}\,dr$$

we obtain

(5.6)
$$c_1^{(0)}(r,\tau) = -j\frac{\omega\mu}{\Lambda}\frac{J_{p+1/2}e^{jr(p+1/2)\Lambda}}{\sum_m \overline{c}_1^{(m)}P_{-m-r/K}(\cos \Delta)}\frac{\sin \pi r/K}{k_o^2 - \tau^2}$$

$$-e_p\frac{2\tau}{\Lambda(k_o^2 - \tau^2)}\frac{e_p e^{jrp\Lambda}\sin \pi r/K}{\sum_m \overline{c}_1^{(m)}P_{-m-r/K}(\cos \Delta)}$$

$$\times \frac{\sum_m \overline{f}_2^{(m)}P_{-m-r/K}(\cos \Delta)}{\sum_m (-1)^m \overline{f}_2^{(m)}P_{-m-r/K}(-\cos \Delta)}\,,$$

which can now be applied to evaluate all other EM fields.

Particularly, we are interested in evaluation of the difference of potentials of strips placed around $x = (q + 1/2)\Lambda$, that is $U_{q+1/2}$ (this explains the extraordinary index applied to that discrete function), and the total current flowing along the strip placed at $x = p\Lambda$, that is j_p, both dependent on $J_{p+1/2}$ and e_q. We obtain

$$
U_{q+1/2}(\tau) = -\frac{\omega\mu}{k_o^2 - \tau^2} \int_0^K \frac{\sum_m (-1)^m \bar{c}_1^{(m)} P_{-m-r/K}(-\cos\Delta)}{\sum \bar{c}_1^{(m)} P_{-m-r/K}(\cos\Delta)}
$$

$$
\times \sin\pi\frac{r}{K}\left[J_{p+1/2}e^{-jr(q-p)\Lambda} \right.
$$

(5.7)
$$
\left. -j\frac{2\tau(\omega\mu)^{-1}\bar{f}_2^{(m)} P_{-m-r/K}(\cos\Delta)}{(-1)^m \bar{f}_2^{(m)} P_{-m-r/K}(-\cos\Delta)} e_p e^{-j(q-p+1/2)\Lambda} \right] dr/K,
$$

$$
j_p(\tau) = \frac{2\tau}{k_o^2 - \tau^2} \int_0^K \left[J_{q+1/2}e^{-jr(p-q-1/2)\Lambda} \right.
$$

$$
\left. -j\frac{4\omega\varepsilon}{k_o^2 - \tau^2}\frac{\bar{f}_2^{(m)} P_{-m-r/K}(\cos\Delta)}{(-1)^m \bar{f}_2^{(m)} P_{-m-r/K}(-\cos\Delta)} e_q e^{-j(p-q)\Lambda}\sin\pi r/K \right] dr/K,
$$

which fully describe the considered system, if the applied fields depend on z as $\exp(-j\tau z)$.

Generally, the above relations give us Fourier transforms in the z axis with τ being a spectral variable of the transformation. If the exciting forces $J_{p+1/2}$ and e_q are z-dependent functions, they have the corresponding τ-dependent transforms, which should be introduced in Eqs. (5.7). Inverse transforms are

(5.8) $$ U_{p+1/2}(z) = \frac{1}{2\pi}\int_{-\infty}^{\infty} U_{p+1/2}(\tau)e^{-j\tau z}\,d\tau, \qquad j_q(z) = \frac{1}{2\pi}\int_{-\infty}^{\infty} j_q(\tau)e^{-j\tau z}\,d\tau. $$

This concludes the solution of an inhomogeneous 3-dimensional problem.

It should be noted that the solution is quite formal; further analysis must include computations, at least numerical evaluation of $\bar{c}^{(m)}$, and evaluation of the above integrals. What concerns Eqs. (2.20), let us note that for larger value of τ, the system is larger, too. This results from the approximation condition (2.21). Thus it will be more difficult to obtain numerical results in cases where $e_q(z)$ and $J_{p+1/2}(z)$ have wide spectra in τ domain (which is the case of a sharp cut shown in Fig. 1). In such cases, we must apply further approximations by reducing the computed spectrum of functions, and then applying the corresponding interpretation of the numerical results.

6. Conclusions

A new 3-dimensional problem for EM wave excitation is stated and solved. We have shown usefulness of the applied method, that was for the first time applied in [4] to an analysis of a certain scalar eigenvalue problem. In this paper the method is generalized to vectorial problems, both electromagnetic and elastic. We have shown that the method is useful in the analysis of layered and anisotropic media. A 3-dimensional excitation problem can also be formulated for elastic body with liquid-filled cracks. The liquid is a medium delivering pressure into the cracks, which is constant in the crack cross-section.

One may also expect that the proposed method of analysis can be applied to boundary problems for certain differential operators, the solutions of which exhibit singularities different from the above discussed square-root type. That is justified by Eq. (B.1), which admits different singularities for different μ. For example, it is expected that a lens-shaped cracks [16] can be analyzed by a generalized method. The field at the tip of such a crack is singular, depending on the crack opening angle.

Appendix A

A.1. Electromagnetic fields

Let us consider an EM harmonic wave in the upper isotropic halfspace $y > 0$

(A.1)
$$e^{-jkx}e^{-jsy}e^{j\omega t}$$

with s chosen following Eq. (2.8) (with substitution of r_n to k, and $\tau = 0$) which is required for an EM field satisfying the radiation conditions at $y \to \infty$. It follows directly from Maxwell's equations that $-jsE_z = -j\omega\mu H_x$ and $-jsH_z = j\omega\varepsilon E_x$. Thus, at the surface $y = 0$, we obtain the following solution for tangential magnetic field $\mathbf{H}^+$ resulting from the applied tangential electric field $\mathbf{E}^+$ to that surface:

$$\mathbf{H}^\pm = [H_x^\pm, H_z^\pm]^T, \qquad \mathbf{E}^\pm = [E_x^\pm, E_z^\pm]^T,$$

(A.2)
$$\mathbf{H}^\pm = \pm\mathbf{G}'\mathbf{E}^\pm, \qquad \mathbf{G}' = \begin{bmatrix} 0 & s/(\omega\mu) \\ -\omega\varepsilon/s & 0 \end{bmatrix}.$$

The signs $-$ concern the solution of the analogous problem for the lower halfspace $y < 0$ (s should be replaced by $-s$ in (A.1) to meet the radiation condition at $y \to -\infty$). $\mathbf{G}'$ is the Fourier transform of a planar Green's matrix function describing the response of the body, in tangential magnetic field, to the applied tangential electric field, both at the $y = 0$ plane.

The electric and magnetic fields of an incident EM wave propagating in the upper halfspace from infinity satisfy Eq.(A.2) taken with indices $-$, because this

wave satisfies the radiation condition at $y \to -\infty$

(A.3) $$\mathbf{H}^I = -\mathbf{G}'\mathbf{E}^I.$$

Let us consider a general case of a wave propagating in an arbitrary direction

(A.4) $$e^{-jrx}e^{-jsy}e^{-j\tau z}.$$

To evaluate the corresponding "planar Greeen's matrix function" let us note that in a new coordinate system x', y, z' rotated around y-axis, as defined by

(A.5) $$[x', z']^T = \boldsymbol{\alpha}[x, z]^T, \qquad \boldsymbol{\alpha} = \begin{bmatrix} r/k & \tau/k \\ -\tau/k & r/k \end{bmatrix}, \qquad k = \sqrt{r^2 + \tau^2},$$

the wave (A.4) is transformed to the form (A.1). Thus in the "primed" system of coordinates the "primed" planar Green's function $\mathbf{G}'$ is given by (A.2). In the original system (x, y, z) we obtain

(A.6) $$\mathbf{G} = \boldsymbol{\alpha}^T \mathbf{G}' \boldsymbol{\alpha} = \frac{\omega\varepsilon}{sk_o^2} \begin{bmatrix} -r\tau & r^2 - k_o^2 \\ k_o^2 - r^2 & r\tau \end{bmatrix}.$$

where $\mathbf{G}$ should be applied in relations (A.2) and (A.3) in that case.

In Sec. 2, we introduced planar current on the $y = 0$ plane. Below, we derive a relation between this current and the electric field. Let us first note that relations (A.2) concern the EM field satisfying the radiation condition at infinity. It results from Eqs. (2.2) that

(A.7) $$\mathbf{H}^+ = \mathbf{H} - \mathbf{H}^I, \qquad \mathbf{E}^+ = \mathbf{E} - \mathbf{E}^I, \qquad \mathbf{E}^- = \mathbf{E}.$$

where $\mathbf{E}$ and $\mathbf{H}$ are full EM fields on the $y = 0$ plane. We thus obtain from (A.2)

(A.8) $$\begin{bmatrix} -J_z \\ J_x \end{bmatrix} = \begin{bmatrix} H_x - H_x^- \\ H_z - H_z^- \end{bmatrix} = \mathbf{H}^+ + \mathbf{H}^I - \mathbf{H}^- = \mathbf{G}(\mathbf{E} - \mathbf{E}^I) - \mathbf{G}\mathbf{E}^I,$$

which can be rewritten in the form ($J_{x,x} = -jrJ_x$ and $E_{z,x} = -jrE_z$)

(A.9) $$[J_{x,x}, J_z]^T = \frac{2}{\omega\mu}\mathbf{g}[E_x, E_{z,x}]^T - \frac{2}{\omega\mu}\mathbf{g}\left[E_x^I, -jrE_z^I\right]^T.$$

$$\mathbf{g} = \begin{bmatrix} \dfrac{-jr}{s}(k_o^2 - \tau^2) & \tau r/s \\ \tau r/s & \dfrac{k_o^2 - r^2}{-jrs} \end{bmatrix}.$$

Asymptotic property of matrix **g** is the following:

(A.10)

$$\mathbf{g}(r \to \pm\infty) = S_r \begin{bmatrix} k_o^2 - \tau^2 & j\tau \\ j\tau & 1 \end{bmatrix} = S_r \mathbf{g}_\infty, \qquad S_r = \begin{cases} 1, & \text{for } r \geq 0, \\ -1, & \text{for } r < 0, \end{cases}$$

$$\mathbf{g}_\infty^{-1}\mathbf{g} = \begin{bmatrix} -jr/s & \tau/(rs) \\ 0 & s/(-jr) \end{bmatrix} = \bar{\mathbf{g}}.$$

Replacing r by r_n in the above relations and noticing that the term with $\mathbf{E}^I$ appears only with $r_I = r + n\mathcal{K}$, we obtain Eq. (2.9). Note that the important asymptotic property (A.10) takes place because we have applied the properly chosen variables E_x, $\partial_x E_z$, $\partial_x J_x$ and J_z which are all square-root singular functions having Fourier transforms with the same asymptotics.

Below, other planar Green's functions are presented which are derived by solving the corresponding inhomogeneous boundary problems. Let us first consider dielectric layer of thickness h, $0 < y < h$. There are electric fields $\mathbf{E}^+$ applied to its surface $y = 0$, and magnetic field $\mathbf{H}^-$ applied to its upper surface $y = h$ (a complementary problem is that $\mathbf{H}^+$ and $\mathbf{E}^-$ are given on $y = 0$, and $y = h$, respectively). We obtain

$$\mathbf{H}^+ = \mathbf{G}\mathbf{E}^+ + \mathbf{G}_1\mathbf{H}^-, \qquad \mathbf{H}^- = -\mathbf{G}\mathbf{E}^- + \mathbf{G}_1\mathbf{H}^+,$$

(A.11)

$$\mathbf{G} = \begin{bmatrix} 0 & \dfrac{s}{\omega\mu}\dfrac{1 - C^2}{1 + C^2} \\ -\dfrac{\omega\varepsilon}{s}\dfrac{1 - C^2}{1 + C^2} & 0 \end{bmatrix}, \qquad \mathbf{G}_1 = \begin{bmatrix} \dfrac{s}{\omega\mu}\dfrac{2C}{1 + C^2} & 0 \\ 0 & \dfrac{\omega\varepsilon}{s}\dfrac{2C}{1 + C^2} \end{bmatrix}.$$

The system of equations is convenient for the description of cascaded layers.

Another case concerns the chiral media governed by Maxwell's and constitutive equations

(A.12)

$$\nabla \times \mathbf{E} = -j\omega\mathbf{B}, \qquad \mathbf{D} = \varepsilon\mathbf{E} + j\backslash\mathbf{H},$$

$$\nabla \times \mathbf{H} = -j\omega\mathbf{D}, \qquad \mathbf{B} = -j\backslash\mathbf{E} + \mu\mathbf{H},$$

which yield, after some transformations

(A.13)

$$(\nabla^2 + k_o^2 + \omega^2\backslash^2)\mathbf{E} + j2\omega^2\mu\backslash\mathbf{H} = 0,$$

$$-j2\omega^2\mu\backslash\mathbf{E} + (\nabla^2 + k_o^2 + \omega^2\backslash^2)\mathbf{H} = 0.$$

Assuming the solution in the form $\exp(-jrx - jsy)$ resulting in $\nabla^2 = -r^2 - s^2 = -k^2$, we obtain two possible values for $k = \sqrt{r^2 + s^2}$,

(A.14) $k_i = k_o \pm \omega\backslash, \qquad k_o = \omega\sqrt{\varepsilon\mu}, \qquad s_l = \sqrt{k_l^2 - r^2}, \qquad l = 1.2.$

Solving the corresponding boundary problem for a halfspace $y > 0$, we obtain

$$(A.15) \quad \begin{bmatrix} H_x^+ \\ H_z^+ \end{bmatrix} = \sqrt{\frac{\varepsilon}{\mu}} \begin{bmatrix} j\dfrac{k_1/s_1 - k_2/s_2}{k_1/s_1 + k_2/s_2} & \dfrac{2}{k_1/s_1 + k_2/s_2} \\ -2\dfrac{(k_1/s_1)(k_2/s_2)}{k_1/s_1 + k_2/s_2} & j\dfrac{k_2/s_2 - k_1/s_1}{k_1/s_1 + k_2/s_2} \end{bmatrix} \begin{bmatrix} E_x^+ \\ E_z^+ \end{bmatrix}$$

(apply substitution $s \rightarrow -s$ to obtain the relation valid for the lower halfspace).

A.2. Mechanical fields

Below, analogous relations are presented for the elastic media characterized by Lamé elastic constants λ, μ and mass density ρ. Elastic field on the surface of the body ($y = 0$) includes the particle displacement vector $\mathbf{u} = (u_x, u_y, u_z)$, and the surface traction ($T_{yx} = T_1$, $T_{yy} = T_2$, $T_{yz} = T_3$). In [17] we can find the following solution of the boundary problem where traction $\mathbf{T}^+ \exp(j\omega t - jkx)$ is applied to the surface of an elastic halfspace $y > 0$:

$$\mathbf{u}^+ = \mathbf{G}'\mathbf{T}^+,$$

$$(A.16) \quad \mathbf{G}' = \begin{bmatrix} \dfrac{jk_t^2 s_l}{\mu w} & \dfrac{jr(k_t^2 - 2r^2 - 2s_l s_t)}{\mu w} & 0 \\ -\dfrac{jr(k_t^2 - 2r^2 - 2s_l s_t)}{\mu w} & \dfrac{jk_t^2 s_l}{\mu w} & 0 \\ 0 & 0 & -j(\mu s_t) \end{bmatrix}.$$

$$w = (k_t^2 - 2r^2)^2 + 4r^2 s_l s_t, \quad k_l^2 = \rho\omega^2/(2\mu + \lambda), \quad k_t^2 = \rho\omega^2/\mu.$$

$$s_i = \sqrt{k_i^2 - r^2}, \quad i = l, t$$

(we assume the rule (2.8) to make sure that the elastic field satisfies the radiation condition at ∞). Substitution $s \rightarrow -s$ results in relations for the $y < 0$ halfspace, and also in that one for an incident wave arriving from infinity. It is important that

$$(A.17) \quad w(r \rightarrow \infty) \rightarrow (k_t^2 - k_l^2)(k_t^2 - 2r^2).$$

In a general case of a traction wave propagating in arbitrary direction on the $y = 0$ plane, we proceed in a similar manner as in the case of Eq. (A.6). This results in

$$(A.18) \quad \mathbf{g} = -j2r\mathbf{G} = -j2r\boldsymbol{\alpha}^T\mathbf{G}'\boldsymbol{\alpha},$$

where coefficient 2 is introduced for convenience, and multiplication by $-jr$ is introduced to obtain the relation between $\partial_x\mathbf{u}(x, z)$ and $\mathbf{T}(x, z)$ in the spectral domain. It is easy to show that

$$(A.19) \quad \mathbf{g}(r \rightarrow \pm\infty) = \mathbf{g}_\infty, \quad \mathbf{g}_\infty = -\frac{1}{\mu}\begin{bmatrix} A & 0 & 0 \\ 0 & A & 0 \\ 0 & 0 & 2 \end{bmatrix}, \quad A = \frac{\lambda + 2\mu}{\lambda + \mu}.$$

Correponding relations for an elastic slab of thickness h are [10]

$$\mathbf{u}^- = \mathbf{G}_0 \mathbf{T}^-, \qquad \mathbf{G} = \frac{1}{\mu}\begin{bmatrix} a_1/D & -a_2/D & 0 \\ a_2/D & a_3/D & 0 \\ 0 & 0 & a_4 \end{bmatrix},$$

$$a_1 = js_t k_t^2 \left[W(1 - L^2 T^2) + (X^2 - z)(T^2 - L^2) \right],$$

$$a_2 = jr\big[W(X - 2s_l s_t)(1 - L^2 T^2) - (X^2 - Z)(X + 2s_l s_t)(T^2 + L^2)$$

$$- 4LTX(Z - 2X s_l s_t)\big],$$

(A.20)

$$a_3 = js_l k_t^2 \left[W(1 - L^2 T^2) + (X^2 - Z)(T^2 - L^2) \right],$$

$$a_4 = \frac{j}{\mu s_t}\frac{1 + T^2}{1 - T^2}, \qquad s_i = \sqrt{k_i - r^2}, \qquad i = l, t,$$

$$D = (1 - L^2)(1 - T^2)W^2 + 4X^2 Z(L - T)^2, \qquad W = X^2 + Z,$$

$$X = k_t^2 - 2r^2, \qquad Z = 4r^2 s_l s_t, \qquad T = e^{js_t h}, \qquad L = e^{js_l h}.$$

Its limit at $\omega \to 0$ (equivalently $r \to \infty$), describing the elastostatic case of a plate, is considered in [9].

A.3. Coupled electro-mechanical field

Analogous planar Green's functions were introduced for piezoelectrics [19, 20]. In [20] a certain special but important case of piezoelectric halfspace is considered, where only transverse particle displacement u_z is piezoelectrically coupled with the electric potential ϕ. The introduced approximation to a planar Green's function is valid in vicinity of a cut-off wave-number of bulk waves. Below we present a slightly modified version of this approximation by using the variable of electric flux density D_y instead of $\Delta D_\perp = D_y + \varepsilon_0 \sqrt{r^2}\phi$ applied in [20]. Corresponding transformations yield equations of the same form as those given in [20], but with modified values of some approximation parameters marked below by primes. We obtain for the upper halfspace (index $+$)

(A.21)

$$\phi^+ = \frac{1}{\varepsilon_0 \varepsilon'}\frac{1}{\sqrt{r^2}}\frac{\sqrt{r^2 - k_s^2} - \alpha\sqrt{r^2}}{\sqrt{r^2 - k_s^2} - \beta'\sqrt{r^2}}D_y^+ + \frac{1}{\sqrt{r^2}}\frac{a'\sqrt{r^2 - k_s^2} - b'\sqrt{r^2}}{\sqrt{r^2 - k_s^2} - \beta'\sqrt{r^2}}T_{yz}^+,$$

$$u_z^+ = \frac{1}{\sqrt{r^2}}\frac{a'^*\sqrt{r^2 - k_s^2} - b'^*\sqrt{r^2}}{\sqrt{r^2 - k_s^2} - \beta'\sqrt{r^2}}D_y^+ + \frac{1}{\sqrt{r^2}}\frac{c'\sqrt{r^2 - k_s^2} - \gamma'\sqrt{r^2}}{\sqrt{r^2 - k_s^2} - \beta'\sqrt{r^2}}T_{yz}^+,$$

which can also be rewitten in the second form

(A.22)

$$D_y^+ = \varepsilon_0 \varepsilon' \sqrt{r^2} \frac{\sqrt{r^2 - k_s^2} - \beta' \sqrt{r^2}}{\sqrt{r^2 - k_s^2} - a\sqrt{r^2}} \phi^+ - \varepsilon_0 \varepsilon' \frac{a'\sqrt{r^2 - k_s^2} - b'\sqrt{r^2}}{\sqrt{r^2 - k_s^2} - a\sqrt{r^2}} T_{yz}^+ ,$$

$$u_z^+ = \varepsilon_0 \varepsilon' \frac{a'^* \sqrt{r^2 - k_s^2} - b'^* \sqrt{r^2}}{\sqrt{r^2 - k_s^2} - a\sqrt{r^2}} \phi^+ + \frac{1}{\sqrt{r^2}} \frac{d\sqrt{r^2 - k_s^2} - \eta \sqrt{r^2}}{\sqrt{r^2 - k_s^2} - a\sqrt{r^2}} T_{yz}^+ .$$

Similar equations hold for the lower halfspace ($y < 0$, field components with index $-$). To obtain them from the equations derived above, substitutions $\sqrt{\cdot} \to -\sqrt{\cdot}$, $a' \to a'^*$ and $b' \to b'^*$ must be made. Justified by the reasoning presented in [20], the relations and identities are found:

(A.23)

$$\varepsilon' = \varepsilon - 1, \qquad \beta' = \frac{\varepsilon}{\varepsilon'}\left(\beta - \frac{a}{\varepsilon}\right), \qquad a' = \frac{\varepsilon}{\varepsilon'}a, \qquad b' = \frac{\varepsilon}{\varepsilon'}b,$$

$$c' = \frac{\varepsilon}{\varepsilon'}\left(c - \frac{d}{\varepsilon}\right), \qquad \gamma' = \frac{\varepsilon}{\varepsilon'}\left(\gamma - \frac{\eta}{\varepsilon}\right).$$

$$|a'|^2 = \frac{c - d}{\varepsilon_0 \varepsilon'}, \qquad |b'|^2 = \frac{a\gamma' - \beta'\eta}{\varepsilon_0 \varepsilon'}.$$

$$a'b'^* + a'^*b' = \frac{ac' + \gamma' - \beta'd - \eta}{\varepsilon_0 \varepsilon'}.$$

which allow us to use the numerically evaluated parameters presented there.

There is still another identity concerning the approximation parameters involved in the above equations. Let us consider the continuous piezoelectric medium, divided for mathematical reasons only, into two halfspaces. Both halfspaces are in perfect contact, thus

(A.24) $$u_z^+ = u_z^-, \qquad T = T_{yz}^+ = T_{yz}^-, \qquad \phi = \phi^+ = \phi^-.$$

Solving the corresponding boundary problem with the help of Eqs. (A.22) we obtain

(A.25)

$$Q = D_y^+ - D_y^- = 2\phi\varepsilon_0 \varepsilon' \sqrt{r^2} \frac{\sqrt{r^2 - k_s^2}}{\sqrt{r^2 - k_s^2} - a\sqrt{r^2}} P .$$

$$P = \frac{(d' - \varepsilon_0 \varepsilon' (\mathrm{Im}\{a\})^2)\sqrt{r^2 - k_s^2} - [\eta + \beta'd + \varepsilon_0 \varepsilon'(a'b' - a'^*b'^*)]\sqrt{r^2}}{d\sqrt{r^2 - k_s^2} - \eta\sqrt{r^2}}.$$

provided that

(A.26) $$\varepsilon_0 \varepsilon' (\mathrm{Im}\{b'\})^2 = -\beta'\eta .$$

what is necessary to obtain a unique solution $r = k_s$ of dispersive equation resulting from Eqs. (A.25) for $D_y^+ - D_y^- = 0$ which, together with Eqs. (A.24), is a condition of continuity of the body at $y = 0$. Indeed, the correct solution should be $r = k_s$ which is a projection of the shear-wave wave number k_b on the $y = 0$ plane [20]. It is interesting, that $\varepsilon_0\varepsilon'(\text{Im}\{a'\})^2 = -d$ is also valid for numerical data presented in [20].

An interesting consequence results from Eqs. (A.21) that a guided wave exists if a conducting plane is embedded in the considered piezoelectric body (at $y = 0$). Particularly, for a perfectly conducting plane, $\phi = 0$ in Eqs. (A.25), and we obtain the wave-number of a guided mode

$$(\text{A.27}) \qquad r = k_s/\sqrt{1 - \alpha^2} \ .$$

The wave decays in the body on both sides of the plane $y = 0$. Theory of propagation, generation and detection of the discussed guided mode by a system of periodic strips is similar to that presented in [20].

Appendix B

B.1. Legendre functions

Legendre functions used in this paper are well presented in [21], where we find

$$P_\nu = P_\nu^0, \quad 0 < \theta < \pi, \quad \text{Re}\{\mu\} < 1/2, \quad P_n(-x) = S_n(-1)^n P_n(x),$$

$$(\text{B.1}) \qquad \Gamma\left(\frac{1}{2} - \mu\right) \sum_{n=0}^{\infty} P_n^\mu(\cos\theta) \cos\left(n + \frac{1}{2}\right)v$$

$$= \begin{cases} \dfrac{(\pi/2)^{1/2}\sin^\mu\theta}{(\cos v - \cos\theta)^{\mu+1/2}}, & 0 \le v < \theta, \\[2ex] 0, & \theta < v < \pi, \end{cases}$$

which can be transformed into two complementary forms [4] (α_m and β_m are arbitrary constants)

$$\sum_{n=-\infty}^{\infty} \alpha_m P_{n-m}(\cos\Delta)e^{-jn\theta} = \begin{cases} \sqrt{2}\dfrac{\alpha_m\exp(-jm\theta)}{\sqrt{\cos\theta - \cos\Delta}}e^{j\theta/2}, & |\theta| < \Delta, \\[2ex] 0, & \Delta < |\theta| < \pi, \end{cases}$$

$$(\text{B.2}) \qquad \sum_{n=-\infty}^{\infty} \beta_m S_{n-m} P_{n-m}(\cos\Delta)e^{-jn\theta}$$

$$= \begin{cases} 0, & |\theta| < \Delta, \\[2ex] -jS_\theta\sqrt{2}\dfrac{\beta_m\exp(-jm\theta)}{\sqrt{\cos\Delta - \cos\theta}}e^{j\theta/2}, & \Delta < |\theta| < \pi, \end{cases}$$

where $S_\nu = 1$ for $\nu \geq 0$, and $= -1$ otherwise. There are also relations resulting from Dougall's expansion [21, 4].

(B.3)
$$\sum_{n=-\infty}^{\infty} \alpha_m \frac{(-1)^n P_{n-m}(\cos \Delta)}{r + nK} = \frac{\pi}{K \sin \pi r/K} \alpha_m P_{-m-r/K}(\cos \Delta),$$

$$\sum_{n=-\infty}^{\infty} \beta_m \frac{S_{n-m} P_{n-m}(\cos \Delta)}{r + nK} = \frac{\pi}{K \sin \pi r/K} (-1)^m \beta_m P_{-m-r/K}(-\cos \Delta),$$

$$P_\nu(\cos \Delta) P_{-\nu}(-\cos \Delta) + P_\nu(-\cos \Delta) P_\nu(\cos \Delta) = 2(\sin \pi \nu)/(\pi \nu).$$

Asymptotic values for $\nu \to 0$ and $\cos \Delta \to 1$ are [21]

(B.4)
$$P_\nu(0) \approx 1 - (\nu/2) \ln 2, \qquad P_\nu(-\cos \Delta) \approx 1 + \nu \ln \frac{1 - \cos \Delta}{2}.$$

B.2. A generalization

Consider an analytical function of complex variable θ having, for real θ, real or imaginary values in separate domains

(B.5)
$$f(\theta; \Delta) = \sqrt{\frac{2}{\cos \theta - \cos \Delta}}.$$

Its expansion can be easily obtained from Eqs. (B.2) (apply $m = 0$, $\alpha_0 = \beta_0 = 1$). A product

(B.6)
$$f_2 = f(\theta - \alpha_1; \Delta_1) f(\theta - \alpha_2; \Delta_2)$$

(Fig. 4) can be expanded into the following series [22] (θ real)

(B.7)
$$\mathrm{Re}\{f_2\} = \sum_{k,m} (1 - S_{m-k} S_m) P_{k-m}(\cos \Delta_2)$$
$$\times P_m(\cos \Delta_1) e^{jk(\theta - \alpha_2)} e^{j(m+1/2)(\alpha_2 - \alpha_1)},$$
$$j\,\mathrm{Im}\{f_2\} = \sum_{k,m} (S_m - S_{m-k}) P_{k-m}(\cos \Delta_2)$$
$$\times P_m(\cos \Delta_1) e^{jk(\theta - \alpha_2)} e^{j(m+1/2)(\alpha_2 - \alpha_1)}.$$

Since

(B.8)
$$1 - S_{m-k} S_m = 2 \quad \text{if } m - k < 0 \text{ and } m \geq 0, \text{ that is } 0 \leq m < k,$$
$$\text{or } m - k \geq 0 \text{ and } m < 0, \text{ that is } k \leq m < 0,$$
$$= 0 \quad \text{otherwise,}$$
$$S_m - S_{m-k} = 2 = 2S_n \quad \text{if } 0 \leq m < k,$$
$$= -2 = 2S_n \quad \text{if } k \leq m < 0,$$
$$= 0 \quad \text{otherwise,}$$
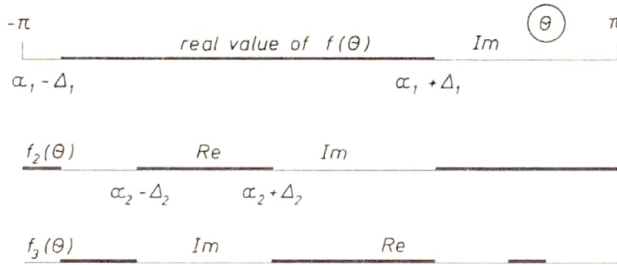
FIG. 4. Sample domains of real and imaginary values of functions f, f_2, and f_3.

we obtain

$$\mathrm{Re}\{f_2\} = \sum_{k=-\infty}^{\infty} X_k e^{jk(\theta-\alpha_2)}, \qquad j\mathrm{Im}\{f_2\} = \sum_{k=-\infty}^{\infty} S_k X_k e^{jk(\theta-\alpha_2)},$$

(B.9)

$$X_k = X_{-k}^* = \sum_{0\leq m < k \cup k \leq m < 0} 2P_{k-m}(\cos \Delta_2)P_m(\cos \Delta_1)e^{j(m+1/2)(\alpha_2-\alpha_1)}.$$

and $X_0 = 0$. Analogously, for

(B.10)
$$f_3 = f_2 f(\theta - \alpha_3; \Delta_3).$$

$$\mathrm{Re}\{f_3\} = \sum_{k=-\infty}^{\infty} Y_k e^{j(k+1/2)(\theta-\alpha_3)}.$$

$$j\mathrm{Im}\{f_3\} = \sum_{k=-\infty}^{\infty} S_k Y_k e^{j(k+1/2)(\theta-\alpha_3)},$$

(B.11)

$$Y_0 = 0, \qquad Y_{-k-1} = Y_k^*,$$

$$Y_k = \sum_{0\leq n < k \cup k < n < 0} 2X_n P_{k-n}(\cos \Delta_3)e^{jn(\alpha_3-\alpha_2)}.$$

Similarly, $f_4 = f_2 f_2$ (the series includes X'), $f_5 = f_3 f_2$ (that function includes Y'), etc., where X' and Y' have the same properties as X and Y described above. In all cases one can easily find domains where these functions have real or imaginary values, by considering the basic function (B.5),

$$\mathrm{Re}\{f_4\} = \sum_{k=-\infty}^{\infty} X_k' e^{jk(\theta-\alpha_4)},$$

(B.12) $$j\mathrm{Im}\{f_4\} = \sum_{k=-\infty}^{\infty} S_k X_k' e^{jk(\theta-\alpha_4)}, \qquad X_0' = 0.$$

$$X_k' = X_{-k}'^* = \sum_{0\leq m < k \cup k \leq m < 0} 2X_{k-m} X_m e^{j(m+1/2)(\alpha_4-\alpha_3)}.$$

(B.12)
[cont.]

$$\mathrm{Re}\{f_5\} = \sum_{k=-\infty}^{\infty} Y'_k e^{j(k+1/2)(\theta - \alpha_5)},$$

$$j\,\mathrm{Im}\{f_5\} = \sum_{k=-\infty}^{\infty} S_k Y'_k e^{j(k+1/2)(\theta - \alpha_5)},$$

$$Y'_0 = 0, \qquad Y'_{-k-1} = Y'^{*}_k,$$

$$Y'_k = \sum_{0 \le n < k \cup k < n < 0} 2X_n Y_{k-n} e^{jn(\alpha_5 - \alpha_3)}.$$

A nice feature of coefficients X' and Y' is that they are expressed by finite sums; their disadvantage is that the relation analogous to Eqs. (B.3) is not known. The derived functions can be used in expansions analogous to (2.14) and (3.7), but additional equations like (2.6) and (3.6) must be computed (either by summation of the series like (B.3), or by evaluation of the corresponding higher-order elliptic integrals of real and imaginary part of functions f_n). Anyway, the introduced expansions for f_2, f_3 ... allows us to obtain Eqs. (2.20) in an explicit form.

Appendix C

It follows from expansions (2.7), (2.14) that

$$J_x(x, z) = \frac{2}{\omega\mu} \sum_{m,n} \frac{(k_o^2 - \tau^2)c_1^{(m)} - j\tau c_2^{(m)}}{-j(r + nK)}$$

(C.1)
$$\times P_{n-m}(\cos \varDelta) e^{-j(r+nK)x} e^{-j\tau z},$$

$$E_z(x, z) = \sum_{m,n} f_2^{(m)} \frac{S_{n-m} P_{n-m}(\cos \varDelta)}{-j(r + nK)} e^{-j(r+nK)x} e^{-j\tau z}.$$

Applying identities (B.3), we easily obtain

(C.2) $$J_{p+\frac{1}{2}} = J_x(x = (p + 1/2)\varLambda, z) = J(r, \tau)e^{-jr(p+1/2)\varLambda} e^{-j\tau z}$$

$$= j\frac{\varLambda/(\omega\mu)}{\sin \pi r/K} \sum_m \left[(k_o^2 - \tau^2)c_1^{(m)} + j\tau c_2^{(m)} \right] P_{-m-r/K}(\cos \varDelta) e^{-jr(p+1/2)\varLambda} e^{-j\tau z}$$

$$= e_q = E_z(x = q\varLambda, z) = e(r, \tau)e^{-jrq\varLambda} e^{-j\tau z}$$

$$= j\frac{\varLambda/2}{\sin \pi r/K} \sum_m (-1)^m f_2^{(m)} P_{-m-r/K}(-\cos \varDelta) e^{-jrq\varLambda} e^{-j\tau z},$$

where fractional indices are applied for convenience.

In a similar way we evaluate

$$U_{q+\frac{1}{2}} = -\int_{q\Lambda+w/2}^{q\Lambda-w/2} E_x(x,z)dx = -\int_{q\Lambda}^{(q+1)\Lambda} E_x dx = U(r,\tau)e^{-jr(p+1/2)\Lambda}e^{-j\tau z}$$

(C.3)
$$= -\Lambda\sum_m(-1)^m f_1^{(m)} P_{-m-r/K}(-\cos\Delta)e^{-jr(q+1/2)\Lambda}e^{-j\tau z},$$

$$j_p = \int_{p\Lambda-w/2}^{p\Lambda+w/2} J_z(x,z)dx = \int_{p\Lambda-\Lambda/2}^{p\Lambda+\Lambda/2} J_z dx = j(r,\tau)e^{-jrp\Lambda}e^{-j\tau z}$$

$$= \frac{2}{\Lambda}\omega\mu\sum_m(j\tau c_1^{(m)} + c_2^{(m)})P_{-m-r/K}(\cos\Delta)e^{-jrp\Lambda}e^{-j\tau z},$$

where we have exploited the property of the considered fields that they vanish on strips (E_x), or between strips (J_z), as stated by boundary conditions (2.5).

Appendix D

In this appendix we consider Fourier transforms of discrete functions that appear in the analysis of periodic systems [23]. They are, for example, the total current flowing along the strip and the difference of potentials of neighbouring strips. Such functions depend rather on the strip number, which is a discrete variable, than on the x-coordinate.

In the scattering and waveguiding problems, for convenience we deal with functions depending on x, z, for example

(D.1) $$\partial_x E_z(x,z) = \sum_m f_2^{(m)} \sum_{n=-\infty}^{\infty} S_{n-m} P_{n-m}(\cos\Delta)e^{-j(r+nK)x}e^{-j\tau z}.$$

It is clear that the "coefficient" $f_2^{(m)}$ can be a function of r. Note, however, that the applied r is confined to one Brillouin zone, $r \in (0, K)$. We can introduce the standard Fourier transform for $E_z(x,z)$ as follows (∂_x corresponds to multiplication by $-jr'$ in the spectral domain)

(D.2) $$E_z(r') = \left\{\sum_m f_2^{(m)}[K(r'-n)]\frac{S_{n-m}P_{n-m}(\cos\Delta)}{-jr'K}\quad\text{for}\quad n<r'<n+1\right\},$$

where r' is a spectral variable spanned over $(-\infty, \infty)$.

Thus the inverse Fourier transform to $E_z(r')$ is

(D.3) $$E_z(x) = \int\limits_{-\infty}^{\infty} E_z(r') e^{-j2\pi r'x/\Lambda}\, dr'$$

$$= \sum_m \frac{1}{K} \sum_{n=-\infty}^{\infty} \int\limits_0^K f_2^{(m)}(r) \frac{S_{n-m}P_{n-m}(\cos\varDelta)}{-j(r+nK)} e^{-jrx}\, dr,$$

where the sum over n can be explicitly evaluated by means of the identities presented in Appendix B. Let us note that similar considerations can be formally applied to other field components, however the resulting sums over n not always can be evaluated explicitly.

Summarizing, the inverse Fourier transform of discrete functions analyzed in this paper includes integration over the spectrum in one Brillouin zone, $(0, K)$ in our case.

Acknowlegments

References

1. W.A. Harrison, *Solid state theory*, Chap. II, McGraw Hill, NY 1970.

2. C-M. Chu, *Propagation of waves in helical wave guides*, J. Appl. Phys., **29**, pp. 88–99, 1958.

3. S.G. Joshi, R.M. White, *Dispersion of surface acoustic waves produced by a conducting grating on a piezo-electric crystal*, J. Appl. Phys., **29**, pp. 5819–5827, 1968.

4. K. Bløtekjær, K.A. Ingebrigtsen, H. Skeie, *A method for analyzing waves in structures consisting of metal strips on dispersive media*, IEEE Trans, **ED-20**, pp. 1133–1138, 1973.

5. K. Bløtekjær, K.A. Ingebrigtsen, H. Skeie, *Acoustic surface waves in piezoelectric materials with periodic metal strips on the surface*, IEEE Trans., **ED-20**, pp. 1139–1146, 1973.

6. E. Danicki, *Theory of periodic interdigital transducer (IDT) of surface acoustic wave (SAW)*, J. Tech. Phys., **19**, pp. 89–102, 1978.

7. E. Danicki, *Theory of surface acoustic wave slant propagation in a periodic electrode system*, J. Tech. Phys., **19**, pp. 69-77, 1978.

8. E. Danicki, *New approach in the theory of microstrip waveguides*, Arch. Acoust., **15**, pp. 45–48, 1990.

9. E. Danicki, *Bending of a layered plate with periodic debondings*, J. Appl. Mech., [accepted for publication 1993].

10. L.A. Wainstein, *Theory of diffraction and a factorization method*, Chap. VIII, [in Russian], Nauka, Moscow 1966.

11. B. Langli, *Electromagnetic waves in periodic structures*, Dissertation, NTH, Trondheim 1992.

12. D.S. Jones, *The theory of electromagnetism*, Chap. 9, McMillan, NY 1964.

13. K. Uchida, T. Noda, T. Matsunaga, *Elctromagnetic wave scattering by an infinite plane metallic grating in case of oblique incidence and arbitrary polarization*, IEEE Trans., **AP-36**, pp. 415–422, 1988.

14. Y.C. ANGELL, J.D. ACHENBACH, *Harmonic waves in an elastic solid, containing a doubly periodic array of cracks*, Wave Motion, **9**, pp. 37–385, 1987.

15. P. JOLY, T. TLILI, *Elastic waves guided by an infinite plane crack*, Wave Motion, **14**, pp. 25–53, 1991.

16. V.V. VARADAN, V.K. VARADAN, *Smart structures – modelling and applications*, 1992 IEEE Ultrason. Symp. Proc., pp. 833–841, 1992.

17. E. DANICKI, *Perturbation theory of surface acoustic wave reflection from a periodic structure with arbitrary angle of incidence*, Arch. Mech. **36**, pp. 623–638, 1984.

18. E. DANICKI, *Analysis of surface acoustic wave in a layered structure with periodic delamination*, [in:] Physical Acoustics, Fundamentals and Applications, O. LEROY and M.A. BREAZEALE [Eds.], Plenum Press, NY 1991, pp. 281–285.

19. E. DANICKI, *Generation and bragg reflection of surface acoustic waves in nearly periodic system of elastic metal strips on piezoelectric half-space*, J. Acoust. Soc. Am., **93**, pp. 115–131, 1993.

20. E. DANICKI, *Propagation of transverse surface acoustic waves in a rotated Y-cut quartz substrates under heavy periodic metal electrodes*, IEEE Trans., SU-3, pp. 304–312, 1983.

21. A. ERDÉLYI, W. MAGNUS, F. OBERHETTINGER, F.G.TRICOMI, *Higher transcendental functions*, v. 1, Chap. 3, McGraw Hill, NY 1953.

22. T. AOKI, K.A. INGEBRIGTSEN, *Acoustic surface waves in split strip periodic gratings on a piezoelectric surface*, IEEE Trans, SU-24, pp. 179–193, 1979.

23. E.I. JURY, *Theory and application of the Z-tansform method*, Chap. 1, A Wiley, NY 1964.

On experimental studies of yield surfaces of metals; a more general approach

W. SZCZEPIŃSKI and J. MIASTKOWSKI (WARSZAWA)

IN ALL EXISTING experimental studies of the effect of plastic deformation on yield condition the results of tests are represented by assuming a certain standard coordinate system. When thin-walled tubular specimens are used, the coordinate axes x, y are assumed to coincide with the axial and circumferential directions of the tube. When specimens are cut out from a prestressed metal sheet, the coordinate axes are so chosen that they are parallel to the edges of the sheet. It is shown in the present study that the interpretation of experimental results may be more instructive if, for the same test, variously oriented coordinate systems x, y are used. Numerous experimental results are recalculated for variously oriented coordinate systems and then represented in the respective stress space corresponding to the assumed orientation of the reference axes. Such various representations of the deformation-induced changes of the yield surface will constitute the experimental basis for a more sound analysis of the theory of deformation-induced anisotropy of metals. If the plastic properties of the tested material in its initial state are isotropic, we can always arbitrarily choose a reference system in which the deformation-induced anisotropy will later be described.

1. Introduction

OVER SIXTY YEARS elapsed since LODE [1] published his classical paper reporting experimental investigations of yield surfaces of some metals in virgin state. For almost thirty years since then no paper reporting experimental tests of this kind has been published, except that by TAYLOR and QUINNEY [2], who used thin-walled tubular specimens made of various metals. The concept of this work was different than that in the Lode's investigations, because each specimen was prestrained by axial stresses beyond the initial yield locus and then, after partial unloading, was additionally loaded by increasing twisting moment while the axial stress was kept constant. The conventional yield loci have been found by extrapolating the smooth portion of the stress-strain diagram back to intersect the extrapolated straight initial portion of the diagram. This was a quite different approach than that used in most recent papers in which the proportional limit during subsequent loading was taken as a conventional yield stress.

Experimental investigations of surfaces of prestrained metals began to attract the attention of numerous scientists in the late fifties, when the strain-hardening phenomenon under complex loadings became one of the most important problems in the development of the theory of plasticity. Numerous experimental works in this field have been described in two survey papers by IKEGAMI [3, 4]. Thus they will not be mentioned here.

The aim of this paper is to present a more general look at an interpretation of the results of experimental studies of yield surfaces of plastically deformed

metals. Our considerations will be based on the fact that most metals in virgin
state display isotropic plastic properties. Thus the analysis presented below is
valid for initially isotropic materials only.

2. The theory of experiments on plastic yielding under plane stress conditions

At first we shall present in brief the foundations of experiments concerning the
behaviour of yield surfaces of metals undergoing complex plastic deformations
(cf. [5]). Such experiments are usually performed under plane stress conditions.
Mostly thin-walled tubular specimens are used. They are loaded simultaneously
by various combinations of axial force, a twisting moment and internal pressure.
At a definite point of an arbitrarily chosen Cartesian coordinate system x, y with
the x, y-plane coinciding with the local plane tangent to the specimen's surface,
there exist three stress components σ_x, σ_y, τ_{xy} only, the stress component σ_z
perpendicular to this surface being equal to zero or being so small that it may
be neglected in the analysis. It is important to emphasize that axes x and y
can be chosen arbitrarily. They not necessarily must coincide with the axial and
circumferential directions on the surface of a tubular specimen.

The Huber – Mises yield condition for isotropic materials under plane stress
conditions assumes the form

$$(2.1) \qquad \sigma_x^2 - \sigma_x\sigma_y + \sigma_y^2 + 3\tau_{xy}^2 = 3k^2,$$

where k is the yield stress under pure shear conditions. In the stress space of
non-vanishing components σ_x, σ_y, τ_{xy} yield condition (2.1) is represented by the
points of the surface of an ellipsoid shown in Fig. 1. One of its principal axes
coincides with the τ_{xy}-axis and other two lie in the $\sigma_x\sigma_y$-plane. They bisect the
right angles made by reference axes σ_x and σ_y. By heavy lines are shown in the
figure certain particular ellipses on the surface of the ellipsoid. They correspond
to the loading modes most commonly used in testing yield surfaces with the use
of tubular specimens. For instance, ellipse AB for which $\sigma_y = 0$ corresponds to
simultaneous torsion and axial tension of the specimen, if x is chosen as the axial
direction. Portion BCD of the ellipse lying in the $\sigma_x\sigma_y$-plane corresponds to the
simultaneous loading of the tubular specimen by the axial force and by internal
pressure.

The paths of proportional loadings are represented in the stress space by
straight lines originating from the central point 0. For instance, if the x and
y-directions coincide with the directions of principal stresses, the path of propor-
tional loading with constant ratio of principal stresses will be represented by a
straight line lying in the plane σ_x, σ_y, such as line $0P$ in Fig. 2. Let us consider
an arbitrary stress state represented by the point P on the line $0P$. Stress compo-
nents written in the system of coordinate axes x, y arbitrarily inclined with respect
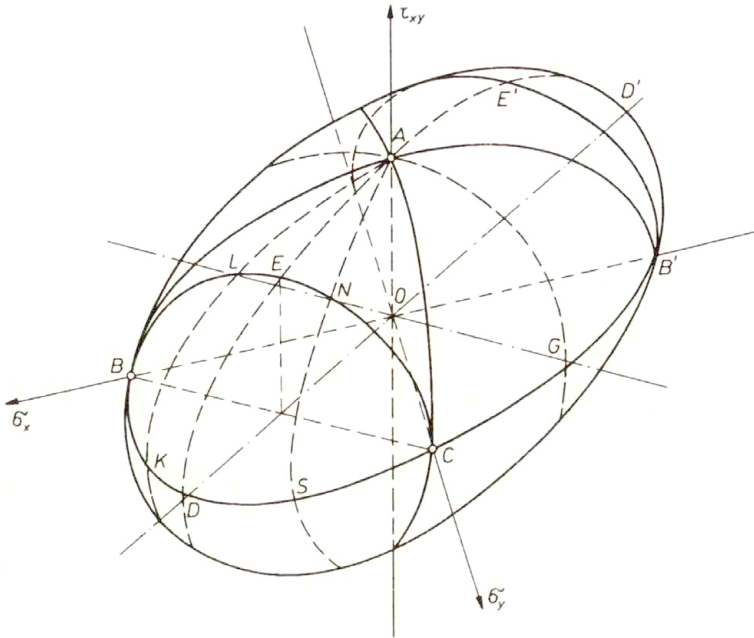
Fig. 1.
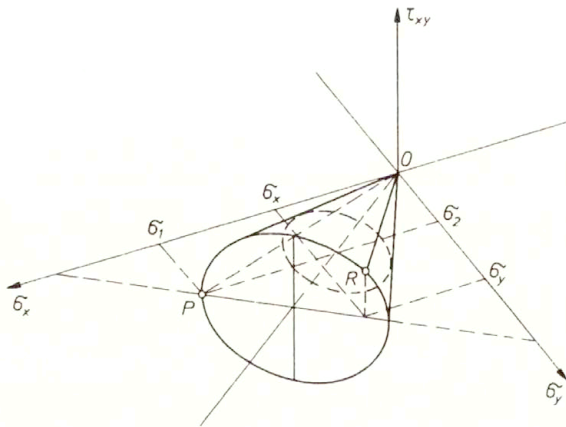
Fig. 2.

to the directions of principal stresses σ_1, σ_2 satisfy the known relations

(2.2)
$$(\sigma_x - \sigma_y)^2 + 4\tau_{xy}^2 = (\sigma_1 - \sigma_2)^2,$$
$$\sigma_x + \sigma_y = \sigma_1 + \sigma_2.$$

These equations represent a certain ellipse lying in the plane perpendicular to the bisector of the right angle between the axes σ_x and σ_y (Fig. 2). All the points

on this ellipse represent the same stress state written in various reference frames. Similarly each straight line connecting the origin 0 with an arbitrary point R on the ellipse corresponds to the proportional loading path $0P$, referred to the different coordinate system. Representations of the same proportional loading path (say $0P$) in various rotated coordinate systems generate the surface of an elliptical cone. Its equation is

$$(2.3) \qquad \kappa \left(\sigma_x^2 + \sigma_y^2 \right) - \left(1 + \kappa^2 \right) \sigma_x \sigma_y + (1 + \kappa)^2 \tau_{xy}^2 = 0.$$

Here $\kappa = \sigma_1 / \sigma_2$ is a parameter characterizing the proportional loading path.

Intersections of cones (2.3) with the yield surface (2.1) shown in Fig. 1 are also ellipses lying in the planes

$$\sigma_x + \sigma_y = \text{const}$$

perpendicular to the axis $0D$ of the ellipsoid from Fig. 1. Thus each such an ellipse on the ellipsoid represents the same stress state described in a rotated coordinate system x, y. This follows from the fact that the yield condition (2.1) is invariant under the rotation of the reference system.

The latter conclusion is of primary importance for programming and interpreting experimental and also numerical studies of the behaviour of yield surfaces of initially isotropic materials. Let us assume, for instance, that the yield stresses of an isotropic metal have been determined by loading a set of tubular specimens, each by a different combination of axial force and internal pressure. Such a loading procedure is usually identified with the ellipse $BDCB'$ lying on the ellipsoid shown in Fig. 1. In such a case the reference system of coordinates is so chosen that the x-axis is parallel to the longitudinal axis of the tubular specimen and y-axis has the circumferential direction. The yield stresses found in this way for a M-63 brass in [6] and [7] are presented in Fig. 3. The experimental points from Fig. 3 may be also presented in the plane determined by τ_{xy}-axis and the symmetry axis $0D$ of the ellipsoid from Fig. 1, if the axes x and y of reference system will make the angle of $45°$ with the axial and circumferential directions on the specimen (Fig. 4). For such a rotated coordinate system the experiment presented in Fig. 3 will correspond to the theoretical ellipse $DEAE'$ on the Huber – Mises ellipsoid (Fig. 5).

In Fig. 6 are presented experimental points from Fig. 3 recalculated for a new reference system with the axes x and y making the angle of $45°$ with the axial direction on the surface of each specimen. Theoretical ellipse $DEAE'$ from Fig. 5 is also shown for comparison. Note that, in order to obtain the experimental points such as those shown in Fig. 6 with the use of the standard reference system coinciding with the axial and circumferential directions on the surface of the specimens, it would be necessary to load tubular specimens simultaneously by axial force, a twisting moment and, moreover, by internal pressure.

C

△ – after [6]
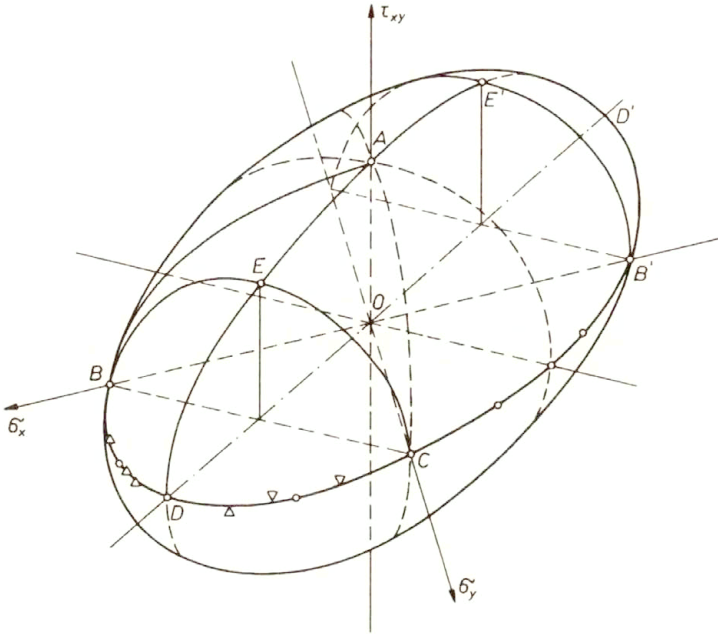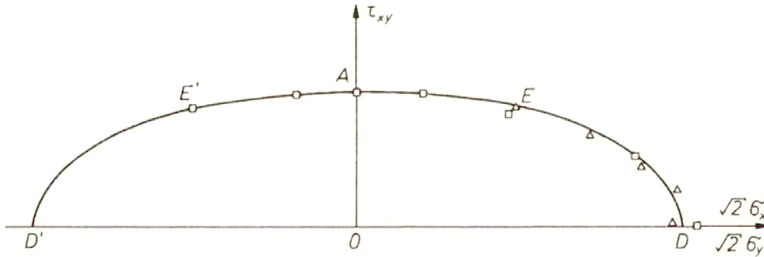□ – after [7]

Fɪɢ. 3.
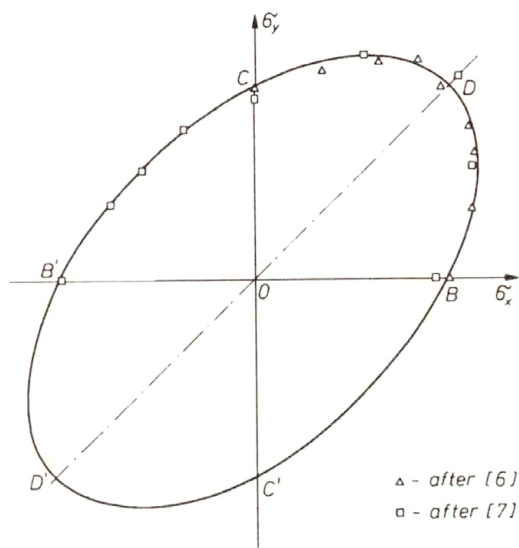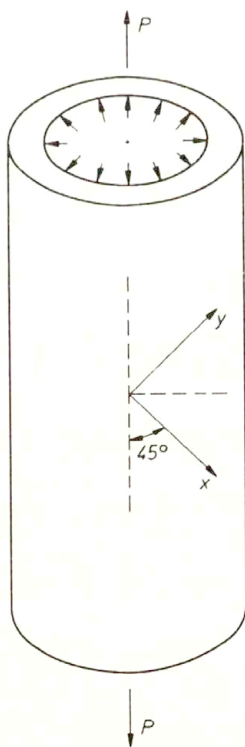
Fɪɢ. 4.

Fig. 5.

Fig. 6.

Numerous experiments concerning behaviour of yield surfaces were performed by simultaneous loading of thin-walled tubular specimens by a tensile force and a torque. The analysis of the results of such experiments was always performed with the use of a reference system with the coordinate axes coinciding with the axial and circumferential directions. In such a reference frame this mode of loading corresponds to the ellipse AB on the Huber–Mises ellipsoid (cf. Fig. 1). An example of the results of experiments performed under simultaneous torsion and tension of thin-walled tubular specimens is shown in Fig. 7. If the tested material is isotropic, such results can be presented in another way by assuming, for instance, for each specimen of the set a reference system x, y coinciding with the directions of principal stresses. The experimental points from Fig. 7

recalculated for such individual reference frames are shown in Fig. 8. It is seen that in this case the latter representation is less informative than that shown in Fig. 7.
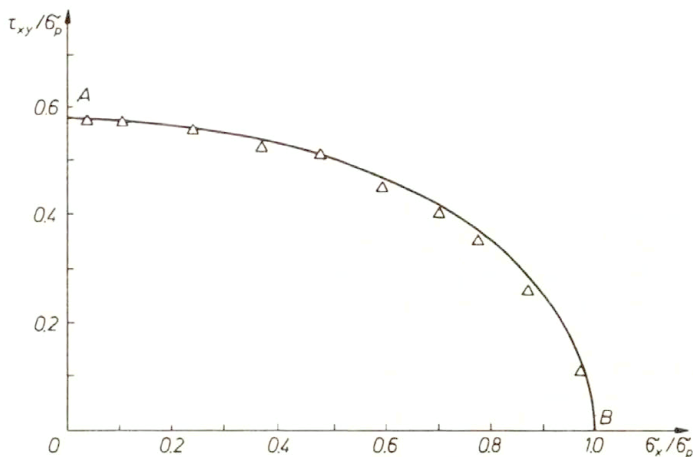
FIG. 7.
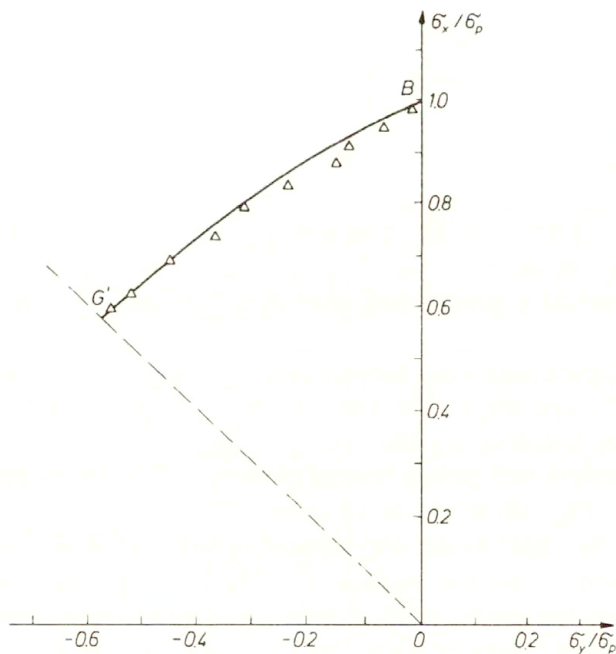
FIG. 8.

When the reference frames are so chosen that for each specimen the axes x and y make the angle $45°$ with the directions of principal stresses, the re-calculated experimental points from Fig. 7 correspond to the sector AE of the

ellipse $DEAE'D'$ (Fig. 1). These points recalculated for such reference frames are shown in Fig. 9. Also in this case such a representation is less instructive than the original representation shown in Fig. 7.
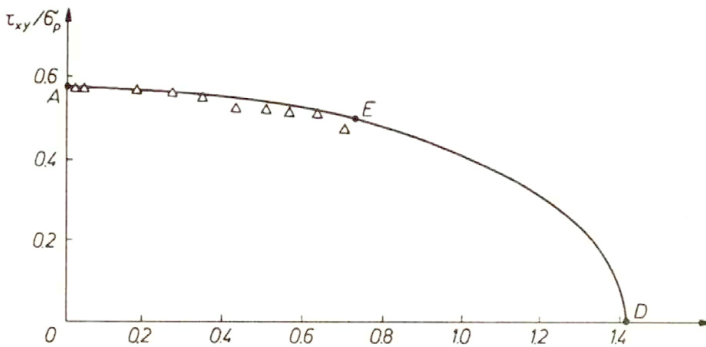
Analysing more generally the equivalence of various representations of experimental results let us assume, for instance, that the yield surface of an *isotropic material* has been determined by loading a set of thin-walled tubular specimens by various combinations of a tensile force and a twisting moment. Such a loading procedure corresponds to the segment AB of the ellipse

$$\sigma_x^2 + 3\tau_{xy}^2 = 3k^2$$

lying on the Huber–Mises ellipsoid (cf. Fig. 1). The experimentally determined form of the curve AB determines the entire portion of the yield surface shaded in Fig. 10a. That portion of the yield surface is generated by ellipses (2.2) passing through the individual experimental points corresponding to the curve AB (cf. Fig. 2).

If the tubular specimens were subject to the simultaneous tension and internal pressure (this corresponds to the segment BD on the Huber–Mises ellipsoid in Fig. 1), then by constructing the family of ellipses (2.2) passing through the experimentally determined points corresponding to BD, the portion of the yield surface shaded in Fig. 10b would be obtained.

Carrying out the experiments corresponding to an arbitrary curve which connects points D and D' on the surface (cf. Fig. 1), such as the arc $DCB'D'$ in Fig. 10c, we obtain the entire yield surface. Additional tests corresponding, for instance, to the arc AB may be considered as a verification whether the material is really isotropic.

Note that this reasoning does not apply to materials exhibiting *plastic anisotropy*, whether natural or induced by previous plastic deformations. This remark applies in particular to considerations concerning the effect of plastic deformation on the yield surface or, in other words, to the analysis of the so-called *secondary yield*
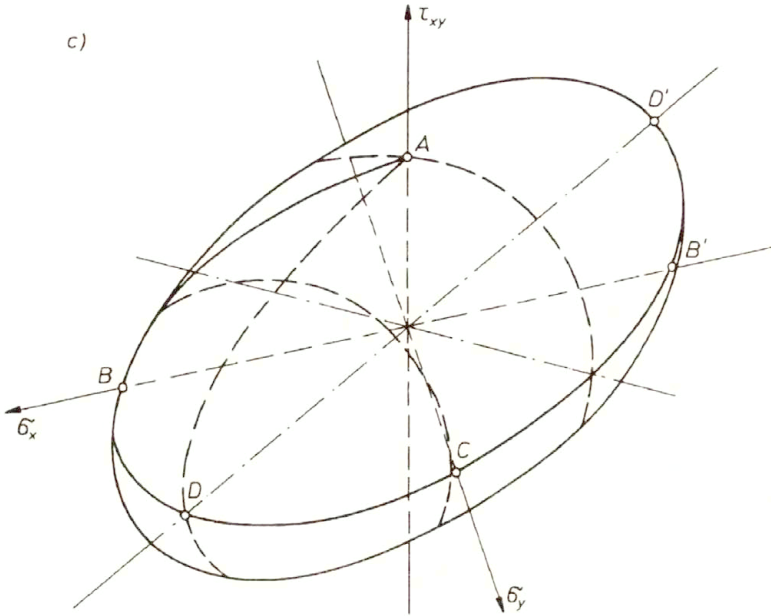
a)

b)
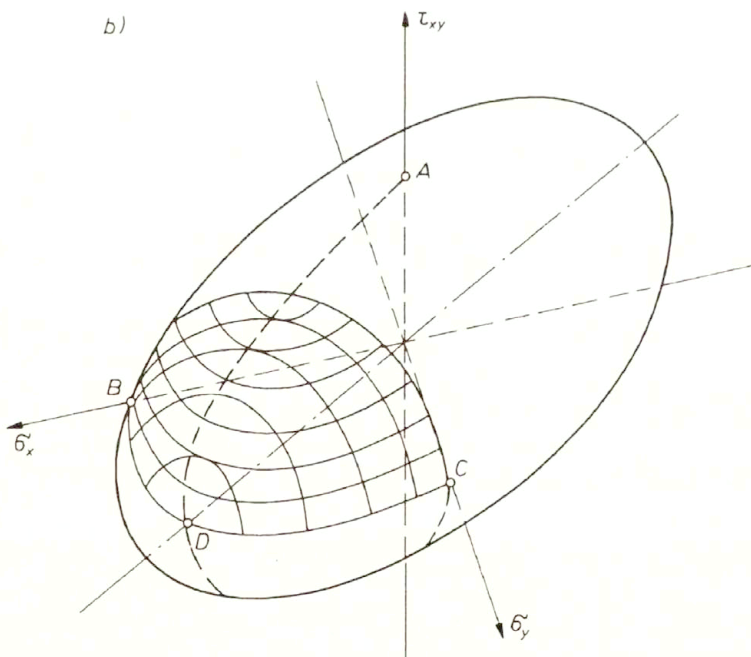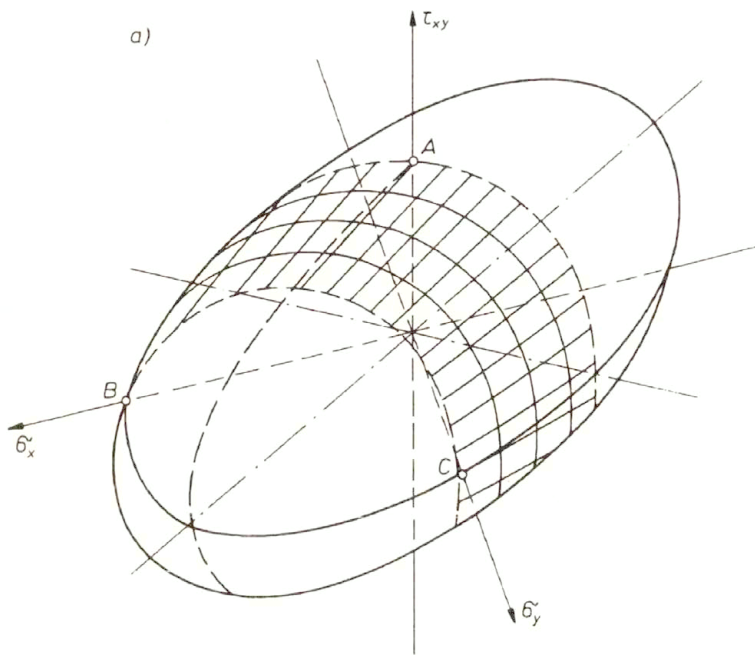
[Fig. 10]

Fig. 10.

surfaces. Such investigations must be referred to a fixed coordinate system chosen at the beginning of the experimental procedure.

However, there exists a certain practically important type of anisotropy when the procedure described above may be used. Such a case of anisotropy occurs in rolled sheet metals and is *referred to as the transversal isotropy*. Let the axes of reference be so chosen that the x and y axes lie in the median plane of the sheet and z-axis is normal to that plane. In most cases the plastic properties of the sheet are isotropic in the x, y-plane. The yield stresses of specimens cut out from the sheet in various direction are of the same magnitude Y_0. Of the same magnitude are also absolute values of yield stresses under uniaxial compressive loading. However, yield stresses in the z-direction are different from Y_0 in the case of transversal isotropy.

If the Bauschinger effect in z-direction is neglected, the yield condition for plane stress state may be written in the following form:

$$(2.4) \qquad \sigma_x^2 - \left[2 - \left(\frac{Y_0}{Y_z}\right)^2\right]\sigma_x\sigma_y + \sigma_y^2 + \left[4 - \left(\frac{Y_0}{Y_z}\right)^2\right]\tau_{xy}^2 = Y_0^2.$$

In this condition Y_z is the yield stress in z-direction under uniaxial tension. It represents also the absolute value of yield stresses under uniaxial compression in that direction. In the stress space σ_x, σ_y, τ_{xy} yield condition (2.4) is represented by the points located on the surface of an ellipsoid shown in Fig. 11. For $Y_z > Y_0$ the ellipsoid is more elongated in the $0D$-direction than that shown in Fig. 1 for

fully isotropic material. Various methods of measuring the yield stress Y_z are discussed in the previous papers [8] and [9].
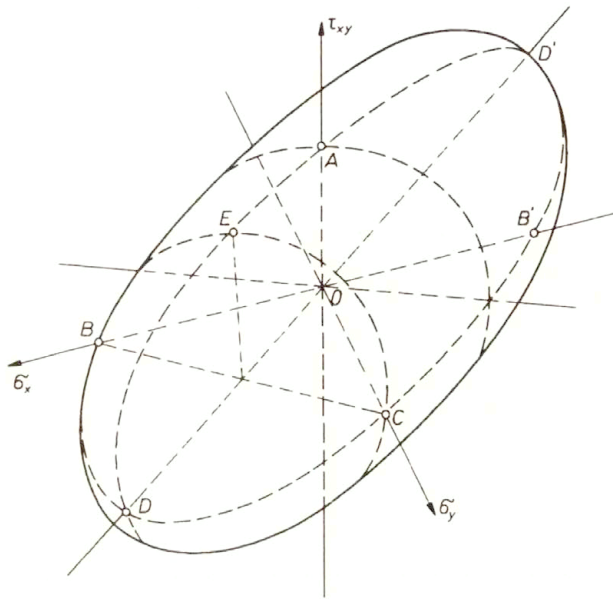
FIG. 11.

3. Presentation of the effect of plastic deformation on yield condition in various reference systems

Plastic deformations in metals produce complex changes in the shape and position of the yield surface. These changes are difficult to be described theoretically. Intensive experimental studies are aimed at explaining them. However, there appear certain difficulties in interpreting such experimental results. They are described for example in the previous paper [5] and will not be discussed here.

In Sec. 2 it was shown that if the material in question is isotropic in initial state, the orientation of the coordinate system in which the stresses are defined can be chosen arbitrarily. Thus it is possible to present the consecutive yield surfaces deformed after plastic prestraining of the material in various reference systems. In such a manner one can generalize the results of experimental studies of the effect of plastic deformation on yield condition. We shall illustrate this by a number of examples.

Let us begin with a simple method of investigating the effect of plastic deformation on the shape of yield surface used in [10]. Simple rectangular specimens cut out from the sheet metal were tested. The sheet was stretched in the

x-direction well above the initial yield locus. Then after unloading, a series of small rectangular specimens were cut out from the sheet, each inclined at different angle α with respect to the x-direction (Fig. 12). These small specimens were tested under uniaxial tensile loading. An example of stress-strain diagram for one of such small specimens is shown in Fig. 13. In the figure is also shown the analogous diagram for the specimen cut out in the same direction from a non-deformed sheet. The two diagrams are displaced, one with respect to the other, by the value of initial plastic prestrain.
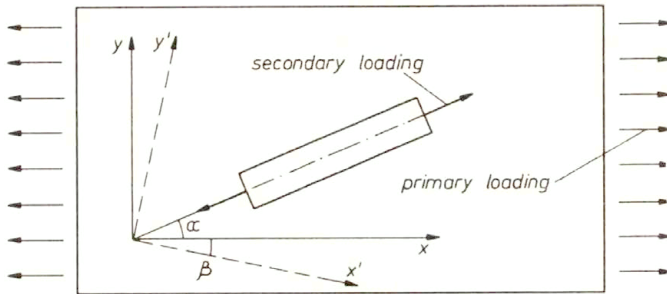
FIG. 12.
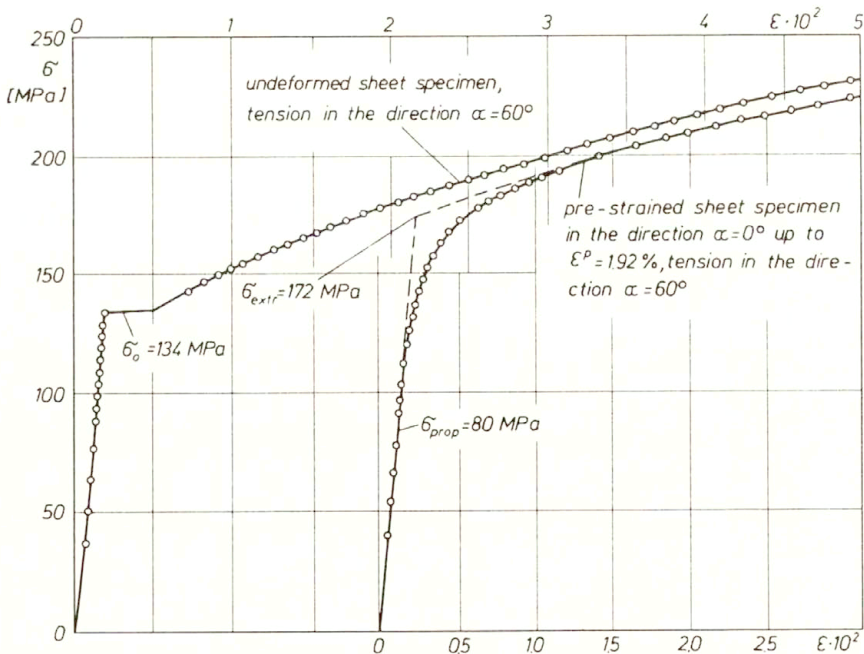
FIG. 13.

Such diagrams for various angles α were then used to determine the stress corresponding to various definitions of the yield point. Then the yield stresses

referred to the x, y coordinate system were calculated from the formulae

(3.1)
$$\sigma_x = \frac{1}{2}\sigma(1 + \cos 2\alpha),$$
$$\sigma_y = \frac{1}{2}\sigma(1 - \cos 2\alpha),$$
$$\tau_{xy} = \frac{1}{2}\sigma \sin 2\alpha.$$

Plotting the calculated values of yield stresses in the stress space σ_x, σ_y, τ_{xy} we obtain a set of curves (Fig. 14) which represent the intersections of various conventional yield surfaces of the prestrained material corresponding to different definitions of yield stresses, with the cone representing uniaxial tensile loading paths (cf. Fig. 2). Assuming that $\sigma_2 = 0$ and that $\kappa = \sigma_2/\sigma_1 = 0$ we obtain from Eq. (2.3) the equation of the cone

(3.2)
$$\sigma_x\sigma_y = \tau_{xy}^2.$$

Figure 14 shows a set of experimentally determined curves projected on the $\sigma_x\sigma_y$-plane and on another plane perpendicular to the bisector of the right angle between the coordinate axes in the $\sigma_x\sigma_y$-plane. Point B denotes the end of the path $0B$ of initial loading of the sheet. The initial yield curve before prestraining is shown by dashed line.

Experimental results shown in Fig. 14 can be represented in other various coordinate systems rotated by an angle β with respect to the original system x, y. Rotation of the coordinate system in the median plane of the sheet causes that in the stress space the end point of the vector $0B$ characterizing the initial loading of the sheet moves along the ellipse corresponding to uniaxial tension (Fig. 15).

The experimental lines shown previously in Fig. 14 for the non-rotated coordinate system are represented in Fig. 16 for the coordinate system x, y rotated by the angle $\beta = 15°$ with respect to the original one. Such a rotation of the coordinate system corresponds to the prestressing path $0B_1$ in the new system (cf. Fig. 15). Similarly, the yield curves shown in Fig. 17 correspond to $\beta = 30°$ and the prestressing path $0B_2$. In the Fig. 18 are presented yield curves for rotation angle $\beta = 45°$ and the prestressing path $0B_3$.

Since the material was found to be initially isotropic, all four representations are fully equivalent because the coordinate system could be chosen arbitrarily.

This simple method of experimental investigation of the effect of plastic deformation on the shape of the yield surfaces was recently extended by R. SZCZEBIOT [11] to the region of compressive stresses in the stress space. Tensile tests for specimens cut out in different directions from a prestressed sheet were performed in the same manner as in [10]. However, now they were complemented by compression tests with the use of another set of specimens cut out in the same directions from the same prestressed large specimen.
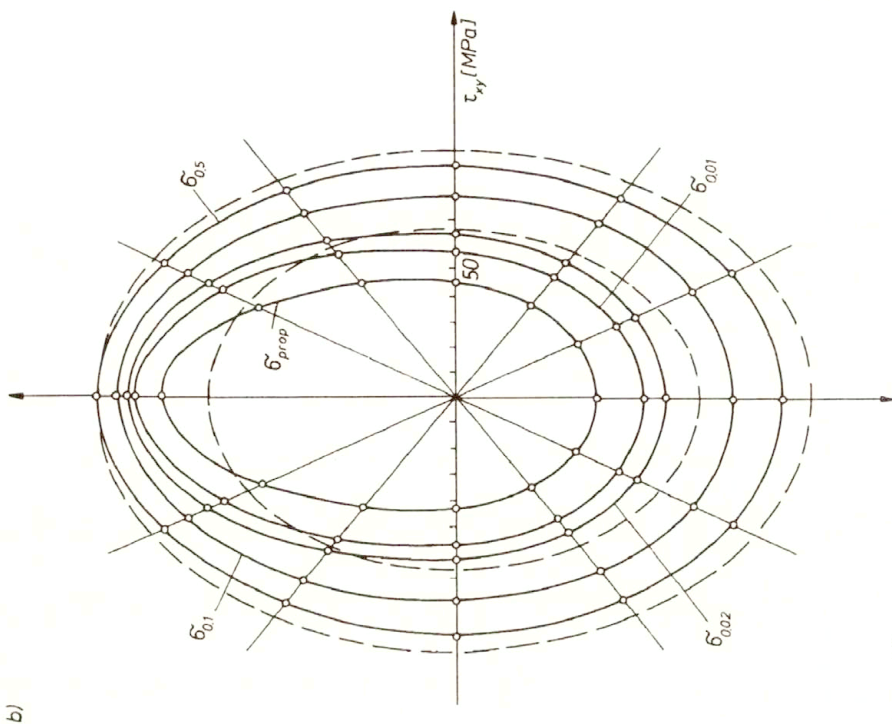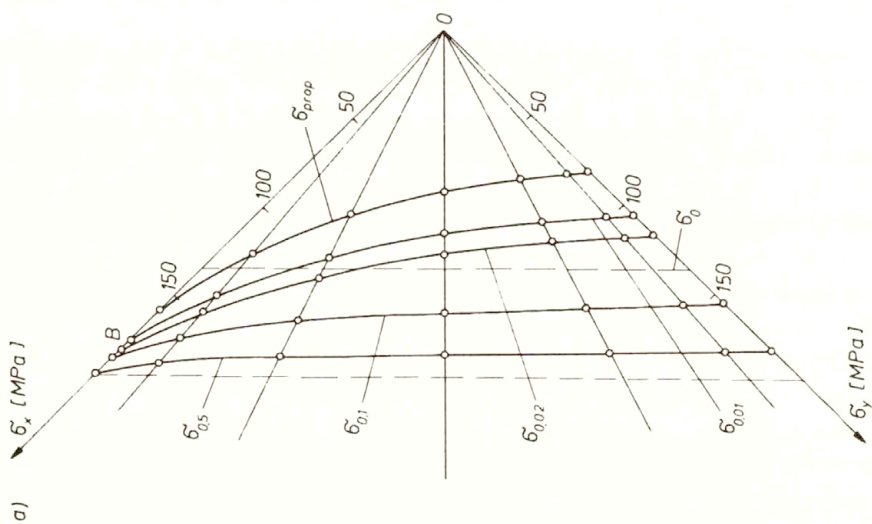
b)

$\sigma_{0.5}$

$\sigma_{0.01}$

$\tau_{xy} \, [MPa]$

50

σ_{prop}

$\sigma_{0.1}$

$\sigma_{0.02}$

Fig. 14.

a)

O

σ_{prop}

50

50

100

100

σ_0

150

B

150

$\sigma_x \, [MPa]$

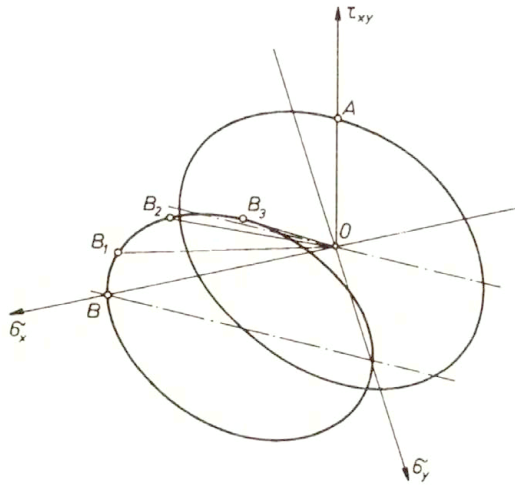$\sigma_{0.5}$

$\sigma_{0.1}$

$\sigma_{0.02}$

$\sigma_{0.01}$
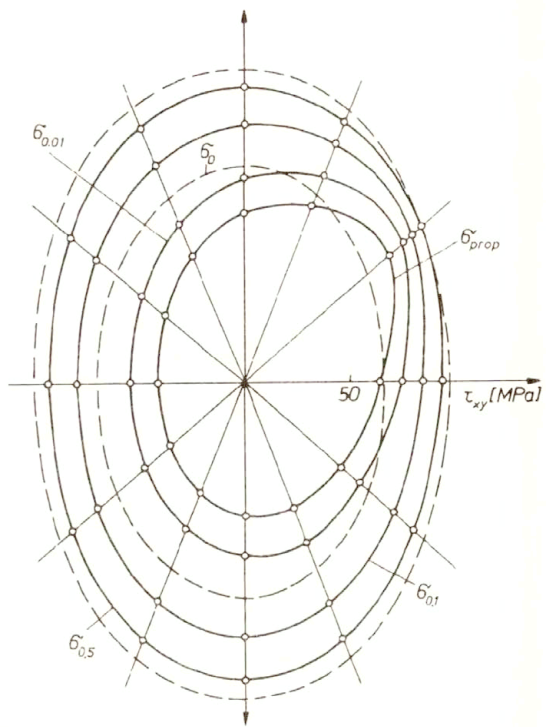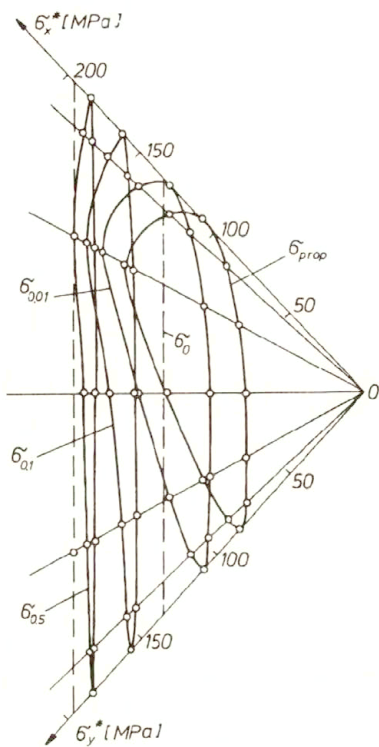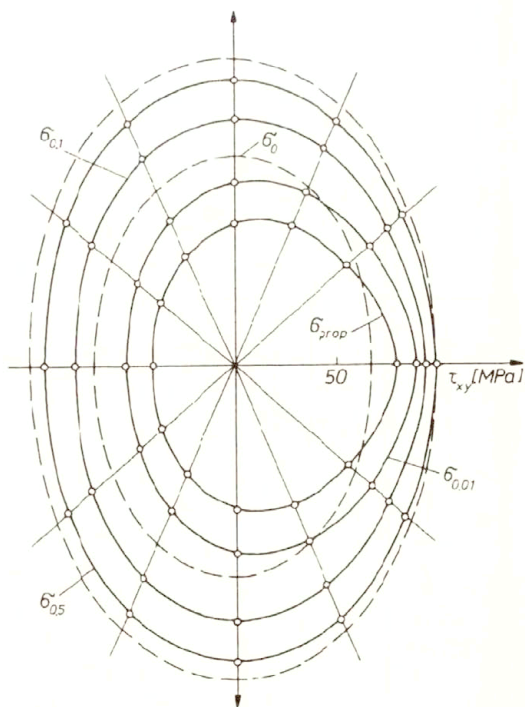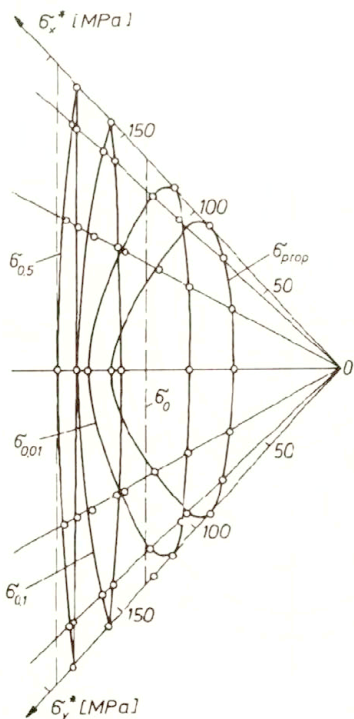
$\sigma_y \, [MPa]$

Fig. 15.
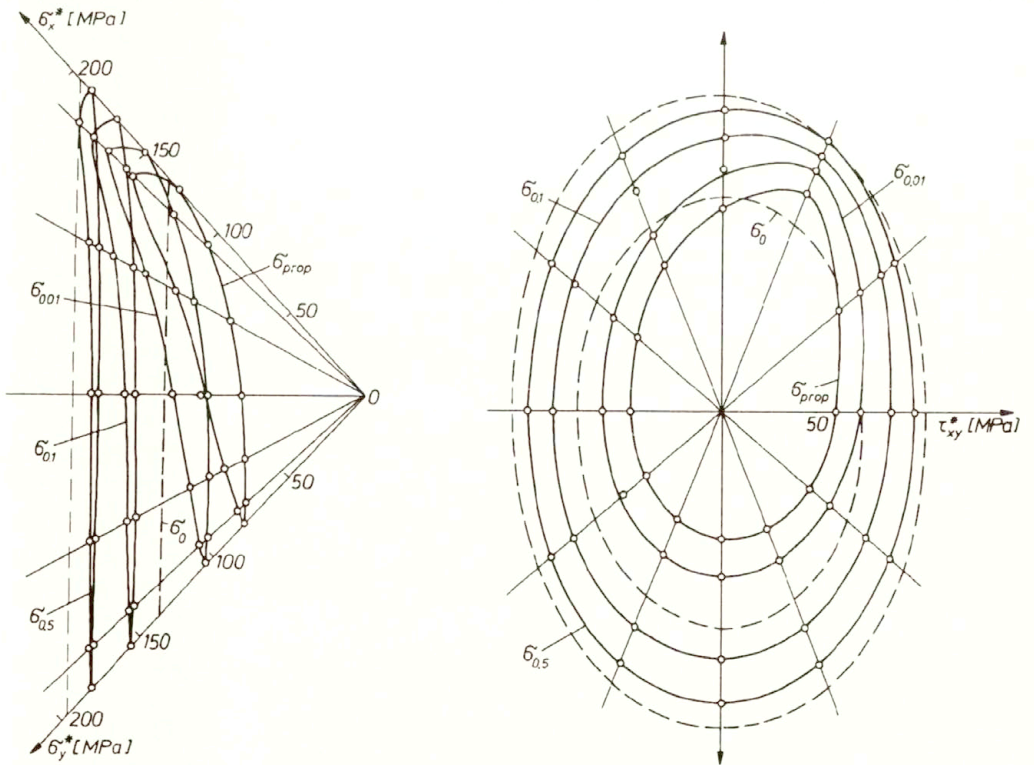
Fig. 16.

Fig. 17.

Fig. 18.

As the material, a sheet 3 mm thick of the aluminium alloy PA2N-M3 (Al2%Mg) was used. Large specimens cut out in the rolling direction, assumed by the author as the x-direction, were plastically deformed each by different stresses $\sigma_A = 124.5\,\text{MPa}$, $\sigma_B = 154.6\,\text{MPa}$, $\sigma_C = 185.5\,\text{MPa}$, respectively. These stress levels were well above the conventional yield stresses $\sigma_{0.5}^0 = 100\,\text{MPa}$ for the off-set strain 0.5 percent of the sheet in the initial state, in which the sheet was found to be fully plastically isotropic in its plane. No Bauschinger effect was observed in the sheet before prestraining.

Compression tests on small specimens cut out from the sheet were performed with the use of special testing device preventing thin specimens from buckling. This device was designed by L. Dietrich and K. Turski [12] – see also [5].

In Fig. 19 are presented original experimental curves given in [11], where the prestressing uniaxial tension $0B$ was chosen to coincide with the assumed x-direction in the sheet's plane. Thus these curves correspond to the case when prestressing level was equal to $\sigma_B = 154.6\,\text{MPa}$.

Note that the projections of the curves shown on the left-hand side of Fig. 19a and their projections shown in Fig. 19b are analogous to those presented in Fig. 14 for another material. On the right-hand side of Fig. 19a and in Fig. 19c are shown projections of the conventional yield curves for the prestressed material, loaded afterwards by uniaxial compression in different directions with respect to the previously chosen x-axis of the reference system. In geometrical terms, the two sets of experimental conventional yield curves in the tension and compression quadrants of the stress space represent the intersections of the deformed conventional yield surfaces of prestressed material with the cones

$$\sigma_x \sigma_y = \tau_{xy}^2$$

on both sides of the symmetry axis $0A$ in the stress space (cf. Fig. 1).

Comparison of the experimental curves σ_{prop}, $\sigma_{0.01}$ and $\sigma_{0.02}$ on both sides of the symmetry axis demonstrates the clearly visible Bauschinger effect induced in the sheet by previous plastic deformation.

In Fig. 20 are shown the same experimental results referred to another reference system x, y rotated by the angle $\beta = 45°$ with respect to that assumed for the previous representation of results in Fig. 19. Thus now the x and y axes make the angle of 45° with the prestressing direction. In such a rotated reference system the initial yield surface was pushed from inside along the straight line $0E$ (cf. Fig. 1) up to the end point B of the prestressing path $0B$.

This bulging of the yield surface caused by previous plastic deformations is even more distinctly demonstrated for still larger prestressing level by the stresses $\sigma_C = 185.5\,\text{MPa}$. In Fig. 21 are presented original experimental curves taken from [11]. The x-axis of the reference system coincides with the direction of the prestressing path $0C$. Figure 22 presents the same experimental results in the coordinate system rotated by an angle of 45° with respect to the original one.
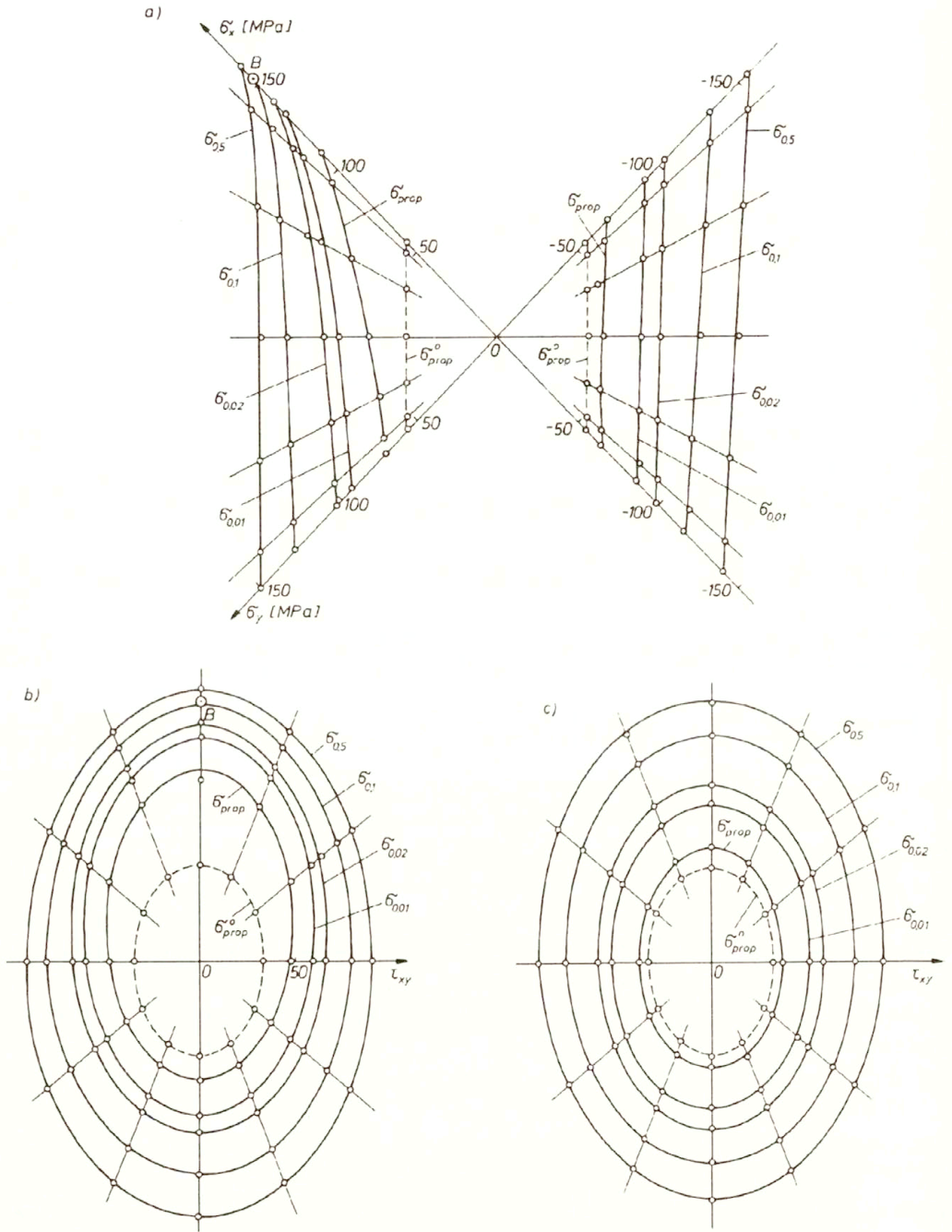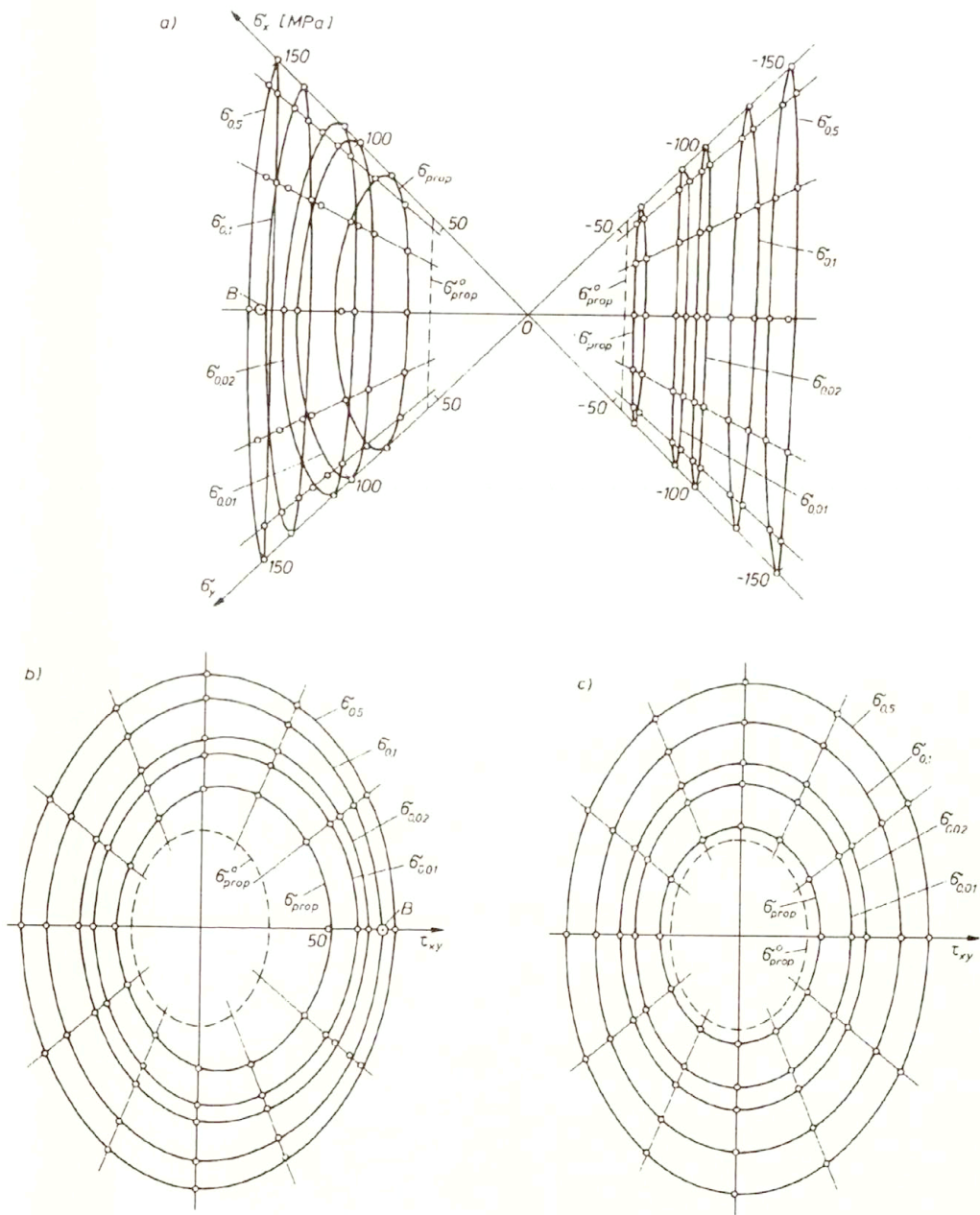
FIG. 19.

a)

b)

c)

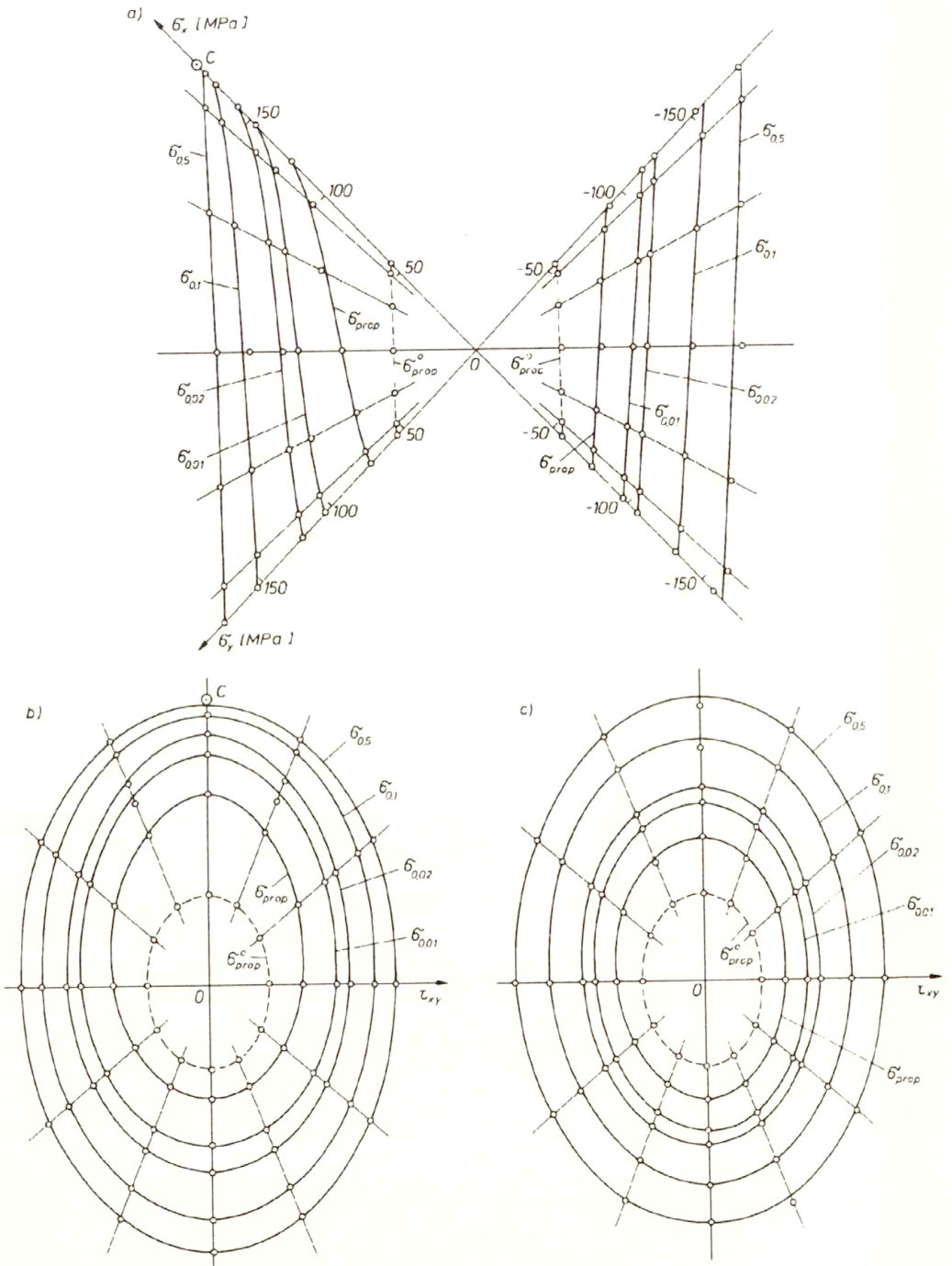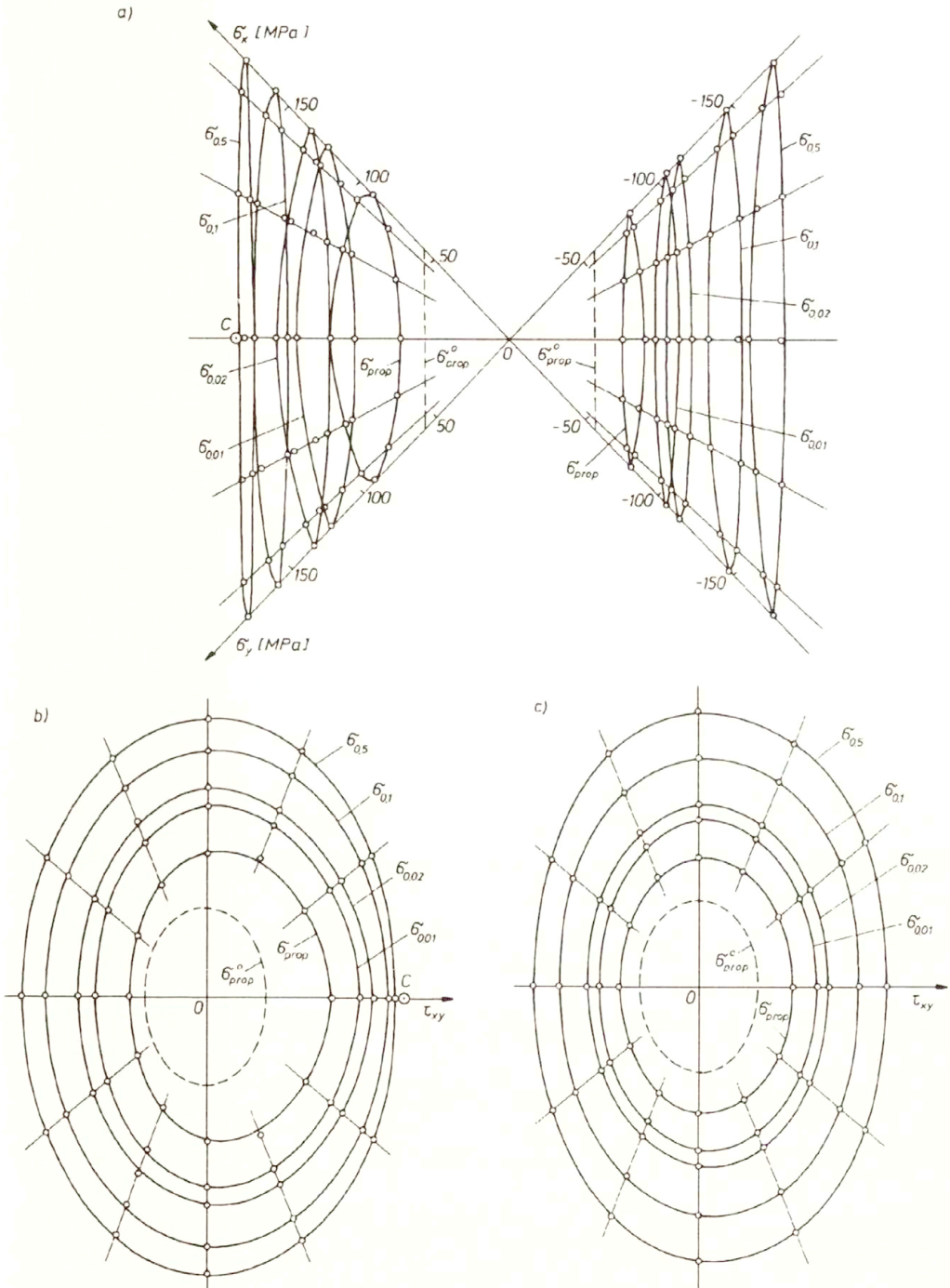Fig. 20.

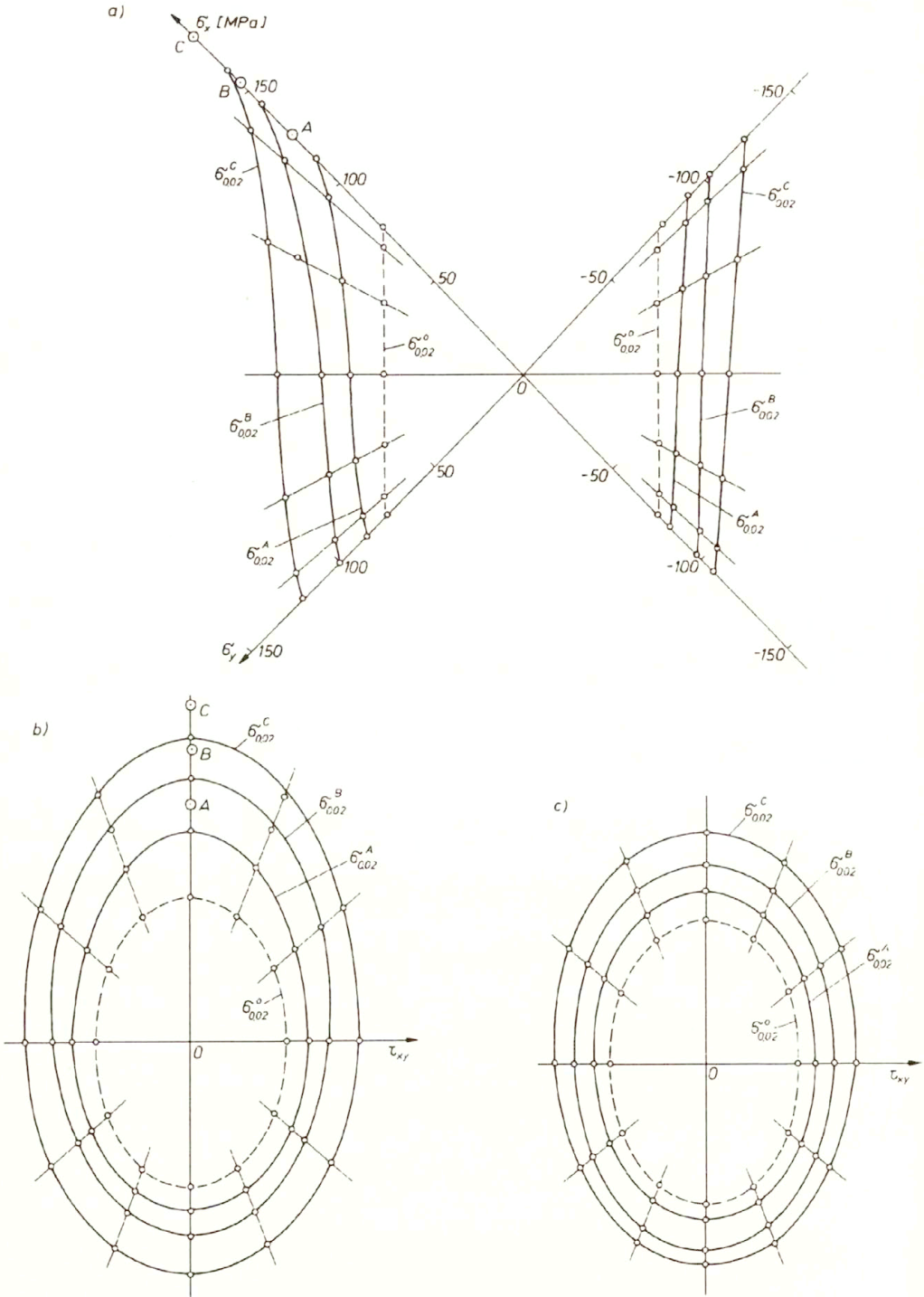Fig. 21.

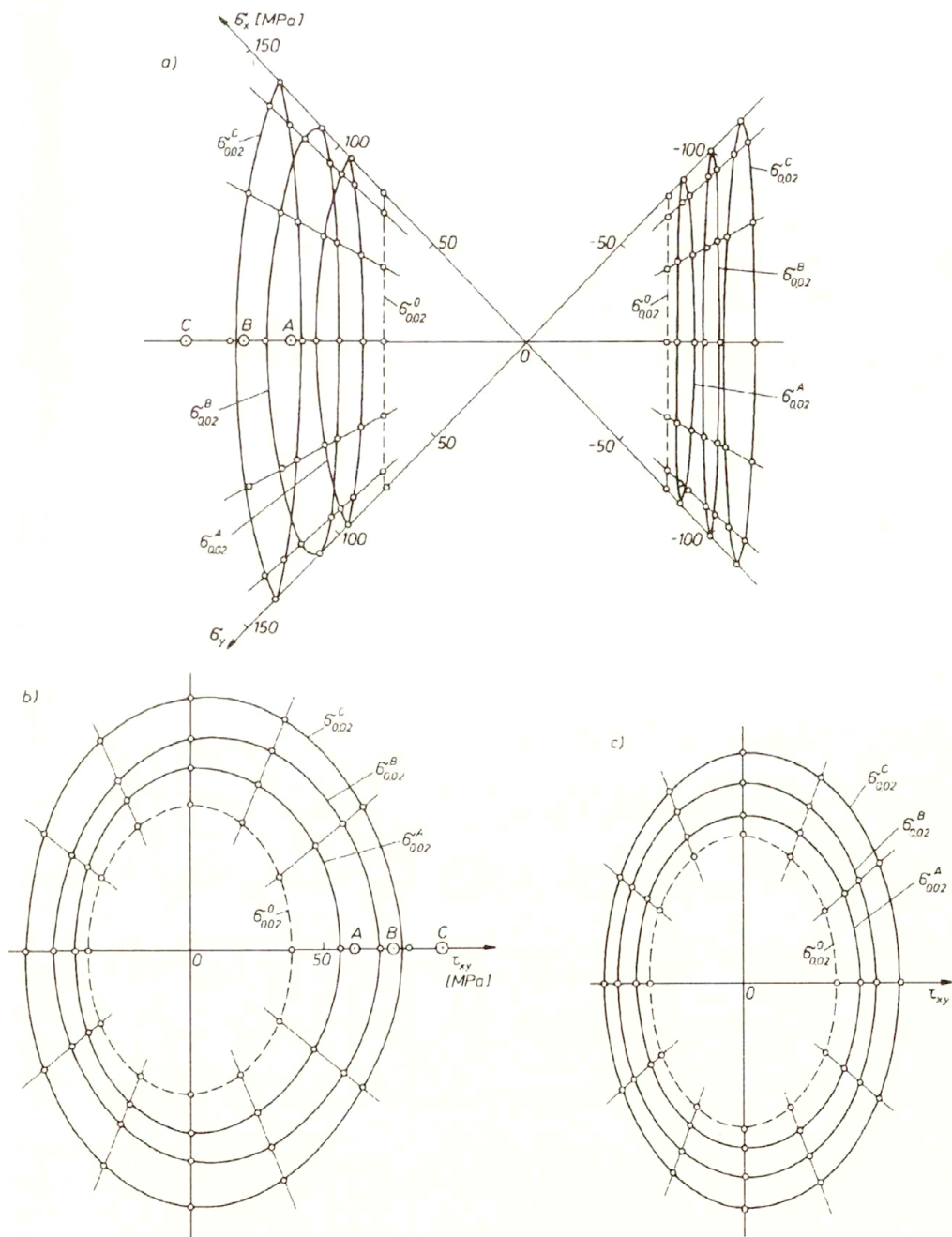a)

b)

c)

Fig. 22.

[171]

a)

b)

c)

FIG. 23.

FIG. 24.

[173]

Evolution of the yield surface during the process of plastic deformation of the material may be observed if the corresponding conventional yield curves for the consecutive stages of prestraining are presented in the same figure, as it has been done in Fig. 23 for the $\sigma_{0.02}$ yield curves in the original coordinate system (cf. [11]). The mode of evolution is even more clearly visible if the same experimental curves are presented in another coordinate system rotated by an angle of 45° (Fig. 24).

As a next example let us transform the experimental conventional yield curve $\sigma_{0.01}$ obtained by R. KIRYK [13] for the duralumin type alloy PA6. A thin-walled tubular specimen was prestressed by uniaxial tension in axial direction far beyond the initial yield stress and then unloaded. Next the conventional yield curve for such prestressed material was determined by consecutive loading of the specimen by various combinations of axial force and torque. The $\sigma_{0.01}$ yield curve is shown in Fig. 25 in the coordinate system standard for such tests, in which the x-axis is parallel to the axis of the tube. In Fig. 26 are presented, in two projections, these experimental results in another coordinate system x, y rotated by an angle of 45° with respect to the original system from Fig. 25.
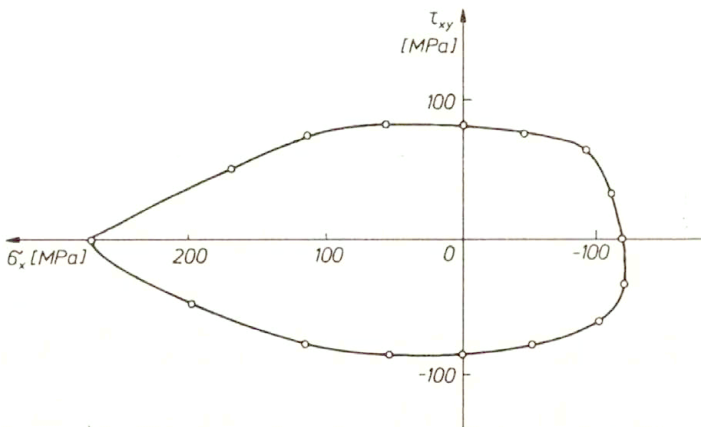

FIG. 25.

Since the material in the initial state displayed fully isotropic plastic properties, the initial yield surface shown in Fig. 1 is valid for any arbitrarily oriented coordinate system x, y. Thus the prestressing path $0B$ in the original reference system corresponds to the path $0E$ in the coordinate system rotated by an angle of 45°.

Variously oriented reference systems may be used when experimental results, such as those shown in Fig. 25, are presented in the stress space. Still another reference system rotated by an angle of 22°30′ is used in Fig. 27 for presentation of the same experimental results. Now the prestressing path passes through origin 0 and a certain point lying on the ellipse BLENC in Fig. 1.
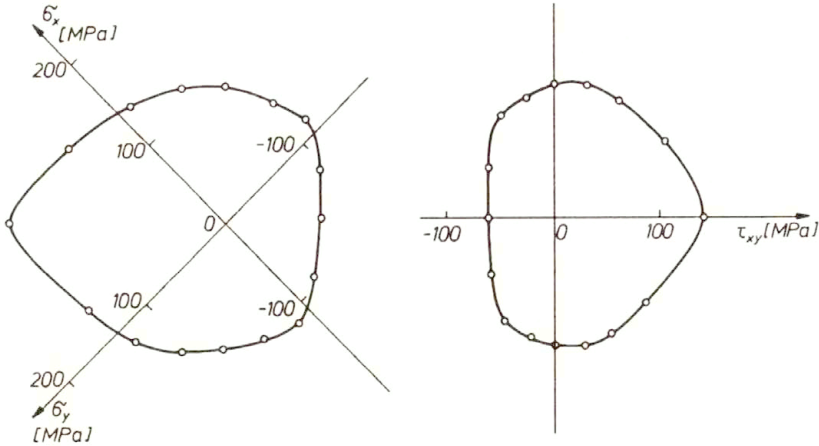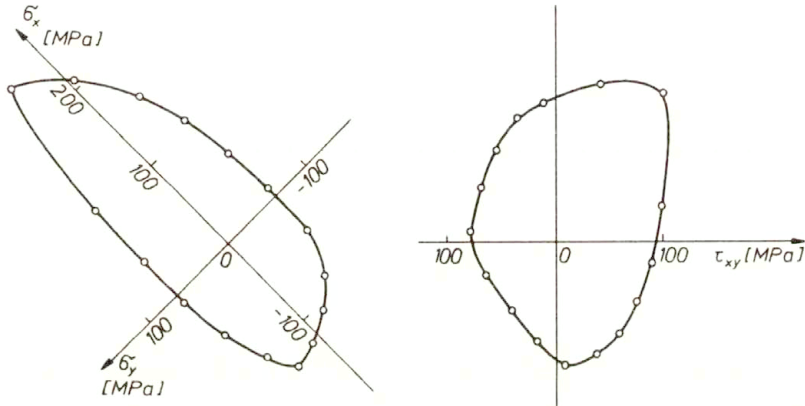
FIG. 26.

FIG. 27.

Acknowledgement

References

1. W. LODE, *Versuche über den Einfluss der mittleren Hauptspannung auf das Fliessen der Metalle Eisen, Kupfer und Nickel*, Zeitschr. für Physik, **36**, 1926.

2. G.I. TAYLOR and H. QUINEY, *The plastic distortion of metals*, Phil. Trans. Roy. Soc., **A230**, 323–362, 1931.

3. K. IKEGAMI, *A historical perspective of the experimental study of subsequent yield surfaces for metals* [in Japanese], J. Soc. Mat. Sci., **24**, 491–505 and 709–719, 1975; English translation by British Industrial and Scientific Translation Service BISITS, BISI 14420, Sept. 1976.

4. K. IKEGAMI, *Experimental plasticity of the anisotropy of metals, in mechanical behaviour of anisotropic solids*, Colloques Internationaux du CNRS, **295**, 201–242, 1982.

5. W. SZCZEPIŃSKI, L. DIETRICH and J. MIASTKOWSKI, *Plastic properties of metals. Part I* [in]: Experimental Methods in Mechanics of Solids, W. SZCZEPIŃSKI [Ed.], PWN-Elsevier, 1990.

6. J. MIASTKOWSKI and W. SZCZEPIŃSKI, *An experimental study of yield surfaces of prestrained brass*, Intern. J. Solids and Structures, 1, 189–194, 1965.

7. K. TURSKI, *Investigations of the effect of plastic prestrain for various paths of secondary loading* [in Polish], Mech. Teor. Stos., 9, 155–199, 1971.

8. W. SZCZEPIŃSKI, *On deformation-induced plastic anisotropy of sheet metals*, Arch. Mech., 45, 3–38, 1993.

9. G. SOCHA, W. SZCZEPIŃSKI, *On experimental determination of the coefficients of plastic anisotropy in sheet metals*, Arch. Mech., 46, 177–190, 1994.

10. W. SZCZEPIŃSKI, *On the effect of plastic deformation on yield condition*, Arch. Mech., 15, 275–296, 1963.

11. R. SZCZEBIOT, *Analysis of the strain hardening phenomena in an aluminium alloy prestrained plastically under complex stress states*, [in Polish], IFTR-Report, 21, 1991.

12. L. DIETRICH, K. TURSKI, *New method of sheet metal compression tests*, [in Polish], Engng Trans., 26, 91–99, 1978.

13. R. KIRYK, *Micromechanical model of the visco-plastic polycrystalline materials*, [in Polish], IFTR-Report, 38, 1992.

POLISH ACADEMY OF SCIENCES
INSTITUTE OF FUNDAMENTAL TECHNOLOGICAL RESEARCH.

On experimental determination of the coefficients of plastic anisotropy in sheet metals

G. SOCHA and W. SZCZEPIŃSKI (WARSZAWA)

PROBLEMS CONNECTED with experimental determination of coefficients of plastic anisotropy in sheet metals are discussed and illustrated by experimental results. Some of the coefficients can be determined directly, the others with the use of various non-direct measuring techniques only. It is shown that various shearing tests techniques are of questionable accuracy. In the theoretical analysis, a certain anisotropic yield condition accounting for the Bauschinger effect is used.

1. Introduction

WHEN ANALYZING theoretically various processes of sheet metal forming it is necessary to know the yield criterion with all the anisotropy coefficients (moduli) experimentally determined. The deformation-induced plastic anisotropy of sheet metals is very complex since the plastic deformation during the manufacturing process depends on numerous factors, such as multistage rolling, hot or cold rolling, frictional conditions that exist the interfaces between the rolls and the work-piece. Thus it is rather difficult to expect that the plastic anisotropy of sheet metals could be described by an universal theory. Recently a number of new proposals concerning the form of the yield condition for sheet metals have been published in order to describe, as accurately as possible, their real plastic properties. A comprehensive review of these works has been given in the previous paper [1] of the second author.

As the basic yield criterion for orthotropic sheet metals the HILL's criterion ([2] and [3]) is commonly used. It can be written in the following form

$$(1.1) \qquad \frac{1}{Y_x^2}\sigma_x^2 - \left(\frac{1}{Y_x^2} + \frac{1}{Y_y^2} - \frac{1}{Y_z^2} \right) \sigma_x\sigma_y + \frac{1}{Y_y^2}\sigma_y^2 + \frac{1}{Q^2}\tau_{xy}^2 = 1,$$

where Y_x, Y_y, Y_z are yield stresses under uniaxial tension (compression) in directions x, y, z, respectively, and Q stands for the yield stress in shear with respect to the principal axes x, y of anisotropy in plane of the sheet. The z-axis is perpendicular to sheet's surface, and the x-axis coincides with the rolling direction.

In most existing proposals of yield conditions for anisotropic sheet metals the Bauschinger effect is not taken into account. However, this effect is very distinctly observed in some sheet metals (see e.g. [4]). If the Bauschinger effect is to be accounted for, the yield condition for three-dimensional stress states may

be assumed in the following form (cf. [5] and also [1]):

$$(1.2) \quad k_{12}(\sigma_x - \sigma_y)^2 + k_{23}(\sigma_y - \sigma_z)^2 + k_{31}(\sigma_z - \sigma_x)^2 + k_{44}\tau_{yz}^2 + k_{55}\tau_{zx}^2$$

$$+ k_{66}\tau_{xy}^2 - b_{12}(\sigma_x - \sigma_y) - b_{23}(\sigma_y - \sigma_z) - b_{31}(\sigma_z - \sigma_x) = 1.$$

Physical interpretation of the anisotropy coefficients k_{ij} and b_{ij} may be found by analysing uniaxial stress states, each with only one non-vanishing stress component. By considering uniaxial tension (compression) states we obtain the relations

$$(1.3) \quad \begin{aligned} k_{12} &= \frac{1}{2}\left(\frac{1}{Y_x Z_x} + \frac{1}{Y_y Z_y} - \frac{1}{Y_z Z_z}\right), \\ k_{23} &= \frac{1}{2}\left(-\frac{1}{Y_x Z_x} + \frac{1}{Y_y Z_y} + \frac{1}{Y_z Z_z}\right), \\ k_{31} &= \frac{1}{2}\left(\frac{1}{Y_x Z_x} - \frac{1}{Y_y Z_y} + \frac{1}{Y_z Z_z}\right), \end{aligned}$$

where Y_x, Y_y, Y_z stand for the yield stresses of the material uniaxially tensioned in the directions x, y, z respectively, and Z_x, Z_y, Z_z are the absolute values of yield stresses under the respective uniaxial compression.

Considering uniaxial tensile (compressive) loadings in the x, y, z directions, respectively, we obtain also the following three relations

$$(1.4) \quad \begin{aligned} b_{31} - b_{12} &= \frac{1}{Y_x} - \frac{1}{Z_x}, \\ b_{12} - b_{23} &= \frac{1}{Y_y} - \frac{1}{Z_y}, \\ b_{23} - b_{31} &= \frac{1}{Y_z} - \frac{1}{Z_z}, \end{aligned}$$

for the moduli b_{12}, b_{23}, b_{31}. This system of equations has no unique solution. By assuming, for example, that $b_{31} = 0$ we obtain the relations

$$(1.5) \quad b_{31} = 0, \qquad b_{12} = -\frac{1}{Y_x} + \frac{1}{Z_x}, \qquad b_{23} = \frac{1}{Y_z} - \frac{1}{Z_z}.$$

From Eqs. (1.4) the relation follows

$$(1.6) \quad \frac{1}{Y_x} + \frac{1}{Y_y} + \frac{1}{Y_z} = \frac{1}{Z_x} + \frac{1}{Z_y} + \frac{1}{Z_z}.$$

The anisotropy of plastic strain increments may be used for indirect measurements of the anisotropy coefficients appearing in yield condition (1.2). For

materials with the Bauschinger effect the expressions for plastic strain increments associated with the yield condition (1.2) are as follows:

(1.7)
$$d\varepsilon_x = d\lambda \left\{ 2\left[k_{12}(\sigma_x - \sigma_y) - k_{31}(\sigma_z - \sigma_x)\right] - b_{12} + b_{31} \right\},$$
$$d\varepsilon_y = d\lambda \left\{ 2\left[-k_{12}(\sigma_x - \sigma_y) + k_{23}(\sigma_y - \sigma_z)\right] + b_{12} - b_{23} \right\},$$
$$d\varepsilon_z = d\lambda \left\{ 2\left[-k_{23}(\sigma_y - \sigma_z) + k_{31}(\sigma_z - \sigma_x)\right] + b_{23} - b_{31} \right\}.$$

2. Yield condition with Bauschinger effect for sheet metals

For sheet metals in which there exists a plane stress state, we have

$$\sigma_z = \tau_{zx} = \tau_{zy} = 0.$$

For plane stress states the yield condition (1.2) takes the following form:

(2.1)
$$\frac{1}{Y_x Z_x}\sigma_x^2 - \left(\frac{1}{Y_x Z_x} + \frac{1}{Y_y Z_y} - \frac{1}{Y_z Z_z}\right)\sigma_x \sigma_y + \frac{1}{Y_y Z_y}\sigma_y^2$$
$$+ \frac{1}{Q^2}\tau_{xy}^2 + \left(\frac{1}{Y_x} - \frac{1}{Z_x}\right)\sigma_x + \left(\frac{1}{Y_y} - \frac{1}{Z_y}\right)\sigma_y = 1,$$

where $Q = 1/\sqrt{k_{66}}$ is the yield locus in shear.

In the space of non-vanishing stress components σ_x, σ_y, τ_{xy} yield condition (2.1) is represented by an ellipsoid shown in Fig. 1. Central point O_1 of the ellipsoid is shifted in the σ_x, σ_y-plane with respect to the origin O of the reference system.

Expressions (1.7) for plastic strain increments take for the plane stress conditions the following form:

(2.2)
$$d\varepsilon_x = d\lambda \left[\frac{2}{Y_x Z_x}\sigma_x - \left(\frac{1}{Y_x Z_x} + \frac{1}{Y_y Z_y} - \frac{1}{Y_z Z_z}\right)\sigma_y + \frac{1}{Y_x} - \frac{1}{Z_x}\right],$$
$$d\varepsilon_y = d\lambda \left[\frac{2}{Y_y Z_y}\sigma_y - \left(\frac{1}{Y_x Z_x} + \frac{1}{Y_y Z_y} - \frac{1}{Y_z Z_z}\right)\sigma_x + \frac{1}{Y_y} - \frac{1}{Z_y}\right],$$
$$d\varepsilon_z = d\lambda \left[-\left(-\frac{1}{Y_x Z_x} + \frac{1}{Y_y Z_y} + \frac{1}{Y_z Z_z}\right)\sigma_y \right.$$
$$\left. -\left(\frac{1}{Y_x Z_x} - \frac{1}{Y_y Z_y} + \frac{1}{Y_z Z_z}\right)\sigma_x + \frac{1}{Y_z} - \frac{1}{Z_z}\right].$$

In the yield condition (2.1) there appear seven coefficients of plastic anisotropy. However, only six of them are independent if the equality (1.6) is to be satisfied. The anisotropy coefficients Y_x, Z_x, Y_y, Z_y and Z_z may in most cases be measured
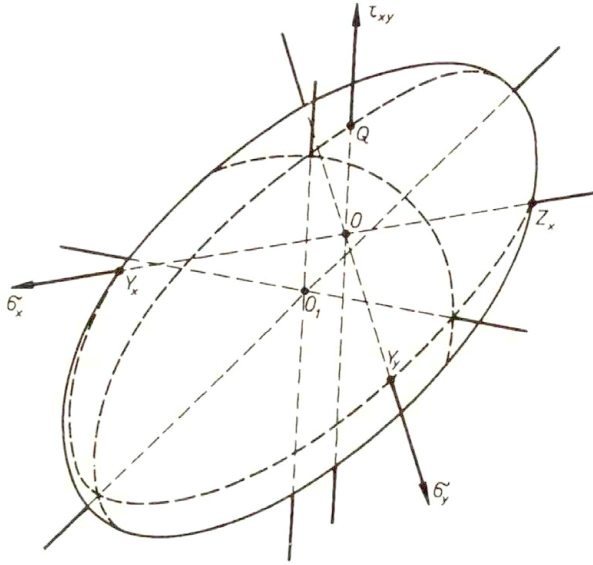
FIG. 1.

by simple uniaxial tension and compression tests. Theoretically the remaining coefficients can be deduced from the measured yield stresses for specimens cut out at various angles with respect to the x-direction and subjected to uniaxial tension or uniaxial compression (cf. HILL [2]).

Another indirect method of experimental determination of the anisotropy coefficients in sheet metals consist in measuring the ratios of strain increments (or strain rates) in longitudinal, transversal and through-thickness directions in uniaxially extended (compressed) specimens cut out from the sheet metal in question. This is the standard technique used in laboratory tests. However, when such a method is used, the values of anisotropy coefficients are usually deduced from the theoretical relations between the measured strain increment ratios resulting from the flow law associated with the yield condition (1.1). Thus the accuracy and credibility of such indirect method may be questioned. The observed differences between the values of certain anisotropy coefficients measured directly and indirectly are in some works, e.g. [6, 7], termed "anomaly" of plastic behaviour of the sheet metal in question.

Most reliable are those values of anisotropy coefficients which have been measured directly. For example, the value of yield stress Z_z under simple compression in the through-thickness direction may be measured on several test-pieces cut out from the sheet and made to adhere to each other by using some adhesive – ref. e.g. [8]. However, it is not possible to measure directly the tensile yield stress Y_z in this direction. Certain technical difficulties arise in direct determination of the yield stress in shear Q. This problem will be discussed later on.

3. Example of experimental determination of the state of plastic anisotropy in a sheet metal

For experimental tests a sheet 6 mm thick of an Al-2%Mg aluminium alloy was used. Stress-strain diagrams for two identical specimens cut out from the sheet in the rolling direction (RD) and loaded by uniaxial tension are shown in Fig. 2. The averaged conventional yield stress $Y_x = 112$ MPa has been estimated in the manner shown in the figure as the point of intersection of extrapolated curvlinear part of the diagram with its extrapolated straight initial portion. All tests have been performed on the INSTRON 1251 machine.
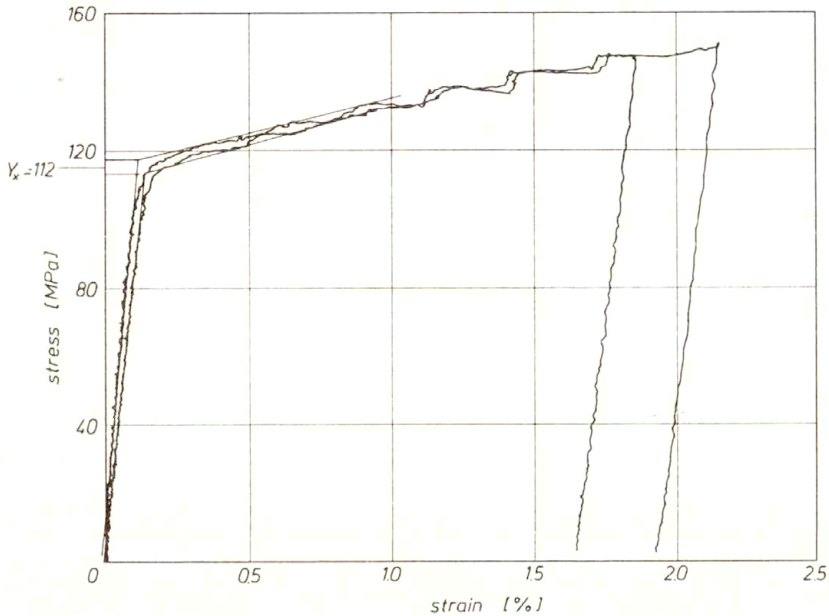

FIG. 2.

For tensile specimens cut out in the direction perpendicular to the rolling direction (TD) the averaged conventional yield stress was found to be $Y_y = 113.5$ MPa – Fig. 3.

In Figs. 4 and 5 are shown stress-strain diagrams for uniaxial compression of specimens cut out in the rolling direction and in the transversal direction, respectively. The conventional values of yield stresses are

$$Z_x = 115.2 \text{ MPa}, \qquad Z_y = 113.6 \text{ MPa}.$$

They differ only slightly from the corresponding yield stresses in tension

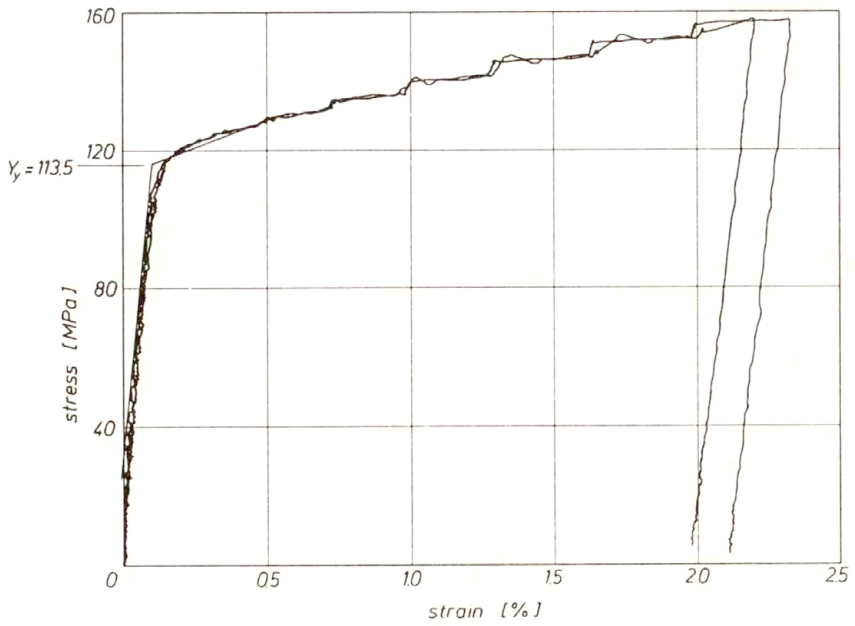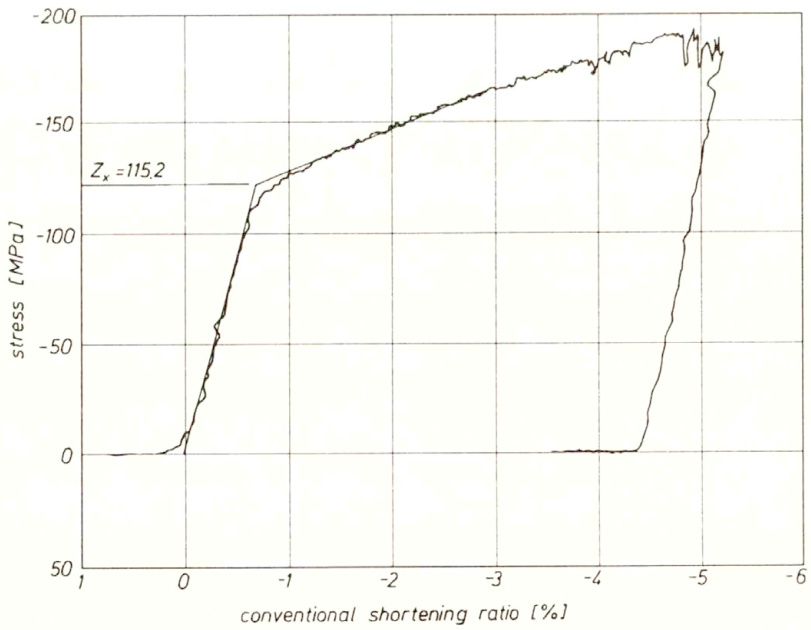$$Y_x = 112 \text{ MPa}, \qquad Y_y = 113.5 \text{ MPa}.$$
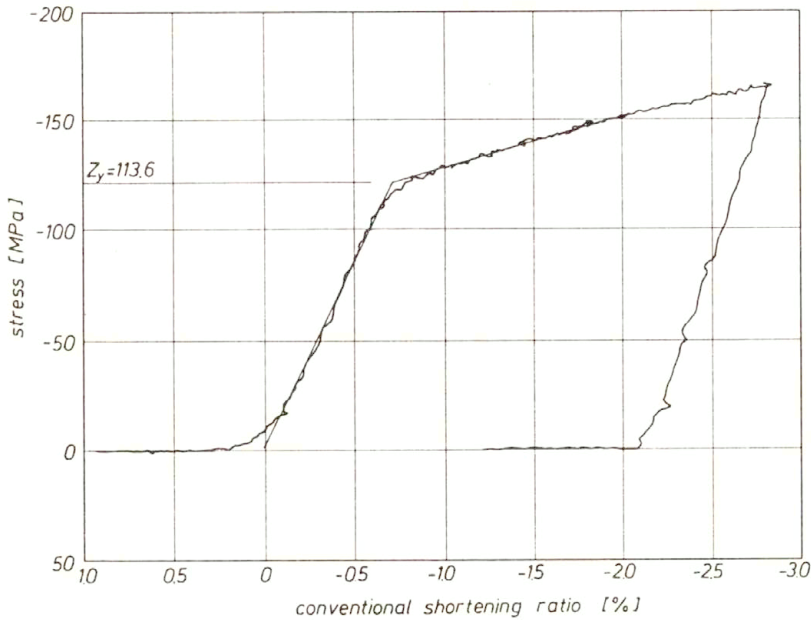
FIG. 3.

FIG. 4.

FIG. 5.

Thus for the material in question we shall aproximately assume that

$$Y_x = Y_y = Z_x = Z_y = Y_0 = 113.6\,\text{MPa},$$

where $Y_0 = 113.6\,\text{MPa}$ is the mean value of all four yield stresses.

Now instead of the general yield condition (2.1) we shall write (cf. [1])

(3.1)
$$\sigma_x^2 - \left(2 - \frac{Y_0^2}{Y_z Z_z}\right)\sigma_x \sigma_y + \sigma_y^2 + \frac{Y_0^2}{Q^2}\tau_{xy}^2 = Y_0^2.$$

However, in this case from the relation (1.6) results the equality $Y_z = Z_z$. We shall show experimentally that for the material in question this equality is not satisfied and that yield condition (2.1) does not describe fully the real plastic properties of the material in question.

The through-thickness yield stress Z_z was measured by a compression test on a set of several penny-shaped test-pieces cut out from the sheet and made to adhere to each other. The height of the cylindrical specimen composed in this manner was three times larger than its diameter. The compression diagram is shown in Fig. 6. The conventional yield locus

(3.2)
$$Z_z = 123.5\,\text{MPa}$$

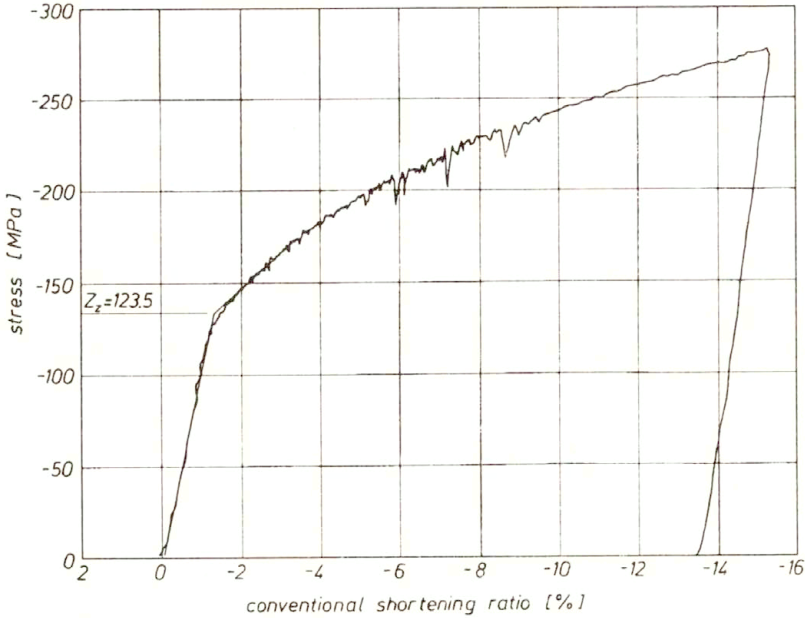has been estimated in the manner shown in the figure.

FIG. 6.

To estimate the value of yield stress in tension Y_z in the through-thickness direction we shall use the indirect method by measuring the strain rates $\dot{\varepsilon}_x, \dot{\varepsilon}_y$ and $\dot{\varepsilon}_z$, in the specimen cut out in the y-direction (transversal direction) and loaded by uniaxial tension (cf. Fig. 3). The diagrams of plastic strain versus time are shown in Fig. 7. These diagrams are curvilinear and therefore the strain rates change their values during the course of the deformation process. Thus a certain convention has to be introduced. For the plastic strain $\varepsilon_y = 0.1\%$ the following values of strain rates have been estimated from the diagrams

$$
\begin{aligned}
\dot{\varepsilon}_x &= -3.19 \cdot 10^{-6} \text{sec}^{-1}\,, \\
\dot{\varepsilon}_y &= 7.32 \cdot 10^{-6} \text{sec}^{-1}\,, \\
\dot{\varepsilon}_z &= -4.97 \cdot 10^{-6} \text{sec}^{-1}\,.
\end{aligned}
$$

(3.3)

Theoretical relations (2.2) take for this particular case the following forms:

$$
\begin{aligned}
d\varepsilon_x &= -d\lambda \left(\frac{2}{Y_0^2} - \frac{1}{Y_z Z_z} \right) \sigma_y\,, \\
d\varepsilon_y &= d\lambda \frac{2}{Y_0^2} \sigma_y\,, \\
d\varepsilon_z &= -d\lambda \left(\frac{1}{Y_z Z_z} \sigma_y + \frac{1}{Y_z} - \frac{1}{Z_z} \right)\,.
\end{aligned}
$$

(3.4)
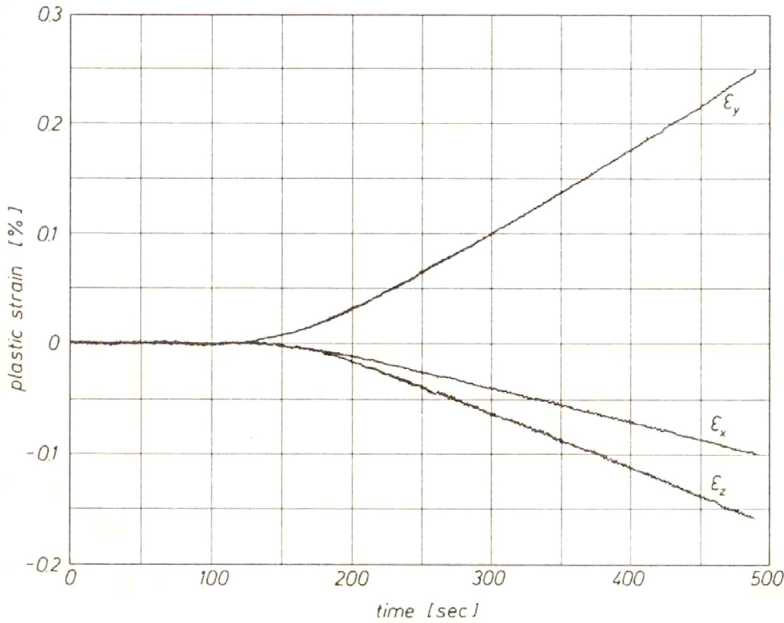
FIG. 7.

In the state of plastic yielding of the specimen the σ_y stress must be equal to the yield stress Y_0. Thus we have $\sigma_y = Y_0$. Now we can write the equation

$$\frac{d\varepsilon_x}{d\varepsilon_z} = \frac{\dot{\varepsilon}_x}{\dot{\varepsilon}_z} = \frac{\dfrac{2}{Y_0} - \dfrac{Y_0}{Y_z Z_z}}{\dfrac{Y_0}{Y_z Z_z} + \dfrac{1}{Y_z} - \dfrac{1}{Z_z}} = 0.642\,,$$

from which the value of Y_z may be found, because all the remaining parameters in this equation have been measured directly. Finally we obtain

(3.5) $$Y_z = 94.4\,\text{MPa}.$$

Note that the value of Y_z may also be found from the relations $d\varepsilon_y/d\varepsilon_z$ or $d\varepsilon_y/d\varepsilon_x$. These alternative values are $Y_z = 95.9\,\text{MPa}$ and $Y_z = 93.0\,\text{MPa}$, respectively. The mean value of Y_z is

(3.6) $$(Y_z)_m = 94.4\,\text{MPa}.$$

It differs remarkably from the yield stress $Z_z = 123.5\,\text{MPa}$ measured directly under compressive loading.

Since in-plane properties of the sheet are found to be almost isotropic without the Bauschinger effect, we shall recalculate the value of Y_z using the expressions

for strain increments associated with the yield condition (1.1). For the test in question these expressions take the following form:

(3.7)
$$d\varepsilon_x = -d\lambda \left(\frac{2}{Y_0^2} - \frac{1}{Y_z^2} \right) \sigma_y,.$$

$$d\varepsilon_y = d\lambda \frac{2}{Y_0^2} \sigma_y,$$

$$d\varepsilon_z = -d\lambda \frac{1}{Y_z^2} \sigma_y.$$

Thus we can write the expression

$$\frac{d\varepsilon_x}{d\varepsilon_z} = \frac{\dot{\varepsilon}_x}{\dot{\varepsilon}_z} = \frac{\dfrac{2}{Y_0} - \dfrac{Y_0}{Y_z^2}}{\dfrac{Y_0}{Y_z^2}} = 0.642$$

from which we obtain

(3.8) $Y_z = 102.9\,\text{MPa}.$

If the relation $d\varepsilon_y/d\varepsilon_z$ or $d\varepsilon_y/d\varepsilon_x$ are used, the alternative values are $Y_z = 97.6\,\text{MPa}$ and $Y_z = 106.9\,\text{MPa}$, respectively. The mean value is

(3.9) $(Y_z)_m = 102.5\,\text{MPa}.$

The numerical difference between Y_z and Z_z calculated according to the two assumptions is thought too great to be attributed to the inaccuracy of measurements of strain rates, or to the use of expressions (3.4) or (3.7) for indirect evaluation of Y_z. It indicates that the material in question really exhibits the Bauschinger effect across the thickness. The existence of the Bauschinger effect in the direction perpendicular to the surface of the rolled sheet metal seems obvious and physically justified, because during the rolling operations the material has been strongly plastically compressed in this direction. This effect neglected in the theories of plastic anisotropy of sheet metals may be called the "hidden" Bauschinger effect. It is not excluded that this "hidden" effect contributes to the so-called "anomalous" behaviour of sheet metals observed in some experimental studies (e.g. [6]).

The discrepancy between the measured value of Y_z and the completely different theoretical value $Y_z = Z_z$ resulting from the relation (1.6) indicates that the yield condition (2.1) does not fully correspond to the real plastic properties of the tested material. Problems connected with the formulation of the yield conditions for metals with deformation-induced anisotropy have been discussed in [1]. Note that non-quadratic yield conditions [7], proposed in connection with the observed so-called "anomalous" behaviour of sheet metals (see e.g. [6]) do not account for the Bauschinger effect and cannot be used in our case.

4. Direct and indirect measurements of the yield stress in shear

Usually the yield stress in shear Q is measured non-directly. It may be deduced from the tension test of a specimen cut out at angle of 45° to the rolling direction (cf. Hill [2]). To estimate the value of Q, two tensile specimens have been cut out from the sheet at the angle $\alpha = 45°$ with respect to the rolling direction. The tension diagrams are shown in Fig. 8. Conventional yield stress for these
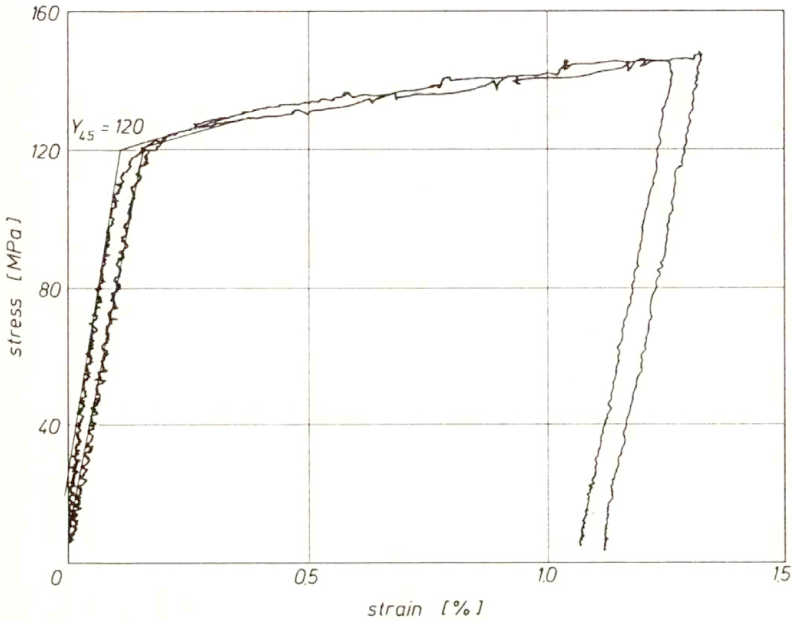
Fig. 8.

specimens is $Y_{45} = 120$ MPa. Thus yield stresses related to the reference system x, y are

(4.1) $$\sigma_x = \sigma_y = \tau_{xy} = \frac{1}{2}Y_{45} = 60\,\text{MPa}.$$

By substituting these values and also the experimentally determined yield stresses Y_0, Y_z and Z_z to the yield condition (3.1), we obtain

(4.2) $$Q = 68.65\,\text{MPa}.$$

Now we shall compare this indirectly estimated value of Q with the results of direct shearing tests. Two various shear tests have been performed, each with the use of a specimen of a different type.

The specimen of the first type is shown in Fig. 9. It is analogous to that used by Sato et al. [9]. Preparation of such a specimen is simple. Standard grips of ordinary testing machine may be used to hold the specimen. The diagram of
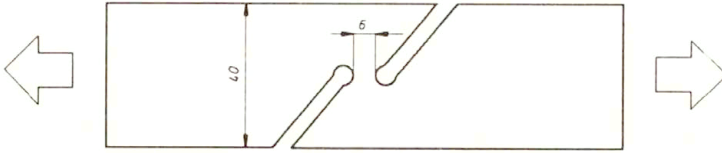
FIG. 9.

conventional shear stress versus displacement is shown in Fig. 10. The diagram is very smoothly curved in contrast to all previous diagrams for tension and compression tests. This is a consequence of the strong stress concentration in the specimen in the initial elastic state, and by further evolution of plastic zones in the deforming region. Additionally the exact determination of the shear strain is very difficult. This problem has been analysed in [10]. Any method of estimating the shear strain is of questionable accuracy. Thus any convention, according to which the yield stress in shear resulting from such tests could be estimated, can hardly be used. For comparison, the value $Q = 68.5\,$MPa measured indirectly [cf. (4.2)] has been shown in figure.
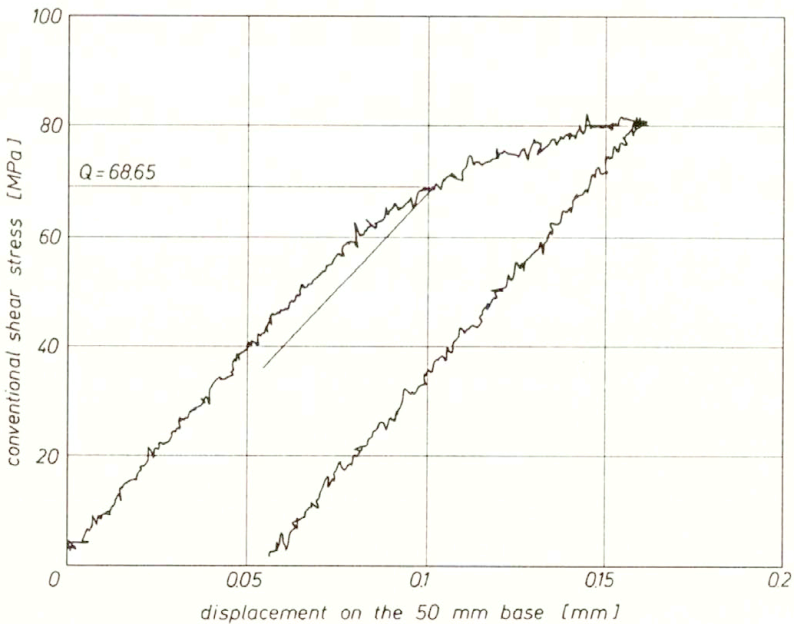
FIG. 10.

Similar difficulties arise when symetrical specimens of the type shown in Fig. 11 are used. The shear stress versus displacement diagram for the test with the use of specimens of this type is shown in Fig. 12. The value $Q = 68.65\,$MPa found indirectly is shown for comparison.
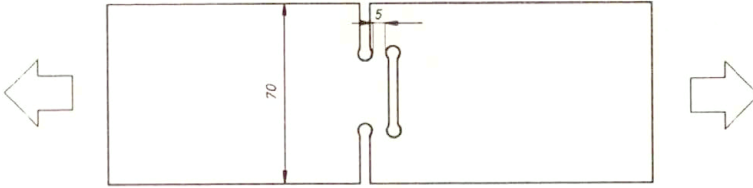
FIG. 11.
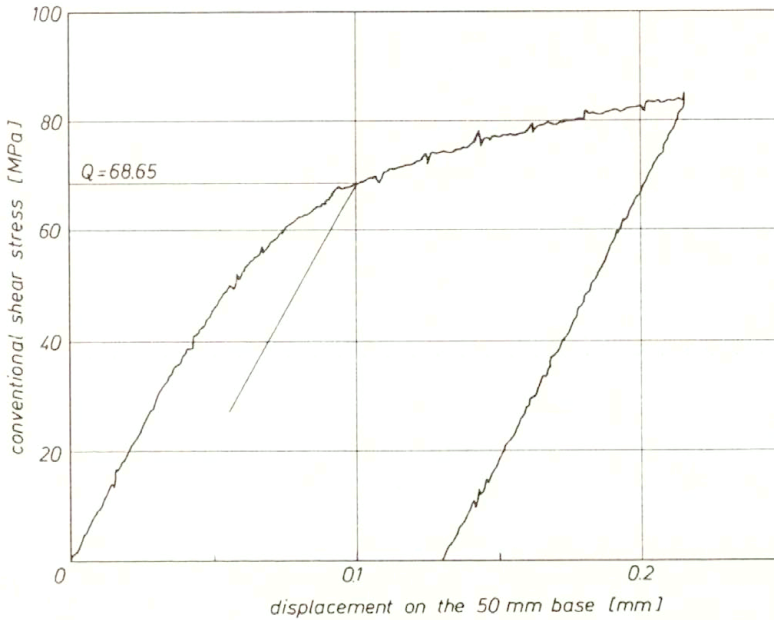
FIG. 12.

5. Conclusions

Experimental results analysed in this paper indicate that yield conditions of the type (2.1) and (3.1) accounting for the Bauschinger effect do not fully correspond to the real plastic behaviour of sheet metals displaying across the thickness this effect, induced by considerable compression in this direction during rolling operations. Neverthless, such yield conditions seem to constitute a certain alternative to yield condition (1.1) or to various so-called non-quadratic conditions, neglecting the Bauschinger effect completely. It is shown, moreover, that indirect methods of measuring the yield stress in shear Q should be recommended as a standard technique, since direct measuring methods are of questionable accuracy.

Acknowledgement

References

1. W. SZCZEPIŃSKI, *On deformation-induced plastic anisotropy of sheet metals*, Arch. Mech., **45**, 3–38, 1993.

2. R. HILL, *A theory of yielding and plastic flow of anisotropic metals*, Proc. Roy. Soc. London, A193, 281–297, 1948.

3. R. HILL, *The mathematical theory of plasticity*, Oxford 1956.

4. A. LITEWKA, *Plastic flow of anisotropic aluminium alloy sheet metals*, Bull. Acad. Polon. Sci., **25**, 475–484, 1977.

5. T. OTA, A. SHINDO, F. FUKUOKA, *A consideration on anisotropic yield criterion*, Proc. 9th Jap. Nat. Congr. Appl. Mech., 117–120, 1959.

6. J. WOODTHROPE and J. PEARCE, *The anomalous behaviour of aluminium sheet under biaxial tension*, Intern. J. Mech. Sci., **12**, 341–347, 1970.

7. R. HILL, *Theoretical plasticity of textured aggregates*, Math. Proc. Cambridge Phil. Soc., **85**, 179–191, 1979.

8. M. GOTOH, *A theory of plastic anisotropy based on a yield function of fourth order (plane stress state)*. I. Intern. J. Mech. Sci., **19**, 505–512, 1977.

9. K. SATO, Y. MIYAKI, Y. TOYABARA, *Inplane single shear deformation of Ti-6Al-4V alloy sheet under transformational superelasticity condition*, Proc. 13th Riso Intern. Symp. on Material Sci., Riso Nat. Lab. Rosklide, Denmark, 423–429, 1992.

10. G. SOCHA, *Optimal design of specimens for pure shear tests of sheet metals*, Engng. Trans., **42**, 1–2, 1994.

POLISH ACADEMY OF SCIENCES
INSTITUTE OF FUNDAMENTAL TECHNOLOGICAL RESEARCH.

Stokes flow about a porous spherical particle

B. S. PADMAVATHI, T. AMARANATH (HYDERABAD) and
D. PALANIAPPAN (BANGALORE)

STOKES FLOW of a viscous, incompressible fluid past a porous spherical particle is considered, using Darcy's law for the flow in the porous region and Saffman's conditions at the surface of the sphere. The velocity and pressure fields of the modified flow in the presence of the porous spherical boundary are obtained. The formulae for drag and torque are found in terms of the undisturbed velocity which are analogous to the well-known Faxén's laws. It is found that the torque on a porous sphere is always less than that on a rigid sphere, whereas the drag in general is not. It is also observed that effective viscosity of a dilute suspension of porous spheres decreases as compared to that of rigid particles of the same size. Some illustrative examples are discussed to justify the usefulness of the results.

1. Introduction

THE PROBLEM OF SLOW, streaming motion of a viscous fluid past a porous spherical particle assuming Darcy's law for the fluid in the porous region ($0 \leq r \leq a$) was studied by JOSEPH and TAO [1]. Assuming the permeability to be small, they have considered the no-slip condition for the exterior tangential velocity as one of the boundary conditions at the permeable surface, the other boundary conditions being continuity of pressure and normal velocity. The no-slip condition was justified by JOSEPH and TAO [2], and several problems relating to the lubrication of porous bearings were solved using this condition (see [2, 3] and the references therein). In [1], it was found that the drag on the porous sphere is that of a rigid sphere with reduced radius. But recently, PADMAVATHI and AMARANATH [4] have shown that by employing the conditions as in [1], in the general case, the drag is not always less than that of a rigid sphere; indeed, it decreases or increases depending on whether the undisturbed velocity is harmonic or purely biharmonic, respectively.

However, the experiments of BEAVERS and JOSEPH [5] suggested that there is actually some slip at the boundary, in particular, when the permeability is large. To accommodate for this, they [5] proposed a slip boundary condition for plane boundaries

$$\frac{du}{dy} = \frac{\alpha}{\sqrt{k}}(u - Q),$$

where u is the velocity parallel to the surface, y is the coordinate normal to the surface, Q is the velocity inside the porous medium, k is the permeability and α is a dimensionless constant whose value depends on the properties of the porous medium. Their experimental values showed a reasonable agreement with

the values predicted by this condition. Using a statistical approach to extend Darcy's law to non-homogeneous porous media, SAFFMAN [6] gave a theoretical justification of the condition proposed by BEAVERS and JOSEPH [5]. He showed that in the limit $k \to 0$

$$u = \frac{\sqrt{k}}{\alpha} \frac{du}{dy} + O(k)$$

at the boundary. NEALE *et al.* [7] have reviewed the different boundary conditions that can be applied to the Darcy law and arrived at the conclusion that the one derived by SAFFMAN [6] was the most satisfactory one. Therefore for small values of k, Saffman's condition is more appropriate than no-slip condition.

In this paper, we shall discuss an arbitrary Stokes flow past a sphere using Darcy's law for the fluid inside the porous region ($r \leq a$) with SAFFMAN'S [6] boundary conditions. We derive the expressions for drag and torque and show that while the torque is reduced as compared to the rigid case, in general the drag may not. However the drag is reduced whenever the velocity of the basic flow is harmonic.

2. Mathematical formulation

Let us consider a stationary porous sphere of radius a in an arbitrary Stokes flow in a viscous, incompressible fluid. For the flow outside the sphere, the governing equations are the Stokes equations

(2.1) $$\mu \nabla^2 \mathbf{V} = \nabla p,$$
(2.2) $$\nabla \cdot \mathbf{V} = 0,$$

where μ is the coefficient of viscosity, $\mathbf{V}$ the velocity and p the pressure of the liquid.

The flow inside the porous sphere ($0 \leq r \leq a$) is governed by Darcy's law

(2.3) $$\mathbf{Q} = -\frac{k}{\mu} \nabla P,$$
(2.4) $$\nabla^2 P = 0,$$

where $\mathbf{Q}$ is the volume rate of flow per unit cross-sectional area, P the pressure and $k > 0$ is the permeability coefficient. $\mathbf{Q}$ represents the filter velocity rather than the actual velocity of the fluid in the pores.

The boundary conditions on $r = a$ (in spherical polar coordinates (r, θ, ϕ)) are:

a) the pressure is continuous at the boundary of the sphere

(2.5) $$p(a, \theta, \phi) = P(a, \theta, \phi);$$

b) the normal velocity is continuous at the boundary of the sphere

(2.6) $$q_r(a, \theta, \phi) = Q_r(a, \theta, \phi);$$

c) Saffman's condition for tangential velocity on the sphere is

(2.7) $$q_\theta(a, \theta, \phi) = \lambda\sqrt{k}\frac{\partial q_\theta}{\partial r}(a, \theta, \phi),$$

and

(2.8) $$q_\phi(a, \theta, \phi) = \lambda\sqrt{k}\frac{\partial q_\phi}{\partial r}(a, \theta, \phi),$$

where λ is a dimensionless constant characteristic of the porous medium. NEALE [7] and HABER and MAURI [8] have noted that much of the data of BEAVERS and JOSEPH [5] can be reasonably correlated by assigning λ the value of unity. Therefore the conditions (2.7) and (2.8) on $r = a$ are

(2.9) $$q_\theta(a, \theta, \phi) = \sqrt{k}\frac{\partial q_\theta}{\partial r}(a, \theta, \phi),$$

(2.10) $$q_\phi(a, \theta, \phi) = \sqrt{k}\frac{\partial q_\phi}{\partial r}(a, \theta, \phi).$$

3. Method of solution

We assume the following representation proposed by PALANIAPPAN *et al.* [9] for the velocity and pressure in the region $r > a$

(3.1) $$V = \operatorname{curl}\operatorname{curl}(rA) + \operatorname{curl}(rB).$$

(3.2) $$p = p_0 + \mu\frac{\partial}{\partial r}(r\nabla^2 A),$$

where

(3.3) $$\nabla^4 A = 0, \qquad \nabla^2 B = 0.$$

In the absence of a porous sphere, suppose the basic flow is given by a biharmonic A_0 and a harmonic B_0 whose form near $r = a$ is as follows:

(3.4) $$A_0(r, \theta, \phi) = \sum_{n=1}^{\infty}\left[\alpha_n r^n + \alpha_n' r^{n+2}\right]S_n(\theta, \phi).$$

(3.5) $$B_0(r, \theta, \phi) = \sum_{n=1}^{\infty}\chi_n r^n T_n(\theta, \phi),$$

where

$$(3.6) \qquad S_n(\theta, \phi) = \sum_{m=0}^{n} P_n^m(\zeta)(A_{nm} \cos m\phi + B_{nm} \sin m\phi),$$

$$(3.7) \qquad T_n(\theta, \phi) = \sum_{m=0}^{n} P_n^m(\zeta)(C_{nm} \cos m\phi + D_{nm} \sin m\phi), \qquad \zeta = \cos\theta,$$

and the constants α_n, α_n', χ_n, A_{nm}, B_{nm}, C_{nm} and D_{nm} are all known, and P_n^m is the Legendre polynomial. Now in the presence of a porous sphere of radius a in the flow field of Eqs. (3.4) and (3.5), the modified field is assumed as follows:

$$(3.8) \qquad A(r, \theta, \phi) = \sum_{n=1}^{\infty} \left[\alpha_n r^n + \alpha_n' r^{n+2} + \frac{\beta_n}{r^{n+1}} + \frac{\beta_n'}{r^{n-1}} \right] S_n(\theta, \phi),$$

$$(3.9) \qquad B(r, \theta, \phi) = \sum_{n=1}^{\infty} \left[\chi_n r^n + \frac{\gamma_n}{r^{n+1}} \right] T_n(\theta, \phi), \qquad r \geq a$$

and

$$(3.10) \qquad P(r, \theta, \phi) = p_0 + \sum_{n=1}^{\infty} \delta_n r^n S_n(\theta, \phi), \qquad r \leq a.$$

The components of velocity and pressure from Eqs. (3.8) and (3.9) for $r > a$ are

$$(3.11) \qquad q_r = \sum_{n=1}^{\infty} n(n+1) \left[\alpha_n r^{n-1} + \alpha_n' r^{n+1} + \beta_n r^{-n-2} + \beta_n' r^{-n} \right] S_n(\theta, \phi),$$

$$(3.12) \qquad q_\theta = \sum_{n=1}^{\infty} \left[(n+1)\alpha_n r^{n-1} + (n+3)\alpha_n' r^{n+1} - n\beta_n r^{-n-2} \right.$$

$$\left. -(n-2)\beta_n' r^{-n} \right] \frac{\partial}{\partial\theta} S_n(\theta, \phi) + \operatorname{cosec}\theta \sum_{n=1}^{\infty} \left[\chi_n r^n + \gamma_n r^{-n-1} \right] \frac{\partial}{\partial\phi} T_n(\theta, \phi),$$

$$(3.13) \qquad q_\phi = \frac{1}{\sin\theta} \sum_{n=1}^{\infty} \left[(n+1)\alpha_n r^{n-1} + (n+3)\alpha_n' r^{n+1} - n\beta_n r^{-n-2} \right.$$

$$\left. -(n-2)\beta_n' r^{-n} \right] \frac{\partial}{\partial\phi} S_n(\theta, \phi) - \sum_{n=1}^{\infty} \left[\chi_n r^n + \gamma_n r^{-n-1} \right] \frac{\partial}{\partial\theta} T_n(\theta, \phi),$$

$$(3.14) \qquad p = p_0 + \mu \sum_{n=1}^{\infty} \left[2(2n+3)(n+1)r^n \alpha_n' + \frac{2n(2n-1)}{r^{n+1}} \beta_n' \right] S_n(\theta, \phi).$$

Similarly, for $r < a$, from Eq. (3.10) we have

$$(3.15) \qquad Q_r = -\frac{k}{\mu} \sum_{n=1}^{\infty} n\delta_n r^{n-1} S_n(\theta, \phi),$$

$$(3.16) \qquad Q_\theta = -\frac{k}{\mu} \sum_{n=1}^{\infty} \delta_n r^{n-1} \frac{\partial}{\partial \theta} S_n(\theta, \phi),$$

$$(3.17) \qquad Q_\phi = -\frac{k}{\mu \sin \theta} \sum_{n=1}^{\infty} \delta_n r^{n-1} \frac{\partial}{\partial \phi} S_n(\theta, \phi),$$

$$(3.18) \qquad P = p_0 + \sum_{n=1}^{\infty} \delta_n r^n S_n(\theta, \phi).$$

The expressions given in Eqs. (3.11)–(3.18) satisfy the boundary conditions given in Eqs. (2.5), (2.6), (2.9) and (2.10) on $r = a$ if

$$\beta_n = \left\{ (n+1)(2n-1) \left[a^3 - a^2\sqrt{k} + 2nka - 2n(n-1)k\sqrt{k} \right] a^{2n+1} \alpha_n \right.$$
$$+ (2n+1) \left[(n+1)a^3 - 3(n+1)a^2\sqrt{k} + 4(n^2+n-3)ka \right.$$
$$\left. -6n(n+1)k\sqrt{k} \right] a^{2n+3} \alpha_n' \Big\} / X_n,$$

$$\beta_n' = - \left\{ (n+1)(2n+1) \left[a + \sqrt{k} \right] a^{2n+1} \alpha_n \right.$$
$$+ (n+1)(2n+3) \left[a^3 + 2nka - a^2\sqrt{k} + 2n(n+2)k\sqrt{k} \right] a^{2n+1} \alpha_n' \Big\} / X_n,$$

$$\delta_n = -2\mu(n+1)(2n+1) \left\{ n(2n-1) \left(a + \sqrt{k} \right) \alpha_n \right.$$
$$+ (2n+3)a^2 \left[(n-2)a - 3n\sqrt{k} \right] \alpha_n' \Big\} / X_n,$$

$$\gamma_n = \frac{\left(n\sqrt{k} - a \right) a^{2n+1}}{\left[(n+1)\sqrt{k} + a \right]} X_n,$$

where

$$X_n = \left[2(n+1)a^3 + 2n^2(2n-1)ka + 4n(n+1)a^2\sqrt{k} + 2n^2(n+2)(2n-1)k\sqrt{k} \right].$$

It may be noted that by setting

$$A(r, \theta, \phi) \equiv A(r, \theta), \qquad B(r, \theta, \phi) \equiv 0, \qquad \frac{\partial A}{\partial \theta} = \frac{\psi}{r \sin \theta}.$$

where ψ is the Stokes stream function, we can recover the corresponding axisymmetric case.

4. Faxén's law for a porous sphere

The force **D** exerted on the sphere by the fluid in the region $r > a$ is found by following the procedure given in [4]:

$$(4.1) \qquad \mathbf{D} = 6\pi\mu a \left(1 - \frac{(3k\sqrt{k} + ka + 2a^2\sqrt{k})}{(2a^3 + 4a^2\sqrt{k} + ka + 3k\sqrt{k})}\right) [\mathbf{V_0}]_0$$

$$+ \pi\mu a^3 \left(1 + \frac{3(3k\sqrt{k} + ka - 2a^2\sqrt{k})}{(2a^3 + 4a^2\sqrt{k} + ka + 3k\sqrt{k})}\right) \left[\nabla^2 \mathbf{V_0}\right]_0.$$

Similarly, the torque on the porous sphere is

$$(4.2) \qquad \mathbf{T} = 4\pi\mu a^3 \left(1 - \frac{3\sqrt{k}}{(2\sqrt{k} + a)}\right) [\nabla \times \mathbf{V_0}]_0,$$

where

$\mathbf{V_0}$ = velocity corresponding to the basic flow,

$[\ ]_0$ = evaluation at the origin $r = 0$.

When $k = 0$, the expressions for **D** and **T** coincide with the well-known Faxén's laws for a rigid sphere. When $\mathbf{V_0}$ is harmonic, $|\mathbf{D}| < |\mathbf{D_0}|$ where $|\mathbf{D_0}|$ is the drag on a rigid sphere (corresponding to $k = 0$). In general, it may increase or decrease depending on the value of k. However, the torque always decreases as compared to the rigid case, as seen from Eq. (4.2).

5. Effective viscosity

The effective viscosity μ^* of a dilute suspension of porous spherical particles, each of radius a, is found to be

$$(5.1) \qquad \mu^* = \mu\left\{1 + \frac{5}{2}\left(1 - \frac{(3a^2\sqrt{k} + 4ak + 16k\sqrt{k})}{(a^3 + 4ak + 4a^2\sqrt{k} + 16k\sqrt{k})}\right)\Phi\right\}.$$

where Φ is the concentration by volume of the fluid containing the spheres. This result coincides with Einstein's [10] result $\mu^* = \mu\{1 + (5/2)\Phi\}$ for a dilute suspension of rigid spheres when $k = 0$. It is observed that the effective viscosity of the dilute suspension of porous particles is lower than that of rigid particles of the same size.

6. Examples

6.1. Stokeslet

Consider a Stokeslet of strength $F_1/8\pi\mu$ located at $(0, 0, c)$, $(c > a)$ whose axis is along the positive direction of the x-axis. The corresponding expressions for

A_0 and B_0 due the Stokeslet are [4]

(6.1) $$A_0 = \frac{F_1}{8\pi\mu} \sum_{n=1}^{\infty} \left[\frac{r^{n+2}}{(n+1)(2n+3)c^{n+2}} - \frac{(n-2)r^n}{n(n+1)(2n-1)c^n} \right] P_n^1(\zeta)\cos\phi,$$

(6.2) $$B_0 = \frac{F_1}{4\pi\mu} \sum_{n=1}^{\infty} \left[\frac{r^n}{n(n+1)c^{n+1}} \right] P_n^1(\zeta)\sin\phi.$$

The modified flow fields in and around the porous sphere can now be written down using Eqs.(3.11)–(3.18). It is of interest to study the asymptotic behaviour (i.e., as $r \to \infty$) of the external flow field.

The asymptotic forms of the velocity components for large r are given by

(6.3) $$q_r(r,\theta,\phi) \sim \frac{F_1}{4\pi\mu} \left\{ 1 - \left(\frac{3a^3(a+\sqrt{k})}{2c(2a^3+4a^2\sqrt{k}+ka+3k\sqrt{k})} \right. \right.$$
$$\left. \left. + \frac{a^3(a^3+2ka-a^2\sqrt{k}+6k\sqrt{k})}{2c^3(2a^3+4a^2\sqrt{k}+ka+3k\sqrt{k})} \right) \right\} \frac{\sin\theta\cos\phi}{r},$$

(6.4) $$q_\theta(r,\theta,\phi) \sim \frac{F_1}{8\pi\mu} \left\{ 1 - \left(\frac{3a^3(a+\sqrt{k})}{2c(2a^3+4a^2\sqrt{k}+ka+3k\sqrt{k})} \right. \right.$$
$$\left. \left. + \frac{a^3(a^3+2ka-a^2\sqrt{k}+6k\sqrt{k})}{2c^3(2a^3+4a^2\sqrt{k}+ka+3k\sqrt{k})} \right) \right\} \frac{\cos\theta\cos\phi}{r},$$

(6.5) $$q_\phi(r,\theta,\phi) \sim \frac{F_1}{8\pi\mu} \left\{ 1 - \left(\frac{3a^3(a+\sqrt{k})}{2c(2a^3+4a^2\sqrt{k}+ka+3k\sqrt{k})} \right. \right.$$
$$\left. \left. + \frac{a^3(a^3+2ka-a^2\sqrt{k}+6k\sqrt{k})}{2c^3(2a^3+4a^2\sqrt{k}+ka+3k\sqrt{k})} \right) \right\} \frac{\sin\phi}{r}.$$

Hence the dominant flow at infinity is that due to a Stokeslet of strength F located at the origin and oriented along the x-axis, where

(6.6) $$F = \frac{F_1}{8\pi\mu} \left\{ 1 - \left(\frac{3a^3(a+\sqrt{k})}{2c(2a^3+4a^2\sqrt{k}+ka+3k\sqrt{k})} \right. \right.$$
$$\left. \left. + \frac{a^3(a^3+2ka-a^2\sqrt{k}+6k\sqrt{k})}{2c^3(2a^3+4a^2\sqrt{k}+ka+3k\sqrt{k})} \right) \right\}.$$

From Eq. (4.1) the drag on the porous sphere is

(6.7) $$\mathbf{D} = \left\{ \frac{3a^3(a+\sqrt{k})}{2c(2a^3+4a^2\sqrt{k}+ka+3k\sqrt{k})} \right.$$
$$\left. + \frac{a^3(a^3+2ka-a^2\sqrt{k}+6k\sqrt{k})}{2c^3(2a^3+4a^2\sqrt{k}+ka+3k\sqrt{k})} \right\} F_1 \hat{\mathbf{i}},$$

and from Eq. (4.2) the torque is

(6.8)
$$\mathbf{T} = \frac{a^3(a - \sqrt{k})}{(2\sqrt{k} + a)c^2} F_1 \hat{\mathbf{j}}.$$

6.2. Rotlet

Consider a rotlet of strength $F_3/8\pi\mu$ located at $(0, 0, c)$ $(c > a)$ whose axis is along the positive direction of z-axis. The basic flow is given by A_0 and B_0, where

(6.9)
$$A_0 = 0,$$

(6.10)
$$B_0 = \frac{F_3}{8\pi\mu c R_1},$$

where $R_1^2 = r^2 + c^2 - 2rc\cos\theta$.

We can rewrite B_0 as

(6.11)
$$B_0 = \frac{F_3}{8\pi\mu} \sum_{n=0}^{\infty} \frac{r^n}{c^{n+1}} P_n(\zeta).$$

The modified flow fields in and around the porous sphere can be obtained using Eqs. (3.11)–(3.18). The drag $\mathbf{D}$ on the porous sphere is zero. The torque $\mathbf{T}$ is

(6.12)
$$\mathbf{T} = \frac{a^3(a - \sqrt{k})}{(2\sqrt{k} + a)c^2} F_3 \hat{\mathbf{k}}.$$

Acknowledgement

References

1. D.D. Joseph and L.N. Tao, *The effect of permeability on the slow motion of a porous sphere in a viscous liquid*, ZAMM, **44**, 361–364, 1964.

2. D.D. Joseph and L.N. Tao, *Lubrication of a porous bearing*, J. Appl. Mech., Trans. ASME, Series E, **33**, 753–760, 1966.

3. D.D. Joseph and C.L. Shir, *Lubrication of a porous bearing – Stokes solution*, J. Appl. Mech., Trans. ASME, Series E, **33**, 761–767, 1966.

4. B.S. Padmavathi and T. Amaranath, *A solution for the problem of Stokes flow past a porous sphere*, ZAMP, **44**, 178–184, 1993.

5. G.S. Beavers and D.D. Joseph, *Boundary conditions at a naturally permeable wall*, J. Fluid Mech., **30**, 1, 197–207, 1967.

6. P.G. SAFFMANN, *On the boundary condition at the surface of a porous medium*, Studies Appl. Math., **50**, 93–101, 1971.

7. G. NEALE and N. EPSTEIN, *Creeping flow relative to permeable spheres*, Chem. Engng. Sci., **28**, 1865–1874, 1973.

8. S. HABER and R. MAURI, *Boundary conditions for Darcy's flow through porous media*, Int. J. Multiphase Flow, **9**, 5, 561–574, 1983.

9. D. PALANIAPPAN, T. AMARANATH, S.D. NIGAM and R. USHA, *Lamb's solution of Stokes equations — A sphere theorem*, Quart. J.Mech. Appl. Math., **45**, 1, 57–66, 1992.

10. A. EINSTEIN, *Investigations on the theory of Brownian movement* [English translation], Dover Publications Inc., 1956.

DEPARTMENT OF MATHEMATICS AND STATISTICS, SCHOOL OF M.C.I.S.
UNIVERSITY OF HYDERABAD, HYDERABAD, INDIA
and
DEPARTMENT OF MATHEMATICS
INDIAN INSTITUTE OF SCIENCE, BANGALORE, INDIA.

Some results and new experimental technique in studies of adiabatic shear bands(*)

J. R. KLEPACZKO (METZ)

SHEAR STRAIN instability and localization at different nominal strain rates are investigated in this paper through numerical analysis of a layer deformed at wide range of nominal strain rates. A one-dimensional model for simple shearing deformation was applied together with constitutive relations based on structural evolution and dislocation dynamics. Generalised condition for instability for adiabatic shearing has been derived and discussed. Since Split Hopkinson Torsional Bar has been used for some time to study catastrophic thermoplastic shear in materials, a short discussion is offered as to the range of applicability of this experimental technique. A new experimental technique implemented in Laboratory of Physics and Mechanics of Materials, Metz, is briefly described. This experimental technique based on the principle of direct impact is more flexible and offers much higher nominal strain rates, of the order $10^5\,\mathrm{s}^{-1}$, than the SHTB technique. A double shear specimen is loaded directly by a projectile launched with a wide range of impact velocities. The range of impact velocities from $2\,\mathrm{m/s}$ to $200\,\mathrm{m/s}$ allows for a wide range of high nominal strain rates, usually not accessible for the SHTB technique. Preliminary series of experiments on annealed mild steel XC18 has been performed with this technique. The results are compared with the numerical data for the same material.

1. Introductory remarks

DURING THE LAST DECADE substantial progress has been made in testing, analytical solutions and numerical calculations of adiabatic shear bands. It has been well known for a long time (for example, see the paper by H. TRESCA [40] and review by W. JOHNSON [14] of early works) that metals can develop a thermal instability of plastic flow due to heat generated during deformation. ZENER and HOLLOMON [45] noted that an increase of strain rate is inevitably associated with a change of the deformation conditions from isothermal to adiabatic. The same authors found that the plastic deformation becomes unstable when the strain hardening rate (the tangent modulus of the stress-strain curve) starts to be negative. Although localisation of plastic deformation in the form of shear bands is common in many materials, a great deal of interest has been recently devoted to study the non-isothermal cases. The present study is also limited to the non-isothermal case when the adiabatic conditions of plastic deformation prevail.

At moderately high and high strain rates plastic deformation in metals is nearly adiabatic; as a consequence, the deformation heating can lead to a sizeable amount of flow softening and hence to flow localization in the form of ASB, called also the thermoplastic catastrophic shear which can lead to fracture. The

---

(*)Part of this paper has been presented at XVIIIth International Congress of Theoretical and Applied Mechanics, Haifa, Israel, August 1992.

ASB are narrow, a small fraction of a millimeter, zones of highly nonhomo-
geneous deformation developed by a complicated interplay of strain hardening,
temperature softening, strain rate sensitivity, dynamic strain ageing and, some-
times, inertia forces. In some materials, especially in steels and titanium alloys,
a phase transformation or amorphous-like microstructure may develop within a
narrow zone of the highest temperatures. It may be mentioned that ASB, with
or without phase transformation, often act as sites of fracture initiation in Mode
II, VARFOLOMEYEV and KLEPACZKO [41]. The importance of the ASB is obvious
in diverse applications like rolling, drawing, machining, impact on structures and
ballistic impact.

A number of analytical, numerical and experimental studies have been per-
formed in attempt to determine the critical conditions for the onset and evolution
of catastrophic thermo-plastic shear. The early review on the subject demon-
strated difficulties in the analysis of the problem, for example ROGERS [36]. A
more recent up-to-date review was published by BAI [1].

Analytical studies of ASB are more numerous and they will not be reviewed in
this paper. Generally, because of simplicity of constitutive relations, in order to
find a closed-form solution, unacceptable simplifications were automatically intro-
duced in some ASB analyses. More recent analytical studies are more acceptable,
for example FRESSENGEAS and MOLINARI [10], FRESSENGEAS [9], WRIGHT [42].

On the other hand, more and more numerical analyses on ASB formation are
available and, in general, the final results are very sensitive to constitutive rela-
tions chosen. Although, most frequently, the fully nonlinear system of equations
is employed in such studies, the material behaviour characterized in the form of
constitutive relations is quite simplified. Such situation may lead to some mis-
interpretations of how ASB evolve as functions of both the initial and boundary
conditions.

The state of the art is that relatively large quantity of theoretical studies have
been published so far with much less effort put into the experiment. Most ex-
perimental studies make use of the Split Hopinson Torsion Bar (torsional Kolsky
apparatus), COSTIN et al. [5], GIOVANOLA [11], MARCHAND and DUFFY [29]. They
are based on fast torsion of thin, short tubular specimens. Such a test with SHTB
has a very limited range (in the logarithmic scale) of the nominal shear strain
rates, usually around $10^3 \, \text{s}^{-1}$, and the boundary conditions imposed during the
test, although well defined, are not constant, cf. LEROY and MOLINARI [25]. Thus,
the majority of experimental studies were limited to a thin tubular geometry and
to the nominal strain rates around $10^3 \, \text{s}^{-1}$. In addition, the effects of length and
stress concentrators in a short tubular specimen have not been properly studied.

The other range of rates, albeit much higher, occurs in external ballistics and
explosive loading. Although it is very easy to produce a network of ASB during
ballistic or explosive loadings, they do not provide a good experimental basis to
study the fundamentals.

The most important, and so far unresolved class of problems, is the effect

of initial and boundary conditions on the onset and formation of the ASB. From the point of view of experiments, the following loading schemes can be specified:

i. Initially uniform deformation field with small initial perturbations; the initial perturbations which are usually assumed:

a) small defect of geometry;

b) small thermal perturbations;

c) heat sinks.

ii. Imposed deformation fields with instantaneous stress or strain concentrators;

a) controlled loading conditions;

b) direct impact at different velocities (including ballistic impact) and different projectile/target geometries.

iii. Explosive loading;

a) expansion of tubes (fragmentation via ASB);

b) shock waves generated on limited surfaces.

iv. Controlled shock waves;

a) plate/plate impact (micro ASB).

v. Metal forming processes;

a) machining;

b) high speed rolling;

c) high speed drawing.

The systematics shown above points out to a wide class of loading conditions and, in turn, to a wide class of initial and boundary conditions under which the ASB can be generated. The cases iii., iv. and v. will not be discussed here; however, the most fundamental cases, i. and ii., are worth discussing. The case i. is clearly related to SHTB technique. It can be pointed out that the active specimen length and initial conditions can influence the outcome in the form of ASB. For example, Litoński [26] has furnished a detailed analysis of the deformation in torsion of a thin-walled tube with an initial geometric imperfection in the form of a slightly thinned section. The analysis was repeated in a similar way by Costin et al. [5] but with comparison to SHTB experiments on 1018 CRS (cold-rolled steel). Some time later Litoński [27] has shown, by a similar analysis, but with the thin-walled tube without geometric imperfection and with the heat sinks at the ends, that the ASB occurs above a certain critical strain rate of the order of $1.0\,\mathrm{s}^{-1}$. Another numerical study was reported by Kamiński [15] where a thin-walled tube of a constant cross-section had a Gaussian imperfection of the yield stress τ_y i.e. $\tau_y(x) = \tau_{y0}G(x)$, where $G(x)$ is the Gaussian distribution and τ_{y0} is the mean yield stress. It was shown in that study that at lower nominal strain rates, of the order of $0.1\,\mathrm{s}^{-1}$, the strain and temperature fields differ for the

adiabatic and heat conduction cases. When the nominal strain rate was increased to $1\,\text{s}^{-1}$, the differences were substantially reduced.

Also later the geometry imperfections were the most frequently studied cases. MERTZER [31] reported numerical simulations of ASB observed on 1020 CRS by COSTIN *et al.* [5]. SEMIATIN *et al.* [37] assumed a geometrical imperfection in the specimen. SEMIATIN *et al.* [38] also studied the effects of material imperfections via geometric imperfections on flow localization in the SHTB test.

SHAWKI and CLIFTON [39] presented a number of analytical solutions and numerical studies, including torsion of a thin tube with geometrical imperfections, with one or more circumferential grooves and with thermally isolated sides. Three simple constitutive relations were used in those calculations. It was found, as expected, that at high nominal strain rates of the order of 10^3 to $10^4\,\text{s}^{-1}$, the localization mechanism which accounts for ASB formation is exclusively adiabatic. For this mechanism, at advanced deformation, the thermal softening dominates in reduction of stress and in increase of local shear strain, leading to catastrophic local shearing. At small strains a positive strain hardening dominates and localization does not occur. The rate of localization depends strongly on the strain-rate sensitivity. The qualitative discussion as offered above is consistent with earlier findings and physical intuition. The qualitative analyses of the ASB formation for particular metals and alloys and for different geometries and boundary conditions are still waiting to be solved.

A more recent numerical study by BURNS [3] has shown that the heat sinks introduced at the ends of a thin-walled tube can modify the whole process of the ASB formation in comparison to the assumption of the adiabatic boundary conditions. In addition to the heat sinks, a temperature perturbation was introduced. A small local maximum in the initial temperature distribution along the tube axis led to formation of the ASB just in this cross-section. A simple linear Arrhenius model combined with a power strain hardening was employed in those calculations, the nominal strain rate was assumed as $1.6 \times 10^3\,\text{s}^{-1}$. Again, numerical results discussed above clearly indicate the influence of the initial and boundary conditions on formation and final geometry of the ASB.

2. Transition from isothermal to adiabatic deformation

The localization of deformation in the form of ASB is observed in thin-walled tubes when the nominal strain rate exceeds a certain value. Obviously, a transition exists between pure isothermal and pure adiabatic regimes of deformation. This transition depends, in the first place, on geometry of the deformed body and on effectiveness of the heat extraction from the heated zones. When correct boundary and initial problems are posed, it is possible to estimate the range of strain rates within which the transition occurs. Preliminary attempts to find an approximate strain rate range of transition were reported by KAMIŃSKI [15]

and LITOŃSKI [27]. In the first case, numerical calculations were performed for the length of tube $L = 30$ mm and initial temperature 673 K, and three cases were studied: isothermal, adiabatic and mixed. Three nominal strain rates were assumed: 0.01; 0.1 and $1.0 \, \text{s}^{-1}$. The final results of those calculations indicate that the difference between adiabatic and mixed cases is substantially reduced for shear strain rate of $1.0 \, \text{s}^{-1}$. A similar calculation was performed by LITOŃSKI [27] for a thin-walled tube, $L = 5.0$ mm, and with the heat sinks at the ends, again the initial temperature was assumed $T_0 = 673$ K, and four values of nominal strain rates were considered: 0.01; 0.1; 1.0 and $10.0 \, \text{s}^{-1}$. Similar results were produced for the complete case (heat conduction included). It was found that the transition must occur between nominal strain rates 0.1 and $1 \, \text{s}^{-1}$.
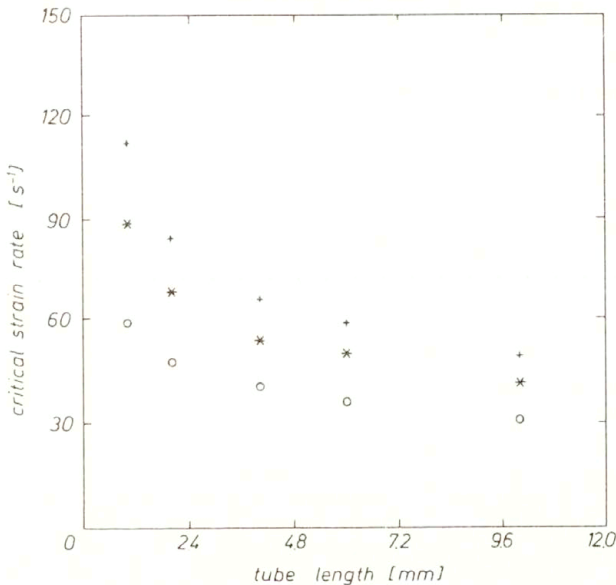
FIG. 1. Critical values of shear strain rates $(\Gamma_n)_{\text{cr}}$ as a function of tube length L; $+$ – copper, $*$ – aluminium, o – steel.

A more exact transition analysis for a thin-walled tube was performed more recently by OUSSOUADDI and KLEPACZKO [34]. The finite difference technique has been applied with relatively exact constitutive relation, and calculations were carried out at different nominal strain rates in shear from $1.0 \, \text{s}^{-1}$ to $10^3 \, \text{s}^{-1}$, at $T_0 = 300$ K. In addition, the effect of length on the isothermal/adiabatic transition was studied. Since the heat sinks were assumed at the tube ends, the transition was defined as the maximum of partial derivative of the temperature gradient with respect to the nominal strain rate

(2.1)
$$\xi = \frac{\partial}{\partial \log \dot{\Gamma}_n} \left(\frac{\partial T}{\partial x} \right).$$

where x is the axial coordinate; $-L/2 \leq x \leq L/2$, T is the absolute temperature and $\dot{\Gamma}_n = d\Gamma_n/dt$ is the nominal strain rate in shear, $\Gamma_n = (r/L)\varphi$, r is the mean radius and φ the angle of twist. It was found that the transition can be well defined by the maximum value of ξ. The critical values of $(\Gamma_n)_{cr}$ are shown in Fig. 1 as a function of L. The results support quantitatively the physical intuition that the critical strain rate increases in proportion to the thermal conductivity, which is the lowest for steel and the highest for copper. When L decreases from 10 mm to 1.0 mm, the critical strain rate increases approximately twofold for all three materials which were studied.

Those results clearly indicate the importance of the boundary and initial conditions, in both experiment and numerical analysis, not only in the case of transition isothermal/adiabatic, but also in formation of ASB.

3. Shear strain of instability

The earliest studies on the onset of the shear localization were limited, by analogy to Considere condition of instability in tension test, to the load instability $dM/d\varphi = 0$. The condition $dM/d\varphi = 0$, where M is the torque and φ is the angle of twist, gives possibility to determine the critical instability strain if a specific constitutive relation is assumed. It was confirmed by LITOŃSKI [26], by numerical application of the flow localization model (MARCINIAK–KUCZYŃSKI [30] approach), that the onset of instability corresponds to the maximum load, that is the condition $dM/d\varphi = 0$ was confirmed as the onset of instablity. Many authors derived formulas for a critical strain using different empirical constitutive relations; a review of those derivations was published by DORMEVAL [6]. Experimental confirmation of the onset condition $dM/d\varphi = 0$ was provided for a low-alloy structural steel by MARCHAND and DUFFY [29]. A high speed photography combined with SHTB technique was applied in those studies.

Since up to the maximum of torque the shear deformation is uniform, the condition for load instability reduces to the formula

$$(3.1) \qquad \frac{d\tau}{d\Gamma} = 0.$$

Since many authors use constitutive relations in the form of multiplication function

$$(3.2) \qquad \tau = f_1(T)f_2(\Gamma)f_3(\dot{\Gamma}),$$

a more general analysis of the condition (3.1) will be given, as compared to the earlier one by KLEPACZKO [20]. If the mechanical equation of state is assumed and the history effects are neglected, one can write

$$(3.3) \qquad \frac{d\tau}{d\Gamma} = \left(\frac{\partial \tau}{\partial \Gamma}\right)_{T,\dot{\Gamma}} + \left(\frac{\partial \tau}{\partial T}\right)_{\Gamma,\dot{\Gamma}} \frac{dT}{d\Gamma} + \left(\frac{\partial \tau}{\partial \dot{\Gamma}}\right)_{T,\Gamma} \frac{d\dot{\Gamma}}{d\Gamma}.$$

then the condition (3.1) leads to

$$(3.4) \qquad \left(\frac{\partial \tau}{\partial \Gamma}\right)_{T,\dot\Gamma} + \left(\frac{\partial \tau}{\partial T}\right)_{\Gamma,\dot\Gamma}\frac{dT}{d\Gamma} + \left(\frac{\partial \tau}{\partial \dot\Gamma}\right)_{T,\Gamma}\frac{d\dot\Gamma}{d\Gamma} = 0.$$

Condition (3.4) can be satisfied only in very specific conditions of deformation. One of them is the adiabatic process of deformation, then

$$(3.5) \qquad \frac{dT}{d\Gamma} = \left(\frac{dT}{d\Gamma}\right)_{\text{ADIABATIC}}.$$

Condition (3.4) can be analysed for a variety of deformation histories $\dot\Gamma(\Gamma)$ and $T(\Gamma)$, but the simplest case is usually limited to the constant strain rate, in general

$$(3.6) \qquad \left(\frac{\partial \tau}{\partial \Gamma}\right)_{T} + \left(\frac{\partial \tau}{\partial T}\right)_{\dot\Gamma}\left(\frac{dT}{d\Gamma}\right)_{A} = 0.$$

It is important, then, to have an estimate of the adiabatic increase of temperature $T_A(\Gamma)$ and $(\partial T/d\Gamma)_A$ due to plastic work converted into heat. Assuming constitutive relation (3.1), it follows from the principle of energy conservation that

$$(3.7) \qquad \left(\frac{dT}{d\Gamma}\right)_{A} = \frac{[1 - \zeta(T,\Gamma)]f_1(T)f_2(\Gamma)f_3(\dot\Gamma)}{\rho(T)C_p(T)},$$

where $\zeta(T,\Gamma)$ is a coefficient taking into account the stored energy in the material, $\rho(T)$ is the mass densiy of the material and $C_p(T)$ is the specific heat at constant pressure, both ρ and C_p are functions of temperature.

The partial differentials can be found after (3.2) as follows:

$$(3.8) \qquad \begin{aligned} \left(\frac{\partial \tau}{\partial T}\right)_{\Gamma,\dot\Gamma} &= f_2(\Gamma)f_3(\dot\Gamma)\frac{\partial f_1}{\partial T}, \\[6pt] \left(\frac{\partial \tau}{\partial \Gamma}\right)_{\dot\Gamma,T} &= f_1(T)f_3(\dot\Gamma)\frac{\partial f_2}{\partial \Gamma}, \\[6pt] \left(\frac{\partial \tau}{\partial \dot\Gamma}\right)_{\Gamma,T} &= f_1(T)f_2(\Gamma)\frac{\partial f_3}{\partial \dot\Gamma}. \end{aligned}$$

Introduction of (3.8) into condition (3.3) yields

$$(3.9) \qquad \frac{1}{f_2(\Gamma_c)}\left(\frac{\partial f_2}{\partial \Gamma}\right) + \frac{1}{f_1(T)}\left(\frac{\partial f_1}{\partial T}\right)\left(\frac{dT}{d\Gamma}\right)_A + \frac{1}{f_3(\dot\Gamma)}\left(\frac{\partial f_3}{\partial \dot\Gamma}\right) = 0.$$

After elimination of $(dT/d\Gamma)_A$ using (3.7), the condition (3.9) is transformed into the following form:

$$(3.10) \quad \frac{1}{f_2(\Gamma_c)}\left(\frac{\partial f_2}{\partial \Gamma}\right) + f_2(\Gamma_c)f_3(\dot{\Gamma})\left(\frac{\partial f_1}{\partial T}\right)\frac{1-\xi}{\rho(T)C_p(T)}$$

$$+ \frac{1}{f_3(\dot{\Gamma})}\left(\frac{\partial f_3}{\partial \Gamma}\right)\left(\frac{d\dot{\Gamma}}{d\Gamma}\right) = 0,$$

where Γ_c is the strain at the onset of instability.

If the strain rate is constant, $(d\dot{\Gamma}/d\Gamma) = 0$, condition (3.10) reduces to

$$(3.11) \quad \frac{\partial f_2}{\partial \Gamma} + f_2^2(\Gamma_c)f_3(\dot{\Gamma})\left(\frac{\partial f_1}{\partial T}\right)\frac{1-\zeta}{\rho(T)C_p(T)} = 0.$$

Since only $f_2(\Gamma_c)$ depends on the critical strain, the explicit equation for $f_2(\Gamma_c)$ is

$$(3.12) \quad f_2(\Gamma_c) = \left[-\frac{(\partial f_2/\partial \Gamma)}{(\partial f_1/\partial T)}\frac{\rho(T)C_p(T)}{f_3(\dot{\Gamma})(1-\zeta)}\right]^{1/2}.$$

The expression $[-A]^{1/2}$ has real and imaginary parts. Inversion of $f_2(\Gamma_c)$ makes it possible to find Γ_c

$$(3.13) \quad \Gamma_c = f_2^{-1}\left[-A(\Gamma, \dot{\Gamma}, T)\right]^{1/2}.$$

where A is the expression in the square brackets of (3.12). Existence of the real $f_2(\Gamma_c)$ is possible only if A is negative. Since ρ, C_p, $(1-\zeta)$ must be always positive, and the function of strain rate sensitivity, $f_3(\Gamma)$, is also assumed in this case to be positive, the only term which may be negative is $(\partial f_2/\partial \Gamma)/(\partial f_1/\partial T)$. The most common case is the thermal softening which leads to negative value of $\partial f_1/\partial T$, of course, if $\partial f_2/\partial \Gamma$ is at the same time positive. Another possibility is if the tangent modulus $\partial f_2/\partial \Gamma$ is negative and at the same time there is no thermal softening. The role of a positive rate-sensitivity is quite interesting, that is if $f_3(\dot{\Gamma})$ is an increasing function of strain rate $\dot{\Gamma}$. The positive rate-sensitivity has a negative effect on the onset of adiabatic instability, that is, Γ_c is reduced when strain rate is increased. The positive rate-sensitivity increases production of plastic work converted into heat. However, after the critical strain Γ_c is reached, $\Gamma > \Gamma_c$, a positive rate sensitivity diminishes local strain gradients in ASB. Since the assumption was made $(d\dot{\Gamma}/d\Gamma) = 0$, function $f_3(\Gamma)$ plays the role of a parameter, it must be constant but rate-dependent.

In many publications constitutive relations are employed which fall into the class of Eq. (3.2). For example, LITOŃSKI [26, 27], KAMIŃSKI [15], COSTIN *et al.* [5], and others, used in numerical studies the following relation

$$(3.14) \qquad \tau = B(1 - aT)\left(1 + b\,\dot{\Gamma}\right)^m \Gamma^n,$$

where n is the strain hardening index and m is the rate sensitivity, a, b, B are empirical constants. In this case the thermal softening term has been linearized. Other authors employed the following constitutive relation

$$(3.15) \qquad \tau = B\left(\frac{T_0}{T}\right)^\nu \left(\frac{\Gamma}{\Gamma_0}\right)^n \left(\frac{\dot{\Gamma}}{\dot{\Gamma}_0}\right)^m,$$

where B, ν, n, m are, respectively, plasticity modulus, temperature index, strain hardening index and logarithmic strain rate-sensitivity, T_0, Γ_0 and $\dot{\Gamma}_0$ are normalization constants. Relation (3.15) falls in the class of nonlinear liquids since $\tau = 0$ if $\Gamma \to 0$. This relation was used many times for both the numerical solutions and perturbation analyses, for example MOLINARI and CLIFTON [33], BUISSON and MOLINARI [2], FRESSENGEAS [8], SHAWKI and CLIFTON [39], and others.

In order to discuss further the condition of adiabatic instability, it is assumed that the flow stress is represented by a more specific relation

$$(3.16) \qquad \tau = B(T)\Gamma^n\,\dot{\Gamma}^m,$$

where $B(T)$ is a known temperature-dependent plasticity modulus. The condition (3.9) yields the following relation

$$(3.17) \qquad n\Gamma_c^{n-1} + \Gamma_c^{2n}\Gamma^m\left(\frac{\partial B}{\partial T}\right)\frac{1 - \zeta}{\rho_0 C_p(T)};$$

it is assumed that the mass density ρ_0 and the coefficient of stored energy remain constant. From (3.17), the critical shear strain at the onset of instability is

$$(3.18) \qquad \Gamma_c = \left[\frac{n\rho_0 C_p(T)}{(1 - \zeta)\,\dot{\Gamma}^m\left(-\dfrac{\partial B}{\partial T}\right)}\right]^{\frac{1}{n+1}}.$$

A positive role of strain hardening in delaying the instability was well documented in early publications. Since the specific heat is an increasing function of temperature, it also delays the instability. The most important factor is the mathematical form of $-(\partial B/\partial T)$, especially in the case of post-critical analyses.

Adiabatic increments of temperature at the point of instability, $\partial \tau/\partial \Gamma = 0$, are usually not very high, and constant n and m are acceptable. Constant values of n and m are only the first approximation for small increments of temperature. Since

it has been shown by HARTLEY *et al.* [12], and later by MARCHAND and DUFFY [29], that post-critical temperature rise for steels is of the order $425\,\text{K} \leq \Delta T \leq 595\,\text{K}$ at the central part of the ASB, the constancy of n and m is a very crude approximation. A similar conclusion was reached by JOHNSON [13] by numerical analysis of a thin-walled torsion test specimen. The thermal softening $-(\partial B/\partial T)$ was assumed to be linear in the first calculations of the post-critical deformation of copper, and bilinear in the second one. Substantial differences were revealed in the evolution of stresses in both stages of deformation, at the instability points and during localization. Another paradox of the temperature-independent logarithmic rate sensitivity, if the thermal softening $(\partial \tau/\partial T)$ is negative, lies in the fact that, according to formula (3.16), the stress differences at two constant strain rates increase when temperature is decreased, what is in complete contradiction to the real behaviour of metals, KLEPACZKO [16]. A more rational approach is to use some form of the Arrhenius relation to take into account, at the same time, thermal softening and temperature-dependent rate sensitivity; see, for example, SHAWKI and CLIFTON [39] and also BURNS [3].

Because of the complexity in formation of the ASB, the analytical studies in this area, although important, have a qualitative character, mostly due to simplistic constitutive relations. The importance must be focused on a full numerical approach with physically-based constitutive relations.

4. Some results of numerical studies

Among publications on numerical analyses of ASB, only few take into account the fully nonlinear system of governing equations. However, the crucial problem, even for the complete formulation, is the choice of constitutive relations.

Two boundary value problems are most interesting from the point of view of experimental techniques:

i) fast torsion of a thin-walled tube (interesting due to SHTB technique),

ii) fast shearing of a layer of finite height (interesting due to new experimental technique described in the next part of this paper).

A relatively complete analysis of torsion was reported by BURNS [3]. A numerical study of a layer as a complete nonlinear problem, fully coupled with temperature, was reported by KLEPACZKO *et al.* [23]. The fully coupled problem was formulated including heat conduction, changes of specific heat as a function of temperature, complete effects of temperature on mechanical properties and inertia. A layer with geometric imperfection was assumed, and the top and bottom of the layer were adiabatically insoluted. A complete phenomenological constitutive relation has been used in those calculations. A more exact analysis and discussion of this constitutive relation is published elsewhere, KLEPACZKO [17]. The fully temperature-coupled constitutive relations are as follows

$$(4.1) \qquad \tau = B(\theta)\,(\Gamma_0 + \Gamma)^{n,(\theta)}\,\dot{\Gamma}^{m(\theta)} + \left\langle \eta(\theta)(\dot{\Gamma} - \dot{\Gamma}_0) \right\rangle.$$

where θ is the homologous temperature, $\theta = T/T_m$, and T_m is the melting temperature of a material under consideration, η is the pseudo-viscosity and $< \cdot >$ is the operator, $< \cdot > = 0$ if $\dot{\Gamma} \leq \dot{\Gamma}_0$ and $< \cdot > = 1$ if $\dot{\Gamma} > \dot{\Gamma}_0$, $\dot{\Gamma}_0$ is the threshold strain rate. Both the strain hardening index n and logarithmic rate sensitivity m are coupled with temperature. For BBC metals m and n are expressed as functions of θ as follows:

(4.2)
$$n(\theta) = n_0 \frac{\mu(\theta)}{\mu_0},$$
$$m(\theta) = a\theta \exp(-b\theta) + \alpha_0 \theta^r,$$

where n_0 is the strain hardening index at $0°$ K, and a, b, α_0 are constants, $\mu(\theta)$ is temperature-dependent shear modulus of elasticity

(4.3)
$$\mu(\theta) = \mu_0 \left[1 - \theta \exp \left(\theta_\mu \left(1 - \frac{1}{\theta} \right) \right) \right].$$

where μ_0 is the shear modulus at 0 K. All constants for two steels (1018 CRS and 1020 HRS) are identified in the paper which was mentioned above. Variation of specific heat was taken into account according to the Debye formulation. Geometric imperfection was assumed in the form

(4.4)
$$w(y) = w_0 \left\{ 1 + \delta \sin \left[\pi \left(\frac{1}{\varepsilon} - 2\varepsilon \frac{y}{h} \right) \right] \right\},$$

where w_0 is the layer thickness and h is the layer height, δ and ε are geometry parameters. Equations of momentum, balance of energy with a suitable Fourier constant for heat conduction and compatibility condition were assumed in their standard form in those calculations. Numerical calculations were performed using the implicit finite difference method. The duration of the successive time increments was chosen in such a way that the algorithm was unconditionally stable. The following boundary conditions were assumed: the bottom surface of the layer was fixed, and a constant velocity V was assumed at the top, a steady state process.

The input for those calculations was the nominal strain rate in shear $\dot{\Gamma}_n = V/h$. The output of calculations consisted of a detailed spatial history of all important physical quantities like shear stress $\tau(y,t)$, strain $\Gamma(y,t)$, strain rate $\dot{\Gamma}(y,t)$, absolute temperature $T(y,t)$ and local velocity $v(y,t)$. Thus, the simulation provided a whole dynamic history of the ASB development at different nominal strain rates $\dot{\Gamma}_n$.

Two values of critical nominal strains were evaluated, the instability strain Γ_c associated with the maximal force and the final localization strain Γ_{LOC} defined as follows:

(4.5)
$$\Gamma_n - \Gamma_{\mathrm{LOC}} \qquad \text{when} \qquad \lim_{\dot{\Gamma}_A \to 0} \dot{\Gamma}_B = \infty.$$

where $\dot{\Gamma}_A$ is the local strain rate in the strongest section of the layer and $\dot{\Gamma}_B$ is the local strain rate in the cross-section where localization occurs. Numerical solutions obtained for two steels within the range of nominal strain rates $10^2\,\mathrm{s}^{-1} \leq \dot{\Gamma}_n \leq 10^4\,\mathrm{s}^{-1}$ (1018 CRS and 1020 HRS) have shown a minimum of both values of Γ_n, i.e. Γ_c and Γ_{LOC}, at the nominal strain rate $\sim 2 \times 10^3\,\mathrm{s}^{-1}$. Values of Γ_{LOC} were obtained numerically using the condition $\dot{\Gamma}_{\mathrm{LOC}} = 10^2\,\dot{\Gamma}_n$. In the range of $\dot{\Gamma}_n$ lower than $\dot{\Gamma}_n = 2 \times 10^3\,\mathrm{s}^{-1}$ both nominal strains Γ_c and Γ_{LOC} decrease when $\dot{\Gamma}_n$ is increased, the trend with agreement to formulas (3.12) and (3.18). In the range of the nominal strain rates higher than $\dot{\Gamma}_n = 2 \times 10^3\,\mathrm{s}^{-1}$ an increase of Γ_c and Γ_{LOC} was observed. Since calculations were performed twice, without pseudo-viscosity $\eta = 0$, and with pseudo-viscosity, the positive effect of excessive strain rate-sensitivity on the localization is obvious. The ratio $\Gamma_{\mathrm{LOC}}/\Gamma_c$ increases at the higher rate if the pseudo-viscosity is included into calculations; if only the logarithmic rate-sensitivity is taken into calculations, the ratio $\Gamma_{\mathrm{LOC}}/\Gamma_c$ increases only slightly as a function of $\dot{\Gamma}_n$. It has been, thus, shown in the paper discussed above that for a given material and a given geometric imperfection, there exists a domain of nominal strain rates $\dot{\Gamma}_n$ where development of the catastrophic shear in the form of the ASB is the most likely to occur. A similar minimum of Γ_c was also found by WRIGHT and WALTER [43] using the finite elements technique and confirmed later by WRIGHT [42] by an approximate method. In both cases the initial temperature defect was assumed. Attempts to find the final thickness of ASB after those numerical results were not quite successful. Although it was found that ASB were formed, the asymptotic width was difficult to estimate since at $\dot{\Gamma}_{\mathrm{LOC}} = 10^2\,\dot{\Gamma}_n$ the evolution of ASB was still not terminated. One of the reasons why it was difficult to specify a finite thickness of the ASB is the excessive strain hardening introduced by the term $\Gamma^{n(T)}$ at large strains, even when the correct relation for $n(T)$ was used.

As a result, a completely new series of numerical calculations were undertaken, but this time a physically based set of constitutive relations has been used. Here only some results will be discussed, a more thorough of that study will be given elsewhere, KLEPACZKO and REZAIG [22]. The constitutive modeling is represented by a consistent approach to the kinetics of macroscopic plastic behaviour of metals with BCC and FCC structures, KLEPACZKO [18, 19]. The constitutive formalism is used here with the one state variable which is the total dislocation density ρ. It is assumed that plastic deformation in shear is the fundamental mode of deformation. It is assumed that at constant microstructure the flow stress τ consists of two components: the internal stress τ_μ and the effective stress τ^*, thus

$$(4.6) \qquad \tau = \tau_\mu \left[h\left(\dot{\Gamma}.T \right), \dot{\Gamma},T \right]_{\mathrm{STR}} + \tau^* \left(\dot{\Gamma}.T \right)_{\mathrm{STR}}.$$

where $h(\Gamma,T)$ are the histories of plastic deformation, Γ and $\dot{\Gamma}$ are, respectively,

plastic strain and strain rate. The internal stress τ_μ is developed by long-range strong obstacles to dislocation motion, and the effective stress τ^* is due to thermally activated short-range obstacles. In fact, the internal stress τ_μ must be also rate- and temperature-dependent via the dynamic recovery processes. To describe completely the strain rate and temperature effects, including evolution of microstructure and strain hardening, an evolution equation must be defined. In this case a simple evolution equation has been adopted which is adequate to account for strain hardening in mild steels, KLEPACZKO [17, 18],

$$(4.7) \qquad \frac{d\rho}{d\Gamma} = M_{II} - k_a(\dot{\Gamma}, T)(\rho - \rho_0),$$

where ρ_0 is the initial dislocation density and $k_a(\dot{\Gamma}, T)$ is the annihilation factor. The multiplication factor M_{II} is related to the mean free path λ of dislocation storage by the formula $M_{II} = 1/b\lambda$, where b is the modulus of Burgers vector. For constant temperature and strain rate, the explicit form for ρ can be found after integration of Eq. (4.7),

$$(4.8) \qquad \rho = \rho_0 + \frac{M_{II}}{k_a(\dot{\Gamma}, T)} \left[1 - \exp\left(-k_a(\dot{\Gamma}, T)\Gamma \right) \right].$$

If the strain rate and temperature are not constant, like in the case of ASB formation, the evolution equation must be numerically integrated to find the current value of ρ. If ρ is found, the internal stress is also found from the relation

$$(4.9) \qquad \tau_\mu = \alpha\mu(T)b\sqrt{\rho}.$$

where α is the dislocation/obstacle interaction constant, and $\mu(T)$, the shear elasticity modulus, is specified by Eq. (4.3). Annihilation factor k_a is given by the formulas

$$k_a = k_0 \qquad \text{for} \quad 0 \le T \le T_*$$

and

$$(4.10) \qquad k_a = k_0 \left(\frac{\dot{\Gamma}_0}{\dot{\Gamma}} \right)^{2m_0(T-T_*)} \qquad \text{for} \quad T_* < T < T_m.$$

A constant value for $k_a = k_0$ for $0 \le T \le T_*$ is a good approximation for mild steels which have the ability to dynamic strain ageing. Equations (4.7) to (4.10) characterize completely the evolution of the internal stress τ_μ.

The effective stress τ^* can be obtained from the generalised Arrhenius relation, KLEPACZKO [17, 18]

$$(4.11) \qquad \dot{\Gamma} = \nu_k(\rho_m, T) \left[\exp - \frac{\Delta G_k(\tau^*, T, \rho_m)}{kT} \right].$$

where ν_k is the frequency factor for the kinetics of double dislocation kink, and ΔG_k is the free energy of activation for this micromechanism. Inversion of Eq. (4.9) leads to the explicit formula for the effective stress, with $\Delta G_k = 2H_k$

$$(4.12) \qquad \tau^* = \tau_0^* \left\{ 1 - \left[\frac{kT}{2H_k} \log \left(\frac{\nu_k}{\dot{\Gamma}} \right) \right]^{1/q} \right\}^{1/p}.$$

In this case the universal form for the free energy ΔG_k was employed, KOCKS *et al.* [24],

$$(4.13) \qquad \Delta G = 2H_k \left[1 - \left(\frac{\tau^*}{\tau_0^*} \right)^p \right]^q$$

with

$$(4.14) \qquad \rho_m = f\rho,$$

where $2H_k$ is the energy of the double kink formation and τ_0^* is the Peierls stress at 0 K, KLEPACZKO [19]. The frequency factor ν_k is assumed in the form

$$(4.15) \qquad \nu_k = f_0 n b^2 \nu_D \rho_0 \left[1 + \frac{f_1}{f_0} \exp \left(\frac{T_r}{2T} \right) \log \left(\frac{\rho}{\rho_0} \right) \right].$$

where f_0 is the initial fraction, Eq. (4.14), ρ_m is the mobile dislocation density, ν_D is Debye frequency, f_1, T_r are constants. The set of Eqs. (4.12) to (4.15) provide complete evolution of the effective stress τ^*.

This constitutive modeling involves two kinds of constants, the absolute physical constants and the constants also based on physics but specified for a particular metal or alloy. The complete discussion of all constants will be given elsewhere, by KLEPACZKO and REZAIG [22], but some basic values are given below: $M_{II} = 1.2 \times 10^{10}\,\text{cm}^{-2}$; $T_* = 558\,\text{K}$; $T_r = 300\,\text{K}$; $m_0 = 1.47 \times 10^{-4}$, $\Gamma_0 = 10^4\,\text{s}^{-1}$; $G_0 = 0.315\,\text{eV}$; $k_0 = 9.23$; $f_1 = 7$; $\tau_0^* = 520\,\text{MPa}$; $n = 2$; $f_0 = 0.05$; $\rho_0 = 6.2 \times 10^8\,\text{cm}^{-2}$; $q = 4/3$; $p = 3/4$. Those constants are representative for a mild steel XC18 (French Standards) after annealing, 0.17% C; 0.58% MN; 0.21% Si.

Numerical calculations were performed using a similar finite difference procedure outlined previously, but the height of the layer was assumed to be $h = 2.0\,\text{mm}$ and the number of elementary sublayers was 100, so that the elementary sublayer had the thickness $\Delta h = 20\,\mu\text{m}$. With such a value of Δh, an analysis of the terminal thickness of the ASB could be attempted.

Results of seventeen computer simulations for different nominal strain rates, $80\,\text{s}^{-1} \leq \dot{\Gamma}_n \leq 4.5 \times 10^4\,\text{s}^{-1}$, will be briefly presented here. The nominal instability strain Γ_c and the nominal localization strain Γ_{LOC} are shown as a function of
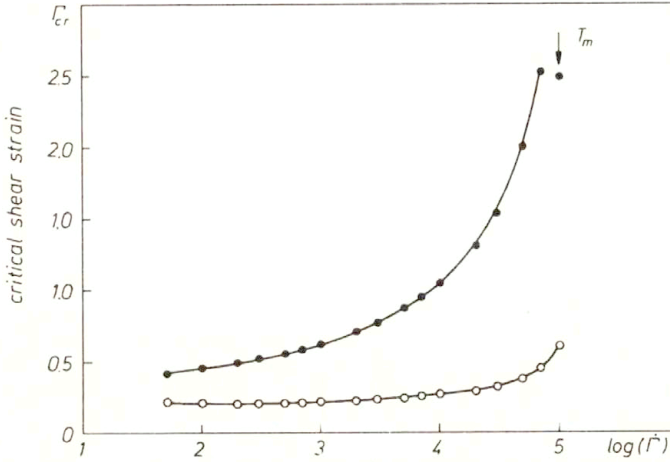
FIG. 2. Nominal values of instability strain Γ_c and localization strain Γ_{LOC} as a function of the nominal strain rate $\dot{\Gamma}_n = V/h$, numerical simulation for XC18 steel.

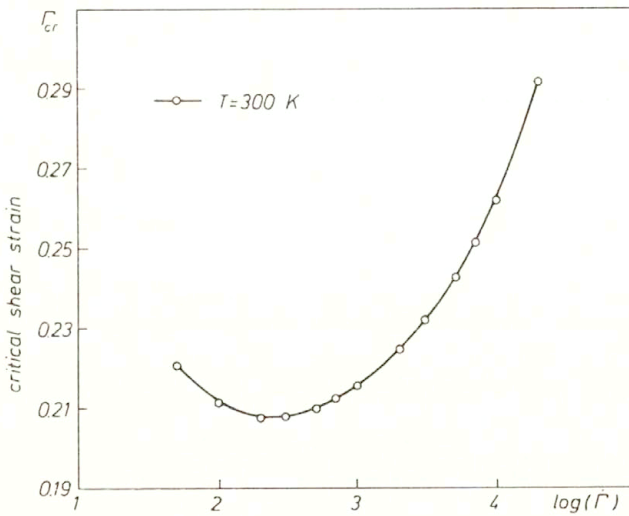FIG. 3. Nominal values of instability strain Γ_c in expanded scale as a function of the nominal strain rate $\dot{\Gamma}_n$, numerical simulation for XC18 steel.

log $\dot{\Gamma}_n$ in Fig. 2. The minimum of the instability strain Γ_c is found again in the region of nominal strain rates above $10^2\,\mathrm{s}^{-1}$, log $\dot{\Gamma}_n \approx 2.3$, $\dot{\Gamma}_n \approx 200\,\mathrm{s}^{-1}$. This is visible better in Fig. 3 with expanded scale of Γ_c. The stabilizing effect of strain rate and perhaps inertia are clearly shown in Fig. 4, where the ratio Γ_c/Γ_{LOC} is plotted as a function of log $\dot{\Gamma}_n$. The ratio begins with a value around 2.0 at $\dot{\Gamma}_n = 10^2\,\mathrm{s}^{-1}$ and ends with ~ 5.0 at $\dot{\Gamma}_n \approx 10^5\,\mathrm{s}^{-1}$. Around the nominal strain rates $\sim 5 \times 10^4\,\mathrm{s}^{-1}$ the maximum temperatures at the center of the ASB are found

to be quite close to the melting point for iron $T_m = 1785$ K. This is why the last point of localization strain Γ_{LOC} calculated for the highest $\dot{\Gamma}_n$ is on the same level in Fig. 2 as the preceding point, $\Gamma_{LOC} \approx 2.5$. A high probability that at the latest stages of material separation the temperature exceeds the melting point was suggested by MAKEL and WILSDORF [28]. It was found after examination of fracture surfaces formed during tensile tests of high strength steels that the tops of the dimples separated by a fast shearing are spheroidized, apparently due to melting.
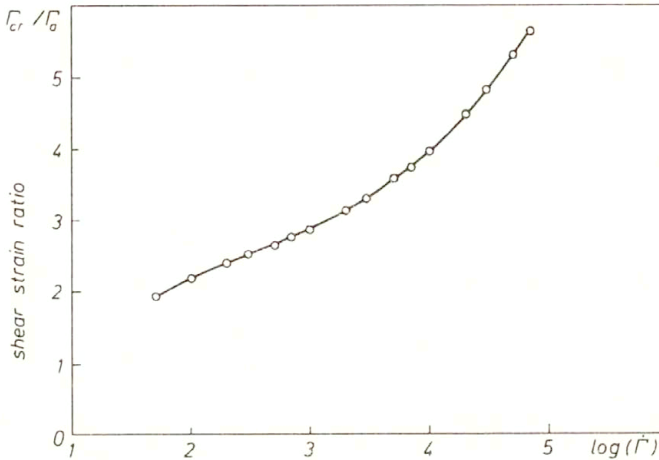

FIG. 4. The ratio of Γ_c/Γ_{LOC} as a function of log $\dot{\Gamma}_n$, numerical simulation for XC18 steel.

The most sensitive parameter for numerical analyses of the ASB is the final width of the band. In the present analysis a gradient method was assumed to define the final width of shear band. The profiles of shear strain $\Gamma(y)$ and temperature $T(y)$ as shown in Fig. 5 and Fig. 6 for $\dot{\Gamma}_n = 10^3$ s^{-1} and for different levels of the nominal strains Γ_n, served as a basis for all strain rates analysed to find strain and temperature gradients $g_\Gamma(y)$ and $g_T(y)$ at different levels of the nominal strain. The strain gradients $g_\Gamma(y)$ obtained after such procedure for $\dot{\Gamma}_n = 10^3$ s^{-1} at different levels of nominal strain are shown in Fig. 7. The width of the ASB has been defined as an asymptotic value of the distance between the gradient maxima,

$$(4.16) \qquad \lim_{\Gamma \to \Gamma_{LOC}} \Delta y_m = 2a \qquad \text{or} \qquad \lim_{T \to T_{LOC}} \Delta y_m = 2a,$$

where Δy_m is the distance between the gradient maxima, both for strain and temperature. Figure 8 shows how the asymptotic half-value a of the ASB thickness was determined. The dashed line shows terminal evolution of the band thickness. The same procedure was applied to the temperature gradients. The final result is shown in Fig. 9 where the asymptotic values of the shear band width $2a$ is
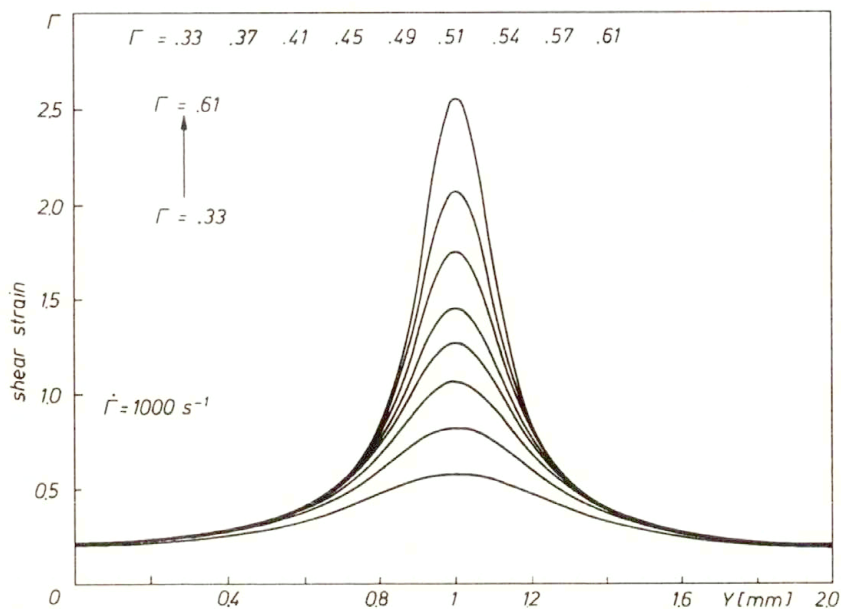
FIG. 5. Localization of shear strain at different levels of the nominal strain Γ_n at $\dot{\Gamma}_n = 10^3\,\mathrm{s}^{-1}$.
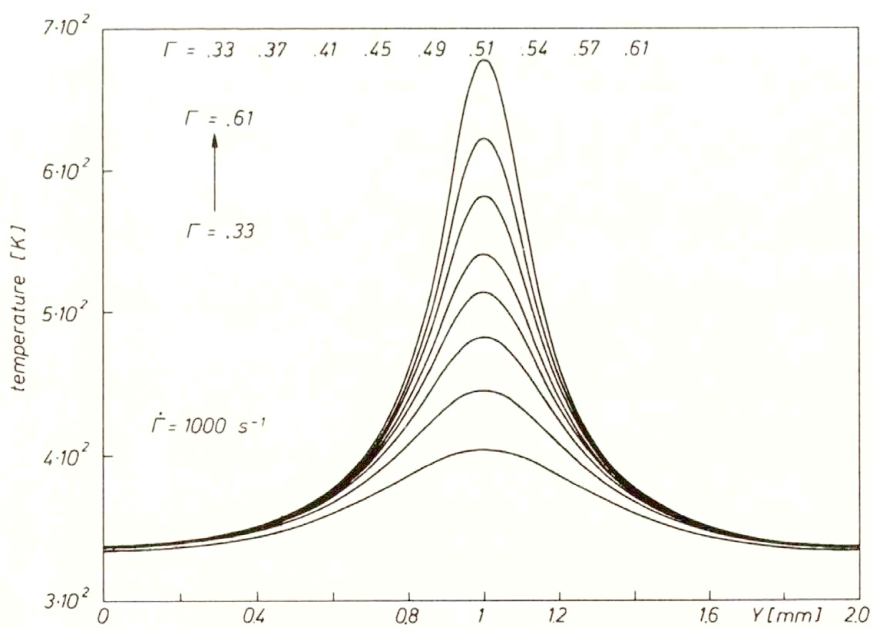
FIG. 6. Localization of temperature at different levels of the nominal strain Γ_n at $\dot{\Gamma}_n = 10^3\,\mathrm{s}^{-1}$.
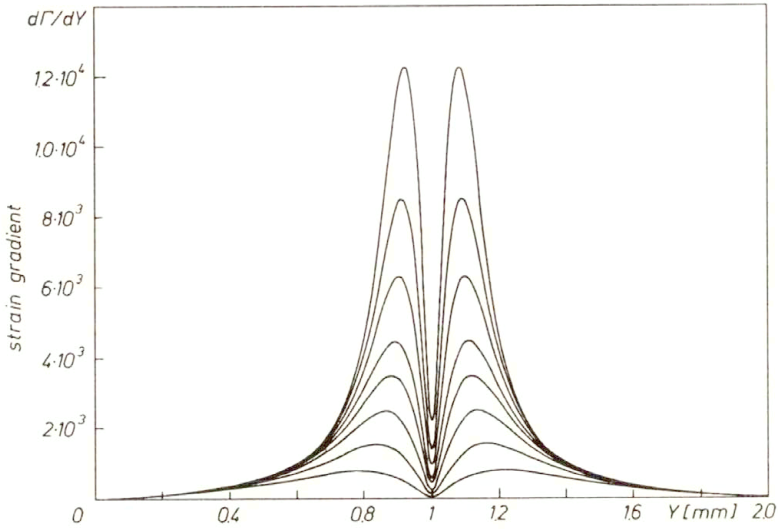
FIG. 7. Evolution of strain gradients $g_\Gamma(y)$ at the same levels of the nominal strains as indicated in Fig. 7, nominal strain rate $\dot{\Gamma}_n = 10^3\,\mathrm{s}^{-1}$.

FIG. 8. Evolution of strain gradients in the half-thickness of the layer at $\dot{\Gamma}_n = 10^3\,\mathrm{s}^{-1}$ and different levels of nominal strain Γ_n; dashed line shown the asymptotic procedure in finding the ASB thickness.

plotted versus logarithm of the nominal strain rate, $\log \dot{\Gamma}_n$. The points illustrate the values of the band width obtained by deformation gradients, asterisks are obtained by the temperature gradient method. Differences between those two approaches increase when the nominal strain rate decreases. This is due to a more intensive effects of heat conduction at l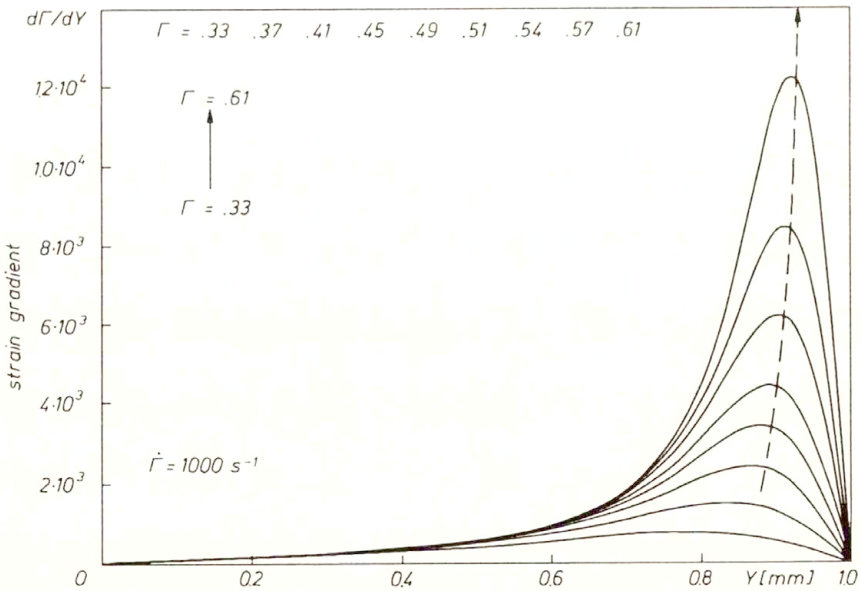ower strain rates. The shear band widths were found to have a minimum of $2a_{min} \approx 140\,\mu m$ at $\dot{\Gamma}_n \approx 3.2 \times 10^3\,s^{-1}$. Figure 9 shows also that at lower strain rates the shear bands are more diffused. At high strain rates inertia and rate sensitivity may again increase the width of ASB. However, the dimensions of the widths are in general agreement with experimental observations for annealed mild steels, including the XC18 one. Some steels with a high yield stress and low strain hardening may substantially reduce the ASB widths. For example, MARCHAND and DUFFY [29] have found the shear band width about $20\,\mu m$ for HY-100 low alloy steel tested at $\dot{\Gamma}_n = 1.6 \times 10^3\,s^{-1}$.
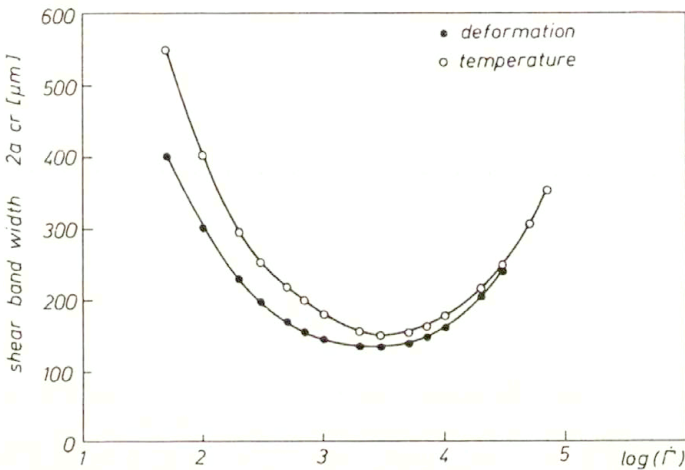
FIG. 9. Evolution of the ASB band thickness as a function of the nominal strain rate; o – analysis based on strain gradients; * – analysis based on temperature gradients.

Seventeen computer simulations of deforming layer with thickness $h = 2.0\,mm$ and with adiabatic boundary conditions, for seventeen values of the nominal strain rate $\dot{\Gamma}_n$, $80\,s^{-1} \leq \dot{\Gamma}_n \leq 10^5\,s^{-1}$, have revealed existence of the strain rate range within which the development of the catastrophic shear is the easiest. This region lies around the nominal strain rate of $10^3\,s^{-1}$. Also this study has confirmed existence of the minimum of both the instability strain and the final localization strain, reported earlier by WRIGHT and WALTER [43], and KLEPACZKO et al. [19]. The minimum of the ASB thickness was also revealed at the nominal strain rate $\dot{\Gamma}_n \approx 3.2 \times 10^3\,s^{-1}$. Evolution of the critical values Γ_c, Γ_{LOC} and $2a$ at different nominal strain rates found by numerical simulation has provided a strong argument for experiment in this area.

5. New experimental technique of impact shearing

The torsion tests of thin-walled tubular specimens are a very effective method to study advanced plastic deformation, for both quasi-static and dynamic loadings. In the literature three types of torsion devices are reported: the rotary flywheel machines, the high-speed hydraulic testing machines and the SHTB. All those systems of loading have their limitations. For example, the SHTB technique has a strong limitation in maximum strain (the net angle of rotation), maximum nominal strain rate of the order $\dot{\Gamma} \approx 2 \times 10^3 \, \text{s}^{-1}$ (for a standard specimen length) and, finally, the variation of strain rate during the test are quite high. At high strain rates the finite risetime of the incident wave may cause relatively large specimen deformation in absence of the mechanical equilibrium between the incident and transmitter bar.

Another experimental technique very useful in material testing is the double shear test introduced by FERGUSON et al. [7] and perfected by CAMPBELL and FERGUSON [4]. Since one of the promising specimen geometries to study dynamic plasticity and ASB is the Double-Notch Shear specimen, it has been decided to use a similar concept in shear testing at medium and high strain rates. Originally, Campbell and Ferguson applied the loading scheme consisting of the incident Hopkinson bar and transmitter Hopkinson tube to study the temperature and strain-rate dependence of the yield stress of a mild steel. Interpretation of oscillograms was the same as that for the Split Hopkinson Pressure Bar (SHPB or original Kolsky apparatus). Due to combination of a small gage length, $L_s = 0.84 \, \text{mm}$, that is the shearing part of the DS specimen, and a standard risetime in the incident bar, $t_r \approx 20 \, \mu\text{s}$, relatively advanced plastic deformation was reached during the risetime period. This negative feature of the bar/tube configuration was recently discussed by KLEPACZKO [21].

It was decided, then, to develop a new experimental configuration based on a Modified Double Shear specimen. The new experimental technique combines several positive factors already experienced with the other setups. This new technique has been described in some detail elsewhere, KLEPACZKO [20, 21]. The scheme of the loading setup and measuring devices are shown in Fig. 10. The fundamental change has been introduced, the direct impact is applied to load the MDS specimen. In this way the risetime in specimen loading present in the bar/tube configuration is practically eliminated. The flat-ended projectiles of different lengths made of maraging steel and of diameter $d_p = 10 \, \text{mm}$ are launched from an air gun with desired velocities V_0, $1 \, \text{m/s} \leq V_0 \leq 200 \, \text{m/s}$. The impact velocity is measured by the setup consisting of three sources of light, fiber optic leads 1, 2, 3 and three independent photodiodes. The time intervals of dark signals from the photodiodes generated during passage of a projectile are recorded by two time counters. The setup with three light axes makes it possible to determine acceleration/deceleration of a projectile just before impact thus, the exact value of V_0 can be determined.
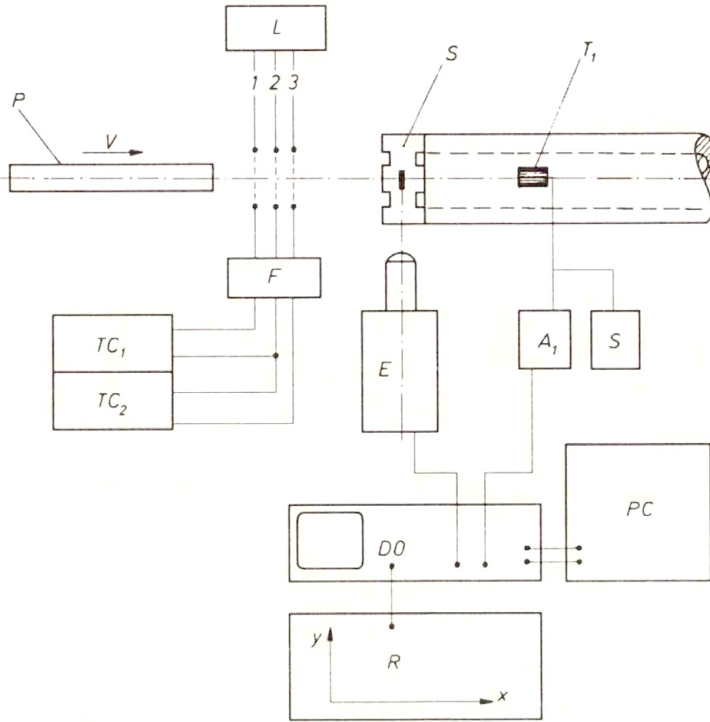
FIG. 10. New configuration of experimental setup developed in LPMM-Metz; P – projectile, S – double shear specimen, L – source of light, $1, 2, 3$ – fiber optics, F – photodiodes, $TC1$, $TC2$ – time counters, E – optical extensometer, T_1 – strain resistance gage, S – DC – supply unit, $A1$ – amplifier, DO – digital oscilloscope, PC – microcomputer, R – XY – recorder or graphic printer.

Axial displacement $U_x(t)$ of the central part of the MDS specimen is measured as a function of time by an optical extensometer E, acting as an non-contact displacement gage. The optical extensometer reacts to the axial movement of a small black and white target cemented to the central part of the MDS specimen.

Axial force transmitted by the specimen symmetric supports can be determined as a function of time from the transmitted longitudinal wave $\varepsilon_T(t)$ measured by strain gages T_1, DC supply unit S_1 and amplifier A_1. All electric signals are recorded by digital oscilloscope DO, and next stored in the computer hard disc. In addition, a hard copy of the recorded signals can be produced with an XY recorder or a printer. This new configuration of experimental setup permits a wide variation of the nominal strain rate. Direct determination of the axial displacement enables also a more exact evaluation of deformation history, a very important piece of information in development of adiabatic shear bands. After elimination of time, a force-displacement curve can be constructed for the MDS specimen, and next $\tau(\Gamma)$ or $\Gamma(\Gamma)$ curves can be found. The experimental technique described above has proved to be quite effective and flexible for material

testing at high strain rates as well as for studies of adiabatic shear bands. Detailed description of stress calibration of the MDS specimen by FE is given elsewhere, KLEPACZKO [21].

The net displacement δ_s imposed on the central part of the MDS specimen is

$$(5.1) \qquad \delta_s(t) = \delta_A(t) - C_0 \int_0^t \varepsilon_T(\vartheta)\, d\vartheta,$$

where $\delta_A(t)$ is displacement measured by the optical extensometer/displacement gage shown by E in Fig. 10, $\varepsilon_T(t)$ is the transmitted wave signal, measured by the strain gage station T_1 cemented on the transmitter tube surface, C_0 is the elastic wave speed in the tube. If h is the deforming gage length of the MDS specimen, the nominal shear strain can be found from the formula

$$(5.2) \qquad \Gamma(t) = \frac{1}{h}\left[\delta_A(t) - C_0 \int_0^t \varepsilon_T(\vartheta)\, d\vartheta\right].$$

The nominal strain rate can be also found,

$$(5.3) \qquad \dot{\Gamma}(t) = \frac{1}{h}\left[\frac{d\delta_A}{dt} - C_0\varepsilon_T(t)\right].$$

In the elementary approach it is assumed that the transmitted signal $\varepsilon_T(t)$ in the Hopkinson tube is sufficient to find the axial force transmitted by the MDS supports into the tube

$$(5.4) \qquad F(t) = E A_E \varepsilon_T(t),$$

where A_E is the cross-section of the tube and E is Young's modulus. The cross-section A_E is related to the external and internal tube diameter

$$A_E = \frac{\pi}{4}\left(D^2 - d^2\right).$$

The shear stress in the MDS specimen can be found from the formula, KLEPACZ-KO [21],

$$(5.5) \qquad \tau(t) = \xi\frac{F(t)}{2ab},$$

where ab is the active cross-section of one side of the MDS specimen, ξ is the calibration factor, $\xi \geq 1$ and F is the axial force in the Hopkinson tube. The final formula for the shear stress is

$$(5.6) \qquad \tau(t) = \frac{\pi\left(D^2 - d^2\right)\xi E}{8ab}\varepsilon_T(t).$$

Thus, the shear stress in the MDS is proportional to the current signal of the transmitted longitudinal wave ε_T. All those relations have been derived using the elementary wave theory of longitudinal elastic waves. In addition, it was assumed in derivation of Eq. (3.14) that the local pressures applied by MDS specimen at the end of the Hopkinson tube are transmitted uniformly at the distance $x \approx 3D$; this is the dynamic St. Venant rule. Preliminary FE calculations by a dynamic code confirm this assumption when four SR gages are cemented with the circumferential distribution of $90°$. At the impact velocity $V \approx 100\,\text{m/s}$ time to fracture of the MDS specimen is relatively short, for example, for $\Gamma_{\text{cr}} = 1.0$ the time to fracture is $t_{\text{cr}} \approx 20\,\mu\text{s}$, it gives the wavelength $\lambda \approx 100\,\text{mm}$ and the relative wavelength is $\bar{\lambda} = 2\lambda/(D-d) = 11.1$; $D = 32\,\text{mm}$ and $d = 14\,\text{mm}$. Those wavelengths indicate that some geometry dispersion may be present, but the so-called Pochhammer – Chree vibrations, and of course the geometry dispersion, are much smaller in a tube of the same external diameter than in a solid bar. A more exact analysis of wave dispersion in tubes is in progress and will not be discussed in this paper.

Another important parameter is the length of projectile L_p. It is desirable to reach the time to fracture t_r during the first cycle of elastic wave propagation in a projectile. If the nominal strain rate $\dot{\Gamma}_n$ is assumed and the critical shear strain Γ_{cr} can be estimated, the length of the projectile L_p which assures the contact with the MDS specimen up to fracture can be found from the formula

$$(5.7) \qquad L_p = \frac{\Gamma_{\text{cr}}}{2\,\dot{\Gamma}}C_0.$$

For example, when $\Gamma_{\text{cr}} = 1.0$ and $\dot{\Gamma}_n = 5 \times 10^4\,\text{s}^{-1}$, the projectile length is reduced to $L_p = 50\,\text{mm}$, but for $\dot{\Gamma}_n = 10^3\,\text{s}^{-1}$ the length should be $L_p = 2500\,\text{mm}$. It appears that at lower strain rates it is almost impossible to deform and fracture the MDS specimen during the contact time $t_p = 2L_p/C_0$. The longest projectile used in this study was $L_p = 300\,\text{mm}$.

Nevertheless, the elementary wave theory can be applied, as the first approach, to obtain a complete information on the whole process of deformation and fracture of the MDS specimen; the following data can be obtained from one test: $\tau(t)$; $\Gamma(t)$; $\dot{\Gamma}(t)$; $\tau(\Gamma)$ and $\dot{\Gamma}(\Gamma)$. Since a two-channel fast digital oscilloscope was used (sampling rate 1 GHz), the useful portion of the digital memory could be taken for analysis to determine all the functions needed. A computer program was made to calculate all those functions.

6. Preliminary results of experiments

A preliminary series of experiments was performed on low-alloy steel XC18 (French Standards) of the following composition in %: C 0.17; Mn 0.58; Si 0.21;

S 0.032; P 0.024. The specimen material was supplied in the form of cold drawn
bars DIA 12 mm. After precision machining, all specimens were vacuum annealed
at $\sim$ 1000 K for 1 1/2 hrs and furnace cooled. Metallographic examination showed
a uniform microstructure with evenly distributed grains of ferrite. The tests on
MDS specimens were performed within two ranges of strain rates: medium rates
$10^2\,s^{-1} \leq \dot{\Gamma}_n \leq 10^3\,s^{-1}$ with closed-loop fast testing machine and high rates
$10^4\,s^{-1} \leq \dot{\Gamma}_n \leq 10^5\,s^{-1}$ with the new experimental technique. One of oscillo-
grams obtained with impact velocity $V =\approx$ 35 m/s is shown in Fig. 11. The upper
trace comes from the strain gages on the transmitter tube and the lower one from
the optical extensometer. It can be seen from Fig. 11 that, after the upper yield
peak, there are small oscillations on the upper trace; those longitudinal vibrations
of the transmitter tube were also revealed by the FE dynamic calculations.
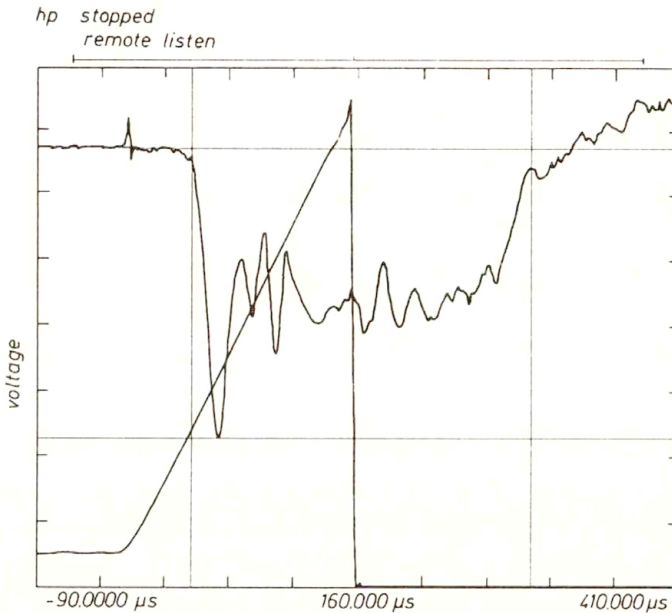
FIG. 11. Oscillogram from the test at impact velocity V_0 = 35.08 m/s; upper trace is the signal
from SR station $T1$; lower trace is the displacement signal from the optical extensometer.

Since the length of the projectile was L_p = 180 mm and t_p = 74 µs, around
three full cycles of wave reflexions had occured during specimen deformation.
They are recognizable in the oscillogram. As a whole, both the upper and lower
yield stresses can be found, as well as the plastic flow curve up to fracture. The
signal from the optical extensometer shows that the displacement rate of the
central part of the MDS specimen is almost constant. The optical contact was
lost before the specimen fractured.

A number of MDS specimens was tested at different impact velocities from
30 m/s to about 100 m/s. The deformed part of the MDS specimen had the follow-

ing dimensions: $h = 2.0$ mm, $a = 5$ mm and $b = 6.0$ mm. Value of $h = 2.0$ mm was the same as the assumed thickness layer in the numerical study. In addition to the dynamic plasticity parameters like the upper and lower yield stress, Klepaczko [21], the nominal strain to fracture and the total energy to fracture by ASB were determined at impact velocities $V_0 \approx 30$ m/s, the nominal strain rates are, respectively, $\dot{\Gamma}_n \approx 1.5 \times 10^4 \, \text{s}^{-1}$ and $5 \times 10^4 \, \text{s}^{-1}$. Estimated value of the localization strain Γ_{LOC} from the five tests performed at $\dot{\Gamma} \approx 1.5 \times 10^4 \, \text{s}^{-1}$ is $\Gamma_{LOC} \approx 2.60$ (from the formula (5.2)) and from three tests performed at $\dot{\Gamma} \approx 5 \times 10^4 \, \text{s}^{-1}$, $\Gamma_{LOC} \approx 0.85$. This surprising result is in complete contradiction to the numerical results shown in Fig. 2. The experimental mean values for Γ_{LOC} are perhaps slightly too high because of a small additional displacement which has occurred due to some plastic deformation of the specimen supports. However, the two groups of specimens tested at two impact velocities were deformed in a similar way. The most plausible explanation of this severe discrepancy is the existence of different initial and boundary conditions in the form of stress concentrators in the corners of the MDS specimen. In addition, the numerical simulation was performed for the *steady state* of shearing, whereas the experiments were performed for the case of *impact* shearing where accelerations play an important role. In general, all stress concentrators activated during impact loading will change to a high degree the formation and development of the ASB. At high impact velocities stress concentrators and inertia will ease the shear band formation. This hypothesis must be again verified in the future.

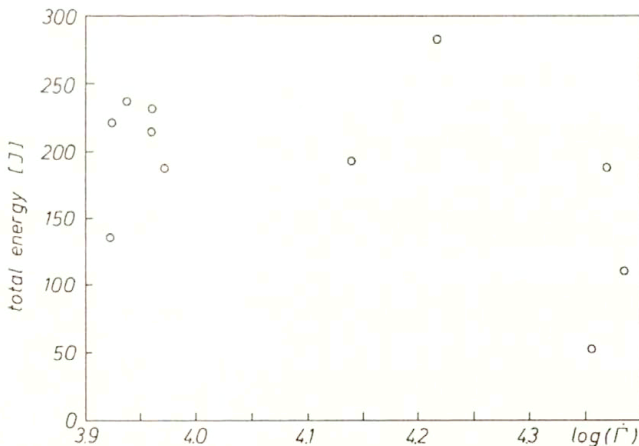
FIG. 12. Energy of fracture for MDS specimens tested at high nominal strain rates as a function of log Γ_n, XC18 steel.

Non-direct confirmation of this finding was attempted by energy analysis. The total energy to fracture was determined for all specimens tested at high strain rates. The result is shown in Fig. 12. The tendency is obvious, the total energy

of fracture decreases as a function of log $\dot{\Gamma}_n$. The trend is not so strong in comparison to changes of Γ_{LOC} because of a positive strain rate-sensitivity. A similar observation concerning energy consumption during fracture by ASB formation was reported by PINTAT *et al.* [35]. The so-called "hat" specimens made of two plain carbon steel of the garde 1010 and 1045 were deformed with SHPB at different velocities, $5.5\,\mathrm{m/s} \leq V_0 \leq 8.3\,\mathrm{m/s}$; strain rates are difficult to estimate, probably around $10^3\,\mathrm{s}^{-1}$. In both cases the fracture energy decreased with the loading velocity, more than twofold in the cases of the softer versions of those steels, that is for annealed states. In the logarithmic scale reduction of the energy would be very abrupt.

7. Concluding remarks

There is a general agreement that the critical instability strain is related to the zero hardening condition, $d\tau/d\Gamma = 0$, of the adiabatic stress-strain curve. The post-instability behaviour is much more complex. In addition to material behaviour, initial and boundary conditions could play a decisive role in development and formation of ASB and also in fracture. The steady-state solutions, like the numerical one reported in this paper, or analytical ones, are very useful tools in ASB studies, they can depict the late stage morphology during ASB development as a function of initial and boundary conditions. However, the steady state solutions neglect the stress concentrators which are always present in real situations including the experiment. It has been shown in this study that the stress concentrators and perhaps inertia invert the post-localization behaviour as a function of the nominal strain rate. To study further those effects, a variety of experimental techniques must be applied with well specified initial and boundary conditions. The next inevitable step is a superposition of fracture dynamics on ASB morphology. Comparison of all available approaches for the same or similar materials may provide a data base on development and formation of ASB.

Up to now, majority of analytical and numerical solutions have been obtained for rigid-viscoplastic constitutive relations. When elasticity is included into analyses of the ASB, the post-instability behaviour will change in a manner similar to fracture dynamics where the elastic energy in the loading train interferes with a crack. In addition, the wave dynamics makes the problem still more complex. Because of rapid interactions between the ASB and elastic boundaries, some oscillations can be excited, WRIGHT and WALTER [44]. At very high strain rates where a local wave interaction is expected, the development of the ASB may be controlled by elastic unloading waves, for example FRESSENGEAS [9].

Another important problem, not addressed in this paper, are *post factum* metallographic examination of ASB. Electron microscopy, both in transmission and scanning, is a very important tool, for example MEYERS *et al.* [32], GIOVANOLA [11].

Since morphology of ASB is closely related to several branches of mechanics

and materials science like plasticity, thermodynamics, fracture mechanics and metallurgy, a concerted action must be pursued to clarify the remaining problems.

Acknowledgements

References

1. Y. Bai, *Adiabatic shear banding*, Res Mechanica, 31, 133, 1990.

2. M.V. Buisson and A. Molinari, *Bandes de cisaillement stationnaires dans un acier*, [in:] Proc. Int. Conf. on Mechanical and Physical Behaviour of Materials Under Dynamic Loading, Les éditions de physique, Les Ulis, C3-167, 1988.

3. T.J. Burns, *A mechanism of shear band formation in the high strain-rate torsion test*, J. Appl. Mech., 57, 836, 1990.

4. J.D. Campbell and W.G. Ferguson, *The temperature and strain rate dependence of the shear sthength of mild steel*, Phil. Mag., 21, 63, 1970.

5. L.S. Costin, E.E. Crisman, R.H. Hawley and J. Duffy, *On the localization of plastic flow in mild steel tubes under dynamic torsional loading*, [in:] Proc. 2-nd Conf. on the Mechanical Properties of Materials at High Rates of Strain, Inst. Phys. Conf. ser. No. 47, p.90, Bristol 1979.

6. R. Dormeval, *Adiabatic shear phenomenon*, [in:] Materials at High Strain Rates, Elsevier Appl.Sci., p.47, London 1987.

7. W.G. Ferguson, F.E. Hauser and J.E. Dorn, *Dislocation damping in zinc single crystals*, Brit. J. Appl. Phys., 18, 411, 1967.

8. C. Fressengeas, *Analyse dynamique élasto-viscoplastique de l'hétérogénéité de la déformation plastique de cisaillement*, Proc. Int. Conf. on Mechanical and Physical Behaviour of Materials Under Dynamic Loading, Les éditions de physique, Les Ulis, C3-277, 1988.

9. C. Fressengeas, *Adiabatic shear morphology at very high strain rates*, Int. J. Impact Engng, 8, 141, 1989.

10. C. Fressengeas and A. Molinari, *Non-linear approximate analysis of shear band formation*, [in:] Impact Loading and Dynamic Behaviour of Materials, DGM Informationsgesellschaft Verlag, Oberursel, 2, 761, 1988.

11. J.H. Giovanola, *Adiabatic shear bending under pure shear loading*, Mechanics of Materials, 7, part I, 59; part II, 73, 1988.

12. K.A. Hartley, J. Duffy and R.H. Hawley, *Measurement of the temperature profile during shear band formation in steels deforming at high strain rates*, J. Mech. Phys. Solids, 35, 283, 1987.

13. G.R. Johnson, *Dynamic analysis of a torsion test specimen including heat conduction and plastic flow*, J. Engng. Materials and Technol., 103, 201, 1981.

14. W. Johnson, *Henri Tresca as the originator of adiabatic heat lines*, Int. J. Mech. Sci., 29, 301, 1987.

15. M. Kamiński, *Coupling of strain and temperature fields in the problem of torsion of a thin-walled tube*, Engng. Trans., [in Polish], 24, 185, 1976.

16. J.R. Klepaczko, *The relation of thermally activated flow in BCC metals and ferritic steels to strain rate history and temperature history effects*, Technical Report DMR-79-23257/2, Materials Research Laboratory, Brown University, Providence 1981.

17. J.R. Klepaczko, *A practical stress-strain-strain rate-temperature constitutive relation of the power form*, J. Mech. Working Technology, 15, 143, 1987.

18. J.R. KLEPACZKO, *Modelling of structural evolution at medium and high strain rates, FCC and BCC metals*, [in:] Constitutive Relations and Their Physical Basis, Risö Natl. Laboratory, p.387, Roskilde, Denmark 1987.

19. J.R. KLEPACZKO, *A general approach to rate sensitivity and constitutive modelling of FCC and BCC metals*, [in:] Impact: Effects of Fast Transient Loadings, A.A. Balkema, p.3, Rotterdam 1988.

20. J.R. KLEPACZKO, *Adiabatic shear bands, review of experimental techniques and results*, [in:] Mécanique, Modélisation Numérique et Dynamique des Matériaux, Publications LMA-CNRS, No. 124, p.335, Marseille 1991.

21. J.R. KLEPACZKO, *An experimental technique for shear testing at high and very high strain rates, case of a mild steel*, Int. J. Impact Engng., 15, 25, 1994.

22. J.R. KLEPACZKO and B. REZAIG, *A numerical study of rate effects in shear band formation*, 1992 [in preparation].

23. J.R. KLEPACZKO, P. LIPIŃSKI and A. MOLINARI, *An analysis of the thermoplastic catastrophic shear in some metals*, [in:] Impact Loading and Dynamic Behaviour of Materials, DGM Informationsgesellschaft Verlag, Oberursel, 2, 695, 1988.

24. U.F. KOCKS, A.S. ARGON and M.F. ASHBY, *Thermodynamics and kinetics of slip*, Pergamon Press, Oxford 1976.

25. Y.M. LEROY and A. MOLINARI, *Stability of steady states in shear zones*, J. Mech. Phys. Solids, 40, 181, 1992.

26. J. LITOŃSKI, *Plastic flow of a tube under adiabatic torsion*, Bull. Acad. Polon. Sci., Série Sci. Tech., 25, 7, 1977.

27. J. LITOŃSKI, *Numerical analysis of plastic torsion processes with account of heat generated during deformation*, [in Polish], IFTR Reports, 33, Warsaw 1985.

28. D.D. MAKEL and G.F. WILSDORF, *Localized melting during the separation of high strength tensile samples*, [in:] Shock-Wave and High-Strain-Rate Phenomena in Materials, M.Dekker, Inc., p.693, New York 1992.

29. A. MARCHAND and J. DUFFY, *An experimental study of the formation process of adiabatic shear bands in a structural steel*, J. Mech. Phys. Solids, 36, 251, 1988.

30. Z. MARCINIAK and K. KUCZYŃSKI, *Limit strains in the process of stretch-forming sheet metal*, Int. J. Mech. Sci., 9, 609, 1967.

31. A.M. MERZER, *Modelling of adiabatic shear band development from small imperfections*, J. Mech. Phys. Solids, 30, 323, 1982.

32. M.A. MEYERS, C.L. WITTMAN, H.R. PAK and S. KURIYAMA, *Observation and modelling of high-strain-rate shear localization*, [in:] Impact Loading and Dynamic Behaviour of Materials, DGM Informationsgesellschaft Verlag, Oberrursel, vol. 2, 719, 1988.

33. A. MOLINARI and R.J. CLIFTON, *Localisation de la déformation viscoplastique en cisaillement simple: résultats exacts en théorie non linéaire*, C.R. de l'Acad. Sci., Sér. II, 296, 1, 1983.

34. O. OUSSOUADDI and J.R. KLEPACZKO, *An analysis of transition between isothermal and adiabatic deformation for the case of torsion of a tube*, [in:] Proc. 3rd Intern. Conf. on Mechanical and Physical Behaviour of Materials under Dynamic Loading, Les éditions de physique, Les Ulis, C3-323, 1991.

35. T. PINTAT, B. SCHOLZ, H.D. KUNZE and O. VÖHRINGER, *The influence of carbon content and grain size on energy consumption during adiabatic shearing*, [in:] Proc. Int. Conf. on Mechanical and Physical Behaviour of Materials Under Dynamic Loading, Les éditions de physique, Les Ulis, C3-237, 1988.

36. H.C. ROGERS, *Adiabatic plastic deformation*, Ann. Rev. Mater. Sci., 9, 283, 1979.

37. S.L. SEMIATIN, M.R. STAKER and J.J. JONAS, *Plastic instability and flow localization in shear at high rates of deformation*, Acta Metall., 32, 1347, 1984.

38. S.L. SEMIATIN, J.J. JONAS, T.G. SHAWKI and J. DUFFY, *Effect of material imperfections on flow localization in torsion*, Scripta Metall., 21, 669, 1987.

39. T.G. SHAWKI and R.J. CLIFTON, *Shear band formation in thermal viscoplastic materials*, Mech. of Materials, 8, 13, 1989.

40. H. TRESCA, *On further applications of the flow of solids*, Proc. Inst. Mech. Engrs., 30, 301, 1878.

41. I.V. VARFOLOMEYEV and J.R. KLEPACZKO, *Approximate analysis on strain rate effects and behaviour of stress and strain fields at the crack tip in Mode II in metallic materials*, Appendix No. 1 to the Technical Report submitted to the European Research Office, US Army RDSG, Contract DAJA 45-90-C-0052; also Technical Report ISGMP-LPMM, Metz University, 1992.

42. T.W. Wright, *Approximate analysis for the formation of adiabatic shear bands*, J. Mech. Phys. Solids, **38**, 515, 1990.

43. T.W. Wright and J.W. Walter, *On stress collapse in adiabatic shear bands*, J. Mech. Phys. Solids, **35**, 701, 1987.

44. T.W. Wright and J.W. Walter, *Adiabatic shear bands in one dimension*, [in:] Mechanical Properties of Materials at High Rates of Strain 1989, Int. Phys. Conf., Ser. No. 102, p. 119, Bristol 1989.

45. C. Zener and J.H. Hollomon, *Effect of strain rate upon plastic flow of steel*, J. Appl. Phys, **15**, 22, 1944.

FACULTÉ DES SCIENCES
UNIVERSITÉ DE METZ, METZ, FRANCE.

Many-sphere Oseen hydrodynamic interactions

I. PIEŃKOWSKA (WARSZAWA)

IN THIS PAPER the hydrodynamic interactions of N rigid spheres, immersed in an incompressible, unbounded fluid, are considered. The velocity and pressure fields of the fluid obey the Oseen equations. The paper concerns the weak inertial effects, arising in the hydrodynamic interactions. The scope of the paper is specified by the condition Re < 1, where Re is the characteristic Reynolds number. The forces, exerted on the spheres by the fluid, are presented as due to the multiple scattering processes.

1. Introduction

THE PRESENT PAPER deals with the Oseen hydrodynamic interactions of a finite number N of rigid spheres, immersed in an incompressible, unbounded fluid. The paper is a continuation of the paper [1], in which the notion of the Oseen hydrodynamic interaction tensors has been introduced. Here we present the further analysis of the properties of the tensors, relevant for the consideration of the forces, exerted on the spheres by the fluid. The dependence of these forces on the spatial distribution of the spheres, and on the weak momentum convection (Re < 1) is analysed.

The properties of the Oseen boundary-value problems of flows past a body have been examined not only on their own but also in view of the fact that the knowledge of these properties can be useful in the analysis of the related Navier–Stokes problems. For example, in the series of papers by FINN [2, 3], we can find the analysis of the mathematical aspects of the Navier–Stokes boundary-value problem, for the case of small data, based on the consideration of the respective linearized problem. The papers by GALDI [4], and SALVI [5], being devoted to the mathematical questions arising in the Oseen boundary-value problem for a single body, contain also the considerations on the relations between the linearized and the nonlinear cases.

The first results for the flows past two spheres have been obtained by Oseen himself [6]. The author used the Smoluchowski's method of description of the hydrodynamic interactions. In the papers by KANEDA and ISHII [7], and by VASSEUR and COX [8], the case of two spheres has been considered in the framework of the Navier–Stokes equation. To examine the velocity, and the pressure fields, the authors applied the matched asymptotic expansions approach (for more details see the paper [1]).

In this paper, to examine the properties of the Oseen hydrodynamic interactions of N rigid spheres, the integral equation approach is used. It involves the second order hydrodynamic interaction tensors, related to the Green tensor of

the problem considered. The properties of the interaction tensors are analysed in the range of small Reynolds number, $\mathrm{Re} < 1$. As an example, the drag forces acting on two spheres, being at rest in a fluid, are calculated up to terms of the order of $O(\mathrm{Re})$ and $O(a/R)$ (a – the radius of the spheres, R – the typical distance between the centres of two spheres, $\mathbf{U}$ – the uniform velocity of the fluid at infinity, ν – the kinematic viscosity, $\mathrm{Re} = a|\mathbf{U}|/\nu$).

2. Basic equations

The spatial distribution of the spheres, being at rest, is described in the fixed Cartesian coordinate system $\mathbf{r}(x, y, z)$. The positions of the centres of the spheres are given by $\mathbf{R}_j^0$, $j = 1, \ldots, N$, and the positions of the surfaces of the spheres are given by $\mathbf{R}_j$. We introduce also the local coordinate system for each sphere: $\mathbf{r}_j = \mathbf{R}_j - \mathbf{R}_j^0, \mathbf{r}_j(a, \Omega_j)$.

The presence of the spheres in the flow accounts for the induced forces $\mathbf{f}_j(\mathbf{R}_j)$ [9, 15], distributed on the surfaces of the spheres. These surfaces are indicated by the appropriate δ – functions: $\delta(\mathbf{r} - \mathbf{R}_j)$. The forces $\mathbf{f}_j(\mathbf{r}_j)$ give rise to the source term in the Oseen equation of motion:

$$\rho \mathbf{U} \cdot \nabla \mathbf{v} - \mu \Delta \mathbf{v} + \nabla p = \sum_{j=1}^{N} \int d\Omega_j \delta \left[\mathbf{r} - \mathbf{R}_j(\Omega_j) \right] \mathbf{f}_j(\Omega_j),$$

(2.1)

$$\nabla \cdot \mathbf{v} = 0,$$

where ρ is the density, μ – the dynamic viscosity, $\mathbf{v}(\mathbf{r})$ – the velocity, p – the pressure of the incompressible fluid. On the surfaces of the spheres, we assume the no-slip boundary conditions

(2.2) $$\dot{\mathbf{R}}_j(\Omega_j) = \mathbf{v}(\mathbf{R}_j(\Omega_j)),$$

$\dot{\mathbf{R}}_j$ denotes the velocity of the j-th sphere.

In the volumes of the spheres we determine the divergence of the stress tensor $\mathbf{P}(\mathbf{r})$ by the following relation:

(2.3) $$\nabla \cdot \mathbf{P}(\mathbf{r}_j) = 0, \qquad |\mathbf{r}_j| < a.$$

Next, the velocity field of the fluid is expressed in terms of the Green tensor $\mathbf{T}(\mathbf{r})$, acting on the induced forces $\mathbf{f}_j$:

$$\mathbf{v}(\mathbf{r}) = \mathbf{v}^0(\mathbf{r}) + \int d\mathbf{r}' \mathbf{T}(\mathbf{r} - \mathbf{r}') \cdot \sum_{j=1}^{N} \int d\Omega_j' \delta \left[\mathbf{r}' - R_j'(\Omega_j') \right] \mathbf{f}_j'(\Omega_j'),$$

(2.4)

$$\mathbf{v}^0(\mathbf{r}) = \mathbf{U}.$$

$\mathbf{v}^0(\mathbf{r})$ denotes the fluid velocity in the absence of the spheres. Below the Green tensor is presented by means of the space-Fourier representation [10]:

(2.5)
$$T(\mathbf{r}) = \int \frac{d\mathbf{k}}{(2\pi)^3} \frac{\exp(i\,\mathbf{k}\cdot\mathbf{r})}{\mu(k^2 + i\nu^{-1}\mathbf{U}\cdot\mathbf{k})} \left(1 - \hat{\mathbf{k}}\hat{\mathbf{k}}\right),$$

$$\nu = \mu/\rho, \qquad \hat{\mathbf{k}} = \mathbf{k}/|\mathbf{k}|, \qquad k = |\mathbf{k}|.$$

Using the expression for the velocity field and the boundary conditions on the surfaces of the spheres, we obtain N coupled integral equations [11]:

(2.6)
$$\dot{\mathbf{R}}_j\,(\Omega_j) = \mathbf{v}^0(\mathbf{R}_j(\Omega_j)) + \int d\Omega_j' \mathbf{T} \left[\mathbf{R}_j(\Omega_j) - \mathbf{R}_j'(\Omega_j')\right] \cdot \mathbf{f}_j'(\Omega_j')$$

$$+ \sum_{k \neq j}^{N} \int d\Omega_k \mathbf{T}\left[\mathbf{R}_j(\Omega_j) - \mathbf{R}_k(\Omega_k)\right] \cdot \mathbf{f}_k(\Omega_k),$$

$$\mathbf{V}_j(\Omega_j) = \dot{\mathbf{R}}_j\,(\Omega_j) - \mathbf{v}^0(\mathbf{R}_j(\Omega_j)),$$

where $\mathbf{V}_j$ is the relative velocity of the j-th sphere with respect to the fluid. The first integral on the r.h.s. describes the interaction of the j-th sphere with the fluid, the second integral concerns the hydrodynamic interactions between the spheres.

3. The set of algebraic equations

To transform the set of integral equations (2.6), we apply the technique of expansion in an infinite series of normalized spherical harmonics [13]:

(3.1)
$$\mathbf{V}_j(\Omega_j) = \sqrt{4\pi} \sum_{lm}^{\infty} \mathbf{V}_{j,lm} Y_l^m(\Omega_j),$$

$$\mathbf{f}_j(\Omega_j) = \frac{1}{\sqrt{4\pi}\,a^2} \sum_{lm}^{\infty} \mathbf{f}_{j,lm} Y_l^m(\Omega_j),$$

$$|m| \leq l, \qquad 0 \leq l < \infty.$$

In the considered case of the uniform velocity of the fluid at infinity, the expansion coefficients $\mathbf{V}_{j,lm}$ read:

(3.2)
$$\mathbf{V}_{j,lm} = -\mathbf{v}_{j,lm}^0 = \begin{cases} -\mathbf{U}, & l = 0, \\ 0, & l \geq 1. \end{cases}$$

The forces $\mathbf{F}_j$, exerted by the fluid on the spheres, can be expressed in terms of the coefficients $\mathbf{f}_{j,lm}$ as follows:

(3.3)
$$\mathbf{F}_j = -\int \nabla \cdot \mathbf{P}(\mathbf{r}_j) d\mathbf{r}_j = -\mathbf{f}_{j,00}.$$

In view of the orthogonality property of spherical harmonics, the set of integral equations (2.6) leads to the following relations for the expansion coefficients:

$$(3.4) \qquad V_{j,l_1m_1} = \sum_{l_2m_2} \mathbf{T}_{l_1m_1}^{l_2m_2}(\mathbf{O}_j) \cdot \mathbf{f}_{j,l_2m_2} + \sum_{k \neq j}^{N} \sum_{l_2m_2} \mathbf{T}_{l_1m_1}^{l_2m_2}(\mathbf{R}_{jk}) \cdot \mathbf{f}_{k,l_2m_2} \,,$$

where $\mathbf{R}_{jk} = \mathbf{R}_k^0 - \mathbf{R}_j^0$ is the distance between the centres of two spheres, $\mathbf{T}_{l_1m_1}^{l_2m_2}$ are the hydrodynamic interaction tensors. The interaction tensors are given by the following expressions:

(i) self-interaction tensors:

$$(3.5) \qquad \mathbf{T}_{l_1m_1}^{l_2m_2}(\mathbf{O}_j) = \frac{1}{2\pi^2\mu} i^{l_1-l_2} \int d\mathbf{k} \frac{\left(1 - \hat{\mathbf{k}}\hat{\mathbf{k}}\right)}{k^2 + i\nu^{-1}\mathbf{U}\cdot\mathbf{k}} Y_{l_1}^{-m_1} Y_{l_2}^{m_2} j_{l_1}(ak) j_{l_2}(ak),$$

where j_{l_1}, j_{l_2} are the spherical Bessel functions,

(ii) mutual-interaction tensors:

$$\mathbf{T}_{l_1m_1}^{l_2m_2}(\mathbf{R}_{jk}) = \sum_{l_3m_3} \mathbf{T}_{l_1m_1,l_3m_3}^{l_2m_2}(|\mathbf{R}_{jk}|) Y_{l_3}^{m_3}(\Omega_{jk}),$$

(3.6)

$$\mathbf{T}_{l_1m_1,l_3m_3}^{l_2m_2} = \frac{2}{\pi\mu} i^{l_1-l_2-l_3} \int d\mathbf{k} \frac{\left(1 - \hat{\mathbf{k}}\hat{\mathbf{k}}\right)}{k^2 + i\nu^{-1}\mathbf{U}\cdot\mathbf{k}}$$

$$\times Y_{l_1}^{-m_1} Y_{l_2}^{m_2} Y_{l_3}^{-m_3} j_{l_1}(ak) j_{l_2}(ak) j_{l_3}(R_{jk}k).$$

The properties of the above tensors follow from the properties of the Green tensor (2.5).

To discuss the relations of the forces $\mathbf{F}_j$, exerted on the spheres by the fluid, to the fluid velocity $\mathbf{U}$, we present the basic set of the algebraic equations (3.4) in the following form:

$$(3.7) \qquad \mathbf{f}_{j,l_1m_1} = \sum_{l_2m_2} \tilde{\mathbf{T}}_{l_1m_1}^{l_2m_2}(\mathbf{O}_j) \cdot \left[V_{j,l_2m_2} - \sum_{k \neq j}^{N} \sum_{l_3m_3} \mathbf{T}_{l_2m_2}^{l_3m_3}(\mathbf{R}_{jk}) \cdot \mathbf{f}_{k,l_3m_3} \right].$$

The inverse self-interaction tensors $\tilde{\mathbf{T}}_{l_1m_1}^{l_2m_2}$, appearing in the above relations, fulfil the condition

$$(3.8) \qquad \sum_{l_3m_3} \tilde{\mathbf{T}}_{l_1m_1}^{l_3m_3}(\mathbf{O}_j) \cdot \mathbf{T}_{l_3m_3}^{l_2m_2}(\mathbf{O}_j) = \mathbf{1}\delta_{m_1m_2}\delta_{l_1l_2} \,.$$

Starting from the relations (3.7), we can calculate the forces $\mathbf{F}_j$ within the assumed approximation with respect to Re and σ (cf. Sec. 5), $\sigma = a/R$.

4. The properties of the hydrodynamic interaction tensors

To perform the analysis of the weak interial effects arising in the hydrodynamic interactions, we will examine the dependence of the interaction tensors on Re, in the range of Re < 1, and on the spatial distribution of the spheres.

4.1. Self-interaction tensors $T^{l_2 m_2}_{l_1 m_1}(O_j)$

To evaluate the interaction tensors (3.5), we introduce spherical coordinates in the k-integrals. The $|k|$ integration leads to the following formulae:

(i) For the cases $|l_1 - l_2| = 2n$, $n = 0, 1, 2, \ldots$, $\beta = 1$,

$$(4.1) \qquad T^{l_2 m_2}_{l_1 m_1}(O_j) = \frac{\beta}{4\pi a\mu} i^{l_1 - l_2 + |l_1 - l_2|} \int d\hat{k} \left(1 - \hat{k}\hat{k}\right) Y^{-m_1}_{l_1} Y^{m_2}_{l_2} I_A(\mathrm{Re}\xi) K_\lambda(\mathrm{Re}\xi),$$

where

$$A = \max\left(l_1 + \frac{1}{2}, l_2 + \frac{1}{2}\right), \qquad \lambda = \min\left(l_1 + \frac{1}{2}, l_2 + \frac{1}{2}\right).$$

A and λ are the larger and smaller number, respectively, of $l_1 + \frac{1}{2}$ and $l_2 + \frac{1}{2}$, symbols $I_{l_1+1/2}$, $K_{l_1+1/2}$ denote the modified Bessel functions of the first, and third kind, respectively,

$$\hat{U} = U/|U|, \qquad \xi = \cos(\hat{U}, \hat{k});$$

(ii) and respectively for the cases $|l_1 - l_2| = 2n + 1$, $\beta = -1$.

From the properties of the Bessel functions in the range Re < 1 it follows that tensors $T^{l_2 m_2}_{l_1 m_1}(O_j)$ behave as follows:
For $|l_1 - l_2| = 2n$, $\beta = 1$,

$$(4.2) \qquad T^{l_2 m_2}_{l_1 m_1}(O_j) = \frac{\beta}{8\pi a\mu} i^{l_1 - l_2 + |l_1 - l_2|} \left(\frac{1}{2}\right)^{|l_1 - l_2|} \frac{\Gamma(\lambda)}{\Gamma(A + 1)}$$

$$\times \int d\hat{k} \left(1 - \hat{k}\hat{k}\right) Y^{-m_1}_{l_1} Y^{m_2}_{l_2} (\mathrm{Re}\xi)^{|l_1 - l_2|} + \text{h.o.t},$$

and, respectively, for the cases $|l_1 - l_2| = 2n + 1$, $\beta = -1$.

Hence, for the particular case of $l_1 = l_2$, the leading order terms of the self-interaction tensor are independent of Re. These terms refer to the regime of Stokes flows, which do not exhibit the effects of the inertia of the fluid. At zero Reynolds number the self-interaction tensors become equal to

$$(4.3) \qquad T^{l_1 m_2}_{l_1 m_1}(O_j) = \frac{1}{4\sqrt{\pi}\, a\mu} \frac{1}{(l_1 + 1/2)} K^{l_1 m_2}_{l_1 m_1, 00}.$$

where

$$\mathbf{K}^{l_2 m_2}_{l_1 m_1, l_3 m_3} = i^{l_1 - l_2 - l_3} \int d\hat{\mathbf{k}} \left(\mathbf{1} - \hat{\mathbf{k}}\hat{\mathbf{k}}\right) Y_{l_1}^{-m_1} Y_{l_2}^{m_2} Y_{l_3}^{-m_3}.$$

The second order tensors $\mathbf{K}$ have been examined, in the context of Stokes conditions, by Yoshizaki, and Yamakawa [13]. Here, as $\mathrm{Re} \Rightarrow 0$, we recover the Stokes self-interaction tensors; for example, the tensor $\mathbf{T}^{00}_{00}(\mathbf{O}_j)$ describing the interaction of a single sphere with fluid, having at infinity the velocity $\mathbf{U}$, reads:

(4.4) $$\mathbf{T}^{00}_{00}(\mathbf{O}_j) = \frac{1}{2\sqrt{\pi}\,a\mu} \mathbf{K}^{00}_{00,00} = \frac{1}{6\pi\mu a} \mathbf{1}.$$

Examining weak inertia effects, we are interested in the contributions, of the order of $O(\mathrm{Re})$ to the relevant tensors. From the properties of the modified Bessel functions we see that there are two sources of such contributions. Firstly, we have a group of the self-interaction tensors, being of the leading order of Re (specified by the condition $|l_1 - l_2| = 1$). These self-interaction tensors are equal to

(4.5) $$\mathbf{T}^{l_2 m_2}_{l_2 + 1 m_1}(\mathbf{O}_j) = \frac{\mathrm{Re}}{8\sqrt{3}\sqrt{\pi}\,a\mu(l_2 + 1/2)(l_2 + 3/2)}$$

$$\times \left[\hat{U}_z \mathbf{K}^{l_2 m_2}_{l_2 + 1 m_1, 10} + \frac{1}{\sqrt{2}}\left(\hat{U}_x - i\hat{U}_y\right) \mathbf{K}^{l_2 m_2}_{l_2 + 1 m_1, 1-1}\right.$$

$$\left. + \frac{1}{\sqrt{2}}\left(\hat{U}_x + i\hat{U}_y\right) K^{l_2 m_2}_{l_2 + 1 m_1, 11}\right] + \text{h.o.t.},$$

and, respectively, to

(4.6) $$\mathbf{T}^{l_1 + 1 m_2}_{l_1 m_1}(\mathbf{O}_j) = \frac{\mathrm{Re}}{8\sqrt{3}\sqrt{\pi}a\mu(l_1 + 1/2)(l_1 + 3/2)}\left[\hat{U}_z \mathbf{K}^{l_1 + 1 m_2}_{l_1 m_1, 10}\right.$$

$$+ \frac{1}{\sqrt{2}}\left(\hat{U}_x - i\hat{U}_y\right) \mathbf{K}^{l_1 + 1 m_2}_{l_1 m_1, 1-1} + \frac{1}{\sqrt{2}}\left(\hat{U}_x + i\hat{U}_y\right) \mathbf{K}^{l_1 + 1 m_2}_{l_1 m_1, 11}\right] + \text{h.o.t.}.$$

We see that here the tensors $\mathbf{K}^{l_2 m_2}_{l_1 m_1, l_3 m_3}$ have higher values of the indices $(l_3 m_3)$ in comparison with the tensors $\mathbf{K}$, referring to the Stokes flow regime. For example, the tensor $\mathbf{T}^{1m}_{00}(\mathbf{O}_j)$ reads:

(4.7) $$\mathbf{T}^{1 m_2}_{00}(\mathbf{O}_j) = \frac{\mathrm{Re}}{6\sqrt{6}\pi\mu a}\left\{\sqrt{2}\,\hat{U}_z \mathbf{K}^{1 m_2}_{00, 10} - \left(\hat{U}_x - i\hat{U}_y\right) \mathbf{K}^{1 m_2}_{00, 1-1}\right.$$

$$\left. + \left(\hat{U}_x + i\hat{U}_y\right) \mathbf{K}^{1 m_2}_{00, 11}\right\} + \text{h.o.t.}.$$

Secondly, we have the contributions linear in Re in a series expansion of the tensor $\mathbf{T}^{00}_{00}$ with respect to Re. It can be presented in the following form:

(4.8) $$\mathbf{T}^{00}_{00}(\mathbf{O}_j) = \mathbf{T}^{(1)00}_{00}(\mathbf{O}_j) + \mathbf{T}^{(2)00}_{00}(\mathbf{O}_j),$$

where

$$\mathbf{T}_{00}^{(1)00}(\mathbf{O}_j) = \frac{1}{6\pi\mu a}\hat{\mathbf{I}}$$

describes the Stokes interactions, and

$$\mathbf{T}_{00}^{(2)00}(\mathbf{O}_j) = \frac{1}{6\pi\mu a}\left[-\frac{3}{16}\mathrm{Re}\left(3\mathbf{I} - \hat{\mathbf{U}}\hat{\mathbf{U}}\right)\right]$$

describes the Oseen interaction, in the approximation considered.

Thus we have brought together all contributions linear in Re to the self-interaction tensors, needed to discuss the weak inertia effects of the interaction of a single sphere with the fluid.

4.2. Mutual-interaction tensors $\mathbf{T}_{l_1 m_1, l_3 m_3}^{l_2 m_2}(\mathbf{R}_{jk}, \mathrm{Re})$

To consider the effects of Re, the tensors $\mathbf{T}_{l_1 m_1, l_3 m_3}^{l_2 m_2}$ are presented in terms of a series expansion, using the formula (7) from §7.15 of [14]:

$$(4.9) \quad \mathbf{T}_{l_1 m_1, l_3 m_3}^{l_2 m_2} = \sum_{m=0}^{\infty} \mathbf{T}_{l_1 m_1, l_3 m_3}^{l_2 m_2, m} = \frac{\sqrt{\pi}}{2a\mu\Gamma(l_1 + 3/2)\Gamma(l_2 + 3/2)}i^{l_1 - l_2 - l_3}$$

$$\times \left(\frac{a}{R_{jk}}\right)^{l_1 + l_2 + 1} \sum_{m=0}^{\infty} \frac{(l_1 + l_2 + 2m + 1/2)\Gamma(l_1 + l_2 + m + 1/2)}{m!}$$

$$\times F_4\left[-m, l_1 + l_2 + m + \frac{1}{2}; l_1 + \frac{3}{2}, l_2 + \frac{3}{2}; \left(\frac{a}{R_{jk}}\right)^2, \left(\frac{a}{R_{jk}}\right)^2\right]$$

$$\times \int d\hat{\mathbf{k}}\left(\mathbf{1} - \hat{\mathbf{k}}\hat{\mathbf{k}}\right)Y_{l_1}^{-m_1}Y_{l_2}^{m_2}Y_{l_3}^{-m_3}$$

$$\times \int d\kappa\frac{\kappa - iR_{jk}\alpha\xi}{\kappa^2 + (R_{jk}\alpha\xi)^2}J_{l_1 + l_2 + 2m + 1/2}(\kappa)J_{l_3 + 1/2}(\kappa),$$

where F_4 is the hypergeometric series of two variables, $J_{n+1/2}$ are the Bessel functions, and where, for $|l_1 + l_2 + 2m - l_3| = 2n$, $\beta = 1$,

$$(4.10) \quad \int d\kappa\frac{\kappa - iR_{jk}\alpha\xi}{\kappa^2 + (R_{jk}\alpha\xi)^2}J_{l_1 + l_2 + 2m + 1/2}(\kappa)J_{l_3 + 1/2}(\kappa)$$

$$= \beta i^{|l_1 + l_2 + 2m - l_3|}I_Z(R_{jk}\alpha\xi)K_\zeta(R_{jk}\alpha\xi),$$

and for $|l_1 + l_2 + 2m - l_3| = 2n + 1$, $\beta = -1$,

$$(4.11) \quad Z = \max\left(l_1 + l_2 + 2m + \frac{1}{2}, l_3 + \frac{1}{2}\right),$$

$$\zeta = \min\left(l_1 + l_2 + 2m + \frac{1}{2}, l_3 + \frac{1}{2}\right). \qquad \alpha = \frac{|\mathbf{U}|}{\nu}.$$

Similarly to the self-interaction tensors, the dependence on Re of the mutual-interaction tensors is given in the form of a product of two modified Bessel functions. However, the arguments of these functions contain the quotients $\mathrm{Re}_m = \mathrm{Re}/(a/R_{jk})$ in view of the fact that the distances R_{jk} are characteristic for the mutual interactions. In view of the properties of the modified Bessel functions in the considered range of $\mathrm{Re}_m < 1$, we see that the Stokes regime is described by the following leading order contributions to the respective mutual-interaction tensors:

$$(4.12) \quad \mathbf{T}^{l_2 m_2}_{l_1 m_1, l_3 m_3} = \sum_{m=0}^{\infty} \mathbf{T}^{l_2 m_2, m}_{l_1 m_1, l_3 m_3} = \frac{\sqrt{\pi}}{4 a \mu \Gamma(l_1 + 3/2)\Gamma(l_2 + 3/2)} \left(\frac{a}{R_{jk}}\right)^{l_1 + l_2 + 1}$$

$$\times \mathbf{K}^{l_2 m_2}_{l_1 m_1, l_3 m_3} \sum_{m=0} \frac{(l_1 + l_2 + 2m + 1/2)\Gamma(l_1 + l_2 + m + 1/2)}{m!} \frac{\Gamma(\zeta)}{\Gamma(Z+1)}$$

$$\times F_4\left[-m, l_1 + l_2 + m + \frac{1}{2}; l_1 + \frac{3}{2}, l_2 + \frac{3}{2}; \left(\frac{a}{R_{jk}}\right)^2, \left(\frac{a}{R_{jk}}\right)^2\right],$$

for the cases $|l_1 + l_2 + 2m - l_3| = 0$, $l_1 + l_2 + l_3 = 2n$, $l_1 + l_2 - l_3 \geq -2$.

Thus the hydrodynamic Stokes interactions are described by means of the tensors being of the leading order of $(a/R)^{l_1 + l_2 + 1}$,

$$(4.13) \quad \begin{array}{ll} \text{(i)} & T^{l_2 m_2, 0}_{l_1 m_1, l_3 m_3}, \quad \text{for the cases} \quad l_3 = l_1 + l_2, \quad \text{and} \\[2ex] \text{(ii)} & T^{l_2 m_2, 1}_{l_1 m_1, l_3 m_3}, \quad \text{for the cases} \quad l_3 = l_1 + l_2 + 2. \end{array}$$

Hence we have recovered the dependence on the inverse powers of the interparticle distances, characteristic for Stokes flows. For example, the tensor $\mathbf{T}^{00}_{00}(\mathbf{R}_{jk})$ reads:

$$(4.14) \quad \mathbf{T}^{00}_{00}(\mathbf{R}_{jk}) = \mathbf{T}^{00}_{00,00}(|\mathbf{R}_{jk}|)Y^0_0(\Omega_{jk}) + \sum_m \mathbf{T}^{00}_{00,2m}(|R_{jk}|)Y^m_2(\Omega_{jk})$$

$$= \frac{1}{8\pi\mu R_{jk}}\left[1 + \hat{\mathbf{e}}_{jk}\hat{\mathbf{e}}_{jk} + \frac{2a^2}{R^2_{jk}}\left(\frac{1}{3} - \hat{\mathbf{e}}_{jk}\hat{\mathbf{e}}_{jk}\right)\right] = \mathbf{T}^{(1)00}_{00}(\mathbf{R}_{jk}),$$

where

$$R_{jk} = |\mathbf{R}_{jk}|, \qquad \hat{\mathbf{e}}_{jk} = \frac{\mathbf{R}_{jk}}{|\mathbf{R}_{jk}|}.$$

Similarly to the self-interaction case, we are interested in these mutual-interaction tensors, which contain terms linear in Re. As follows from Eq. (4.10), the respective contributions to the tensors $\mathbf{T}^{l_2 m_2}_{l_1 m_1, l_3 m_3}$ are given by

$$(4.15) \qquad \mathbf{T}^{l_2 m_2}_{l_1 m_1, l_3 m_3} = \sum_{m=0}^{\infty} \mathbf{T}^{l_2 m_2, m}_{l_1 m_1,, l_3 m_3} = -\frac{i^{1-l_3} \mathrm{Re} \sqrt{2\pi(2l_3+1)}}{16 a \mu \, \Gamma(l_1 + 3/2) \Gamma(l_2 + 3/2)} \varepsilon(-m_3)$$

$$\times \left\{ \sum_{rs} i^r \sqrt{2r+1} \mathbf{K}^{l_2 m_2}_{l_1 m_1, rs} (-1)^{-s} \varepsilon(-s) \begin{pmatrix} l_3 & 1 & r \\ 0 & 0 & 0 \end{pmatrix} \right.$$

$$\times \left[\sqrt{2} \hat{U}_z \begin{pmatrix} l_3 & 1 & r \\ -m_3 & 0 & s \end{pmatrix} - \left(\hat{U}_x - i\hat{U}_y \right) \begin{pmatrix} l_3 & 1 & r \\ -m_3 & 1 & s \end{pmatrix} \right.$$

$$\left. \left. + \left(\hat{U}_x + i\hat{U}_y \right) \begin{pmatrix} l_3 & 1 & r \\ -m_3 & -1 & s \end{pmatrix} \right] \right\}$$

$$\times \left(\frac{a}{R_{jk}} \right)^{l_1 + l_2} \sum_{m=0}^{\infty} \frac{(l_1 + l_2 + 2m + 1/2)\Gamma(l_1 + l_2 + m + 1/2)}{m!}$$

$$\times \frac{\Gamma(\zeta)}{\Gamma(Z+1)} F_4 \left[-m, l_1 + l_2 + m + \frac{1}{2}; l_1 + \frac{3}{2}, l_2 + \frac{3}{2}; \right.$$

$$\left. \left(\frac{a}{R_{jk}} \right)^2, \left(\frac{a}{R_{jk}} \right)^2 \right] + \text{h.o.t.},$$

where (:::) is the Wigner $3-j$ symbol [12],

$$\left\{ \begin{array}{ll} r = 1, & \text{for the cases of } l_3 = 0 \\ r = l_3 - 1, \quad \text{and} \quad r = l_3 + 1 & \text{for the cases of } l_3 \geq 1 \end{array} \right\},$$

and the following relations should be fulfilled:

$$|l_1 + l_2 + 2m - l_3| = 1,$$

$$l_1 + l_2 + l_3 \pm 1 = 2n, \qquad l_1 + l_2 - l_3 \pm 1 \geq -2,$$

$$\varepsilon(-m) = (-1)^{\frac{-3m-|m|}{2}}.$$

Thus the mutual-interaction tensors, being of the leading order of Re, can be written down as follows:

$$(4.16) \qquad \begin{array}{llll}
\text{(i)} & \mathbf{T}^{l_2 m_2}_{l_1 m_1, l_3 m_3} = \mathbf{T}^{l_2 m_2, 0}_{l_1 m_1, l_3 m_3} & \text{for} \quad l_1 + l_2 - l_3 = 1, \\[2mm]
\text{(ii)} & \mathbf{T}^{l_2 m_2}_{l_1 m_1, l_3 m_3} = \displaystyle\sum_{m=0,1} \mathbf{T}^{l_2 m_2, m}_{l_1 m_1, l_3 m_3} & \text{for} \quad l_1 + l_2 - l_3 = -1, \\[2mm]
\text{(iii)} & \mathbf{T}^{l_2 m_2}_{l_1 m_1, l_3 m_3} = \displaystyle\sum_{m=1,2} \mathbf{T}^{l_2 m_2, m}_{l_1 m_1, l_3 m_3} & \text{for} \quad l_1 + l_2 - l_3 = -3.
\end{array}$$

On the basis of Eq. (4.15) we see that the considered mutual-interaction tensors are, with respect to a/R, of the leading order of $\left(\dfrac{a}{R_{jk}} \right)^{l_1 + l_2}$. We note that,

similarly to the Stokes regime, the Oseen hydrodynamic interactions, in the approximation considered, are described by means of a finite number of the tensors $\mathbf{T}^{l_2 m_2, m}_{l_1 m_1, l_3 m_3}$, with m being equal, respectively, to $0, 1, 2$. Below we give two examples of that kind of the tensors:

$$\mathbf{T}^{00}_{00,1m_3}(\mathbf{R}_{jk}, \mathrm{Re}) = \mathbf{T}^{00,0}_{00,1m_3} + \mathbf{T}^{00,1}_{00,1m_3} + \text{h.o.t.} ,$$

(4.17)

$$\mathbf{T}^{00}_{00,1m_3} = -\frac{1}{2}\sqrt{\frac{3}{2}}\varepsilon(-m_3)\frac{\mathrm{Re}}{a\mu}\left\{\sum_{rs} i^r\sqrt{2r+1}\mathbf{K}^{00}_{00,rs}(-1)^{-s}\varepsilon(-s)\right.$$

$$\times \begin{pmatrix} 1 & 1 & r \\ 0 & 0 & 0 \end{pmatrix}\left[\sqrt{2}\hat{U}_z\begin{pmatrix} 1 & 1 & r \\ -m_3 & 0 & s \end{pmatrix} - (\hat{U}_x - i\hat{U}_y)\begin{pmatrix} 1 & 1 & r \\ -m_3 & 1 & s \end{pmatrix}\right.$$

$$\left.\left. + (\hat{U}_x + i\hat{U}_y)\begin{pmatrix} 1 & 1 & r \\ -m_3 & -1 & s \end{pmatrix}\right]\right\} \cdot \left(1 - \frac{2}{3}\left(\frac{a}{R_{jk}}\right)^2\right) + \text{h.o.t.};$$

$$\mathbf{T}^{00}_{00,3m_3}(\mathbf{R}_{jk}, \mathrm{Re}) = \mathbf{T}^{00,1}_{00,3m_3} + \mathbf{T}^{00,2}_{00,3m_3} + \text{h.o.t.},$$

(4.18)

$$\mathbf{T}^{00}_{00,3m_3} = \frac{1}{8}\sqrt{\frac{7}{2}}\varepsilon(-m_3)\frac{Re}{a\mu}\left\{\sum_{rs} i^r\sqrt{2r+1}\mathbf{K}^{00}_{00,rs}(-1)^{-s}\varepsilon(-s)\right.$$

$$\times \begin{pmatrix} 3 & 1 & r \\ 0 & 0 & 0 \end{pmatrix}\left[\sqrt{2}\hat{U}_z\begin{pmatrix} 3 & 1 & r \\ -m_3 & 0 & s \end{pmatrix} - (\hat{U}_x - i\hat{U}_y)\begin{pmatrix} 3 & 1 & r \\ -m_3 & 1 & s \end{pmatrix}\right.$$

$$\left.\left. + (\hat{U}_x + i\hat{U}_y)\begin{pmatrix} 3 & 1 & r \\ -m_3 & -1 & s \end{pmatrix}\right]\right\} \cdot \left(1 - 4\left(\frac{a}{R_{jk}}\right)^2\right) + \text{h.o.t.},$$

where

$$\mathbf{K}^{00}_{00,00} = \frac{1}{3\sqrt{\pi}}\mathbf{I} \qquad \text{and} \qquad \mathbf{K}^{00}_{00,2s} = \frac{1}{2\sqrt{30}\sqrt{\pi}}\mathbf{K}_s \text{ [13]}.$$

Similarly to the case of self-interaction tensors, we have also the second source of contributions linear in Re. Namely, expanding the tensor $\mathbf{T}^{00}_{00,00}$ with respect to Re, we obtain

(4.19) $$\mathbf{T}^{00}_{00,00}(|\mathbf{R}_{jk}|)Y^0_0(\Omega_{jk}) = \frac{1}{6\pi\mu R_{jk}}\left[\mathbf{I} - \frac{3}{16}\mathrm{Re}_m\left(3\mathbf{I} - \hat{U}\hat{U}\right)\right] + \text{h.o.t.}$$

Collecting the terms linear in Re, we denote:

$$\mathbf{T}^{(2)00}_{00}(\mathbf{R}_{jk}, \mathrm{Re}) = -\frac{\mathrm{Re}}{32\pi\mu a}\left(3\mathbf{I} - \hat{U}\hat{U}\right) + \sum_{m_1}\mathbf{T}^{00}_{00,1m_1}Y^{m_1}_1 + \sum_{m_3}\mathbf{T}^{00}_{00,3m_3} + \text{h.o.t.}$$

We see that the expression resembles that for the self-interaction tensors having, however, as the characteristic length the distance R_{jk}.

4.3. The inverse self-interaction tensors $\widetilde{\mathbf{T}}^{l_2 m_2}_{l_1 m_1}(\mathbf{O}_j)$

For the particular case of the hydrodynamic Stokes interactions, the inverse self-interaction tensors are given by

$$(4.20) \qquad \sum_{m_3} \widetilde{\mathbf{T}}^{l_1 m_3}_{l_1 m_1} \cdot \mathbf{T}^{l_1 m_2}_{l_1 m_3} = \mathbf{I}\delta_{m_1 m_2}.$$

For example, the tensor $\widetilde{\mathbf{T}}^{00}_{00} = 6\pi\mu a \mathbf{I}$ describes the Stokes drag force, exerted by the fluid on the single sphere.

To examine the properties of the tensors $\widetilde{\mathbf{T}}^{l_2 m_2}_{l_1 m_1}(\mathbf{O}_j)$, we apply the approximate formula, used in the paper [15]:

$$(4.21) \qquad \widetilde{\mathbf{T}} = \widetilde{\mathbf{T}}_d - \widetilde{\mathbf{T}}_d \cdot \widetilde{\mathbf{T}}_{od} \cdot \widetilde{\mathbf{T}}_d + \widetilde{\mathbf{T}}_d \cdot \widetilde{\mathbf{T}}_{od} \cdot \widetilde{\mathbf{T}}_d \cdot \widetilde{\mathbf{T}}_{od} \cdot \widetilde{\mathbf{T}}_d - \ldots.$$

where $\widetilde{\mathbf{T}}_d$ and $\widetilde{\mathbf{T}}_{od}$ are the diagonal (in l), and off-diagonal self-interaction tensors, respectively. The above approximate formula leads to the power series expansion in Re of the inverse self-interaction tensors. Considering the tensors, being of the leading order of Re, we obtain

$$(4.22) \qquad \widetilde{\mathbf{T}}^{l_1 + 1 m_2}_{l_1 m_1}(\mathbf{O}_j) = -\sum_{m_3}\sum_{m_4} \widetilde{\mathbf{T}}^{l_1 m_3}_{l_1 m_1} \cdot \mathbf{T}^{l_1 + 1 m_4}_{l_1 m_3} \cdot \widetilde{\mathbf{T}}^{l_1 + 1 m_2}_{l_1 + 1 m_4} + \text{h.o.t.},$$

and, respectively,

$$\widetilde{\mathbf{T}}^{l_2 m_2}_{l_2 + 1 m_1}(\mathbf{O}_j) = -\sum_{m_3}\sum_{m_4} \widetilde{\mathbf{T}}^{l_2 + 1 m_3}_{l_2 + 1 m_1} \cdot \mathbf{T}^{l_2 m_4}_{l_2 + 1 m_3} \cdot \widetilde{\mathbf{T}}^{l_2 m_2}_{l_2 m_4} + \text{h.o.t.}$$

Thus we have, for example

$$\widetilde{\mathbf{T}}^{1 m_2}_{00} = -\sum_{m_3} \widetilde{\mathbf{T}}^{00}_{00} \cdot \mathbf{T}^{1 m_3}_{00} \cdot \widetilde{\mathbf{T}}^{1 m_2}_{1 m_3} + \ldots.$$

$$(4.23) \qquad \widetilde{\mathbf{T}}^{1 m_2}_{00} = \sqrt{6}\pi\mu a \,\text{Re}\left\{\sqrt{2}\hat{U}_z\delta_{m_2 0} + \left(\hat{U}_x - i\hat{U}_y\right)\delta_{m_2(-1)}\right.$$

$$\left. + \left(\hat{U}_x + i\hat{U}_y\right)\delta_{m_2(1)}\right\}\mathbf{1} + \text{h.o.t.},$$

where [11]:

$$\widetilde{\mathbf{T}}^{1 m_2}_{1 m_3} = 6\sqrt{\pi}\mu a \widetilde{\mathbf{K}}^{1 m_2}_{1 m_3, 00}.$$

Similarly to the case of the self-interaction tensors, we calculate the contribution to $\widetilde{\mathbf{T}}^{00}_{00}(\mathbf{O}_j)$ linear in Re,

$$\widetilde{\mathbf{T}}^{00}_{00}(\mathbf{O}_j) = \widetilde{\mathbf{T}}^{(1)00}_{00}(\mathbf{O}_j) + \widetilde{\mathbf{T}}^{(2)00}_{00}(\mathbf{O}_j) + \text{h.o.t.}.$$

with the respective tensors equal to

$$(4.24) \qquad \widetilde{\mathbf{T}}^{(1)00}_{00}(\mathbf{O}_j) = 6\pi\mu a \mathbf{1}.$$

$$(4.25) \qquad \widetilde{\mathbf{T}}^{(2)00}_{00}(\mathbf{O}_j) = 6\pi\mu a \left[\frac{3}{16}\text{Re}\left(3\mathbf{I} - \hat{\mathbf{U}}\hat{\mathbf{U}}\right)\right].$$

5. The multiple scattering representation of the hydrodynamic interactions

Using the relations (3.7), we can write $f_{k,l_3 m_3}(\mathbf{O}_k)$ in terms of $\mathbf{V}_{j,l_2 m_2}(\mathbf{O}_j)$ as follows:

$$(5.1) \qquad f_{j,l_1 m_1} = \sum_{l_2 m_2} \tilde{\mathbf{T}}^{l_2 m_2}_{l_1 m_1}(\mathbf{O}_j) \cdot \mathbf{V}_{j,l_2 m_2}$$

$$- \sum_{k \neq j} \sum_{l_2 m_2} \sum_{l_3 m_3} \sum_{l_4 m_4} \tilde{\mathbf{T}}^{l_2 m_2}_{l_1 m_1}(\mathbf{O}_j) \cdot \mathbf{T}^{l_3 m_3}_{l_2 m_2}(\mathbf{R}_{jk}) \cdot \tilde{\mathbf{T}}^{l_4 m_4}_{l_3 m_3}(\mathbf{O}_k) \cdot \mathbf{V}_{k,l_4 m_4} + \ldots .$$

Thus we obtain the multiple scattering representation for the expansion coefficients $f_{j,lm}$ of the induced forces. The different sequences of the admissible interactions, appearing on the r.h.s of Eq. (5.1), are expressed in terms of the respective interaction tensors. In view of the properties of these tensors, discussed in Sec. 4, we have to take into account only a finite number of the admissible sequences, assuming an approximation with respect to σ and Re. Thus we obtain the following series for the expansion coefficients $f_{j,00}$, appearing in the expression for the vector forces, exerted on the spheres:

$$(5.2) \qquad f_{j,00} = \tilde{\mathbf{T}}^{00}_{00}(\mathbf{O}_j) \cdot \mathbf{V}_{j,00}$$

$$- \sum_{k \neq j} \sum_{l_3 m_3} \tilde{\mathbf{T}}^{00}_{00}(\mathbf{O}_j) \cdot \mathbf{T}^{l_3 m_3}_{00}(\mathbf{R}_{jk}) \cdot \tilde{\mathbf{T}}^{00}_{l_3 m_3}(\mathbf{O}_k) \cdot \mathbf{V}_{k,00} + \ldots .$$

The different sequences of the interactions, described by the above series, are listed below, and the contributions up to $O(\sigma)$ and $O(\text{Re})$ are retained. The inverse self – and mutual – interaction tensors entering the sequences are given by the formulae (4.24), (4.25), (4.14) and (4.19). We apply the following shorthand notation:

$$(5.3) \qquad \begin{aligned} \tilde{\mathbf{T}}^{(1)00}_{00}(\mathbf{O}_j) &= \tilde{\mathbf{T}}^1_j , & \tilde{\mathbf{T}}^{(2)00}_{00}(\mathbf{O}_j) &= \tilde{\mathbf{T}}^2_j , \\ \mathbf{T}^{(1)00}_{00}(\mathbf{R}_{jk}) &= \mathbf{T}^1_{jk} , & \mathbf{T}^{(2)00}_{00}(\mathbf{R}_{jk}) &= \mathbf{T}^2_{jk} , \\ \mathbf{V}_{j,00} &= \mathbf{V}_{k,00} = \mathbf{V}_{l,00} = -\mathbf{U} . \end{aligned}$$

The Stokes contributions to the coefficients $f_{j,00}$, describing the linear dependence of the forces exerted on the spheres, on the velocity of the fluid, read:

$$(5.4)$$

σ^0	$-\tilde{\mathbf{T}}^1_j \cdot \mathbf{U}$
σ^1	$\tilde{\mathbf{T}}^1_j \cdot \sum_{k \neq j} \mathbf{T}^1_{jk} \cdot \tilde{\mathbf{T}}^1_k \cdot \mathbf{U}$

Here we have two sequences of the interactions, generated by the relevant relative velocity $\mathbf{V}_{j,00}$, which are described by means of the two tensors. These sequences

are related, respectively, to the interaction of a single sphere, and a pair of spheres with the fluid. Thus, the property of non-additivity of the interactions does not appear for that case.

The Oseen contributions to the coefficients $\mathbf{f}_{j,00}$, giving quadratic relations between the forces on the spheres and the velocity of the fluid, are as follows:

(5.5)

$$
\begin{array}{c|l}
\sigma^0 & -\tilde{\mathbf{T}}_j^2 \cdot \mathbf{U} \\[4pt]
 & \tilde{\mathbf{T}}_j^1 \cdot \displaystyle\sum_{k \neq j} \mathbf{T}_{jk}^2 \cdot \tilde{\mathbf{T}}_k^1 \cdot \mathbf{U} \\[14pt]
\hline
\sigma^1 & \tilde{\mathbf{T}}_j^1 \cdot \displaystyle\sum_{k \neq j} \mathbf{T}_{jk}^1 \cdot \tilde{\mathbf{T}}_k^2 \cdot \mathbf{U} \\[14pt]
 & \tilde{\mathbf{T}}_j^2 \cdot \displaystyle\sum_{k \neq j} \mathbf{T}_{jk}^1 \cdot \tilde{\mathbf{T}}_k^1 \cdot \mathbf{U} \\[14pt]
 & -\tilde{\mathbf{T}}_j^1 \cdot \displaystyle\sum_{k \neq j}\sum_{l \neq k} \{ \mathbf{T}_{jk}^2 \cdot \tilde{\mathbf{T}}_k^1 \cdot \mathbf{T}_{kl}^1 \\[4pt]
 & + \mathbf{T}_{jk}^1 \cdot \tilde{\mathbf{T}}_k^1 \cdot \mathbf{T}_{kl}^2 \} \cdot \tilde{\mathbf{T}}_l^1 \cdot \mathbf{U}
\end{array}
$$

Here we have the six sequences of the interactions, which are expressed in terms of the four tensors. These sequences describe the interaction, respectively, of a single sphere, a pair of spheres, and three spheres. Hence here the non-additivity of the interactions plays a role in the determination of the forces, exerted on the spheres.

Qualitatively speaking, the structure of the Oseen hydrodynamic interactions is, in comparison with the Stokes interactions, more complex. We also note that the mutual interactions yield to the particular type of the contributions to $\mathbf{f}_{j,00}$, being of the zero order with respect to σ. Such contributions are not generated in the Stokes regime.

The contributions to $\mathbf{f}_{j,00}$, being of the order of $O(\sigma^2)$, and $O(\mathrm{Re}^1)$, are listed in the Appendix.

Here, as an example, we consider the drag forces $\mathbf{F}_j^d$, $j = 1, 2$, exerted on two fixed spheres by the fluid, having at infinity the uniform velocity $\mathbf{U}(O, O, U_z)$. The line connecting the centers of the spheres, is perpendicular to the velocity of the fluid. We obtain the following expression for the vector forces, retaining the terms linear in Re and σ:

(5.6)
$$
\mathbf{F}_j = \left\{ \tilde{\mathbf{T}}_j^1 + \tilde{\mathbf{T}}_j^2 - \sum_{k \neq j} \tilde{\mathbf{T}}_j^1 \cdot \left[\mathbf{T}_{jk}^1 \cdot \tilde{\mathbf{T}}_k^1 + \mathbf{T}_{jk}^2 \cdot \tilde{\mathbf{T}}_k^1 \right] \right\} \cdot \mathbf{U}.
$$

To express explicitly the components of the drag forces, we specify the relative distance between the two spheres in terms of the vectors $\mathbf{R}_{12}$ ($|\mathbf{R}_{12}|$, $\theta_{12} = 90°$, $\phi_{12} = 0°$), and respectively, $\mathbf{R}_{21}$ ($|\mathbf{R}_{12}|, \theta_{21} = 90°, \phi_{21} = 180°$).

Using the relation (5.6), we arrive at

$$(5.7) \qquad (F_1^d)_z = (F_2^d)_z = 6\pi\mu a U_z \left[1 - \frac{3a}{4|\mathbf{R}_{12}|} + \frac{3}{4}\mathrm{Re} + \mathrm{h.o.t}\right].$$

We note that the terms linear in Re are due to the two sources: self-interaction of the respective sphere (3/8Re), and the mutual interactions of the spheres (3/8Re). The above formula agrees, to within the approximation assumed here, with that part of the results of VASSEUR, COX [8], and KANEDA, ISHII [7], which is related to the drag forces acting on two spheres. To examine the hydrodynamic interactions of two spheres, the authors used the asymptotic expansion method of solving of the Navier–Stokes equations.

We note that the different terms of the mutual-interaction tensor $T_{00}^{00}(\mathbf{R}_{jk}, \mathrm{Re})$ describe the different vector components of the forces exerted on the spheres by the fluid. The tensors $T_{00,00}^{00}$ and $T_{00,2m}^{00}$ describe the contributions to the drag forces, whereas the tensors $T_{00,1m}^{00}$ and $T_{00,3m}^{00}$ give rise to the contributions to the lift forces (cf. [1]).

Appendix

The Stokes contributions of the order of $O(\sigma^2)$ to the coefficients $\mathbf{f}_{j,00}$, describing the linear dependence of the forces on the fluid velocity, read:

$$(A.1) \qquad -\sum_{k\neq j}\sum_{l\neq k} \tilde{\mathbf{T}}_j^1 \cdot \mathbf{T}_{jk}^1 \cdot \tilde{\mathbf{T}}_k^1 \cdot \mathbf{T}_{kl}^1 \cdot \tilde{\mathbf{T}}_l^1 \cdot \mathbf{U}.$$

Hence we have one type of the admissible sequence of the interactions, which is described by means of two tensors. Two, or three different spheres take part in the above events, giving rise to the non-additivity of the considered contributions to $\mathbf{f}_{j,00}$.

The Oseen contributions of the order of $O(\sigma^2)$, and $O(\mathrm{Re}^1)$, describing the respective quadratic relations, are given by

$$(A.2) \qquad \tilde{\mathbf{T}}_j^1 \cdot \sum_{k\neq j} \mathbf{T}_{jk}^2 \cdot \tilde{\mathbf{T}}_k^1 \cdot \mathbf{U}$$

$$+ \sum_m \tilde{\mathbf{T}}_{00}^{1m}(\mathbf{O}_j) \cdot \sum_{k\neq j} \mathbf{T}_{1m}^{00}(\mathbf{R}_{jk}) \cdot \tilde{\mathbf{T}}_k^1 \cdot \mathbf{U}$$

$$+ \tilde{\mathbf{T}}_j^1 \cdot \sum_{k\neq j}\sum_m \mathbf{T}_{00}^{1m}(\mathbf{R}_{jk}) \cdot \tilde{\mathbf{T}}_{1m}^{00}(\mathbf{O}_k) \cdot \mathbf{U}$$

$$- \tilde{\mathbf{T}}_j^1 \cdot \sum_{k\neq j}\sum_{l\neq k} \mathbf{T}_{jk}^1 \cdot \tilde{\mathbf{T}}_k^2 \cdot \mathbf{T}_{kl}^1 \cdot \tilde{\mathbf{T}}_l^1 \cdot \mathbf{U}$$

$$- \tilde{\mathbf{T}}_j^1 \cdot \sum_{k\neq j}\sum_{l\neq k} \mathbf{T}_{jk}^1 \cdot \tilde{\mathbf{T}}_k^1 \cdot \mathbf{T}_{kl}^1 \cdot \tilde{\mathbf{T}}_l^2 \cdot \mathbf{U}$$

$$-\tilde{\mathbf{T}}_j^2 \cdot \sum_{k \neq j} \sum_{l \neq k} \mathbf{T}_{jk}^1 \cdot \tilde{\mathbf{T}}_k^1 \cdot \mathbf{T}_{kl}^1 \cdot \tilde{\mathbf{T}}_l^1 \cdot \mathbf{U}$$

$$+\tilde{\mathbf{T}}_j^1 \cdot \sum_{k \neq j} \sum_{l \neq k} \sum_{n \neq l} \left\{ \mathbf{T}_{jk}^1 \cdot \tilde{\mathbf{T}}_k^1 \cdot \mathbf{T}_{kl}^2 \cdot \tilde{\mathbf{T}}_l^1 \cdot \mathbf{T}_{ln}^1 \right.$$

$$+\mathbf{T}_{jk}^2 \cdot \tilde{\mathbf{T}}_k^1 \cdot \mathbf{T}_{kl}^1 \cdot \tilde{\mathbf{T}}_l^1 \cdot \mathbf{T}_{ln}^1$$

$$\left. +\mathbf{T}_{jk}^1 \cdot \tilde{\mathbf{T}}_k^1 \cdot \mathbf{T}_{kl}^1 \cdot \tilde{\mathbf{T}}_l^1 \cdot \mathbf{T}_{ln}^2 \right\} \cdot \tilde{\mathbf{T}}_n^1 \cdot \mathbf{U}.$$

In that case we have the nine different sequences, described in terms of the eight interaction tensors. Two, three, or four different spheres contribute to the above interactions. Hence here the non-additivity of the interactions can possibly be more pronounced in comparison with the Stokes regime.

References

1. I. Pieńkowska, Arch. Mech., **45**, 6, 665, 1993.

2. R. Finn, ARMA, **19**, 363, 1965.

3. R. Finn, Rocky Mountain J. Math., **3**, 107, 1973.

4. G.P. Galdi, [in:] The Navier – Stokes Equations II, J.G. Heywood, K. Masuda, R. Rautmann, S.A. Solonnikov [Eds.], Springer, 1992.

5. R. Salvi, [in:] The Navier–Stokes Equations II, J.G. Heywood, K. Masuda, R. Rautmann, S.A. Solonnikov [Eds.], Springer, 1992.

6. R. Berker, [in:] Handbuch der Physik, vol. VIII/2, Springer, 1963.

7. Y. Kaneda, K. Ishii, J. Fluid Mech., **124**, 209, 1982.

8. P. Vasseur, R.G. Cox, J. Fluid Mech., **80**, 561, 1977.

9. P. Mazur, W. van Saarloos, Physica, **115A**, 21, 1982.

10. P. Mazur, A.J. Weisenborn, Physica, **123A**, 209, 1984.

11. I. Pieńkowska, Arch. Mech., **36**, 749, 1984.

12. A.R. Edmonds, *Angular momentum in quantum mechanics*, Princeton University Press, 1957.

13. T. Yoshizaki, H. Yamakawa, J. Chem. Phys., **73**, 578, 1980.

14. A. Erdelyi, [Ed.] *Higher transcendental functions*, vol. II, McGraw-Hill, 1953.

15. K.F. Freed, M. Muthukumar, J. Chem. Phys., **69**, 2657 (1978).

The periodical *ARCHIVES OF MECHANICS (ARCHIWUM MECHANIKI STOSOWANEJ)* deals with the printing of original papers which should not appear in any other publications. The authors may publish in the Bull. Acad. Polon. Sci. short papers only, announcing the solutions of any problems as well as informing that the full text will be inserted in the columns of the *ARCHIVES OF MECHANICS (ARCHIWUM MECHANIKI STOSOWANEJ)*.

As a rule, the volume of a paper should not exceed 40 000 typographic signs, that is about 20 type-written pages, format: 210×297 mm, leaded. The papers should be submitted in two copies. They must be set in accordance with the norms established by the Editorial Office. Special importance is attached to the following directions:

1. The title of the paper should be as short as possible.

2. The text should be preceded by a brief introduction; it is also desirable that a list of notations used in the paper be given.

3. Short papers should be divided into sections and subsections, long papers into sections, subsections and points. Each section, subsection or point must bear a title.

4. The formula number consists of two figures: the first represents the section number and the other the formula number under that section. Thus the division into subsections does not influence the numbering of formulae. Only such formulae should be numbered to which the author refers throughout the paper, also the resulting formulae. The formula number should be written on the left-hand side of the formula; brackets are to be only to avoid any misunderstanding. For instance, if the author refers to formula 3 of the set (2.1), a subscript should be added to denote the set of formula, viz. $(2.1)_3$.

5. All the notations should be written very distinctly. Special care must be taken to write small and capital letters as precisely as possible. Semi-bold type must be underlined in black pencil. Explanations should be given on the margin of the manuscript in case of special type face.

6. It has been established to denote vectors semi-bold type, transforms of the corresponding functions by tilded symbols. Trigonometric functions are denoted by sin, cos, tg and ctg, inverse functions – by arc sin, arc cos, arc tg and arc ctg; hyperbolic functions are denoted by sh, ch, th and cth, inverse functions – by Arsh, Arch, Arth and Arcth.

7. Figures in brackets denote reference titles. Items appearing in the reference list should include the initials of the Christian name of the author and his surname, also the full title of the paper (in the language of the original paper); moreover;

    a) in the case of books, the publisher's name, the place and year of publication should be given, e.g.,
        5. S. Ziemba, *Vibration analysis*, PWN, Warszawa 1970;

    b) in the case of a periodical, the full title of the periodical, consecutive volume number, current issue number, pp. from ... to ..., year of publication should be mentioned; the annual volume number must be marked in black pencil so as to distinguish it from the current issue number, e.g.,
        6. M. Sokołowski, *A thermoelastic problem for a strip with discontinuous boundary conditions*, Arch. Mech., **13**, 3, 337–354, 1961.

8. The authors should enclose a summary of the paper. The volume of the summary is to be about 100 words.

9. If the paper is to be translated into another language than that of the manuscript, the author is requested to include a glossary of special terms.

Upon receipt of the paper, the Editorial Office forwards it to the reviewer. His opinion is the basic for the Editorial Committee to determine whether the paper can be accepted for publication or not.

The printing of the paper completed, the author receives 25 copies of reprints free of charge. The authors wishing to get more copies should advise the Editorial Office accordingly, not later than the date of obtaining the galley proofs.

The papers submitted for publication in the journal should be written in English. No royalty are paid to the authors.

If possible, please send us, in addition to the typescript, the same text prepared on a diskette (floppy disk) 3 1/2″ or 5 1/4″.